

**Functional characterization of phospholipases
during blood stage development of *Plasmodium
falciparum***

Dissertation

with the aim of obtaining a

Doctor rerum naturalium (Dr. rer. nat.)

of the Faculty of Mathematics, Informatics and Natural Sciences,
Department of Biology, at the University of Hamburg

in collaboration with the Bernhard Nocht Institute for Tropical Medicine
(BNITM) and the Centre for Structural Systems Biology (CSSB)

submitted by

Emma Luise Pietsch

Hamburg 2022

For my mom and my sister

Dissertationsgutachter: Prof. Dr. Tim-Wolf Gilberger
Prof. Dr. Michael Filarsky

Datum der Disputation: 09.12.2022

Eidesstattliche Versicherung

Hiermit erkläre ich, Emma Luise Pietsch, an Eides statt, dass ich die vorliegende Dissertationsschrift selbst verfasst und keine anderen als die angegebenen Quellen und Hilfsmittel benutzt habe.

I, Emma Luise Pietsch, hereby declare upon oath that I have written the present dissertation independently and have not used further resources and aids than those stated in the dissertation.

Hamburg, den 20.10.2022

Place, Date

Emma Luise Pietsch

Signature

Erklärung zur Abgabe der Dissertation

Ich, Emma Luise Pietsch, versichere, dass dieses gebundene Exemplar der Dissertation und das in elektronischer Form eingereichte Dissertationsexemplar (über den Docata-Upload) sowie das bei der Fakultät (Studienbüro Biologie) zur Archivierung eingereichte gedruckte gebundene Exemplar der Dissertationsschrift identisch sind.

I, Emma Luise Pietsch, declare that this bound copy of the dissertation and the dissertation submitted in electronic form (via the Docata upload) and the printed bound copy of the dissertation submitted to the faculty (Academic Office Biology) for archiving are identical.

Hamburg, den 20.10.2022

Place, Date

Emma Luise Pietsch

Signature

Acknowledgments

First, I would like to thank Prof. Tim Gilberger and Dr. Paul-Christian Burda. To Tim for the opportunity to work in his group, for our discussions and his critical comments – and our Friday runs. To Paul for the trust, he put into me with this project, for his supervision and support, and for giving me the chance to start the gametocyte project from scratch. I would also like to thank Prof. Michael Filarsky for all his advice and encouragement over the past three years, for the co-supervision of my work and for examining this thesis, and Prof. Iris Bruchhaus for her co-supervision. Moreover, I owe a huge debt to Dr. Tobias Spielmann for his time and advice as a mentor. Our meetings were of great value to me and I appreciate all the effort he has put into them.

For supporting and funding my work, I want to thank the funding agencies DFG and EMBO and the BNITM for handling not only my salary but also all the more or less complicated travel expenses. I will keep my trips to the BioMalPar and the MPM conference in the best memories.

Over the three years of my PhD candidature, I had the chance to work with great collaborators. Thanks to Prof. Michael J. Blackman and Dr. Abhinay Ramaprasad for the collaboration on the phospholipase story, and to Dr. Markus A. Keller and Yvonne Wohlfarter for their lipidomic analysis. A special thanks also to Prof. Dominique Soldati-Favre who welcomed me into her lab and to her staff Dr. Joachim Kloehn and Dr. Bohumil Maco as well as to all the members of the Soldati and Brochet lab. My time in Geneva was certainly one of the most fun times during my PhD. I appreciate how much time Jo and Bohumil took to discuss my project, run experiments, drink hot lemon tea or coffee, and simply chat. Thanks also to Nico who interrupted writing his thesis to teach me how to do expansion microscopy. Now that I am writing these words, I am even more thankful that you dedicated some of your valuable time to me. I also want to thank the Core Facilities that made my work possible, in particular Dr. Roland Thürnauer as the head of the ALFM facility at the CSSB. Thank you for your advice and enthusiasm and for your patience with our tricky *Plasmodium* samples.

A very special thank you to all the past and present members of the Gilberger and Filarsky lab. I consider myself very lucky to have worked with such fantastic people who supported me not only with their technical expertise but also emotionally whenever I hit a rough patch. I spent many hours, nights, and weekends at CSSB but having great colleagues around certainly made life easier. A special thanks to Monja, Arne and Sarah for preparing liters and liters of medium and ordering tons of blood for my large-scale experiments. I could not have done any of it without you. I also want to thank Sabrina who started the phospholipase project and has done the groundwork this thesis is built on. I am sure you will make your way and I wish you only the best for your future. A huge thank you also to all the TA apprentices for their work and especially their cloning efforts. Supervising them has been a truly rewarding experience. I also want to thank everyone who ever has fed my tiny parasites over the weekends – you helped to keep me sane by giving me some time off to breathe.

Working at CSSB has put me in touch with fantastic researchers beyond our malaria group. From the bottom of my heart, I want to thank Josie, Emily and Katharina for their

friendship and support. The three of you are an inspiration and I consider myself so lucky to have found you. Thanks for sharing coffee and laughter, for drying all my tears, for taking care of the kittens, and for being there whenever I needed you. Having you around made life so much easier and more fun and I already miss you so much. I also would like to thank Yannick, Janne and Maurice for their friendship. I cannot express how much the time with you meant to me and reminded me of what is important in life. Thanks for our shared coffees and aperol spritz' and for paddling with me on the canals of my favorite city.

I would like to thank all the CSSB PhD students who have trusted me as their PhD Representative, and the CSSB Forum members who have listened to all my comments and thoughts. I am eager to see how the CSSB will develop in the next few years.

Thanks also to Jessica Kehrer. Five years ago, I did my first internship in a malaria lab supervised by you – and I am still here. In some ways, you have made me the malaria researcher I am today and I am truly thankful for that. I am sure we will share many more bottles of sparkling wine whenever our paths cross, be it at a conference or the Oktoberfest. I will see you soon.

For their unconditional love and support and their understanding, I would like to thank my family and my wonderful partner Matthias. I am beyond lucky to have them as my rock in stormy waters. I also want to thank Nike and Lakritz who are not able to read these lines but who gave me a reason to leave the lab in the evening and come to a place that is home only when they are there. They will never understand how much they have helped me by doing nothing more than purr and cuddle.

Finally, the biggest thank you to my mother Renée and my sister Charlotte who expressed nothing but love and encouragement to me throughout my life. This thesis is dedicated to them.

Table of Contents

SUMMARY	1
ZUSAMMENFASSUNG.....	3
LIST OF FIGURES	5
LIST OF TABLES.....	6
ABBREVIATIONS	7
1. INTRODUCTION.....	10
1.1 MALARIA	10
1.1.1 Malaria epidemiology	11
1.1.2 Malaria intervention and vaccine strategies	12
1.2 THE COMPLEX LIFE CYCLE OF THE MALARIA PARASITE <i>PLASMODIUM</i>.....	14
1.3 PARASITE ULTRASTRUCTURE.....	17
1.3.1 Merozoites	19
1.3.2 Ring, trophozoite and schizont stages	19
1.3.3 Gametocytes.....	21
1.4 THE FUNCTION OF THE MITOCHONDRION THROUGHOUT THE STAGES	21
1.4.1 The TCA cycle	22
1.4.2 The electron transport chain	22
1.4.3 Biosynthetic mitochondrial pathways	26
1.4.4 The mitochondrion as a drug target	27
1.5 LIPIDS IN THE MALARIA PARASITE.....	28
1.5.1 Scavenging and synthesis	30
1.5.2 The importance of cardiolipins in mitochondria.....	31
1.6 THE DIVERSE ROLES OF PHOSPHOLIPASES IN <i>P. FALCIPARUM</i>.....	33
1.6.1 Essential phospholipases	33
1.6.2 Lysophospholipases	34
1.6.3 Patatin-like phospholipases	34
1.6.4 Other phospholipases of interest	35
1.7 AIM OF THIS THESIS	35
2. MATERIAL AND METHODS.....	37
2.1 MATERIAL.....	37
2.1.1 Chemicals and Reagents.....	37
2.1.2 Media	39
2.1.3 Buffers and Solutions.....	40
2.1.4 Antibiotics and Antimalarials	43
2.1.5 Antibodies	44
2.1.6 Enzymes	44
2.1.7 Inhibitors	44
2.1.8 DNA and Protein Standards.....	45
2.1.9 Oligonucleotides (primers)	45
2.1.10 Plasmids	45
2.1.11 Kits	46
2.1.12 Cell lines	46
2.1.13 Technical equipment and Microscopes.....	47
2.1.14 Labware and Disposables.....	49
2.1.15 Software and Databases.....	50
2.2 METHODS	50
2.2.1 Polymerase Chain Reaction (PCR)	50
2.2.2 Agarose gel electrophoresis	51
2.2.3 Purification of PCR products	51
2.2.4 Restriction digest	52

Table of Contents

2.2.5 Ligation	52
2.2.6 Production of heat-shock competent <i>E. coli</i>	53
2.2.7 Heat-shock transformation of <i>E. coli</i>	53
2.2.8 Plasmid isolation from <i>E. coli</i> culture	53
2.2.9 Cloning of pSLI constructs	54
2.2.10 Sequencing of plasmid DNA	57
2.2.11 DNA precipitation using sodium acetate	57
2.2.12 Isolation of genomic DNA from <i>P. falciparum</i>	57
2.2.13 SDS gel electrophoresis and Western Blot.....	57
2.2.14 Sterilization of solutions and materials.....	58
2.2.15 Cultivation of <i>P. falciparum</i>	58
2.2.16 Production of synchronous <i>P. falciparum</i> gametocytes	59
2.2.17 Giemsa staining of blood smears for routine culture and stage quantifications	59
2.2.18 Freezing and Thawing of <i>Plasmodium</i> cryostabilates.....	60
2.2.19 Isolation of parasites using saponin lysis.....	60
2.2.20 Isolation of schizonts using Percoll	61
2.2.21 Synchronization of rings using sorbitol	61
2.2.22 Tight synchronization of parasites via reinvasion	61
2.2.23 Transfection of <i>P. falciparum</i>	61
2.2.24 Immunofluorescence assays (IFA) of transgenic parasites	62
2.2.25 Mitochondrial staining using MitoTracker or Rhodamine	62
2.2.26 Fluorescence microscopy	63
2.2.27 Electron microscopy.....	63
2.2.28 Proliferation assay with <i>P. falciparum</i>	64
2.2.29 Drug susceptibility assays.....	65
2.2.30 Measurement of oxygen consumption rates (Seahorse Assay)	65
2.2.31 Lipidomic analysis.....	67
2.2.32 Exflagellation assays of mature <i>P. falciparum</i> gametocytes.....	69
2.2.33 Imaging-based egress assay of mature <i>P. falciparum</i> gametocytes	69
2.2.34 Protein sequence alignment	69
2.2.35 Modeling of protein structures.....	69
2.2.36 Statistical analysis.....	70
3. RESULTS	71
3.1 CHARACTERIZATION OF THE MITOCHONDRIAL PHOSPHOLIPASE PNPLA2.....	71
3.1.1 PF3D7_1358000 is a patatin-like phospholipase.....	71
3.1.2 PNPLA2 localizes to the mitochondrion.....	73
3.1.3 KO of PNPLA2 leads to a growth defect.....	73
3.1.4 Loss of PNPLA2 leads to abnormal mitochondrial staining and an ultrastructural abnormality	76
3.1.5 PNPLA2-KO parasites are hypersensitive to drugs targeting the mtETC.....	81
3.1.6 Loss of PNPLA2 leads to lower mitochondrial respiration	82
3.1.7 PNPLA2-KO parasites show a lower mitochondrial membrane potential	83
3.1.8 Deletion of PNPLA2 is associated with changes in the mitochondrial phospholipid cardiolipin.....	85
3.1.9 PNPLA2-KO parasites fail to form mature gametocytes	87
3.2 CHARACTERIZATION OF PHOSPHOLIPASES IN GAMETOCYTES.....	89
3.2.1 The six selected phospholipases show various localization patterns in blood stages	91
3.2.2 LPL1 is not essential for asexual intraerythrocytic development	99
3.2.3 Loss of individual phospholipases does not impair gametocyte development.....	101
3.2.4 None of the tested phospholipases is required for gametogenesis	102
4. DISCUSSION.....	107
4.1 PNPLA2 IS AN IMPORTANT MITOCHONDRIAL PHOSPHOLIPASE FOR INTRAERYTHROCYTIC PARASITE DEVELOPMENT	107
4.1.1 Loss of the mitochondrial phospholipase PNPLA2 leads to ultrastructural aberrations.....	107
4.1.2 PNPLA2 might be required for full activity of Complex IV	109
4.1.3 Loss of PNPLA2 might affect cardiolipin composition.....	110
4.1.4 Is the phospholipase activity of PNPLA2 required for regular mitochondrial function?.....	114
4.1.5 PNPLA2 is required for gametocyte maturation.....	115
4.2 PHOSPHOLIPASES SHOW HIGH REDUNDANCY IN GAMETO(CYTO)GENESIS	116
4.3 FUTURE PERSPECTIVES.....	118
REFERENCES	120

Table of Contents

PUBLICATIONS	135
PRESENTATIONS	136

Summary

Malaria is one of the most important infectious diseases worldwide and represents a persistent socio-economic burden on mankind. The disease is caused by the unicellular Apicomplexan parasite *Plasmodium* whose asexual reproduction within red blood cells is responsible for all clinical symptoms of malaria. Among the human-infecting malaria parasite species, *Plasmodium falciparum* is the most lethal one.

For all cells, but especially for fast proliferating ones, such as the intraerythrocytic malaria parasite, a well-orchestrated lipid metabolism is essential. Enzymes involved in the respective metabolic pathways such as phospholipases have been shown to play crucial physiological roles and represent potential drug targets. The aims of this thesis are i) to functionally characterize the mitochondrial patatin-like phospholipase PNPLA2 (PF3D7_1358000) throughout intraerythrocytic parasite development and ii) to investigate the role of six additional phospholipases during gametocyte development and egress.

Towards the first aim, I showed that parasites lacking PNPLA2 displayed a severe growth phenotype and defects in their organellar ultrastructure. Moreover, PNPLA2-deficient parasites showed decreased mitochondrial respiration rates and had a lower mitochondrial membrane potential. The impaired organelle function rendered these mutant parasites hypersensitive to the anti-malarial drugs Proguanil and Atovaquone along with other inhibitors of the mitochondrial electron transport chain. However, the observed mitochondrial phenotypes were shown to be independent of ROS levels as well as ubiquinone recycling and thus pyrimidine biosynthesis. In line with the results from asexual stages, PNPLA2-KO parasites showed impaired gametocyte development with the majority of parasites only developing to stage III before displaying an aberrant morphology. Taken together, these data point towards an important function of PNPLA2 in mitochondrial physiology.

To study the effects of PNPLA2 deficiency on the lipid metabolism of the parasite, a cardiolipin-tailored lipidomic analysis of *P. falciparum* was executed. While this approach represents the first comprehensive investigation of cardiolipins of the malaria parasite, it also showed that upon loss of PNPLA2, the carbon chains of cardiolipins tend to be shorter and more saturated, implying a role of PNPLA2 in cardiolipin remodeling. We hypothesize that the modification of cardiolipin composition in PNPLA2-deficient parasites might be linked to the impairment of mitochondrial functions.

Towards the second aim, I explored the role of six additional phospholipases during gametocyte development by studying their localization and investigating whether their individual loss impairs gametocytogenesis or gamete egress. Interestingly, the dispensable

PL38 phospholipase appeared to be localized to the rhoptries of asexual blood stages suggesting it might be involved in parasite egress or merozoite invasion.

To our surprise, five of the six phospholipases - LPL1 (PF3D7_1476700), LPL4 (PF3D7_0731800), PL38 (PF3D7_1412000), PL39 (PF3D7_1411900) and PARE (PF3D7_0709700) - were shown to be dispensable for gametocyte development and gamete egress. However, PNPLA3 (PF3D7_0924000)-deficient parasites showed a significant delay in efficient exflagellation of male gametocytes indicating an important, albeit not essential, role of PNPLA3 in male gametogenesis. Taken together, these results illustrate a high level of redundancy of parasite phospholipases during gametocytogenesis under *in vitro* conditions and indicate a complex interplay of the individual members of this enzyme family.

Zusammenfassung

Malaria ist eine der bedeutendsten Infektionskrankheiten der Welt. Etwa die Hälfte der Weltbevölkerung ist dem Risiko einer Infektion ausgesetzt, was Malaria bis heute zu einer enormen sozio-ökonomischen Belastung für die Menschheit macht. Verursacht wird die Krankheit durch den einzelligen, eukaryotischen Parasiten *Plasmodium*, dessen ungeschlechtliche Vermehrung in den roten Blutkörperchen alle klinischen Symptome der Malaria verursacht. Unter den humaninfektiösen Malariaparasiten ist *Plasmodium falciparum* die tödlichste Art.

Lipide, insbesondere Phospholipide, sind essentielle Bestandteile aller lebender Zellen, die als Strukturelemente, Energiespeicher und Signalmoleküle dienen. Aufgrund dieser zentralen Bedeutung ist die differenzielle Regulation des Lipidmetabolismus von besonderer Bedeutung. Das trifft insbesondere für solche Zellen zu, die sich sehr schnell vermehren, wie beispielsweise Malariaparasiten in unseren roten Blutkörperchen. Die Modifikation und Regulation von Phospholipiden wird unter anderem von Enzymen wie Phospholipasen geleistet, die Lipide in Fettsäuren und weitere lipophile Moleküle hydrolysieren, um sie so verschiedensten Stoffwechselwegen zur Verfügung zu stellen. Durch ihre zentrale physiologische Rolle stellen diese Enzyme potenzielle Angriffspunkte für Medikamente dar. Ziel der vorliegenden Arbeit war daher die funktionelle Charakterisierung ausgewählter Phospholipasen des Malariaparasiten *P. falciparum*. Im ersten Teil der Arbeit wurde die Funktion der Patatin-ähnlichen Phospholipase PNPLA2 (PF3D7_1358000) während der gesamten intraerythrozytären Entwicklung des Parasiten eingehend untersucht. Im zweiten Teil der Arbeit wurde die Rolle von sechs weiteren Phospholipasen während der zweiwöchigen Gametozytenentwicklung und Gametenfreisetzung charakterisiert.

Im Hinblick auf das erste Ziel konnte zunächst gezeigt werden, dass PNPLA2 im Mitochondrium des Parasiten lokalisiert. Mit Hilfe von verschiedenen Methoden der reversen Genetik wurde dann gezeigt, dass PNPLA2-Defizienz zu einem schweren Wachstumsphänotypen sowie zu Defekten in der zellulären Ultrastruktur führt. Nachfolgende Untersuchungen zeigten, dass PNPLA2-defiziente Parasiten eine verminderte mitochondriale Respiration und ein niedrigeres mitochondriales Membranpotenzial aufwiesen. Diese Beeinträchtigung der Mitochondrienfunktion führte zudem zu einer Überempfindlichkeit der Parasiten gegenüber den Malariamedikamenten Proguanil und Atovaquone sowie anderen Inhibitoren der Atmungskette. Die beobachteten Defekte waren dabei unabhängig vom Level an reaktiven Sauerstoffspezies sowie vom Ubiquinon-Zyklus und damit von der Pyrimidin-Biosynthese. In Übereinstimmung mit den Ergebnissen aus dem asexuellen Stadium zeigten PNPLA2-defiziente Parasiten starke Defekte in der Gametozytenentwicklung: Die Mehrheit der Parasiten entwickelte sich lediglich bis zum Stadium III, bevor sie eine anomale Morphologie aufwiesen. Zusammengenommen deuten diese Daten auf eine wichtige Funktion von PNPLA2 in der mitochondrialen Physiologie hin.

Um die Auswirkungen des Verlusts von PNPLA2 auf den Lipidstoffwechsel des Parasiten zu untersuchen, wurde anschließend das Lipidom von *P. falciparum* mit einem speziellen Fokus auf Cardiolipinen untersucht. Diese erste, umfassende Cardiolipin-Analyse des Malariaparasiten zeigte, dass die Kohlenstoffketten der Cardiolipine nach dem Verlust von PNPLA2 tendenziell kürzer und stärker gesättigt sind, was auf eine Rolle von PNPLA2 beim Umbau der Cardiolipine hindeutet. Die veränderte Zusammensetzung der Cardiolipine in PNPLA2-defizienten Parasiten könnte dabei mit der Beeinträchtigung der mitochondrialen Funktionen zusammenhängen.

Im Hinblick auf das zweite Ziel wurde die Rolle von weiteren sechs weiteren Phospholipasen während der Gametozytenreifung und der Freisetzung der sexuell differenzierten Gameten untersucht. Zunächst wurde die Expression und Lokalisation der entsprechenden Enzyme experimentell ermittelt, bevor die phänotypische Auswirkung von individuellen Gen-Knockouts der Phospholipasen auf Gametozytogenese und Gametogenese untersucht wurde. Interessanterweise wurde hierbei die Phospholipase PL38 als ein Rhoptrien-Protein identifiziert, was auf eine Rolle dieser Lipase für die Zell-Zell-Interaktion während des Austritts aus der Wirtszelle oder der Merozoiteninvasion nahelegt.

Die detaillierte Analyse der Phospholipase-Knockout-Linien erwies überraschenderweise, dass fünf der sechs Phospholipasen - LPL1 (PF3D7_1476700), LPL4 (PF3D7_0731800), PL38 (PF3D7_1412000), PL39 (PF3D7_1411900) und PARE (PF3D7_0709700) - entbehrlich für die Gametozytogenese und den Gametenaustritt sind. Lediglich PNPLA3 (PF3D7_0924000)-defiziente Parasiten zeigten eine deutlich verzögerte Exflagellation, was auf eine Rolle von PNPLA3 bei der männlichen Gametogenese hindeutet. Zusammengenommen konnte gezeigt werden, dass Phospholipasen in der Gametozytenentwicklung unter In-vitro-Bedingungen ein hohes Maß an Redundanz aufweisen, was ein komplexes Zusammenspiel der Enzyme dieser Familie vermuten lässt.

List of Figures

Figure 1.	Phylogeny and epidemiology of malaria.	12
Figure 2.	Life cycle of <i>Plasmodium falciparum</i> .	15
Figure 3.	Organelle structure and dynamics during intraerythrocytic development of <i>P. falciparum</i> .	18
Figure 4.	Schematic of the mitochondrial TCA cycle and the mitochondrial electron transport chain.	23
Figure 5.	General structure of phospholipids and common head groups.	29
Figure 6.	Predicted 3D structure of PF3D7_1358000 (PNPLA2).	72
Figure 7.	PNPLA2 localizes to the mitochondrion.	74
Figure 8.	Deletion of PNPLA2 leads to slower asexual growth.	75
Figure 9.	PNPLA2-KO parasites display an abnormal mitochondrial staining.	77
Figure 10.	Ultrastructural analysis of WT parasites by FIB-SEM.	78
Figure 11.	Ultrastructural analysis of PNPLA2-KO parasites by FIB-SEM.	79
Figure 12.	3D reconstructions of segmented schizonts.	80
Figure 13.	Susceptibility of PNPLA2-KO parasites to antimalarial drugs.	82
Figure 14.	PNPLA2-KO parasites show lower oxygen consumption rates (OCRs) and a lower $\Delta\Psi_m$.	84
Figure 15.	Lipidomic analysis of PNPLA2-KO parasites.	86
Figure 16.	PNPLA2-KO parasites show defects in gametocyte development.	88
Figure 17.	Analytical PCRs of mScarlet/mNeon-tagged parasite lines in the NF54/iGP2 and 3D7CH background.	91
Figure 18.	PARE localizes to the PPM.	92
Figure 19.	LPL4 localizes mainly to the DV.	94
Figure 20.	PNPLA3 shows an unspecific localization pattern.	95
Figure 21.	PL39 cannot be localized with high confidence.	96
Figure 22.	PL38 localizes to rhoptries.	98
Figure 23.	LPL1 localizes to the PPM.	100
Figure 24.	Analytical PCRs of KO parasite lines in the NF54/iGP2 background.	101
Figure 25.	Individual KO of six phospholipases does not impair gametocyte survival.	102
Figure 26.	Individual KO of the six phospholipases does not impair gametocyte maturation.	103
Figure 27.	PNPLA3-KO shows a delay in exflagellation.	104
Figure 28.	None of the phospholipase-KO lines shows a defect in gamete egress.	105

List of Tables

Table 1.	Phospholipases studied in this PhD thesis.	36
Table 2.	PCR reaction mixes.	51
Table 3.	PCR cycling programs.	51
Table 4.	Reaction mixes for restriction digests.	52
Table 5.	Reaction mix for T4 ligation.	52
Table 6.	Primers used for cloning of SLI-based KO constructs for PNPLA2 and LPL1.	54
Table 7.	Primers used for SLI-based tagging constructs.	55
Table 8.	Primers used for analytical PCRs.	56
Table 9.	Recipes for SDS gels.	57
Table 10.	HPLC gradients for lipidomic analysis.	68
Table 11.	Mass spectrometer parameters for lipidomic analysis.	68
Table 12.	Sequence identities of PNPLA2 orthologs.	73
Table 13.	Putative lipases with mass spectrometric evidence for expression in gametocytes.	90

Abbreviations

ACP	Acyl carrier protein
ACT	Artemisinin combination therapy
ALA	δ -Aminolevulinate
ALCAT1	Acyl CoA:lysocardiolipin acyltransferase 1
APS	Ammonium persulfate
BSA	Bovine serum albumin
C2	Compound 2
CCCP	Carbonyl cyanide m-chlorophenylhydrazone
CDP-DAG	Cytidine diphosphate diacylglycerol
CEPT	Choline/Ethanolamine phosphotransferase
CL	Cardiolipin
CLS	Cardiolipin synthase
CTP	Cytidine triphosphate
CytC	Cytochrome <i>c</i>
DAG	Diacylglycerol
DAPI	4',6-Diamidino-2-Phenylindole
DCUQ	Decylubiquinone
DHA	Dihydroartemisinin
DHE	Dihydroethidium
DHODH	Dihydroorotate dehydrogenase
DMSO	Dimethyl sulfoxide
dNTP	Desoxyribonucleotide
DTT	1,4-Dithiothreitol
DV	Digestive vacuole
ER	Endoplasmic reticulum
FA	Fatty acid
FAD	Flavin Adenine Dinucleotide
FCCP	Carbonyl cyanide-p-trifluoromethoxyphenylhydrazone
FV	Food vacuole
G3P	Glycerol-3-phosphate
G3PDH	Glycerol-3-phosphate dehydrogenase
GDPD	Glycerophosphodiesterase
hpi	Hours post infection
IMC	Inner membrane complex
iPLA2	Calcium-independent phospholipase(s) A2
IRS	Indoor residual spraying
ITN	Insecticide-treated net
KI	Knockin
KO	Knockout

Abbreviations

LPL	Lysophospholipase
lysoPC	Lysophosphatidylcholine
MLCL	Monolysocardiolipin
MQO	Malate:quinone oxidoreductase
mtETC	Mitochondrial electron transport chain
NAD	Nicotinamide Adenine Dinucleotide
NDH2	Type II NADH dehydrogenase
OCR	Oxygen consumption rate
OCR _{basal}	Basal oxygen consumption rate
OCR _{TMPD}	TMPD-elicited OCR
OMC	Ovoid mitochondrial cytoplasmic (complex)
ORS	Outdoor residual spraying
PA	Phosphatidic acid
PbPL	<i>Plasmodium berghei</i> phospholipase
PbPla1	<i>Plasmodium berghei</i> phosphatidic acid-preferring phospholipase A1
PC	Phosphatidylcholine
PC-PLC	Phosphatidylcholine-specific phospholipase C
PCR	Polymerase chain reaction
PE	Phosphatidylethanolamine
PG	Phosphatidylglycerol
PI	Phosphatidylinositol
PI-PLC	Phosphoinositide-specific phospholipase C
PNPLA	Patatin-like phospholipase
pplp2	<i>Plasmodium</i> perforin-like protein 2
PS	Phosphatidylserine
PV	Parasitophorous vacuole
PVM	Parasitophorous vacuole membrane
Q	Ubiquinone
QH ₂	Dihydroubiquinone
RBC	Red blood cell
RBCM	Red blood cell membrane
RDT	Rapid diagnostic test
ROS	Reactive oxygen species
SDH	Succinate dehydrogenase
SDS	Sodium dodecyl sulfate
SLI	Selection-linked integration
SM	Sphingomyelin
TAG	Triacylglycerol
TAG	Tagging line
TAZ	Tafazzin
TCA	Tricarboxylic cycle
TEMED	Tetramethylethylenediamine

Abbreviations

TGD	Targeted gene deletion
TM	Transmembrane domain
TMPD	N,N,N,N'-tetramethyl-p-phenylenediamine
WGA	Wheat Germ Agglutinin
WL	Wildtype locus
WT	Wildtype
$\Delta\Psi_m$	Mitochondrial membrane potential

1. Introduction

1.1 Malaria

Malaria has been a major global health problem throughout history. With around half of the world population at risk of getting infected today, it still poses a massive clinical and economic challenge. Over the last decades, control efforts have reduced the malaria burden tremendously, raising the prospect that elimination and perhaps eradication may be possible (Cowman *et al.*, 2016). Achieving this goal requires the development of novel drugs, new diagnostics, sustainable vector control approaches and efficient vaccines. The development of these tools requires a profound understanding of the disease and the biology of the causative agent, the *Plasmodium* parasite, and its vector.

Plasmodium spp. are unicellular protozoan parasites that infect a wide range of vertebrates, from reptiles and birds to mammals. To date, more than 200 species have been described, each of them infecting a narrow range of hosts (Figure 1A) (Pegoraro and Weedall, 2021; Sato, 2021). There are six *Plasmodium* species able to infect humans which pose an important health threat: *P. falciparum* is the most lethal species accounting for the majority of deaths, mainly in children under the age of five in Sub-Saharan Africa (WHO, 2021). It can be cultured *in vitro* (Trager and Jensen, 1976) which enables its genetic modification for research purposes (Wu *et al.*, 1995; Wu, Kirkman and Wellems, 1996; Crabb *et al.*, 1997; VanWye and Haldar, 1997; Mamoun *et al.*, 1999). Basic *in vitro* research has tremendously advanced our knowledge about the parasite's biology. *P. vivax* is estimated to have caused about 2 % of malaria cases in 2020 (WHO, 2021). However, *P. vivax* is the most widely distributed plasmodial species and accounts for the majority of cases in South-East Asia and the Americas while in Africa the widespread lack of the Duffy antigen, a chemokine receptor on red blood cells (RBCs) that is used for *P. vivax* invasion, constraints transmission (Flannery, Markus and Vaughan, 2019). As there is no *in vitro* system available for *P. vivax*, progress in research has been limited to field isolates. *P. ovale curtisi*, *P. ovale wallikeri*, and *P. malariae* are less common causes of disease and are considered understudied (Cowman *et al.*, 2016; WHO, 2021). Lastly, the simian parasite *P. knowlesi* has emerged as a local but important cause of disease in humans in South-East Asia although it is predominantly a zoonosis affecting macaques (Cowman *et al.*, 2016; Mohammad *et al.*, 2022). Experts warn about other possible spill-over events of ape or simian malaria species to humans which could hinder malaria eradication (WHO, 2021).

Transmission of *Plasmodium* spp. between vertebrate hosts depends on mosquito vectors. The range of insect species that can support *Plasmodium* development depends on the parasite species but all human-infecting *Plasmodium* spp. are transmitted by *Anopheles* mosquitoes (Sato, 2021).

Malaria infection in a naïve individual such as a child or a traveler almost invariably causes fever with accompanying unspecific symptoms such as rigors, headache, nausea, vomiting, anemia, and muscle pain (uncomplicated malaria). If left untreated, the patient's condition might rapidly decline from these symptoms. In severe (complicated) malaria, complications such as severe anemia and end-organ damage might arise including cerebral malaria in which the parasite crosses the blood-brain barrier. Mortality is high if not treated promptly. After acquisition of immunity, *Plasmodium* infection might result in asymptomatic malaria with circulating parasites but no symptoms in the patient (Marsh *et al.*, 1995; Rénia *et al.*, 2012; Cowman *et al.*, 2016; WHO, 2021). In addition to the malaria-imposed risk for the individual, placental malaria during pregnancy has an added toll on the fetus as it often results in preterm delivery and/or low birth weight, increasing the risk for neonatal and childhood mortality (McLean *et al.*, 2015; WHO, 2021).

1.1.1 Malaria epidemiology

In 2020, there were an estimated 241 million malaria cases in 85 malaria-endemic countries resulting in 627,000 deaths (Figure 1B) (WHO, 2021). The increase in malaria cases (+ 14 million) and malaria deaths (+ 69,000) compared to 2019 were mostly due to service disruptions during the COVID-19 pandemic, highlighting the severe consequences of even moderate service disruptions in health care when large populations are at risk (WHO, 2021). However, even before the emergence of COVID-19 and even though China and El Salvador were certified malaria-free by the WHO in 2020, global efforts to eradicate malaria have leveled off and progress against malaria remains uneven (WHO, 2021).

Two WHO Regions are of major concern: the WHO South-East Asia Region and the WHO African Region. While the WHO South-East Asia Region is of high concern due to the rise of multi-drug resistance, the WHO African Region carries the highest malaria burden. The latter accounts for 95 % of malaria cases globally with Nigeria, the Democratic Republic of Congo, Uganda, Mozambique, Angola and Burkina Faso alone carrying the burden of about 55 % of global cases (Figure 1B) (WHO, 2021).

In stably endemic areas severe disease and death are restricted mainly to young children, as older individuals develop a degree of protective, however not sterile, immunity (Cowman *et al.*, 2016). In moderate-to-low transmission settings, all ages are susceptible to infection which will result in clinical disease in most cases. Interestingly, the relationship between severe malaria and transmission rates is non-linear implying that the implementation of effective control measures in high-transmission areas might lead to substantial reductions in transmission with less effect on severe cases until transmission falls to a critical point, following which reductions in disease might be rapid (Cowman *et al.*, 2016). This can give guidance when implementing control measures (Cowman *et al.*, 2016).

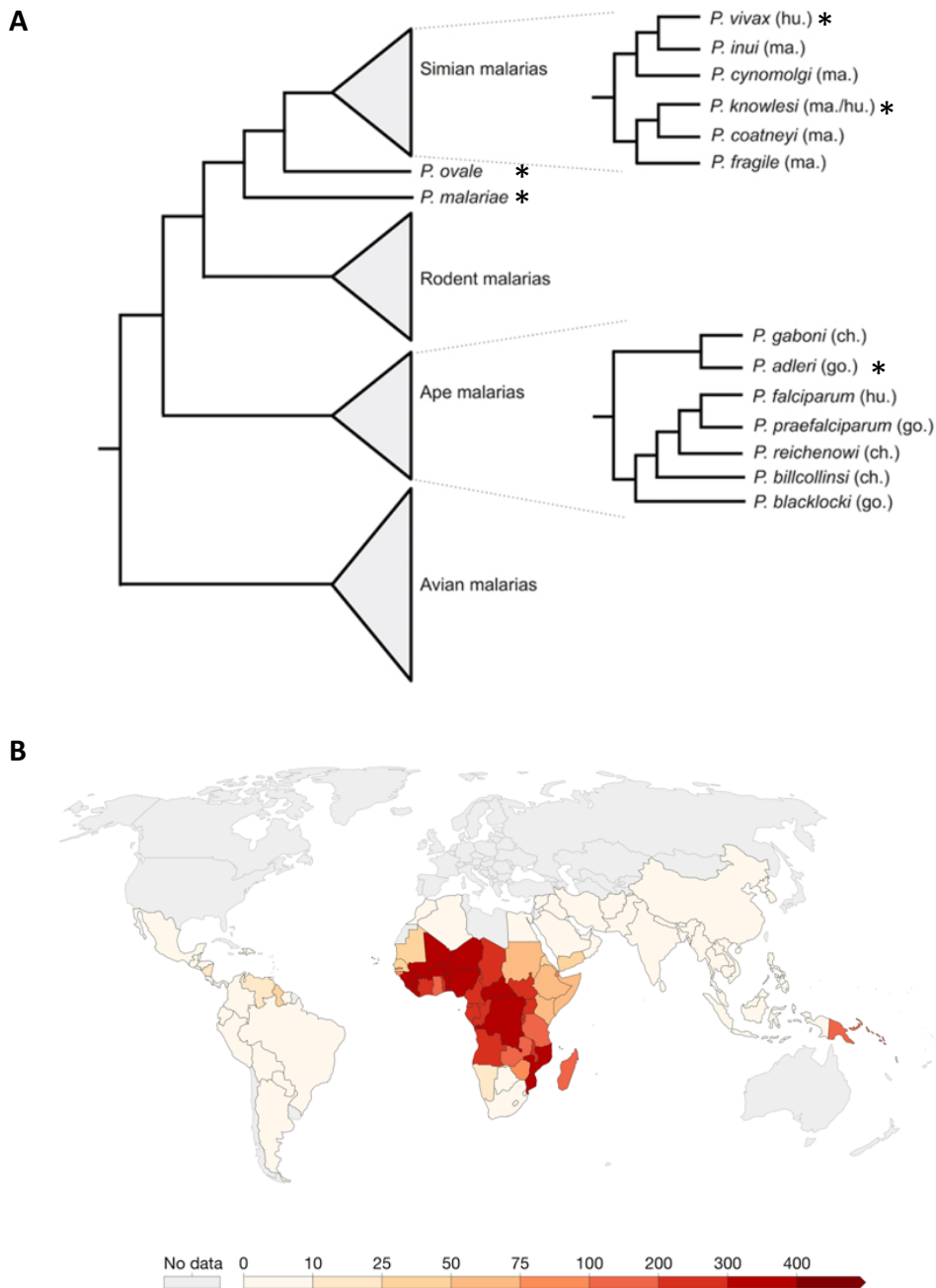


Figure 1. Phylogeny and epidemiology of malaria. (A) Schematic diagram of a phylogenetic tree of malaria parasites showing the relationships among human-infecting species. Branch lengths are not to scale. Host species are indicated in brackets (hu = human; ma = macaque; ch = chimpanzee; go = gorilla). Taken from Pegoraro *et al.* (2021). (B) Incidence of malaria in 2020. Incidence is the number of new cases per 1,000 population at risk within a given period of time (1 year). Data source: World Health Organization (via World Bank). Map taken from: <https://ourworldindata.org/malaria>.

1.1.2 Malaria intervention and vaccine strategies

Efforts to control malaria infections include vector control measures, new diagnostics, and novel antimalarial drugs and vaccines.

Controlling malaria transmission by targeting the mosquito vector has been successful in dramatically reducing malaria cases. In 2020, manufacturers delivered more than 200 million insecticide-treated nets (ITNs) to malaria-endemic countries (WHO, 2021). Additionally, Indoor and Outdoor Residual Spraying (IRS or ORS, respectively) are effective measures to kill mosquitoes that rest on surfaces after a blood meal. To ensure the effectiveness of IRS, the insecticide must cover at least 80 % of the walls inside a house and needs to be applied every three to six months which poses logistical challenges (Mohammad *et al.*, 2022). In addition, the majority of malaria-endemic countries have reported vector resistance to at least one insecticide class reducing the effectiveness of ITNs and IRS/ORS (WHO, 2021).

Another important tool in combating malaria are rapid diagnostic tests (RDTs) as early detection and treatment of malaria can avert serious disease. However, deletions in the malaria parasite's *pfhrp2* and *pfhrp3* genes have been reported that render parasites undetectable by most RDTs and thus might result in the undertreatment of cases (WHO, 2021). Taken together with the rising insecticide resistance, this raises global concerns that the malaria burden might increase again as we fail to control transmission and detect infections efficiently.

Currently, there are potent antimalarial drugs available to treat *P. vivax* and *P. falciparum* malaria. They are administered as artemisinin combination therapies (ACT, artemisinin combined with a partner drug). However, after reports about rising artemisinin resistance in the Greater Mekong subregion, the independent emergence of artemisinin partial resistance in the WHO African Region has raised serious concerns about the long-term utility of ACTs (WHO, 2021; Ward, Fidock and Bridgford, 2022). Although in the WHO African Region they remain efficacious for now, artemisinin resistance might be involved in the spread of resistance to ACT partner drugs, thus further limiting treatment options (WHO, 2021). This highlights the need for novel therapeutics that act broadly to cure the asexual blood stage, which is associated with all clinical symptoms, to kill off gametocytes to prevent transmission, and to clear the liver stage that can result in relapses in *P. vivax* and *P. ovale* malaria (Cowman *et al.*, 2016).

In addition to potent drugs, malaria eradication will require an effective vaccine. In October 2021, the WHO recommended the RTS,S/AS01 vaccine for broad use for children in moderate to high transmission areas because the vaccine had shown a favorable safety profile in pilot introductions (WHO, 2021). RTS,S is a recombinant protein comprised of the regions of the *P. falciparum* circumsporozoite protein which are known to induce humoral and cellular immune responses, linked to the hepatitis B virus surface antigen. Although the vaccine efficacy was comparably low even after three doses, hospital admissions for severe malaria could be significantly reduced in vaccinated children (Agnandji *et al.*, 2014). Nevertheless, more research is needed to develop more potent vaccines for broad use.

The WHO clearly states that no single tool that is available today will solve the problem of malaria in moderate- and high-burden settings (WHO, 2021). Investments in research and development will bring new diagnostics, vector control approaches, antimalarial medicines and vaccines that are needed to meet global eradication targets. This challenge is – among other reasons – hindered by our limited knowledge about the parasite’s biology as our need for continued identification of novel protein drug targets requires a profound understanding of parasite-specific processes.

1.2 The complex life cycle of the malaria parasite *Plasmodium*

The availability of the *Plasmodium* genome sequence (*P. falciparum* clone 3D7; Gardner *et al.*, 2002) and data from several large-scale functional studies such as genomic (e.g., Otto *et al.*, 2014), transcriptomic (e.g., Bozdech *et al.*, 2003; Wichers *et al.*, 2019) and proteomic analyses (e.g., Lasonder *et al.*, 2016) have advanced our knowledge of the parasite’s biology tremendously.

The nuclear genome has a size of about 23 Mb distributed to 14 chromosomes with an overall (A + T) composition of 80.6 %, which poses a challenge for sequencing and genetic modification. It encodes approximately 5300 proteins with more than half of them having insufficient similarity to proteins in other organisms to confidently identify them (Gardner *et al.*, 2002). Since publication of the genome sequence, efforts have continued to improve both the sequence and annotation. Updates are publicly available on PlasmoDB (Aurrecochea *et al.*, 2009; latest update by Amos *et al.*, 2022). Despite the recent efforts to study individual protein function throughout the parasite life cycle, many genes remain annotated to code for either hypothetical (putative) proteins or proteins of unknown function. Characterization of these proteins is a slow but critical process to identify new targets that might be exploited for drug or vaccine development.

Plasmodium parasites have a complex multistage life cycle alternating between the *Anopheles* mosquito vector and the vertebrate host (Figure 2A) (Dixon and Tilley, 2021). The asexual life cycle begins with the blood meal of an infected mosquito on the vertebrate host. During the blood meal, motile sporozoites are injected into the host skin where they move until they invade a blood or lymph vessel which transports them to the liver (Amino *et al.*, 2006). Sporozoites traverse several hepatocytes until they find their final host cell in which they start an asexual replication process called exoerythrocytic schizogony. Towards the end of liver stage development, thousands of merozoites have formed encapsulated within the parasitophorous vacuolar membrane (PVM) that surrounds parasites during their intracellular replication (Meis *et al.*, 1983; Vaughan *et al.*, 2012). Merozoites are released into the bloodstream in membrane-enclosed structures called merozoites that burst shortly after, thereby initiating the blood stage of the parasite (Sturm *et al.*, 2006). Some species such as *P. vivax* and *P. ovale* can form dormant stages called hypnozoites in the liver that can lead to

relapse infections (Krotoski *et al.*, 1982), a feature that has not been reported for the most virulent malaria species, *P. falciparum*.

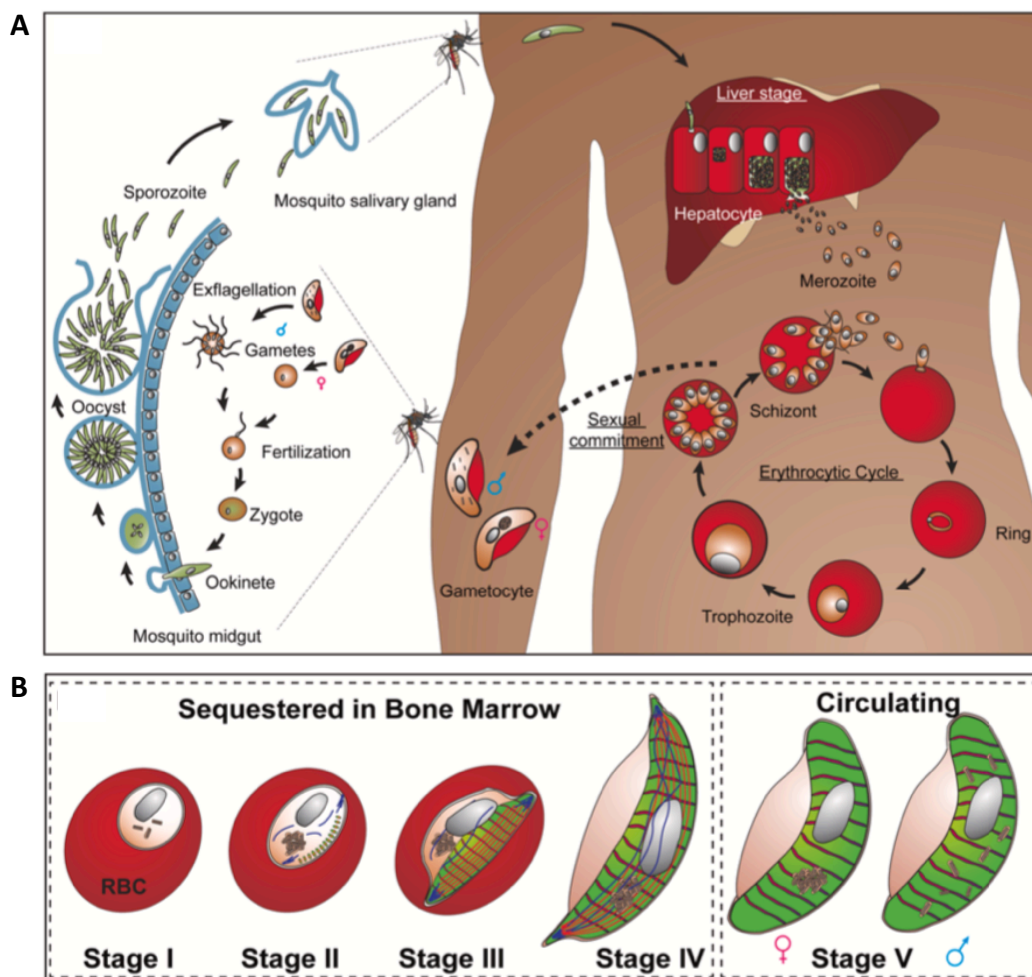


Figure 2. Life cycle of *Plasmodium falciparum*. (A) Schematic depiction of the *P. falciparum* life cycle in the *Anopheles* mosquito vector and the human host. A feeding mosquito initiates the infection by injecting motile sporozoites into the host's skin. Sporozoites invade hepatocytes, initiating the liver stage in which the parasite undergoes asexual replication to form thousands of merozoites that are released into the blood stream in merozoites (not depicted) that burst shortly after. Merozoites then invade RBCs initiating the blood stage (intraerythrocytic cycle), which is responsible for malaria pathology. Parasites develop into ring, trophozoite and schizont stages finally releasing the daughter merozoites that continue the asexual cycle. Some parasites commit to sexual stage development, eventually leading to the formation of sexually mature gametocytes that can be taken up by a feeding mosquito. In the mosquito midgut, male and female gametocytes are activated to form micro- and macrogametes. The gametes fuse to form a zygote that develops into a motile ookinete, which penetrates the mosquito midgut wall and forms an oocyst. Inside the oocyst, sporozoites are formed and released into the hemolymph from where they can migrate to the salivary glands, thus completing the lifecycle. (B) *P. falciparum* gametocytes take 10–12 days to develop through five distinct morphological stages. Stage I-IV gametocytes are sequestered in the bone marrow and spleen and do not circulate in the bloodstream, while stage V gametocytes circulate freely, allowing them to be taken up by feeding mosquitos. Green: IMC plates. Red: IMC sutures. Orange: Microtubules. Blue: Actin. Grey: Nucleus. Brown: Hemozoin/DV. Figure taken from Dixon *et al.* (2021).

While the liver stage remains clinically silent, the following mass proliferation within the host's red blood cells (RBCs) causes all clinical symptoms of malaria. After their release into the bloodstream, merozoites rapidly adhere to and invade RBCs (Cowman and Crabb, 2006). Inside the RBC, a single merozoite residing within the parasitophorous vacuole (PV) matures through the ring, trophozoite and schizont stage (Figure 2A). During the late stages, the parasite undergoes multiple rounds of asynchronous nuclear divisions resulting in the formation of 8-64 daughter merozoites (Gerald, Mahajan and Kumar, 2011). These new merozoites exit from the host cell in a tightly controlled process called egress by breaking down the PVM and the host cell membrane in a sequential inside-out manner (Gulati *et al.*, 2015; Tan and Blackman, 2021). Free merozoites are then ready to reinvade another RBC. Parasites repeat this intraerythrocytic propagation cycle every 24 (*P. knowlesi*), 48 (*P. falciparum*, *P. ovale*, *P. vivax*) or 72 (*P. malariae*) hours (Sato, 2021).

The mass proliferation of parasites within the RBCs and their subsequent rupture releases parasite proteins, toxins, degradation products such as hemozoin (heme biocrystals produced by the parasite) and cell debris into the bloodstream. The following cytokine storm induced by the immune system is an inflammatory reaction resulting in fever (Angulo and Fresno, 2002; Oakley *et al.*, 2011; Dunst, Kamena and Matuschewski, 2017). The synchronous growth of *P. knowlesi*, *P. vivax*, *P. ovale* and *P. malariae* leads to characteristic fever waves: *P. knowlesi* infection is accompanied by daily fever peaks while the longer 48-hour replication cycle of *P. vivax* and *P. ovale* results in *Malaria tertiana* (3-day fever) with a characteristic pattern of one day of fever followed by a fever-free day. *P. malariae* infection leads to *Malaria quartana* (4-day fever) with a first day of fever followed by two fever-free days. Interestingly, *P. falciparum* shows asynchronous growth in its 48-hour replication cycle. The accompanying high fever without a characteristic rhythm is termed *Malaria tropica*.

Asexual proliferation greatly increases parasite mass in the host. However, in order to be successfully transmitted to the mosquito vector, parasites need to develop into male and female sexual stages called gametocytes. Interestingly, male and female gametocytes have very different proteomes indicating that they are strikingly divergent concerning sex-specific processes (Khan *et al.*, 2005). Sexual differentiation (gametocytogenesis) is a complicated process that in *P. falciparum* takes 9-12 days – substantially longer than the gametocyte development in the other human malaria species or rodent malaria species such as *P. berghei* (Gautret and Motard, 1999). *P. falciparum* gametocytogenesis is divided into five morphologically distinct stages (Figure 2B) (Talman *et al.*, 2004): while stage I gametocytes are morphologically indistinguishable from trophozoites, stage II gametocytes display an elongated, lemon-shaped morphology within the RBC. As they mature into stage III, one side of the parasite flattens while the opposite membrane curves resulting in a characteristic D-shape that slightly distorts the RBC. Developing into stage IV, gametocytes mature into highly elongated forms with pointed ends. Distortion of the RBC is enabled by a strong cytoskeleton which is disassembled in stage V, letting the gametocyte collapse into a falciform, crescent shape with rounded extremities (Figure 2B) (Talman *et al.*, 2004; Ngotho

et al., 2019). Like *P. falciparum* asexual stage parasites, stage I-IV gametocyte sequester away from the peripheral circulation, thereby avoiding passage through and potential clearance by the spleen (Figure 2B) (Rogers *et al.*, 1996; Day *et al.*, 1998; Dearnley *et al.*, 2012; Dixon and Tilley, 2021). Mature circulating stage V gametocytes are taken up by the mosquito vector when it feeds on an infected individual.

Within the mosquito midgut the gametocytes are activated by three factors to form gametes: a drop in temperature, an increase in pH, and the presence of xanthurenic acid (previously described as gametocyte-activating factor) (Billker *et al.*, 1998; Garcia *et al.*, 1998; Bennink, Kiesow and Pradel, 2016). After activation, female and male *P. falciparum* gametocytes round up before exiting from the RBC, a process that is controlled by protein kinase G (McRobert *et al.*, 2008). Female gametogenesis (formation of the macrogamete) is regulated by translational repression of messenger RNAs (Mair *et al.*, 2006). Male gamete maturation entails three mitotic divisions and the assembly of axonemes to form eight motile gametes (microgametes) within 10-15 minutes. Nearly concomitant with the rupture of the RBC membrane, the male gamete flagella start beating and detach from the residual body of the cytoplasm (Andreadaki *et al.*, 2018). A microgamete fertilizes the macrogamete to produce a zygote that will further develop into a motile ookinete (Figure 2A) (Siciliano *et al.*, 2020). Ookinetes traverse the midgut wall and form an oocyst in which thousands of motile sporozoites are formed within about two weeks (Vaughan, 2007; Gerald, Mahajan and Kumar, 2011). They are released into the mosquito's hemolymph from where they invade the salivary glands to be passed on to another vertebrate host thereby completing the life cycle (Frischknecht and Matuschewski, 2017).

1.3 Parasite ultrastructure

Plasmodium parasites undergo a series of remarkable morphological transformations during their multistage life cycle. As eukaryotic cells, they harbor all typical features such as a nucleus, an endoplasmic reticulum (ER), a rudimentary Golgi, and a mitochondrion (Figure 3A). In addition, the motile stages (sporozoites, merozoites, and ookinetes) possess the apical complex, a special feature of the phylum of Apicomplexa which is organized around an apical polar ring. The apical polar ring is a unique microtubule-organizing center, that nucleates an array of subpellicular microtubules (Ferreira *et al.*, 2022). These microtubules subtend the inner membrane complex (IMC), a double lipid bilayer formed by flattened membrane vesicles that lies closely beneath the parasite plasma membrane and is involved in many essential parasite-specific functions including host cell invasion, by anchoring glideosome proteins required for actinomyosin-based gliding motility (Morrissette and Sibley, 2002; Baum *et al.*, 2006; Yeoman *et al.*, 2011; Kono *et al.*, 2013; Absalon, Robbins and Dvorin, 2016).

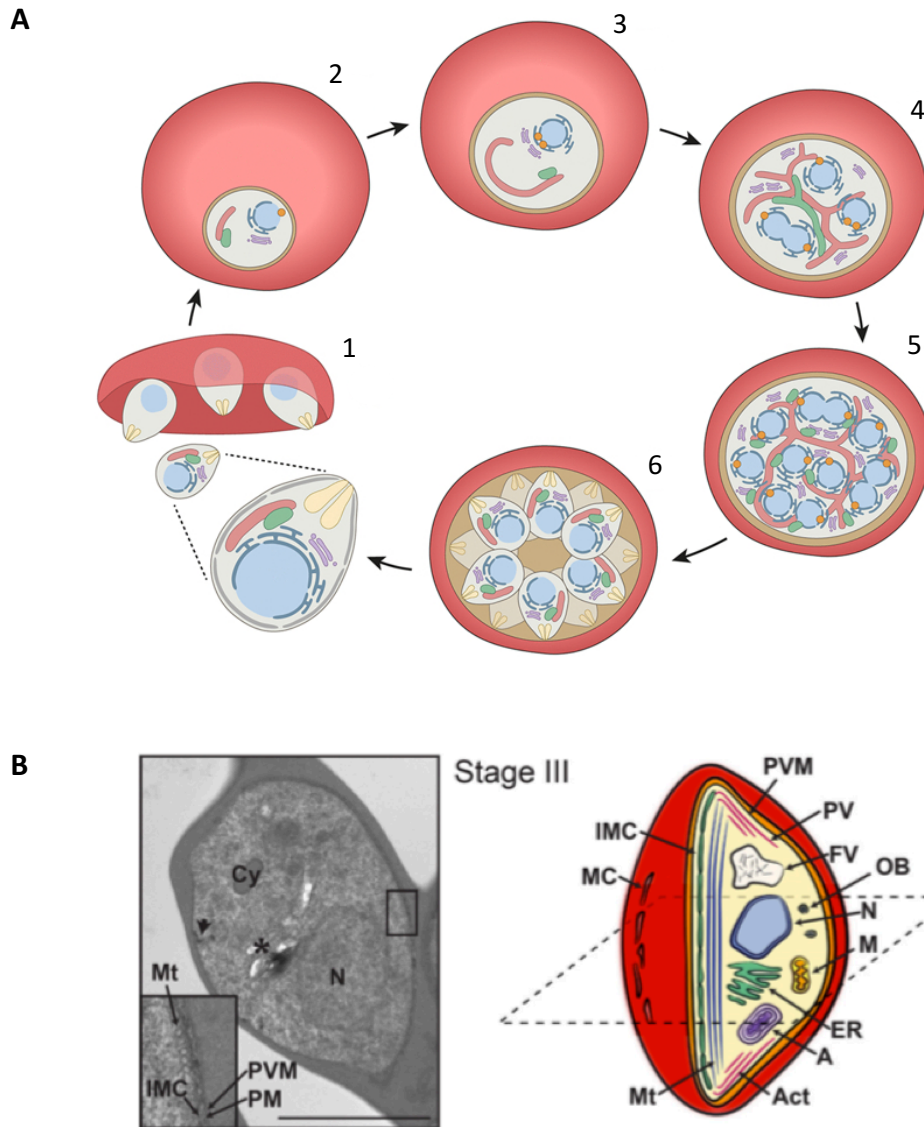


Figure 3. Organelle structure and dynamics during intraerythrocytic development of *P. falciparum*. (A) Schematic of the parasite ultrastructure throughout asexual blood stage development. Blue: Nucleus (light) and ER (dark). Orange: Centriolar plaques. Violet: Golgi. Red: Mitochondrion. Green: Apicoplast. Yellow: Rhoptries. Grey: IMC. Not depicted: Apical secretory organelles, DV. (1) Egress of merozoites. (2) Ring stage. (3) Late ring/early trophozoite stage. Elongation of the mitochondrion and division of the centriolar plaque and Golgi. ER forms extensions into the cytosol. (4) Trophozoite. Further elongation and branching of the mitochondrion and apicoplast. Further replication of the Golgi and nuclei as well as expansion of the ER surrounding the dividing nuclei. (5) Schizont stage. The apicoplast divides and associates with mitochondrial branches. (6) Segmenter. Mitochondrial division and full formation of the daughter parasites ready for egress. Figure taken from Verhoef *et al.* (2021). (B) Morphological features of *P. falciparum* gametocytes. Left: Representative electron microscopy image. Right: Schematic drawing. Shown are inner membrane complex (IMC), Maurer's clefts (MC), the PVM, mitochondrion (M), apicoplast (A), nucleus (N), ER, DV/food vacuole (FV), plasma membrane (PM), the IMC, and osmiophilic bodies (OB). Microtubules (Mt) and actin filaments (Act) are assembled during gametocytogenesis but disassembled in stage V gametocytes. Figure taken from Ngotho *et al.* (2019).

In addition to the apical polar ring, the apical complex also comprises secretory apical organelles (exonemes, rhoptries, micronemes) that are deposited at the apical pole of polarized stages to secrete their content when needed (Bannister *et al.*, 2000; Patra and Vinetz, 2012; Frischknecht and Matuschewski, 2017). Of note, rhoptries are absent in ookinetes.

A second characteristic feature of Apicomplexa is the apicoplast, a non-photosynthetic plastid surrounded by four layers of membrane that was acquired by secondary endosymbiosis of a red algae (Janouškovec *et al.*, 2010). It is involved in plant-type metabolic pathways such as isoprenoid biosynthesis, type II fatty acid biosynthesis and heme biosynthesis (Ralph *et al.*, 2004; Van Dooren, Stimmler and McFadden, 2006; Lim and McFadden, 2010). The apicoplast has its own circular 35-kb genome encoding 30 proteins. All other apicoplast proteins are encoded in the nucleus and have to be imported. Similar to the mitochondrial DNA, the apicoplast genome is inherited solely through the female gamete (Creasey *et al.*, 1994).

1.3.1 Merozoites

Merozoites are ovoid, polar cells of about 1-2 μm in length (Figure 3A (1)). Their shape is supported by the IMC. Despite their small size, they contain all the organelles needed to egress from the host cell and invade another. The nucleus harboring the haploid genome is placed basally while the apex contains ribosomes, the mitochondrion and the apicoplast as well as the secretory vesicles required for invasion (Bannister *et al.*, 2000).

The apicoplast of merozoites appears rounded while the mitochondrion has a slightly elongated tubular structure (van Dooren *et al.*, 2005). The apical vesicles have different appearances and contain very different protein factors. Exonemes are secretory vesicles that release their protein content to mediate egress. The only known exoneme protein factors are SUB1 and Plasmepsin X (Yeoh *et al.*, 2007; Mukherjee *et al.*, 2022). Micronemes and rhoptries are needed for invasion. Micronemes appear as small elongated vesicles that discharge their content when parasites are in contact with the new host cell to mediate parasite attachment (Bannister *et al.*, 2000; Kats *et al.*, 2007). Rhoptries stand out as twin pear-shaped organelles with high protein density. Many rhoptry proteins have been shown to be involved in creating the moving junction, a tight connection between parasite and host cell through which the parasite enters into the host during invasion, and in constructing the PV (Bannister *et al.*, 2000; Kats *et al.*, 2007; Shen and Sibley, 2012). Dense granules are electron-dense rounded vesicles that are generally involved in establishment of the PVM and modifications of the host cell (Bannister *et al.*, 2000; Kats *et al.*, 2007).

1.3.2 Ring, trophozoite and schizont stages

While invading, the parasite establishes the PV in which it resides throughout intraerythrocytic development. Recent evidence suggests that the nascent PVM is

predominantly formed from the host RBC membrane (RBCM) (Geoghegan *et al.*, 2021). During invasion and intraerythrocytic development, the PVM is continuously remodeled. Within the PV, the parasite flattens and loses its IMC. All organelles are arranged at the rim giving it a ring shape in Giemsa-stained thin blood smears (Bannister *et al.*, 2000). The ER typically has a simple crescent shape around the nucleus with the single Golgi apparatus localizing close by (Figure 3A (2)-(3)) (Struck *et al.*, 2005; van Dooren *et al.*, 2005). As the parasite starts to endocytose host cytoplasm and digest hemoglobin for amino acid acquisition, it forms a digestive vacuole (DV, also called food vacuole, FV) in which it crystallizes the toxic byproduct heme to form hemozoin (Dorn *et al.*, 1995; Rosenthal and Meshnick, 1996; Bannister *et al.*, 2000).

In trophozoites, the ER extends into the cytosol and around the DV (van Dooren *et al.*, 2005). The nucleus starts to multiply. In *P. falciparum* mitosis, the nuclear envelope remains intact (closed mitosis) and must be divided at the end of mitosis to complete genome separation before another round of genome replication starts (Figure 3A (4)). *Plasmodium* blood stage parasites undergo repeated asynchronous mitosis without cell division (schizogony) creating multinuclear cells called schizonts (Gerald, Mahajan and Kumar, 2011). In late-stage schizonts that have already formed a number of nuclei, the ER forms a highly branched mesh-like network while the Golgi further multiplies and divides (Figure 3A (5)) (Struck *et al.*, 2005, 2008). The DV resides near the center of the parasite mass. How and when the ER is divided and distributed to the developing daughter merozoites remains largely unknown. However, it is clear that organelles linked to the endomembrane system, such as ER, Golgi, and secretory organelles, generally are distributed to the daughter cells using a combination of *de novo* synthesis and recycling. Only after segmentation is complete, the PVM and the RBCM are breached in a tightly controlled process called egress (Figure 3A (6)-(1)) (Tan and Blackman, 2021). The DV is left behind as the residual body. Recent evidence suggests that daughter cell fission from the DV occurs relatively late in the process of segmentation as some merozoites remain attached to it even after PVM rupture (Rudlaff *et al.*, 2020).

In contrast to the other organelles, the parasite's endosymbiotic organelles apicoplast and mitochondrion cannot be derived *de novo* but like their bacterial ancestors need to replicate their own genomes and undergo division. These processes need to be highly organized as organelle loss is lethal for the parasite (Verhoef, Meissner and Kooij, 2021). During intraerythrocytic parasite development, apicoplast and mitochondrion grow from single, small, discrete organelles into highly branched structures that show several transient contact sites facilitating their metabolic exchange (Figure 3A) (Ralph *et al.*, 2004; van Dooren *et al.*, 2005; Van Dooren, Stimmler and McFadden, 2006). In early-segmenting schizonts, they do not reach up into the developing daughter parasite buds but instead curve through the interior of the parasites winding around the nuclei which fill much of the available space (Figure 3A (4)-(5)) (Rudlaff *et al.*, 2020). By mid-segmentation, the branched apicoplast divides to produce a daughter organelle for each nascent merozoite (Figure 3A (5)) (Rudlaff *et al.*, 2020). Each new apicoplast is in close spatial proximity to the branched mitochondrion. Together, they reach up into the forming merozoite buds. Finally, in fully segmented

merozoites, mitochondria have also divided into individual daughter organelles (Figure 3A (6)) (Rudlaff *et al.*, 2020). Unlike organelle fission in mammalian, yeast, and plant cells, very little is known about the molecular mechanisms of organelle fission in Apicomplexan parasites.

1.3.3 Gametocytes

Unlike the majority of blood stage parasites, a small subpopulation of parasites will exit from the asexual replication cycle and commit to gametocyte differentiation. In general, the overall cellular architecture of gametocytes is similar to the asexual stages (Figure 3B), but they lack an apical complex and polarity. The IMC biogenesis commences in stage II and reveals a more complex structure (Dearnley *et al.*, 2012; Kono *et al.*, 2012) that together with the assembly of a microtubule network is supposed to drive elongation of the *P. falciparum* gametocyte (Dearnley *et al.*, 2012). Stage V gametocytes harbor their own specialized set of egress-related secretory vesicles: osmiophilic bodies and “egress vesicles” (characterized by the presence of the perforin-like protein 2 (pplp2)) that are discharged upon gametocyte egress to disrupt the PVM and the RBCM (Ngotho *et al.*, 2019; Bennink and Pradel, 2021).

During gametocyte development, the mitochondrion undergoes massive morphological changes. It forms cristae and elongates and branches throughout gametocytogenesis forming a cluster around the small apicoplast that stays morphologically surprisingly static (Krungkrai, Prapunwattana and Krungkrai, 2000; Okamoto *et al.*, 2009; Evers *et al.*, 2021). Similar to asexual development, the apicoplast and mitochondrion remain closely associated throughout this pre-sexual development which facilitates their metabolic cooperation in shuttling metabolites or even sharing pathways such as the heme biosynthesis pathway (Van Dooren, Stimmler and McFadden, 2006; Okamoto *et al.*, 2009). After activation and egress, the female gamete has a spherical shape while male microgametes are beating flagella (Janse *et al.*, 1988; Billker *et al.*, 1998; Garcia *et al.*, 1998; Bennink, Kiesow and Pradel, 2016; Andreadaki *et al.*, 2018). Apicoplast and mitochondrion are inherited solely through the female gamete (Creasey *et al.*, 1994).

1.4 The function of the mitochondrion throughout the stages

The parasite’s mitochondrion has important functions throughout the life cycle. As it differs greatly from the host’s mitochondria on a molecular and functional level, it represents an attractive target for selective antimalarial drugs (Goodman, Buchanan and McFadden, 2017).

As in other eukaryotes, the *Plasmodium* mitochondrion has its own DNA. However, it encodes only three proteins, namely subunits of the mitochondrial electron transport chain (mtETC): Cox1 and Cox3 (subunits of Complex IV) and cytochrome *b* (subunit of Complex III) (Aldritt, Joseph and Wirth, 1989; Vaidya, Akella and Suplick, 1989; Feagin, 1992). All other subunits

and mitochondrial factors are encoded in the nuclear DNA and must be imported into the mitochondrion.

The textbook function of mitochondria is the oxidation of substrates in the tricarboxylic acid (TCA) cycle which feeds electrons into the mitochondrial electron transport chain (mtETC), ultimately producing ATP. However, mitochondrial functions extend from there as mitochondria are also involved in several biosynthetic processes (Alberts *et al.*, 2002).

1.4.1 The TCA cycle

In eukaryotic cells, sugars are metabolized and finally degraded to CO₂ in the mitochondrial TCA cycle. The canonical TCA cycle releases electrons via electron carriers, namely Nicotinamide Adenine Dinucleotide (NAD⁺) and Flavin Adenine Dinucleotide (FAD). The flow of these electrons drives the mtETC (Alberts *et al.*, 2002). Both asexual and sexual *Plasmodium* blood stages utilize a conventional TCA cycle to catabolize glucose and glutamine. Glucose provides acetyl-CoA and to some extent oxaloacetate while glutamine enters the cycle via α -ketoglutarate (Figure 4) (Cobbold *et al.*, 2013; MacRae *et al.*, 2013; Storm *et al.*, 2014). While asexual stages prefer carbon skeletons derived from glutamine, gametocytes favor glucose as their carbon source (MacRae *et al.*, 2013). However, when the normal flux of carbon is disrupted, parasites show remarkable plasticity of the TCA metabolism by switching between these carbon sources (Ke *et al.*, 2015).

Although malaria parasites encode all TCA cycle enzymes, genetic ablation of these enzymes has no significant impact on intraerythrocytic parasite growth indicating that the TCA cycle is dispensable in asexual blood stages (Ke *et al.*, 2015; Rajaram *et al.*, 2022; Yang *et al.*, 2022). However, independent deletion of aconitase (ACO) and isocitrate dehydrogenase (IDH) arrests gametocyte differentiation at stage III/IV with parasites failing to develop into transmission-competent mature stages indicating that gametocytes rely on a functional TCA cycle (Ke *et al.*, 2015; Yang *et al.*, 2022). This is in line with previous observations that the transcription of TCA cycle enzymes is upregulated in gametocytes (Young *et al.*, 2005). In contrast, another study has indicated that halting TCA metabolism is not harmful to gametocyte or gamete development but prevents parasite development in mosquitoes providing an explanation for why the parasite has kept all necessary enzymes (Srivastava *et al.*, 2016).

1.4.2 The electron transport chain

The TCA cycle and other biochemical reactions feed electrons into the mtETC which is embedded into the inner mitochondrial membrane and consists of a series of protein complexes (Figure 4). It is responsible for the transfer of electrons from donors to acceptors using redox reactions. The electron flow is coupled to the transfer of protons across the mitochondrial membrane resulting in an electrochemical gradient called the mitochondrial

membrane potential ($\Delta\Psi_m$) which typically drives the synthesis of adenosine triphosphate (ATP), the universal “currency” of energy within cells (Alberts *et al.*, 2002).

Asexual intraerythrocytic *P. falciparum* parasites do not rely on mitochondrial oxidative phosphorylation for ATP production. Instead, they redirect 60-70 % of glucose to lactic fermentation thus incompletely oxidizing the sugar (Jensen, Conley and Helstowski, 1983). Nevertheless, maintaining a functional mtETC is critical for parasite survival as indicated by the parasite’s sensitivity to mtETC inhibitors as antimalarial drugs (Figure 4).

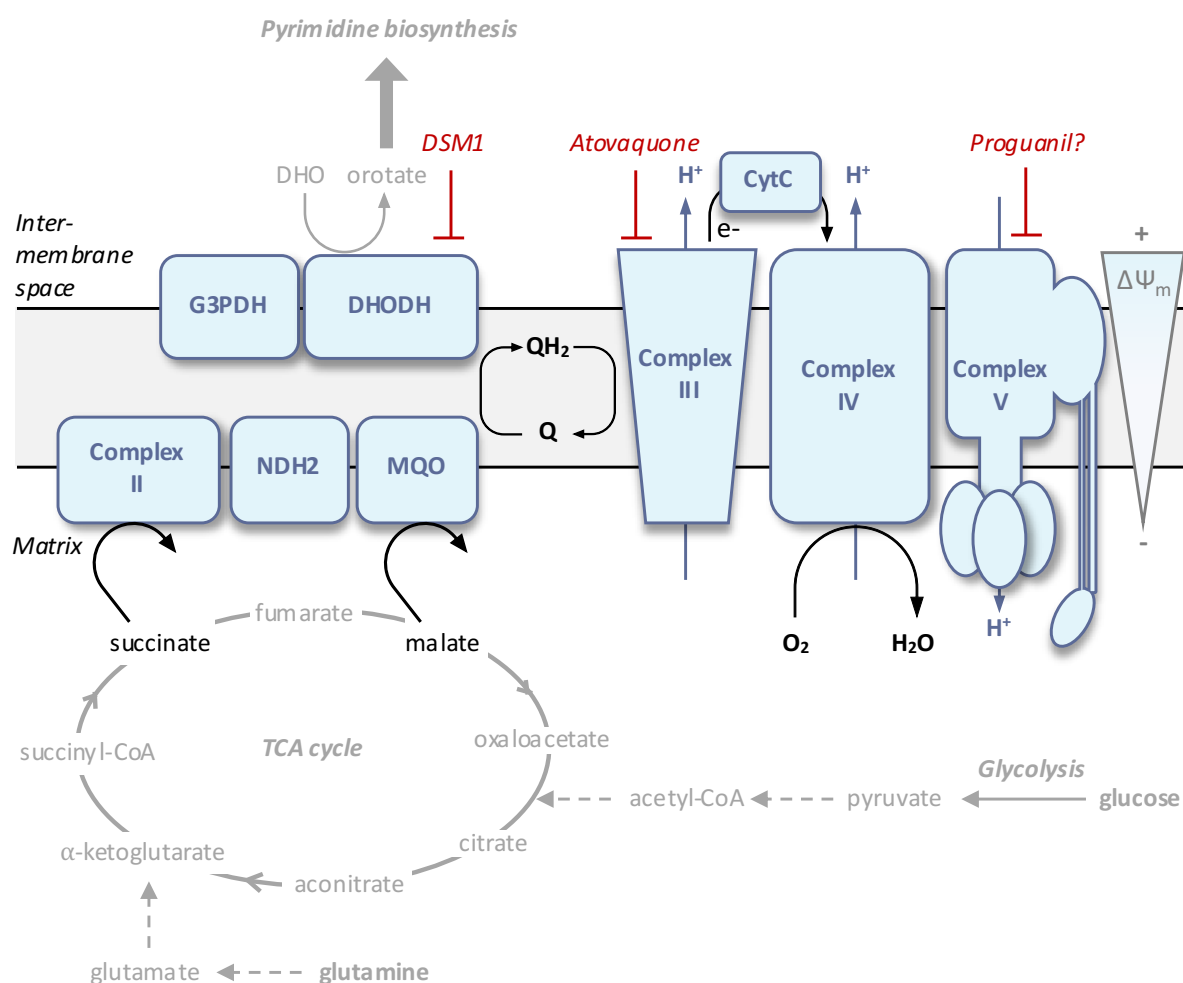


Figure 4. Schematic of the mitochondrial TCA cycle and the mtETC. Glucose is converted to pyruvate by glycolysis. A small fraction of pyruvate is transported to the mitochondrion where it is converted into acetyl-CoA, which enters the TCA cycle. The main source of carbon for the TCA cycle is glutamine, which feeds into the cycle as α -ketoglutarate. The TCA cycle intermediates succinate and malate feed into the mtETC. The DHODH catalyzes the reaction from DHO to orotate which is required for pyrimidine biosynthesis, and contributes to the mtETC by transferring electrons to ubiquinone (Q). Like the other four dehydrogenases, it reduces ubiquinone (Q) to ubiquinol (QH₂) which is reoxidized at Complex III. Complex III transfers the electrons to Cytochrome C (CytC) which passes them to Complex IV. The pumping of protons along the mtETC creates the mitochondrial membrane potential ($\Delta\Psi_m$). Indicated in red are inhibitors.

Electrons fed into the *Plasmodium* mtETC (sourced from several biochemical reactions) all converge at ubiquinone (Q), a hydrophobic, isoprenoid-containing molecule embedded in the inner mitochondrial membrane (Van Dooren, Stimmler and McFadden, 2006). Ubiquinone is the electron acceptor for five dehydrogenases (Figure 4) (Van Dooren, Stimmler and McFadden, 2006):

- (1) the type II NADH dehydrogenase (NDH2),
- (2) the succinate dehydrogenase (complex II, SDH),
- (3) the malate:quinone oxidoreductase (MQO),
- (4) the glycerol-3-phosphate dehydrogenase (G3PDH), and
- (5) the dihydroorotate dehydrogenase (DHODH).

The NDH2 is dispensable for asexual blood stage growth but is required for the establishment of oocysts in the mosquito midgut (Boysen and Matuschewski, 2011). Similarly, SDH and MQO are dispensable for intraerythrocytic growth (Ke *et al.*, 2015; Rajaram *et al.*, 2022).

The mitochondrial G3PDH is localized on the outer surface of the inner mitochondrial membrane. It produces glycerol-3-phosphate (G3P) that can be fed into the lipid synthesis pathway or pass through the permeable outer mitochondrial membrane where it is reoxidized by the cytosolic G3PDH (Fisher *et al.*, 2014). Both GD3PDH enzymes are believed to perform the G3P shuttling function at the central junction of glycolysis, phospholipid biosynthesis, and oxidative phosphorylation (Fisher *et al.*, 2014). It was suggested that this shuttle provides an alternative way to transport electrons from the cytosolic NADH to the mitochondrial ubiquinone pool (Van Dooren, Stimmler and McFadden, 2006). Of the five dehydrogenases, G3PDH has the largest potential as an electron donor (Sakata-Kato and Wirth, 2016).

The most important mitochondrial dehydrogenase in intraerythrocytic stages is the DHODH. It catalyzes the oxidation of dihydroorotate to orotate that subsequently exits the mitochondrion into the cytosol and feeds into the pyrimidine biosynthesis pathway. DHODH-mediated pyrimidine synthesis is the only essential pathway in intraerythrocytic stages that requires ubiquinone and one of the reasons the parasite relies on a functional mtETC (Van Dooren, Stimmler and McFadden, 2006; Painter *et al.*, 2007). The importance of this pathway is underlined by the parasite's susceptibility to DSM1, an inhibitor of the DHODH (Phillips *et al.*, 2008; Guler *et al.*, 2013).

Each of the five dehydrogenases can donate electrons to the mtETC by reducing ubiquinone to ubiquinol (dihydroubiquinone, QH₂) which is re-oxidized to ubiquinone at Complex III (ubiquinol:cytochrome *c* oxidoreductase, cytochrome *b*) (Figure 4). The substrates succinate, malate, G3P, and glutamate were shown to increase oxygen consumption by the mtETC indicating that all dehydrogenases actively contribute electrons to the *Plasmodium* mtETC (Sakata-Kato and Wirth, 2016).

By oxidizing ubiquinol to ubiquinone, Complex III passes electrons on to the small, soluble protein cytochrome *c* (CytC). Complex IV (cytochrome *c* oxidase complex) accepts the electrons from CytC and passes them on to oxygen in the terminal electron transfer step (Figure 4). This reaction accounts for about 90 % of the total oxygen consumption in most cells. The oxygen consumption rate (OCR) at Complex IV is an indicator of the electron flow through the mtETC and therefore has been used to bioenergetically assess the mtETC enzymes and to characterize mitochondrial dysfunction and disease states (Sakata-Kato and Wirth, 2016; Jaber, Yadava and Polster, 2020; Hayward, Makota, *et al.*, 2022; Hayward, Rajendran, *et al.*, 2022). Using freed schizonts, the OCR can also be measured in *Plasmodium* parasites (Seahorse assay) (Sakata-Kato and Wirth, 2016; Hayward, Makota, *et al.*, 2022; Hayward, Rajendran, *et al.*, 2022). Of note, mtETC complex components and linked metabolic pathways are up to 40-fold more prevalent in gametocytes compared to asexual blood stage parasites (Evers *et al.*, 2021).

The electron transfer along the mtETC is coupled to proton shuttling, which generates the $\Delta\Psi_m$ across the inner mitochondrial membrane (Figure 4). The $\Delta\Psi_m$ is typically used by Complex V (ATP synthase) to synthesize ATP thereby converting the energy contained in the electrochemical gradient into biologically useful, chemical-bond energy (Nina *et al.*, 2011). However, as mentioned before, the contribution of the mtETC to the cellular ATP pool in *Plasmodium* remains minimal (Krungkrai *et al.*, 1999; Uyemura *et al.*, 2004) as energy for intracellular survival and growth is primarily derived from glycolysis (Srivastava *et al.*, 2016). Interestingly, it was suggested that Complex V might be able to operate in reverse as an ATPase hydrolyzing ATP into ADP and P_i and pumping protons into the intermembrane space, thereby further establishing a proton gradient. This reverse reaction was described to be important in some mammalian tissues to maintain the $\Delta\Psi_m$ during anoxia, as well as in organisms that lack or have downregulated the mitochondrial respiratory enzymes, such as blood-stage trypanosomes (Nina *et al.*, 2011). Similarly, Complex V was suggested to act in reverse under conditions in which the activity of the mtETC is impaired in *Plasmodium*, an action that might be inhibited by the drug Proguanil (Painter *et al.*, 2007).

Maintenance of the $\Delta\Psi_m$ is crucial as it is tightly linked to the flux of a variety of metabolites, nucleotides and coenzymes across the inner mitochondrial membrane. Their transport is catalyzed by mitochondrial carrier proteins that utilize either the electrical and/or the chemical component of the $\Delta\Psi_m$ as well as the concentration gradient of the solutes as driving force(s). The importance of mitochondrial carriers is demonstrated by their wide distribution in all eukaryotes, their role in numerous metabolic pathways and cellular functions, and the identification of several diseases caused by alterations of the respective genes (Palmieri and Pierri, 2010). In *P. falciparum*, several mitochondrial carriers have been identified and characterized as transporters (Nozawa *et al.*, 2020). Interestingly, their activity was shown to be dependent on cardiolipin, a special mitochondrial lipid class (Nozawa *et al.*, 2020).

The proton gradient across the inner mitochondrial membrane can be dissipated using uncoupling agents such as carbonyl cyanide-p-trifluoromethoxyphenylhydrazone (FCCP) which is often used to quantify the mitochondrial reserve capacity (or maximum respiratory capacity) because it uncouples the oxygen consumption at complex IV from the functionality of complex V (Sakata-Kato and Wirth, 2016).

The mtETC, especially Complex III, is a major site of production of reactive oxygen species (ROS) which contribute to DNA mutations and other undesirable biochemical reactions. In *P. falciparum*, mitochondrial respiration and hemoglobin digestion are pathways for the production of ROS that potentially act synergistically. To attenuate oxidative stress, parasites have developed preventive antioxidant defense mechanisms, including antioxidative enzymes such as thioredoxins and the glutathione oxidase/reductase pair (Bozdech and Ginsburg, 2004; Torrentino-Madamet *et al.*, 2010).

1.4.3 Biosynthetic mitochondrial pathways

Several biochemical pathways take place in the mitochondrion of almost all eukaryotes. They include the biosynthesis of iron-sulfur (Fe-S) clusters, the biosynthesis of heme and the production of acetyl-CoA.

Fe-S clusters are required for several proteins that often localize to the mitochondrion itself, such as proteins of the mtETC. *Plasmodium* parasites harbor two Fe-S cluster synthesis pathways — one in the mitochondrion and one in the apicoplast, highlighting the importance of Fe-S clusters in key cellular functions (Van Dooren, Stimmler and McFadden, 2006; Van Dooren and Striepen, 2013).

While *Plasmodium* has two independent Fe-S cluster synthesis pathways, the heme biosynthesis pathway is not present in either apicoplast or mitochondrion, but rather represents an unusual hybrid pathway shared between the two organelles. Heme synthesis is initiated in the mitochondrion — where glycine and succinyl-CoA are converted to δ -aminolevulinate (ALA). However, the pathway proceeds in the apicoplast, before concluding back in the mitochondrion (Ralph *et al.*, 2004; Van Dooren, Stimmler and McFadden, 2006). It remains unknown why *Plasmodium* parasites synthesize their own heme *de novo* throughout the life cycle instead of utilizing hemoglobin-derived heme that they ingest in large quantities and break down in their DV during intraerythrocytic development (Van Dooren, Stimmler and McFadden, 2006). Most likely, heme biosynthesis is required in mosquito and liver stages providing an explanation why the pathway has not been lost. Alternatively, heme crystallized in hemozoin might be inaccessible for the parasite resulting in the need for biosynthesis (Van Dooren, Stimmler and McFadden, 2006).

Additionally, the parasite's mitochondrion is central for posttranslational modifications of cytoplasmic and nuclear proteins (Nair *et al.*, 2022). Mitochondrial acetyl-CoA produced by ketoacid dehydrogenases is used for protein acetylation (Nair *et al.*, 2022).

Taken together, the *Plasmodium* mitochondrion has crucial functions not only in cellular respiration but also in several, unusual biosynthetic processes, providing interesting potential drug targets.

1.4.4 The mitochondrion as a drug target

The mitochondrion, especially the mtETC has proven itself to be a valuable target for antimalarial drugs. Best known might be Atovaquone (2-[trans-4-(4'-chlorophenyl)cyclohexyl]-3-hydroxy-1.4-naphthoquinone), a hydroxynaphthoquinone compound that is a structural analog and thus competitive inhibitor of ubiquinone (Wendel, 1946; Hudson, 1993). Atovaquone resistance appears with high natural frequency in the form of cytochrome *b* mutants (Torrentino-Madamet *et al.*, 2010). To minimize emerging resistances, Atovaquone is combined with a partner drug such as Proguanil. The combination of Atovaquone and Proguanil displayed synergistic effects and is best known as Malarone™ today (Canfield, Pudney and Gutteridge, 1995; Radloff *et al.*, 1996).

Atovaquone blocks the ubiquinol oxidation site (Q₀) of Complex III thereby preventing the regeneration of the electron carrier ubiquinone, effectively inactivating the five mitochondrial dehydrogenases that depend on ubiquinone, inhibiting the TCA cycle, and collapsing the mitochondrial membrane potential (Figure 4) (Painter *et al.*, 2007). Most deleterious for the parasite is the indirect inhibition of the pyrimidine biosynthesis pathway. Other Complex III inhibitors include Antimycin A which binds to the Q_i site of Complex III and results in the formation of large quantities of ROS, and Myxothiazol which blocks the electron transport within Complex III (Torrentino-Madamet *et al.*, 2010).

The target of Proguanil remains unknown. Several hypotheses have been proposed but fail to be supported by biological proof. Proguanil has a slow-acting activity that is independent of folate metabolism, pyrimidine synthesis and isoprenoid biosynthesis (Skinner-Adams *et al.*, 2019). Interestingly, parasites with an impaired mtETC function are hypersensitive to Proguanil, supporting its function within mitochondria and explaining the synergistic effect of Atovaquone and Proguanil. Some studies suggest Complex V as the target of Proguanil since Proguanil might prevent the alternative mechanism to sustain the mitochondrial membrane potential by reverse action of Complex V (Skinner-Adams *et al.*, 2019). However, recent evidence from a yeast model indicates that Proguanil acts not (mainly) via the alternative (Proguanil-sensitive) system to generate the membrane potential. Instead, it might accumulate at concentrations within the mitochondria that impair multiple mitochondrial functions and block transporters finally resulting in cell death (Mounkoro, Michel and Meunier, 2021).

Another antimalarial drug that potentially targets the mitochondrion is Primaquine. Although its mode of action is not completely understood, studies show that it attacks Fe-S clusters and raises ROS levels potentially decreasing parasite survival rates (Lalève *et al.*, 2016).

As the mitochondrion presents a good drug target, researchers continue exploring and exploiting the parasite's unique mitochondrial features. Recently, Lamb *et al.* (2022) published a list of 122 “putative mitochondrial” proteins based on an experimental biotinylation approach. The authors point out that phenotypic characterization from candidates of their list could be a valuable resource in understanding basic mitochondrial biology and in aiding further antimalarial drug discovery efforts (Lamb *et al.*, 2022). Moreover, a recent preprint showed antiparasitic activity for the anti-cancer drug MitoTam. MitoTam is a mitochondrially targeted drug conjugated with tamoxifen and was developed to accumulate in the mitochondria proportionally to $\Delta\Psi_m$. It disrupts respiratory supercomplexes, increases ROS levels, and rapidly breaks down $\Delta\Psi_m$, ultimately leading to cell/parasite (*Trypanosoma brucei*) death. Interestingly, the authors show that MitoTam is effective against *Plasmodium* asexual blood stages (Arbon *et al.*, 2022) underlining the importance of the mitochondrion as an antimalarial drug target.

1.5 Lipids in the malaria parasite

Intraerythrocytic asexual proliferation of *P. falciparum* is associated with a massive increase in phospholipids. In *Plasmodium*-infected RBCs the total amount of phospholipids increases approximately 5-fold (Beaumelle and Vial, 1986; Déchamps *et al.*, 2010; Gulati *et al.*, 2015), and even 6-fold in RBCs containing gametocytes (Tran *et al.*, 2016), compared to uninfected RBCs. Moreover, infected RBCs showed increased levels of neutral lipids and lipid-associated fatty acids (FAs) indicating an active lipid metabolism in *P. falciparum* (Nawabi *et al.*, 2003). Indeed, parasites require a large amount of lipids during their massive intracellular replication to form daughter merozoites and to expand the PVM and the associated tubovesicular network. Additionally, lipids and fatty acids are needed for signaling events, protein trafficking, hemoglobin degradation, and to generate storage lipids, triacylglycerol (TAG) and cholesteryl-esters (Vial *et al.*, 1989; Vielemeyer *et al.*, 2004; Yu *et al.*, 2008; Vaughan *et al.*, 2009; Déchamps *et al.*, 2010; Bullen *et al.*, 2016; Wein *et al.*, 2018; Asad *et al.*, 2021).

In uninfected mature RBCs, the main phospholipids are phosphatidylcholine (PC) (30–40%), phosphatidylethanolamine (PE) (25–35%), sphingomyelin (SM) (15%), and phosphatidylserine (PS) (10–20%) (Aktas *et al.*, 2014; Wein *et al.*, 2018). Other phospholipids such as phosphatidylinositol (PI), phosphatidic acid (PA), and lysophosphatidylcholine (lysoPC) represent only about 1 % of the total phospholipids (Figure 5) (Dodge and Phillips, 1967; Wein *et al.*, 2018). Interestingly, after infection by *P. falciparum*, changes in the phospholipid profile can be observed. Studies describe an increase of PC (to 45-55 %) and a

decrease of PS (4-8 %) while PE (to 20-35 %) and SM (3-20%) showed broader ranges (Gulati *et al.*, 2015; Wein *et al.*, 2018).

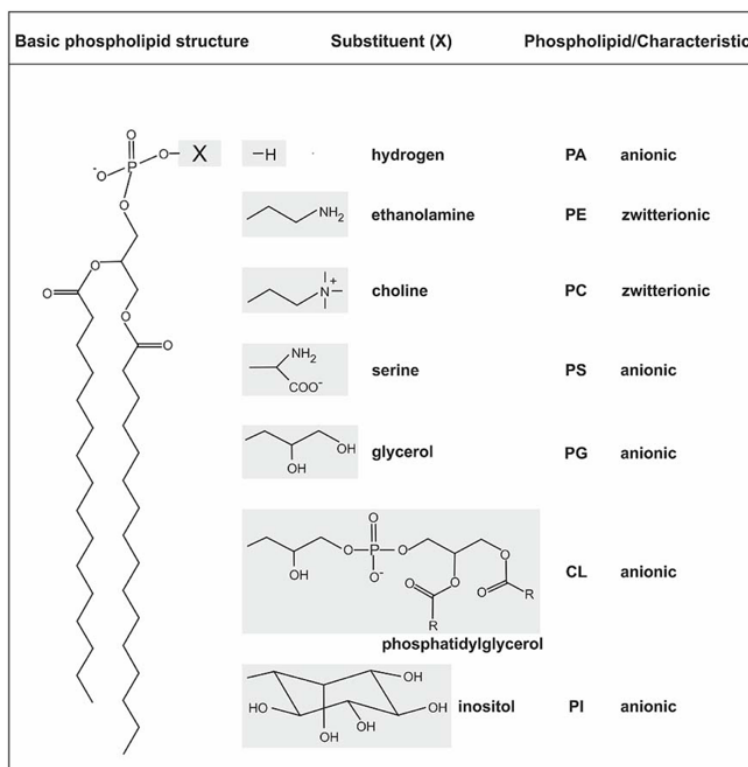


Figure 5. General structure of phospholipids and common head groups. Phospholipids contain two fatty acids ester-linked to glycerol at C-1 and C-2, and a polar head group attached at C-3 via a phosphodiester bond. The fatty acids in phospholipids can vary in carbon group length and saturation degree. The different common polar head groups and charges are indicated. PA, phosphatidic acid; PE, phosphatidylethanolamine; PC, phosphatidylcholine; PS, phosphatidylserine; PG, phosphatidylglycerol; CL, cardiolipin; PI, phosphatidylinositol. Figure taken from Aktas *et al.* (2014).

Differences in the phospholipid composition cannot only be observed between the uninfected and *Plasmodium*-infected RBC but also between the membrane of an infected RBC and parasite-derived membranes indicating that the parasite remodels the host cell membrane and actively synthesizes membranes itself (Holz, 1977; Maguire and Sherman, 1990). Modification of host cell membranous structures includes the formation of the tubulovesicular network, Maurer's clefts and knobs (Déchamps *et al.*, 2010). Moreover, there are significant differences in the lipid composition of asexual stages and gametocytes and between male and female gametocytes reflecting the different roles these stages play (Gulati *et al.*, 2015; Tran *et al.*, 2016; Ridgway *et al.*, 2022). The overall phospholipid and glycerolipid levels are decreased in gametocyte stages, probably as a result of altered substrate utilization following the switch to gametocytogenesis (Tran *et al.*, 2016; Brancucci *et al.*, 2017; Ngotho *et al.*, 2019). Gametocytes may require fewer lipids for membrane biosynthesis compared to the proliferative asexual stages. Interestingly though, sphingolipids, and in particular

ceramide levels, are increased in gametocytes and essential for their maturation (Gulati *et al.*, 2015; Tran *et al.*, 2016; Ngotho *et al.*, 2019).

1.5.1 Scavenging and synthesis

Plasmodium parasites can synthesize fatty acids *de novo* using a type II fatty acid biosynthesis pathway in the apicoplast (Tarun, Vaughan and Kappe, 2009), a process that is dispensable in asexual blood stages but essential in mosquito and liver stages (Yu *et al.*, 2008; Vaughan *et al.*, 2009; van Schaijk *et al.*, 2014). To support membrane biogenesis during their intraerythrocytic multiplication, parasites scavenge lipids and lipid-precursors from the host plasma and utilize them for lipid synthesis. However, exogenous lipids from the host serum were shown to contribute only marginally to the total amount of phospholipids in the parasite underlining the importance for the parasite's ability to synthesize (phosphor)lipids *de novo* using FAs and precursors (Gulati *et al.*, 2015; Guca *et al.*, 2016).

In particular, the parasite relies on the import of C_{16:0} (palmitic acid) and C_{18:1,n-9} (oleic acid) to proliferate (Mitamura *et al.*, 2000; Mi-Ichi, Kita and Mitamura, 2006; Mi-Ichi, Kano and Mitamura, 2007). Because palmitic acid, oleic acid, and stearic acid (C_{18:0}) can be generated by *de novo* biosynthesis in humans, it is interesting to speculate that *P. falciparum* evolved to adapt to human hosts in which the other FAs vary according to diet and health (Mi-Ichi, Kita and Mitamura, 2006). FAs scavenged from the host cell and host serum are subjected to a limited set of modifications by parasitic elongases and desaturases, and are finally incorporated into membrane glycerides. The two-carbon units necessary for elongation are provided by acetyl-CoA (Olszewski and Llinás, 2011).

From scavenged and modified precursors (polar heads, lysolipids, FAs) the parasite is able to assemble and synthesize all lipid precursors – such as phosphatidic acid, diacylglycerol (DAG), and cytidine diphosphate diacylglycerol (CDP-DAG) – as well as all major phospholipid classes - PC, PE, PS, PI, PG and cardiolipin (CL) – via the respective biosynthetic pathways (Kilian *et al.*, 2018; Wein *et al.*, 2018).

PC is the most abundant membrane lipid in the malaria parasite (Gulati *et al.*, 2015). Its *de novo* synthesis via a Kennedy pathway requires prior scavenging of exogenous lysophosphatidylcholine (lysoPC, C_{16:0}), especially of its polar head phosphocholine. Sufficient lysoPC levels are required to maintain high asexual division rates (Brancucci *et al.*, 2017). Reduced levels of exogenous lysoPC drive sexual differentiation, likely by the lack of PC used as building material for active asexual division (Brancucci *et al.*, 2017).

Inhibition of the Kennedy pathways for PC and PE biosynthesis results in parasite death (Guca *et al.*, 2016). These Kennedy pathways, also named CDP-choline and CDP-ethanolamine pathways, respectively, consist of three enzymatic reactions for the synthesis of PC from choline or PE from ethanolamine. The polar heads choline and ethanolamine are taken from

host plasma and are phosphorylated by kinases in the parasite cytoplasm. The products phosphocholine and phosphoethanolamine are then coupled to cytidine triphosphate (CTP) by transferases to form CDP-choline and CDP-ethanolamine. The last step involves the transfer of CDP-choline and CDP-ethanolamine to diacylglycerol (DAG), a reaction that is catalyzed by a single enzyme (Choline/Ethanolamine phosphotransferase, CEPT) in the *Plasmodium* ER, to generate the final products PC and PE (Déchamps *et al.*, 2010; Guca *et al.*, 2016).

Of note, there is no evidence that *Plasmodium* can synthesize cholesterol *de novo*. Nevertheless, upon invasion the nascent PVM shows elevated cholesterol levels compared to the RBCM it is derived from. This indicates that cholesterol might be actively recruited to the PVM or that RBCM lipids are mechanically redistributed during membrane deformations (Geoghegan *et al.*, 2021).

1.5.2 The importance of cardiolipins in mitochondria

The phospholipid composition of mitochondrial membranes is critical for several different processes, including mitochondrial dynamics, apoptosis, oxidative phosphorylation and membrane architecture (Hoffmann and Becker, 2022). While most phospholipids are produced in the ER, mitochondria synthesize CL, a characteristic mitochondrial phospholipid (Hoffmann and Becker, 2022). Additionally, eukaryotic organisms including *T. gondii* are capable of PE synthesis in the mitochondrion. However, in *Plasmodium* PE synthesis is confined to the ER (Hartmann *et al.*, 2014).

CLs are diphosphatidylglycerols that are characterized by a unique glycerol-bridged head group and four, rather than the typical two, fatty acyl side chains (Figure 5) (Schlame and Greenberg, 2017). The modular structure of lipids contributes to lipid diversity due to the combinatoric variability of possible fatty acyl substitution patterns. Owing to their four acyl side chains, CLs harbor a particularly large potential to contribute to lipid diversification (Keller, 2021).

In eukaryotes, CL is biosynthesized from a PG and a CDP-DAG in a non-reversible reaction catalyzed by a cardiolipin synthase (CLS) that contains a CDP-alcohol phosphatidyltransferase domain (CLS_{cap}) (Tian, Feng and Wen, 2012). In contrast, CL biosynthesis in prokaryotes proceeds through reversible phosphatidyl transfer from one PG molecule to another, or from PE to PG (Ren, Phoon and Schlame, 2014). The enzyme necessary for that reaction is a different kind of CLS, harboring two phospholipase D domains (CLS_{pld}) (Tian, Feng and Wen, 2012). Interestingly, unicellular eukaryotes such as Amoebozoa, Excavata and the Subgroup of Alveolata (including *Plasmodium*) bear the “bacterial” CL synthase CLS_{pld} (Tian, Feng and Wen, 2012).

Only in eukaryotes, the nascent CL is further remodeled to become mature CL by exchanging the fatty acyl side chains (Ye, Shen and Greenberg, 2016). Common to all organisms, only one or two types of unsaturated acyl groups dominate in mature CLs (Ren, Phoon and Schlame, 2014). In the first step of remodeling, nascent CL is deacylated by a phospholipase to form monolysocardiolipin (MLCL). The yeast CL-specific phospholipase CLD1 and the *Drosophila* and mammalian calcium-independent phospholipases A2 (iPLA2) β or γ have been reported to catalyze this reaction (Beranek *et al.*, 2009; Malhotra *et al.*, 2009; Zachman *et al.*, 2010). Subsequently, MLCL is reacylated by acyltransferases or transacylases such as the CoA-independent tafazzin (TAZ) or acyl CoA:lysocardiolipin acyltransferase 1 (ALCAT1) to become mature CL (Gu *et al.*, 2003; Cao *et al.*, 2004). It has been shown that CL fatty acyl rearrangement is not stochastically distributed but largely controlled via the FA availability in other cellular phospholipid pools. This creates a strong link between the FAs available in a given cell or tissue and the observed CL profiles (Oemer *et al.*, 2020, 2021; Keller, 2021) and has consequences for cell culture systems that use lipid/FA-rich medium since the observed CL profile of a given cell in these systems might not resemble the physiological state *in vivo* (Oemer *et al.*, 2021).

The unique conical shape of CLs allows them to be functionally involved in fundamental mitochondrial tasks, including proton gradient buffering (Haines and Dencher, 2002), mtDNA protection (Luévano-Martínez *et al.*, 2015), and cristae formation (Ikon and Ryan, 2017) as well as apoptosis (Belikova *et al.*, 2006). Interestingly, CL also plays a direct role in the mtETC at several points. It has been shown that the CL fatty acid composition regulates electron entry into the mtETC via Complex II and is associated with the electron transfer activity of ubiquinone (Schwall, Greenwood and Alder, 2012; Pöyry *et al.*, 2013; Vergeade *et al.*, 2016). Moreover, CL directly interacts with cytochrome *c* as well as several mtETC complexes and plays a stabilizing and functional role (Pinheiro and Watts, 1994; Pfeiffer *et al.*, 2003; Mileykovskaya and Dowhan, 2009; Bazán *et al.*, 2013). In turn, the assembly of the mtETC complexes triggers the remodeling of CLs. This might be caused by packing stress on the lipid bilayer imposed by the mtETC system which could be relieved by CL remodeling (Xu *et al.*, 2019).

In contrast to CL which has been shown to stabilize the supercomplex formation of the mtETC complexes III and IV in yeast, PE is not required for stabilization but rather for full activity of these supercomplexes (Baker *et al.*, 2016). An unbalanced ratio of specific phospholipid species thus might have harmful consequences for mitochondrial morphology and function. For example, the deletion of the mitochondrial phospholipase iPLA₂ γ in mice led to decreased Complex IV activity associated with a decrease in (18:2)₄CL (tetra-18:2 cardiolipin). As a consequence, mice showed growth retardation, cold intolerance, reduced exercise endurance and increased mortality from cardiac stress (Mancuso *et al.*, 2009) highlighting the fact that an imbalance of phospholipid species in the mitochondria might result in significant cellular or even organism-wide defects.

1.6 The diverse roles of phospholipases in *P. falciparum*

Despite our knowledge about scavenging and lipid synthesis pathways in *Plasmodium*, and the importance of correct phospholipid compositions in (mitochondrial) membranes of eukaryotes overall, we still lack a detailed understanding of the parasite's molecular machinery that separates the phospholipid building blocks (FA, polar heads, lysolipids) and reassembles them for the parasite's specific needs. The catabolism of lipid metabolites scavenged from the host must involve phospholipases for manipulation and generation of the proper lipid moieties. Phospholipase activity allows degradation and modification of phospholipids and thereby affects key physiological processes such as changes in membrane curvature, fusion, and turnover as well as membrane stability and lipid homeostasis. Moreover, phospholipases are involved in diverse lipid-mediated signal transduction processes and cell proliferation, and can function as important virulence factors of pathogens (Flammersfeld *et al.*, 2018).

Generally, phospholipases are divided into four categories: A, B, C and D. Phospholipases A1 and A2 hydrolyze ester bonds at the sn-1 or sn-2 position, respectively, thereby producing free FAs and lysophospholipids. These lysophospholipids are intermediates in the metabolism of membrane phospholipids that can be further processed by lysophospholipases (LPLs) which catalyze the hydrolysis of acyl chains from lysophospholipids. LPLs thus play a key role in the recycling of lipids. Phospholipases B attack both ester bonds at the sn-1 and the sn-2 position. Phospholipases C hydrolyze the glycerophosphate bond thereby producing DAG. In general, they show high substrate specificity, which is why they are differentiated into PC-specific and PI-specific phospholipases C (PC-PLC or PI-PLC, respectively) (Goñi, Montes and Alonso, 2012). The last class of phospholipases, phospholipases D, cleaves the polar head group off a phospholipid.

Plasmodium possesses a large family of (putative) phospholipases and several members have been characterized throughout the life cycle. In a recent systematic screen from our group, 20 (putative) *P. falciparum* phospholipases were individually targeted for gene deletion. Surprisingly, their functional analysis revealed a high level of redundancy during asexual blood stage development (Burda *et al.*, 2021). Despite this redundancy, phospholipases have been shown to fulfill important functions during blood stage development and in other life stages.

1.6.1 Essential phospholipases

During *P. falciparum* intraerythrocytic blood stage development, the phosphoinositide-specific phospholipase C (PI-PLC, PF3D7_1013500) has been described as an essential player during trophozoite-to-schizont transition, a function far earlier in the cycle than its proposed role in parasite egress (Burda *et al.*, 2021). PI-PLC-deficient parasites did not only show a maturation defect but also a lower overall lipid content (Burda *et al.*, 2021).

The phospholipase PbPL (PBANKA_1128100, a phospholipase A2) and the phosphatidic acid-preferring phospholipase A1 (PbPla1, PBANKA_1423100) were identified to be key players in PVM rupture during liver stage egress using the rodent malaria model *P. berghei* (Burda *et al.*, 2015; Srivastava and Mishra, 2022). In line with this, their *P. falciparum* orthologues PF3D7_0629300 and PF3D7_0814400 were both dispensable for blood stage development underlining their putative liver stage-specific function (Burda *et al.*, 2021).

1.6.2 Lysophospholipases

As outlined above, LPLs play a key role in lipid recycling. In *P. falciparum* asexual blood stages, the lysophospholipase 1 (LPL1, PF3D7_1476700, Table 1) has been described to have an essential role in the generation of neutral lipids required for hemozoin formation (Asad *et al.*, 2021). The neighboring gene encodes the lysophospholipase 3 (LPL3, PF3D7_1476800). This protein has been shown to display a dynamic localization throughout asexual stages, mainly localizing at the host-parasite interface (Sheokand *et al.*, 2021). Inducible knock-down of LPL3 hindered normal intraerythrocytic development, specifically causing a disruption in parasite development from trophozoites to schizonts, as well as a reduction in the number of merozoite progenies (Sheokand *et al.*, 2021). Detailed lipidomic analyses revealed that LPL3 generates free FAs that fuel the DAG-TAG synthesis pathway for lipid storage. This in turn regulates the timely synthesis of phospholipids, which are required for the membrane biogenesis of merozoites during schizogony (Sheokand *et al.*, 2021).

Another LPL, the lysophospholipase 4 (LPL4, PF3D7_0731800, Table 1), was previously annotated as exported protein GEXP08 and is dispensable in asexual intraerythrocytic growth (Silvestrini *et al.*, 2010; Asad *et al.*, 2021; Burda *et al.*, 2021).

1.6.3 Patatin-like phospholipases

Patatin-like phospholipases (PNPLAs) are highly conserved enzymes in prokaryotes and eukaryotes. They share a common protein domain with the patatin glycoprotein, a non-specific lipid acyl hydrolase of mature potato tubers, and exhibit phospholipase A2 activity (Wilson and Knoll, 2018). PNPLAs were described to have vital functions in lipid homeostasis, membrane degradation and cell signaling, and to act as important virulence factors of pathogenic bacteria such as *Legionella pneumophila* (Wilson and Knoll, 2018).

Of the four putative PNPLAs in *Plasmodium*, only one has been analyzed in detail. The patatin-like phospholipase 1 (PNPLA1 or PfPATPL1, PF3D7_0209100) was identified as a crucial factor for gametocyte commitment in *P. falciparum* (Flammersfeld *et al.*, 2020). Moreover, PNPLA1 was reported to be required for efficient rounding up, egress, and exflagellation of gametocytes following activation (Singh *et al.*, 2019).

The second patatin-like phospholipase, termed patatin-like phospholipase 2 (PNPLA2, PF3D7_1358000, Table 1), localizes to the mitochondrion. Its deletion leads to a significant reduction of asexual growth and aberrant mitochondrial morphology (Burda *et al.*, 2021). Surprisingly, its orthologue in the related Apicomplexan parasite *T. gondii*, TgPL2 (TGME49_231370) localizes to the apicoplast, not the mitochondrion (Lévêque *et al.*, 2017).

A third putative patatin-like phospholipase (PNPLA3, PF3D7_0924000, Table 1) is dispensable for asexual growth (Burda *et al.*, 2021) but has been described to be downregulated in response to inhibition of choline kinase (Razak *et al.*, 2014), thereby linking PNPLA3 to PC biosynthesis.

1.6.4 Other phospholipases of interest

Some *P. falciparum* enzymes harbor features that imply a potential phospholipase activity but are annotated as members of other enzyme classes. This is the case for the prodrug activation and resistance esterase (PARE, PF3D7_0709700, Table 1), also annotated as LPL60 (Asad *et al.*, 2021). PARE showed *in vitro* esterase activity (Istvan *et al.*, 2017) but has an additional predicted phospholipase activity that has not been studied. PARE is dispensable for asexual growth (Burda *et al.*, 2021).

P. falciparum also encodes two proteins with predicted phospholipase C/p1/s1 nuclease domains. Here, we call them PL39 (putative phospholipase with a molecular weight of 39 kDa, PF3D7_1411900, Table 1) and PL38 (putative phospholipase with a molecular weight of 38 kDa, PF3D7_1412000, Table 1). They are dispensable for asexual intraerythrocytic replication (Burda *et al.*, 2021). Interestingly, the genomic proximity of *pl39* and *pl38* and the presence of only one single orthologue in the rodent malaria parasite *P. berghei* at this genomic location (according to PlasmoDB) suggests that these loci are the result of gene duplication. However, since PL39 and PL38 show only 46 % sequence identity, they may have evolved to fulfill different functions.

1.7 Aim of this thesis

Lipid metabolism and its differential and adaptive regulation are essential for living cells. Enzymes involved in these metabolic processes are key regulators. The aims of this thesis are:

- i) A functional analysis of the mitochondrial patatin-like phospholipase (PNPLA2, PF3D7_1358000) in asexual blood stage development and gametocytogenesis, and
- ii) A characterization of six additional phospholipases for their role in gametocyte development.

GENE ID	<i>P. BERGHEI</i> ORTHOLOG	ANNOTATION	LITERATURE
PF3D7_0709700	PBANKA_0201300, PBANKA_0623200, PBANKA_1220200, PBANKA_1220300	PARE, LPL60	Istvan <i>et al.</i> (2017), Asad <i>et al.</i> (2021)
PF3D7_0731800	No ortholog	GEXP08, LPL4	Silvestrini <i>et al.</i> (2010), Asad <i>et al.</i> (2021)
PF3D7_0924000	PBANKA_0824900	PNPLA3	Wilson <i>et al.</i> (2017)
PF3D7_1358000	PBANKA_1134300	PNPLA2	Burda <i>et al.</i> (2021)
PF3D7_1411900	PBANKA_1030600	p1/s1 nuclease (PL 39)	-
PF3D7_1412000	PBANKA_1030600	p1/s1 nuclease (PL38)	-
PF3D7_1476700	PBANKA_0201300, PBANKA_0623200, PBANKA_1220200, PBANKA_1220300	LPL1	Asad <i>et al.</i> (2021)

Table 1. Phospholipases studied in this PhD thesis.

2. Material and Methods

2.1 Material

2.1.1 Chemicals and Reagents

CHEMICAL	MANUFACTURER (LOCATION)
1,4-Dithiothreitol (DTT)	Roth (Karlsruhe)
4',6-Diamidino-2-Phenylindole (DAPI)	Roche (Mannheim)
Acetic acid	Roth (Karlsruhe)
Acetone	Roth (Karlsruhe)
Acrylamide/Bisacrylamide (40%)	Roth (Karlsruhe)
Agar LB (Lennox)	Roth (Karlsruhe)
Agarose	Invitrogen (Karlsruhe)
AlbumaxII	Invitrogen (Karlsruhe)
Albumin Fraction V (BSA)	Biomol (Hamburg)
Ammonium persulfate (APS)	Roth (Karlsruhe)
Bacto™ Peptone	Becton Dickinson (Heidelberg)
Bacto™ Yeast Extract	Becton Dickinson (Heidelberg)
Bromphenol Blue	Merck (Darmstadt)
Calcium chloride (CaCl ₂)	Roth (Karlsruhe)
Choline	Sigma-Aldrich (Steinheim)
Coomassie Brilliantblau R250	Merck (Darmstadt)
D-(+)-Glucosamine hydrochloride	Sigma-Aldrich (Steinheim)
Decylubiquinone (DCUQ)	Cayman Chemical (Ann Arbor)
D-Glucose	Sigma-Aldrich (Steinheim), Roth (Karlsruhe)
Descosept	Dr. Schuhmacher GmbH (Malsfeld)
Deoxyribonucleotides (dNTPs)	Fermentas (St. Leon-Rot)
Digitonin	Roth (Karlsruhe)
Dihydroethidium (DHE)	Biomol (Hamburg)
Dimethyl sulfoxide (DMSO)	Sigma-Aldrich (Steinheim)
Disodium hydrogen phosphate (NaH ₂ PO ₄)	Roth (Karlsruhe)
Disodium phosphate (Na ₂ HPO ₄)	Roth (Karlsruhe)
Dulbecco's Phosphate Buffered Saline (DPBS)	PAN Biotech (Aidenbach)
Durcupan Epoxy Resin	Electron Microscopy Series/VWR (Radnor)
Ethanol, 70 % (denatured)	Roth (Karlsruhe)
Ethanol, absolute	Roth (Karlsruhe)
Ethidium bromide (EtBr)	Sigma-Aldrich (Steinheim)
Ethylene glycol-tetraacetic acid (EGTA)	Roth (Karlsruhe)
Ethylenediaminetetraacetic acid (EDTA)	Roth (Karlsruhe)
FCCP	Biomol (Hamburg)

Material and Methods

Formaldehyde Ultra Pure (methanol-free, 10%)	Polysciences Inc. (Hirschberg)
Giemsa azur eosin methylene blue solution	Merck (Darmstadt)
Glutaraldehyde (25%)	Roth (Karlsruhe)
Glycerol	Roth (Karlsruhe)
Glycine	Merck (Darmstadt)
HEPES (4-(2-hydroxyethyl)-1-piperazineethanesulfonic acid)	Roth (Karlsruhe)
Hoechst333842	Biomol (Hamburg)
Hydrochloric acid (HCl)	Roth (Karlsruhe)
Hypoxanthine	Sigma-Aldrich (Steinheim)
iFluor555 Wheat Germ Agglutinin (WGA)	Biomol (Hamburg)
Immersion Oil TypF Ne23=1,5180/ve=46	Leica (Wetzlar)
Isopropanol	Roth (Karlsruhe)
Isopropyl-beta-D-thiogalactopyranosid (IPTG)	Roth (Karlsruhe)
Magnesium chloride (MgCl ₂)	Sigma-Aldrich (Steinheim)
Malate	Roth (Karlsruhe)
Manganese(II) chloride (MnCl ₂)	Merck (Darmstadt)
Mannitol	Sigma-Aldrich (Steinheim)
Methanol (MeOH)	Roth (Karlsruhe)
Milk powder	Roth (Karlsruhe)
MitoTracker CMXRos	Invitrogen (Waltham)
Mounting medium	Dako (Carpinteria)
Mowiol	Roth (Karlsruhe)
N-Acetyl-glucosamine	Roth (Karlsruhe)
Osmium tetroxide	Electron Microscopy Series/VWR (Radnor)
Percoll	GE Healthcare (Freiburg)
PIPES [1,4-Piperazinediethanesulfonic acid]	Sigma-Aldrich (Steinheim)
Poly-D-Lysine	ThermoFisher (Waltham)
Potassium chloride (KCl)	Sigma (Karlsruhe)
Potassium dihydrogen phosphate (KH ₂ PO ₄)	Merck (Darmstadt)
Potassium ferrocyanide	Electron Microscopy Series/VWR (Radnor)
Potassium hydroxide (KOH)	Roth (Karlsruhe)
Protease inhibitor cocktail	Roche (Mannheim)
Rhodamine123 (chloride)	Cayman Chemical (Ann Arbor)
RPMI (Roswell Park Memorial Institute) medium	Invitrogen (Waltham), Applichem (Darmstadt)
Saponin	Sigma-Aldrich (Steinheim),

	BDH Bioscience/VWR (Darmstadt)
Sekusept Plus	Ecolab GmbH (Monheim am Rhein)
Sodium acetate (NaCH ₃ COO)	Sigma-Aldrich (Steinheim)
Sodium cacodylate buffer	Electron Microscopy Series/VWR (Radnor)
Sodium chloride (NaCl)	Roth (Karlsruhe)
Sodium dihydrogen phosphate (NaH ₂ PO ₄)	Roth (Karlsruhe)
Sodium dodecyl sulfate (SDS)	Roth (Karlsruhe)
Sodium hydroxide	Merck (Darmstadt)
Sorbitol	Roth (Karlsruhe)
Sucrose	Sigma-Aldrich (Steinheim)
SYBR Gold	ThermoFisher (Waltham)
SYBR Green I	ThermoFisher (Waltham)
Tetramethylethylenediamine (TEMED)	Roth (Karlsruhe), Merck (Darmstadt)
Tris	Roth (Karlsruhe)
Tris-Base	Roth (Karlsruhe)
Triton X-100	United States Biological (Salem)
Trolox (6-hydroxy-2,5,7,8-tetramethylchroman-2-carboxylic acid)	Sigma-Aldrich (Steinheim)
Tryptone	Sigma-Aldrich (Steinheim)
Tween 20	Roth (Karlsruhe)
Uranyl acetate	Electron Microscopy Series/VWR (Radnor)
Xanthurenic acid	Sigma-Aldrich (Steinheim)

2.1.2 Media

MEDIUM	COMPOSITION
Luria-Bertani (LB) medium in ddH ₂ O, autoclaved	1% (w/v) Sodium chloride 1% (w/v) Peptone 1% (w/v) Yeast extract
LB-Agar in LB medium	1.5% (w/v) LB-Agar Lennox
Super Optimal Broth (SOB)-Medium in ddH ₂ O, autoclaved adjusted to pH 7.0 with NaOH	10 mM Sodium chloride 2.5 mM Potassium chloride 2% (w/v) Tryptone 0.5% (w/v) Yeast extract
RPMI complete medium (cRPMI) in ddH ₂ O, sterile-filtered adjusted to pH 7.2 with NaOH	1.587% (w/v) RPMI 1640 12 mM NaHCO ₃ 0.2 mM Hypoxanthine 0.4 mM Gentamycin

0.5% (w/v) Albumax II
2 mM Choline*

*Only for NF54/iGP2 and 3D7CH parasite lines.

Ookinete medium
adjusted to pH 8.0

1.587% (w/v) RPMI 1640
12 mM NaHCO₃
0.2 mM Hypoxanthine
0.4 mM Gentamycin
100 µM Xanthurenic acid

Incomplete ookinete medium was stored at -80 °C. On the day of the assay, an aliquot was thawed and 20 % (v/v) human serum were added freshly.

2.1.3 Buffers and Solutions

MOLECULAR BIOLOGY

BUFFER / SOLUTION	COMPOSITION
Ammoniumpersulfate solution in ddH ₂ O	10% (w/v) APS

MAS (Mitochondrial Assay Solution) buffer
according to Jenni A. Hayward *et al.*, 2022

220 mM Mannitol
70 mM Sucrose
10 mM KH₂PO₄
5 mM MgCl₂
2 mM HEPES
1 mM EGTA
0.2% (w/v) Fatty acid-free BSA*
10 mM Malate*

The assay solution was prepared in ddH₂O without BSA and malate. Using KOH, the pH was adjusted to 7.4. The sterile-filtered incomplete MAS was stored at 4 °C.

*On the day of the assay, BSA and malate were freshly added.

Material and Methods

PBS (10X) in ddH ₂ O (7.4)	17.8 g/L Na ₂ HPO ₄ 80 g/L NaCl 2.4 g/L KH ₂ PO ₄ 2 g/L KCl
SDS Loading Dye (5X) in ddH ₂ O	416 mM SDS 300 mM Tris-HCl (pH 6.8) 596 mM DTT 60% Glycerol 0.01% (w/v) Bromphenol Blue
SDS Running Buffer	25 mM Tris 192 mM Glycin 0.1% (w/v) SDS
Separating gel buffer (for SDS-PAGE) in ddH ₂ O	1.5 M Tris-HCl, pH 8.8
Sodium acetate solution in ddH ₂ O	3 M Sodium acetate
Stacking gel buffer (for SDS-PAGE)	1 M Tris-HCl, pH 6.8
TAE buffer autoclaved	40 mM Tris 1 mM EDTA 20 mM Acetic acid
TBS (10X) in ddH ₂ O (pH 7.4)	1.5 M NaCl 30 mM KCl 250 mM Tris
TBS-Tween in 1X TBS	0.02 % Tween 20
TE buffer (for <i>Plasmodium</i> transfection) pH 8.0, autoclaved	10 mM Tris-HCl (pH 8.0) 1 mM EDTA
Western Blot Blocking Solution in 1X TBS	5% (w/v) Milk powder
Western Blot Transfer Buffer in SDS Running Buffer	20% Methanol

CELL BIOLOGY

BUFFER / SOLUTION	COMPOSITION
60% Percoll sterile filtered	67% (v/v) Percoll stock solution 33% (v/v) RPMI complete medium 0.08 g/mL D-Sorbitol
90 % Percoll stock solution sterile filtered	90% (v/v) Percoll 10% (v/v) 10X PBS
Amaxa transfection buffer (for <i>Plasmodium</i> transfection) in ddH ₂ O, sterile filtered adjusted to pH 7.3	90 mM Na ₂ HPO ₄ 5 mM KCl 50 mM HEPES 150 μM CaCl ₂
DHE in DMSO	0.5 mg/mL DHE
Drug Screen Lysis Buffer in ddH ₂ O pH 7.5	20 mM Tris 5 mM EDTA 0.008% Saponin 0.08% TritonX-100 1X SYBR Gold*
	*SYBR Gold was added freshly on the day of the assay.
Giemsa staining solution in H ₂ O (tap water)	10% (v/v) Giemsa solution
Hoechst33342 in DMSO	0.45 mg/mL Hoechst33342
Malaria Freezing Solution (MFS) in ddH ₂ O, sterile filtered	208 mM D-Sorbitol 139 mM NaCl 35% (v/v) Glycerol
Malaria Thawing Solution (MTS) in ddH ₂ O, sterile filtered	3.5% (w/v) NaCl
Ringer solution in ddH ₂ O	1 mM NaH ₂ PO ₄ 5.4 mM KCl 1.2 mM CaCl ₂

	0.8 mM MgCl ₂ 11 mM D-glucose 10 mM HEPES 122.5 mM NaCl
	Ringer solution was prepared and adjusted to pH 7.4 at 37 °C using NaOH/HCl. It was filter-sterilized and stored at 4 °C.
Saponin in 1X PBS	0.03%-0.15% saponin
Sorbitol solution in ddH ₂ O, sterile filtered	5% (w/v) D-Sorbitol
Transformation buffer for ultra-competent <i>E. coli</i> sterile filtered	3.0 g/L PIPES (10 mM) 2.2 g/L CaCl ₂ -2xH ₂ O (15 mM) 18.6 g/L KCl (250 mM) 10.9 g/L MnCl ₂ -4xH ₂ O*
	*The pH was adjusted to 6.7 before adding MnCl ₂ .

2.1.4 Antibiotics and Antimalarials

DRUG	STOCK	MANUFACTURER (LOCATION)
Ampicillin	100 mg/mL in 70% ethanol	Roche (Mannheim)
Antimycin A	3 mM in DMSO	Biomol (Hamburg)
Atovaquone	2.5 mM in DMSO	Biomol (Hamburg)
Blasticidin S (BSD)	10.9 mg/mL in RPMI	Invitrogen (Karlsruhe)
Dihydroartemisinin (DHA)	250 µM in DMSO	Sigma-Aldrich (Steinheim)
DSM1	3.75 mM in DMSO	Biomol (Hamburg)
FCCP	50 mM in DMSO	Biomol (Hamburg)
Gentamycin	80 mg/ 2 mL SF solution for injection	Ratiopharm (Ulm)
Myxothiazol	5 mM in DMSO	Biomol (Hamburg)
Neomycin	50 mg/mL in RPMI	Sigma-Aldrich (Steinheim)
Primaquine phosphate	10 mg/mL in PBS	Biomol (Hamburg)
Proguanil	10 mM in DMSO	Biomol (Hamburg)
WR99210	20 mM in DMSO	Jacobus Pharmaceuticals (USA)

2.1.5 Antibodies

ANTIBODY	ORGANISM	DILUTION		MANUFACTURER/ORIGIN
		Western Blot	IFA	
anti-BIP	Rabbit	1:2000	-	Struck <i>et al.</i> (2005)
anti-GAPDH	Mouse	1:2000	-	Daubenberger <i>et al.</i> (2000)
anti-GFP	Mouse	1:1000	1:1000	Roche (Mannheim)
anti-GFP	Rabbit	-	1:500	ChromoTek (Planegg)
anti-mouse 680RD	Goat	1:10,000	-	LI-COR (Lincoln)
anti-mouse 800CW	Goat	1:10,000	-	LI-COR (Lincoln)
anti-mouse Alexa488	Goat	-	1:1000	Invitrogen (Karlsruhe)
anti-mouse Alexa594	Goat	-	1:1000	Invitrogen (Karlsruhe)
anti-rabbit 680RD	Goat	1:10,000	-	LI-COR (Lincoln)
anti-rabbit 800CW	Goat	1:10,000	-	LI-COR (Lincoln)
anti-rabbit Alexa488	Goat	-	1:1000	Invitrogen (Karlsruhe)
anti-rabbit Alexa594	Goat	-	1:1000	Invitrogen (Karlsruhe)
anti-RAP1 [2.29]	Mouse	-	1:2000	Hall <i>et al.</i> (1983) [†]
anti-rat 680RD	Goat	1:10,000	-	LI-COR (Lincoln)
anti-rat 800CW	Goat	1:10,000	-	LI-COR (Lincoln)
anti-rat Alexa488	Goat	-	1:1000	Invitrogen (Karlsruhe)
anti-rat Alexa594	Goat	-	1:1000	Invitrogen (Karlsruhe)
anti-RFP [5F8]	Rat	-	1:1000	ChromoTek (Planegg)
anti-RFP [6G6]	Mouse	1:2000	-	ChromoTek (Planegg)
anti-SUB1 [NIMP.M7]	Mouse	-	1:1000	Collins <i>et al.</i> (2013)

[†]The monoclonal antibody 2.29 anti-RAP1 was obtained from The European Malaria Reagent Repository (<http://www.malariaresearch.eu>).

2.1.6 Enzymes

All restriction enzymes were purchased from New England Biolabs (NEB, Ipswich). The phosphatase CIP (5 U/μL), the polymerases FirePol DNA Polymerase (10 U/μL) and Phusion High Fidelity DNA Polymerase (2 U/μL) as well as the T4 DNA Ligase (400 U/μL) were also purchased from New England Biolabs (NEB, Ipswich).

2.1.7 Inhibitors

The PKG inhibitor Compound 2 (C2) was kindly provided by Michael Blackman, Francis Crick Institute, London, UK. The PKG inhibitor ML10 (Baker *et al.*, 2017; Ressurreição *et al.*, 2020) was kindly provided by Mathieu Brochet, University of Geneva, Geneva, Switzerland.

2.1.8 DNA and Protein Standards

For agarose gels, GeneRuler 1kb (Fermantas, St. Leon-Rot) was used. For Western Blots, Chameleon Duo Prestained Protein Ladder (LI-COR, Lincoln) was used.

2.1.9 Oligonucleotides (primers)

Oligonucleotides were ordered from Sigma-Aldrich (Steinheim) as 100 μ M stock solutions. For subsequent use, primers were diluted in ddH₂O to a final concentration of 10 μ M. All stock and working solutions were stored at -20 °C.

2.1.10 Plasmids

The parental plasmid for all constructs (except for ACP-mCherry) was pSLI-TGD (Birnbaum *et al.*, 2017). The cloning strategy is outlined in Chapter 2.2.9 *Cloning of SLI constructs*.

CONSTRUCT NAME	CONSTRUCT DESIGN	INTERNAL REF.
ACP-mCherry	Birnbaum <i>et al.</i> , 2020	-
pSLI-PF3D7_0709700-mScarlet	Emma Pietsch	220
pSLI-PF3D7_0731800-mScarlet	Emma Pietsch	221
pSLI-PF3D7_0924000-mScarlet	Emma Pietsch	219
pSLI-PF3D7_1358000-GFP	Louisa Wilcke [†]	METT73
pSLI-PF3D7_1411900-mScarlet	Emma Pietsch	255
pSLI-PF3D7_1412000-mScarlet	Emma Pietsch	256
pSLI-PF3D7_1476700-mNeon-glmS	Emma Pietsch	281
pSLI-PF3D7_1476700-mScarlet	Emma Pietsch	222
pSLI-TGD-PF3D7_0709700	Paul-Christian Burda/ Sabrina Bielfeld [†]	58
pSLI-TGD-PF3D7_0731800	Paul-Christian Burda/ Sabrina Bielfeld [†]	59
pSLI-TGD-PF3D7_0924000	Paul-Christian Burda/ Sabrina Bielfeld [†]	12
pSLI-TGD-PF3D7_1358000	Paul-Christian Burda/ Sabrina Bielfeld [†]	38-1
pSLI-TGD-PF3D7_1411900	Paul-Christian Burda/ Sabrina Bielfeld [†]	32
pSLI-TGD-PF3D7_1412000	Paul-Christian Burda/ Sabrina Bielfeld [†]	13
pSLI-TGD-PF3D7_1476700	Emma Pietsch	223

[†]Construct design and cloning procedure are published in Burda *et al.* (2021).

2.1.11 Kits

KIT	APPLICATION	MANUFACTURER (LOCATION)
NucleoSpin® Plasmid Kit	Plasmid purification from small bacterial cultures (1.8 mL)	Macherey-Nagel (Düren)
NucleoSpin® Gel and PCR Clean-Up	Purification of PCR fragments or digested vector fragments from agarose gels	Macherey-Nagel (Düren)
QIAamp® DNA Mini Kit	Preparation of parasite genomic DNA	Qiagen (Hilden)
PureYield™ Plasmid Midiprep System	Plasmid purification from bigger bacterial cultures (100-200 mL)	Promega (Madison)

2.1.12 Cell lines

All experiments were performed using the human malaria parasite *P. falciparum*. The NF54 isolate was obtained from a patient in the Netherlands who has never left the country and is considered a case of “airport malaria”. The exact origin of NF54 remains unknown. From NF54, the 3D7 reference strain was cloned. Despite being separated in culture for decades, NF54 and 3D7 are assumed to be genetically identical (Moser *et al.*, 2020). 3D7 has mostly lost its ability to undergo gametogenesis. However, some lines support development into mature stage V gametocytes. In this thesis, 3D7CH refers to a wildtype 3D7 parasite line that supports gametocyte commitment and maturation (Filarsky *et al.*, 2018). Parasites were kindly provided by Michael Filarsky, University of Hamburg, Hamburg, Germany.

The parasite line NF54/iGP2 (Boltryk *et al.*, 2021) was kindly provided by Till Voss, Swiss Tropical and Public Health Institute, Basel, Switzerland. NF54/iGP2 parasites allow conditional overexpression of GDV1 which drives gametocyte commitment. Moreover, their NF54 background allows studies of their transmission competency (micro- and macrogametogenesis).

Parasite lines used in this thesis are listed below. All parasite lines integrated the listed plasmids into the respective gene loci. The cloning strategy is outlined in Chapter 2.2.9 *Cloning of pSLI constructs*.

PARASITE LINE	FULL PLASMID NAME	PARENTAL LINE	GENERATION OF THE LINE	REF. NO.
LPL1-KO	pSLI-TGD-PF3D7_1476700	NF54/iGP2	Emma Pietsch	223
LPL1-mNeon	pSLI-PF3D7_1476700-mNeon-glmS	3D7CH	Emma Pietsch	281
LPL1-mScarlet	pSLI-PF3D7_1476700-mScarlet	NF54/iGP2	Emma Pietsch	222
LPL4-KO	pSLI-TGD-PF3D7_0731800	NF54/iGP2	Emma Pietsch	59
LPL4-mScarlet	pSLI-PF3D7_0731800-mScarlet	NF54/iGP2	Emma Pietsch	221
PARE-KO	pSLI-TGD-PF3D7_0709700	NF54/iGP2	Emma Pietsch	58
PARE-mScarlet	pSLI-PF3D7_0709700-mScarlet	NF54/iGP2	Emma Pietsch	220
PL38-KO	pSLI-TGD-PF3D7_1412000	NF54/iGP2	Emma Pietsch	13
PL38-mScarlet	pSLI-PF3D7_1412000-mScarlet	NF54/iGP2	Emma Pietsch	256
PL39-KO	pSLI-TGD-PF3D7_1411900	NF54/iGP2	Emma Pietsch	32
PL39-mScarlet	pSLI-PF3D7_1411900-mScarlet	NF54/iGP2	Emma Pietsch	255
PNPLA2-GFP	pSLI-PF3D7_1358000-GFP	3D7	Louisa Wilcke [†]	METT73
PNPLA2-KO	pSLI-TGD-PF3D7_1358000	3D7	Paul-Christian Burda / Sabrina Bielfeld [†]	38
		3D7CH	Emma Pietsch	
PNPLA3-KO	pSLI-TGD-PF3D7_0924000	NF54/iGP2	Emma Pietsch	12
PNPLA3-mScarlet	pSLI-PF3D7_0924000-mScarlet	NF54/iGP2	Emma Pietsch	219

[†]Parasite lines are published in Burda *et al.* (2021).

2.1.13 Technical equipment and Microscopes

EQUIPMENT	CATALOG NUMBER / NAME	MANUFACTURER (LOCATION)
-80 °C freezer	CryoCube FC660h	Eppendorf (Hamburg)
Agarose gel chamber	PeqLab PerfectBlue	PeqLab/VWR (Radnor)
Analytical balance	Atilon	Satorius (Göttingen)
	Kern 572	Kern&Sohn (Balingen)
Centrifuges	5412 D (F45-24-11)	Eppendorf (Hamburg)
	5424 R (FA-45-24-11)	
	5810 R (A-4-62)	
CO ₂ Incubator (for bacteria)	CO 150	Eppendorf (Hamburg)
Electroporator	Lonza Nucleofactor II	Lonza (Basel)

Material and Methods

Flow cytometer	NovoCyte 1000	ACEA, Agilent (Santa Clara)
Fume hood	-	Köttermann Labortechnik (Uetze)
Gel Documentation	Molecular Imager® Gel Doc™ XR+ System	Bio-Rad (Hercules)
Heating Plate (Cell culture)	CultureTemp	SP Industries (Warminster)
Ice machine	EF 156 easy fit	Scotsman (Vernon Hills)
Incubators	Hera Therm	ThermoScientific (Waltham)
Magnetic stirrer	RSM-01HS	Phoenix Instruments (Garbsen)
Mass spectrometer	timsTOF	Bruker Daltonics (Bremen)
Microwave	Micromaxx MM41568	Medion (Mühlheim)
PCR cyclor	ThermalCycler C1000 Touch	Bio-Rad (Hercules)
pH meter	766 Calimatic	Knick International (Berlin)
Pipettes	Pipetman L P2L / P20L / P200L / P1000L	Gilson (Middleton)
Pipettor	Pipetboy acu 2	Integra (Zizers)
Plate reader	Multimode Plate Reader EnVision	PerkinElmer (Waltham)
Power supply	PowerPac™ Basic Power / HC High Current Supply	Bio-Rad (Hercules)
Roller mixer	Sun Lab SU1400	Sublab (Aschaffenburg)
SDS-gel electrophoresis chamber	Mini-PROTEAN® Tetra Cell System	Bio-Rad (Hercules)
Seahorse XF96 Analyzer	-	Agilent (Santa Clara)
Shaking incubator	Innova 40 May Q 4000	Eppendorf (Hamburg) ThermoScientific (Waltham)
Spectrophotometer	DS-11+ Spectrophotometer	DeNovix (Wilmington)
Sterile laminar flow bench	Maxisafe 2020	ThermoScientific (Waltham)
Thermoblock	Thermomixer Compact/F1.5	Eppendorf (Hamburg)
Ultrapure water purification system	Milli-Q Q-POD CDUFB1001	Merck (Darmstadt)
Vacuum pump (Cell culture)	BVC control	Vacuubrand (Wertheim)
Vacuum pump (Midi prep)	2522Z-02 Vac Dry Pump	Gardner Denver (Davidson)
Vortexer	VV3	VWR (Radnor)
Waterbath	GFL 1083	Gesellschaft für Labortechnik (Wedel)
Western Blot Documentation	Odyssey® FC Imaging System	LI-COR (Lincoln)

MICROSCOPE	CAMERA	APPLICATION	MANUFACTURER (LOCATION)
Helios 660 NanoLab G3 UC DualBeam	-	FIB-SEM	FEI (Hillsboro)
Leica DM2000 LED	Leica DMC2900	Giema slides	Leica (Wetzlar)
Leica DM6 upright	Leica DFC9000	Live cell, IFA	Leica (Wetzlar)

2.1.14 Labware and Disposables

Plastic disposables were purchased from Sarstedt (Nümbrecht) if not indicated otherwise.

LABWARE	SPECIFICATION	MANUFACTURER (LOCATION)
Autoclaving bags	200x300 mm	neoLab Migge (Heidelberg)
Black 96-well plates	Lumox® multiwell 96 cell culture plate	Sarstedt (Nümbrecht)
Dako pen	-	Dako (Glostrup)
Eppendorf reaction tubes	1.5, 2 mL	Eppendorf (Hamburg)
Erlenmeyer flask	500, 1000, 2000 mL	Kimble Chase Life Science (Meiningen)
Glass beaker	100, 250, 600, 1000 mL	Kimble Chase Life Science (Meiningen)
Glass coverslips	24x65 mm thickness	R. Langenbrinck (Emmendingen)
Glass cuvette for electroporation	2 mm	Bio-Rad (Hercules)
Glass pearls	1.7-2.1 mm	Roth (Karlsruhe)
Glass slides	-	Engelbrecht (Edermünde)
Glass waste container	Sekuroka	Roth (Karlsruhe)
Gloves, nitrile	-	Kimberly-Clark (Koblenz)
LI-COR blotting membrane	-	LI-COR (Lincoln)
Measuring cylinder	100, 250, 500, 1000 mL	Kavalierglass (Sázava)
Parafilm	Bemis	neoLab Migge (Heidelberg)
Pasteur pipettes	-	ThermoScientific (Waltham)
Scalpel	-	Braun (Melsungen)
Sterile filter	0.22 µm Stericup Quick Release	Merck (Darmstadt)
Syringes	5, 20 mL	Braun (Melsungen)
Whatman™ paper	-	Sigma-Aldrich (Steinheim)
Wipes	Incidin Premium Wet Wipes	Ecolab (Monheim am Rhein)

2.1.15 Software and Databases

SOFTWARE / DATABASE	PROVIDER / URL
AlphaFold	https://alphafold.ebi.ac.uk
AutoSlice and View	FEI
AxioVision v4.7	Zeiss
Blender v7.79	https://www.blender.org
ChimeraX v1.4.0	https://www.cgl.ucsf.edu/chimerax/
Clustal Omega	https://www.ebi.ac.uk/Tools/msa/clustalo/
Envision Manager	Perkin Elmer
Fiji/ImageJ	https://imagej.net/software/fiji/
GraphPad Prism 9	GraphPad Software Inc.
Ilastik	https://www.ilastik.org
Interpro	http://www.ebi.ac.uk/interpro/entry/InterPro
Image Lab 5.2	Bio-Rad
Leica Application Suite X	Leica
LI-COR Image Studio	LI-COR
Microsoft Office	Microsoft
MitoProt II – v1.101	https://ihg.helmholtz-muenchen.de/ihg/mitoprot.html
Neuromorph	https://neuromorph.epfl.ch
NovoExpress 1.2.5	ACEA Biosciences Inc.
Parasitemia	http://www.gburri.org/parasitemia/
PlasmoDB	https://plasmodb.org/plasmo/app
RCSB Protein Data Bank	https://www.rcsb.org
Seahorse Wave	Agilent
Serial Cloner 2.6	Franck Perez

2.2 Methods

2.2.1 Polymerase Chain Reaction (PCR)

The polymerase chain reaction (PCR) was used to amplify specific DNA fragments from DNA templates that either subsequently were inserted into cloning vectors (“preparative PCR”) or were used for analytical agarose gels (“analytical PCR”). For preparative PCRs, the Phusion polymerase (NEB) was used which has proof-reading capacity thereby reducing the chance for errors, while for analytical PCRs the FirePol polymerase (NEB) was used. Primers were designed using the sequence information provided on PlasmoDB (www.plasmodb.org).

The reaction mixes for PCR are listed in Table 2. The standard PCR programs for preparative and analytical PCRs are listed in Table 3. PCR products were analyzed using agarose gel electrophoresis.

PREPARATIVE PCR		ANALYTICAL PCR	
5X HF Buffer	5 µL	10X FIRE Buffer	1 µL
dNTPs (2 mM)	2.5 µL	MgCl ₂ (25 mM)	0.8 µL
Primer forward (10 µM)	1 µL	dNTPs (2 mM)	1 µL
Primer reverse (10 µM)	1 µL	Primer forward (10 µM)	0.4 µL
Phusion Polymerase	0.25 µL	Primer reverse (10 µM)	0.4 µL
DNA template (10 ng/µL)	1 µL	FirePol Polymerase	0.16 µL
ddH ₂ O	to 25 µL	DNA template (10 ng/µL)	1 µL
		ddH ₂ O	to 10 µL

Table 2. PCR reaction mixes.

PREPARATIVE PCR			ANALYTICAL PCR		
Initial	94 °C	2:00	Initial	95 °C	3:00
Denaturation			Denaturation		
Denaturation	94 °C	0:20	Denaturation	95 °C	0:35
Annealing	42 °C	0:45	Annealing	42 °C	0:40
Elongation	62.5 °C	0:30/kb	Elongation	62 °C	1:00/kb
Final	72 °C	2:00	Final	64 °C	3:00
Elongation			Elongation		
Storage	4 °C	∞	Storage	12 °C	∞

Table 3. PCR cycling program.

2.2.2 Agarose gel electrophoresis

For agarose gel electrophoresis, 1 % agarose (w/v) was boiled in 1X TAE buffer in the microwave until completely dissolved. Subsequently, four drops of Ethidium bromide solution were added to 50 mL of boiled agarose and the mix was poured into a gel chamber for polymerization. For the formation of gel pockets, a comb was inserted before the gel polymerized. After polymerization, the comb was removed and the gel was transferred into an electrophoresis chamber that was filled with 1X TAE buffer. Loading dye was added to the DNA samples and samples were loaded. For comparison, a DNA ladder (GeneRuler 1kb) was pipetted into the first pocket. Gel electrophoresis was performed at 120 Volt for 30 min (or longer for fragments bigger than 3 kb). DNA fragments were visualized using UV light.

2.2.3 Purification of PCR products

After gel electrophoresis, PCR products can be purified from the agarose gel. The according bands were cut from the gel under low UV exposure. DNA purification was performed using the NucleoSpin® Gel and PCR Clean-Up Kit (Macherey-Nagel) following the manufacturer's

instructions. Products were eluted in 20 μL ddH₂O. Until further use, DNA was stored at 4 °C (for 1-2 days) or at -20 °C (for extended storage).

2.2.4 Restriction digest

To digest DNA plasmids or purified PCR products the reaction mixes listed in Table 4 were used. They were incubated at 37 °C for 2.5 hours (30 min to 2 hours for analytical digest). For the plasmid digest of backbones, 0.5 μL CIP Phosphatase were added to the mix which dephosphorylates the 5' overhangs thereby preventing re-ligation of the vector. The mix was incubated for another 30 min at 37 °C before purification of the fragments on an agarose gel. The respective band was cut and purified from the gel using the NucleoSpin® Gel and PCR Clean-Up Kit (Macherey-Nagel) for DNA purification. Digested PCR products were directly purified using the NucleoSpin® Gel and PCR Clean-Up Kit (Macherey-Nagel) following the manufacturer's instructions. Fragments of analytical plasmid digests were analyzed on an agarose gel but not purified.

	PLASMID DIGEST (BACKBONE)	PCR DIGEST (INSERT)	ANALYTICAL DIGEST OF PLASMIDS
DNA	2 μg	20 μL (after gel purification)	5 μL (after mini prep)
Enzyme 1	0.2 μL	0.2 μL	0.2 μL
Enzyme 2	0.2 μL	0.2 μL	0.2 μL
CutSmart Buffer	1 μL	2.5 μL	1 μL
ddH ₂ O	add to 10 μL	add to 25 μL	add to 10 μL

Table 4. Reaction mixes for restriction digests.

2.2.5 Ligation

To create a new plasmid, the desired insert and backbone were ligated using the overhangs created by restriction digest. For ligation, the reaction mix listed in Table 5 was used. The mix was incubated at room temperature for 20-60 min. Then, the whole mix was transformed into heat-shock competent bacteria.

LIGATION

Backbone DNA	50 ng
Insert DNA	1:3 Molar insert
Ligase Buffer	1 μL
T4 Ligase	0.25 μL
ddH ₂ O	to 10 μL

Table 5. Reaction mix for T4 ligation.

2.2.6 Production of heat-shock competent *E. coli*

E. coli bacteria were used for the amplification of plasmid DNA. The protocol for the production of competent bacteria followed published procedures (Inoue, Nojima and Okayama, 1990). A cryostabilate of *E. coli* XL10 Gold was incubated in 10 mL LB medium containing 50 µg/mL Ampicillin at 37 °C overnight on a shaker. The next day, 1 mL and 5 mL of this starter culture were added to 1 L of SOB medium (containing 10 mM MgCl₂) each. Both cultures were incubated at 18 °C shaking at 160 rpm until an OD₆₀₀ of 0.45-0.6 was reached. Bacteria were then pelleted at 3000 x g and 4 °C for 15 min. The supernatant was discarded and the bacterial pellet was resuspended in 20 mL ice-cold transformation buffer. After incubating it for 10 min on ice, the mix was centrifuged as before and the pellet was resuspended in 16 mL ice-cold transformation buffer. 1.2 mL DMSO were added dropwise while shaking the mix. 100 µL of competent bacteria were then transferred into Eppendorf reaction tubes and quickly frozen in liquid nitrogen. Aliquots were stored at -80 °C until use.

2.2.7 Heat-shock transformation of *E. coli*

Competent *E. coli* bacteria were transformed with plasmid DNA by heat-shock transformation. To do so, 100 µl of competent bacteria were thawed on ice for 10 min. 50-100 ng of plasmid DNA or the whole ligation reaction were added to the bacteria and incubated on ice for 10 min. The heat shock was performed at 42 °C for 45 seconds. After that, the mix was incubated for 3 min on ice and subsequently plated on LB agar plates containing the respective antibiotic(s). For plasmids encoding the resistance to kanamycin, 1 mL LB medium without antibiotics was added to the transformed bacteria. The mix was incubated at 37 °C for 30 min before spinning the bacteria down at 6000 x g for 2 min and subsequently plating them on LB agar plates containing kanamycin.

2.2.8 Plasmid isolation from *E. coli* culture

For the production of smaller amounts of DNA (e.g., for analytical digest), bacterial colonies were picked from agar plates and incubated in 1.8 mL LB medium containing the respective antibiotics at 37 °C, 600 rpm, overnight. The next day, plasmids were purified from the bacterial cultures using the NucleoSpin® Plasmid Kit following the manufacturer's protocol. Plasmids were checked by analytical digest and subsequent agarose gel electrophoresis before sending the DNA of clones of interest for sequencing.

For larger volumes of DNA (e.g., for transfection into *Plasmodium*), one bacterial colony of the correct clone was incubated in 100 mL LB medium containing the respective antibiotics at 37 °C, 200 rpm shaking, overnight using an 1 L Erlenmeyer flask. The plasmid DNA was purified following the manufacturer's instructions of the PureYield™ Plasmid Midiprep System (Promega) and stored at -20 °C until further use.

2.2.9 Cloning of pSLI constructs

For the generation of the SLI-based KO constructs for *pnpla2* and *lpl1* (List in Chapter 2.1.10 *Plasmids*), the 532 bp (*pnpla2*) or 423 bp (*lpl1*) region immediately downstream of the start ATG of the respective gene were amplified by PCR using the primers listed in Table 6 and cloned into the pSLI-TGD vector (Birnbaum *et al.*, 2017) using NotI/MluI restriction sites. The amplified region served as homology region for the single-crossover integration.

PRIMER	SEQUENCE	REF. NO.
1358000-KO-fw	gctat ttaggtgacactatagaataactcgcggccgcTAA GTTAAAAATGTTTATATATACTTTGTTTATTTAGTC	104
1358000-KO-rev	cctccagcaccagcagcagcacctctagcacgcgtTATG TAGTTCAGTTTTTCATGATTGC	105
1476700-KO-fw	gctat ttaggtgacactatagaataactcgcggccgcTAA ATGAATAAAAATGATATAACCATTTGATGAG	491
1476700-KO-rev	cctccagcaccagcagcagcacctctagcacgcgtT TTCGAAATGATTGATTCATAAACAC	492

Table 6. Primers used for cloning of SLI-based KO constructs for PNPLA2 and LPL1. Fw = forward, rev = reverse.

For the generation of pSLI-based tagging constructs (complete list in Chapter 2.1.10 *Plasmids*), cloning strategies were adapted: For pSLI-PF3D7_1358000-GFP, the C-terminal 1,063 bp region of *pnpla2* was amplified using the primers listed in Table 7. The fragment was cloned into the pSLI-GFP vector (Birnbaum *et al.*, 2017) using NotI/MluI.

For pSLI-PF3D7_1476700-mNeon-glmS, the 963 bp C-terminal region of *pf3d7_1476700* was amplified by PCR and cloned into a pSLI-mNeonGreen-glmS construct (kindly provided by Dr. Arne Alder and Maria Medina) using NotI/MluI. The pSLI-mNeonGreen-glmS vector is based on the original pSLI-GFP vector (Birnbaum *et al.*, 2017). However, the GFP cassette was replaced by a mNeonGreen-glmS cassette. All other features were identical to pSLI-GFP.

All other constructs were based on a pSLI-mScarlet plasmid. For its generation, first pSLI-PF3D7_0924000-GFP was cloned: Using the primers listed in Table 7, the C-terminal 973 bp region was amplified and cloned into pSLI-GFP via NotI/MluI restriction sites giving rise to the intermediate construct pSLI-PF3D7_0924000-GFP. The GFP cassette was exchanged for a mScarlet-encoding cassette that was amplified from SP-mScarlet (Mesén-Ramírez *et al.*, 2019) using the primers mScarlet-fw/mScarlet-rev (Table 7) and ligated into the final vector using AvrII/SalI restriction sites giving rise to the final plasmid pSLI-PF3D7_0924000-mScarlet. The backbone vector without the homology region created by PCR is now called pSLI-mScarlet. All other constructs were created by amplifying the respective gene loci by PCR using the primers listed in Table 7 and cloning the PCR products into the pSLI-mScarlet vector using MluI/NotI restriction sites.

Material and Methods

PRIMER	SEQUENCE	REF. NO.
0709700-mScarlet-fw2	ccaagctatTTtaggtgacactatagaataactcgcg gccgcTAAAGCAGTAGTCGATTAGATGG	497
0709700-mScarlet-rev2	gcacctccagcaccagcagcagcacctctagcacg cgtcctaggTACTTGTTCTTCTTGTTTGGG	498
0731800-mScarlet-fw2	ccaagctatTTtaggtgacactatagaataactcgcg gccgcTAAAATCAATCACATGGATTATCAGAGG	499
0731800-mScarlet-rev2	gcacctccagcaccagcagcagcacctctagcacg cgtcctaggGCTAAATATATTATTAAGCCAATCAA CAAATATC	500
1358000-GFP-fw	GCGCGCGGCCGCGAAGAAGAAATTAATTCCTCC	-
1358000-GFP-rev	GCGCACGCGTTGTTTCTTTTTTAAAAAAGAAACAT C	-
1411900-GFP-fw	gctatTTtaggtgacactatagaataactcgcggccg cTAATCTGGTTGGTGTGATGAAGGG	17
1411900-GFP-rev	cctccagcaccagcagcagcacctctagcacgcgt cctaggTTTTGTATTTAGCAAATCGGTTGG	18
1412000-GFP-rev	cctccagcaccagcagcagcacctctagcacgcgt cctaggAAGATCTGGAGGTATGTTAGC	20
1412000-GFP-fw	gctatTTtaggtgacactatagaataactcgcggccg cTAAATAATTTTGTTTCTTCTGTATAAGTG	19
1476700-mScarlet-fw	ccaagctatTTtaggtgacactatagaataactcgcg gccgcTAATATTCATGGGAAGTTAGGGAACC	489
1476700-mScarlet-rev	gcacctccagcaccagcagcagcacctctagcacg cgtcctaggTTCACATTTTTTTATCCAAGTTAAC	490
mNeon-fw	CAAATGCAGAGTCATCACATATAGAAGCACCTAGG atggaagtaagggagaagaagac	639
mNeon-rev	AACGAACATTAAGCTGCCATATCCCTCGACCCGGG TTActtatacaactcatccattcccattacg	640
mScarlet-fw	GAAAAATGTTTTTTTTcctaggacgcgtgctagag gtgctgctgctggtgctggaggtgcaggtagacgt acgATGGTGAGTAAGGGTGAGGC	483
mScarlet-rev	cttcctcttcttcttccGTCGACCTTGTAAGCTC ATCCATACC	484

Table 7. Primers used for SLI-based tagging constructs.

Correct integration of the constructs into the parasitic genome was verified by analytical PCR. Primers are listed in Table 8. Primer design was based on published protocols (Birnbaum *et al.*, 2017). Analytical PCRs consisted of three primer pairs (see Figure 7A + 8A):

Wildtype locus (WL)	WL fw WL rev
5' integration (5'int)	WL fw GFP rev*
3' integration (3'int)	WL rev int fw

*For mScarlet- or mNeon-glmS tagging lines, instead of GFP rev the primer Neo rev was used.

Material and Methods

NAME	SEQUENCE	REF. NO.
GFP-rev	ACCTTCACCCTCTCCACTGAC	63
int-fw	gcggataacaattttcacacagg	64
Neo-rev	gagaacctgcgtgcaatcc	173
0709700-TAG-3I	TTTGGAGTTACATAAAATGTACGTCAG	534
0709700-TAG-5I	ATCGAGGAAGAGCTCCACAG	533
0731800-TAG-3I	TCTTTTAATAACAAAATAGGCACACG	536
0731800-TAG-5I	GGACAATGTCTTATGAAAATAGTTGG	535
0924000-TAG-3I-2	CTACATAATATAACAGCATTTAAGGG	94
0924000-TAG-5I-2	CTATGGATTTTCAAGATAGCTTGG	93
1358000-TAG-5I	GCCAAACAGAAAATCGAAAAGATTC	-
1358000-TAG-3I	AAATTAAAGAATGTAGAAATGAAAGG	106
1411900-TAG-3I	TCTAGTTGTTGTAATGGTCTAATTTG	82
1411900-TAG-5I	CCTTCCCTATTTTCATCCGACC	81
1412000-TAG-3I	AGGATGGCCAGGATTTAGCC	84
1412000-TAG-5I	GATTTGCCTTGTACACAACCG	83
1476700-TAG-3I	AAAATCCGCCATAAATAAATGAAA	509
1476700-TAG-5I	CATTTTCCGAGCTTCTAGTTTTT	508
0709700-KO-3I	AAAACGTAAACCAGGAGTAAGACG	203
0709700-KO-5I	TCCATATTCCCATTTTCTTTTCG	202
0731800-KO-3I	CCACAATTACAATATTTTGAAGACC	231
0731800-KO-5I	TTTTTCTTTAAGTATAGGAAATTTAATGG	230
0924000-KO-3I	CATTTCCGTGACTGTTTCTGGG	88
0924000-KO-5I	TGTTTCTTTAAATGAAGCTTCCGC	87
1358000-KO-3I	AATTCAGTTGAGCTGTCTCTGC	143
1358000-KO-5I	TTTTTCTCCTTCTTTCTTTTATACC	142
1411900-KO-3I	TCTAGTTGTTGTAATGGTCTAATTTG	82
1411900-KO-5I	CCTTCCCTATTTTCATCCGACC	81
1412000-KO-3I	AGGATGGCCAGGATTTAGCC	84
1412000-KO-5I	GATTTGCCTTGTACACAACCG	83
1476700-KO-3I	CATTCCAGCTAAAGAAATAAATGC	538
1476700-KO-5I	AAATTATTAATCGATCTTTGTTTTG	537

Table 8. Primers used for analytical PCRs. Primer names are termed according to the gene ID, the purpose of the construct (TAG = tagging; KO = knockout) and the direction (5I = WL fw, 3I = WL rev).

2.2.10 Sequencing of plasmid DNA

DNA sequencing was performed by Microsynth (Balgach, <https://www.microsynth.com/>). For sequencing, 800-1200 ng of plasmid DNA were sent to Microsynth in a final volume of 12 µL. Typically, standard primers were used. If not, 3 µL of sequencing primers (10 µM) were added before shipping. Sequencing results were available for download the next working day. Sequence alignment was performed using Serial Cloner v2.6.

2.2.11 DNA precipitation using sodium acetate

For transfection into parasites, 50 µg of DNA were precipitated using 2.5X volume 100 % ethanol (ice-cold) and 1/10X volume 3 M sodium acetate. After brief vortexing, the sample was incubated at -20 °C for a minimum of 30 min. Subsequently, the precipitated DNA was spun at 20,000 x g, 30 min, 4 °C. The supernatant was discarded and the pellet was washed in 1 mL 70 % ethanol. After centrifugation at 20,000 x g, 15 min, 4 °C the supernatant was discarded again. The DNA pellet was air-dried under a sterile workbench before resuspending it in 10 µL sterile TE buffer. DNA was stored at 4 °C until transfection.

2.2.12 Isolation of genomic DNA from *P. falciparum*

For isolation of genomic DNA (gDNA) from *P. falciparum*, 5 mL of resuspended parasite culture (min. 2 % parasitemia, preferably trophozoite and schizont stages) were pelleted at 800 x g for 3 min. The supernatant was discarded and the pellet was used for gDNA isolation using the QIAamp® DNA Mini Kit (Qiagen). Isolation followed the manufacturer's instructions. The DNA was finally eluted in 50 µL ddH₂O and stored at -20 °C until further use.

2.2.13 SDS gel electrophoresis and Western Blot

Using denaturing SDS gel electrophoresis proteins can be separated according to their molecular weight. To pour SDS gels, the following mixes were used:

SEPARATING GEL (10 %)		STACKING GEL (6 %)	
40 % Acrylamide	2 mL	40 % Acrylamide	0.75 mL
1.5 M Tris pH 8.8	2 mL	0.5 M Tris pH 6.8	1.25 mL
10 % SDS	80 µL	10 % SDS	50 µL
10 % APS	80 µL	10 % APS	50 µL
TEMED	8 µL	TEMED	5 µL
ddH ₂ O	3.8 mL	ddH ₂ O	2.9 mL

Table 9. Recipes for SDS gels.

The addition of TEMED and APS started the polymerization reaction. The mix for the separating gel was poured into an assembled chamber and overlaid with isopropanol to get an even border at the top. The gel was incubated at room temperature until fully polymerized. After washing the top of the polymerized separating gel with water, the mix for the stacking gel was layered on top and a comb was inserted. Fully polymerized gels could be stored in a humid chamber for up to one week but preferably were used fresh.

The SDS gels were inserted into the gel chamber. Protein samples were boiled in SDS loading dye (final concentration: 1X) at 95 °C for 5 min for denaturation and subsequently spun down at 21,000 x g for 2 min. 15 µL of sample were loaded next to a molecular weight marker (Chameleon Duo Prestained Protein Ladder, 1 µL + 14 µL 1X SDS loading dye to adjust the volume). The gels were run at 100 Volt for 30 min, then at 120 Volt for another ca. 70 min until the loading dye had just run out of the gel. After SDS-PAGE, proteins were transferred onto a nitrocellulose membrane using a tank Western Blot system (Bio-Rad). The transfer of proteins from the gel to the membrane occurred between one sponge and three Whatman papers on each side soaked in Western Blot Transfer Buffer. A cool pack was placed in the blotting chamber. The transfer was performed at 90 Volt for 60 min at 4 °C. After the transfer, membranes were blocked in 5% milk in TBS for 1 hour at room temperature before incubating them with the primary antibody rolling or shaking at 4 °C overnight. Primary antibodies were diluted in TBS-Tween or 5% milk in TBS-Tween. The next day, membranes were washed in TBS-Tween three times for 10 min before incubating with the secondary antibody for more than 2 hours at room temperature in the dark. Secondary antibodies were diluted in TBS-Tween. Subsequently, membranes were washed as before. Antibody-binding was detected using the Odyssey® Fc Imaging System (LI-COR).

2.2.14 Sterilization of solutions and materials

The buffers and materials used for cell biological experiments throughout this thesis were sterilized at 121 °C and 1.5 bar steam pressure. Heat-instable solutions were sterile filtered using Stericup filters with a pore size of 0.22 µm.

2.2.15 Cultivation of *P. falciparum*

P. falciparum blood stages were cultured in cRPMI at 5 % hematocrit (blood group 0+ or B+, Universitätsklinikum Hamburg-Eppendorf). The presence of 2 mM choline in the cRPMI culture medium prevented unwanted induction of gametocyte commitment (Brancucci *et al.*, 2017; Filarsky *et al.*, 2018). Cultures were maintained at 37 °C in an atmosphere of 94 % nitrogen, 5 % carbon dioxide and 1 % oxygen according to standard procedures (Trager and Jensen, 1976). Asexual intraerythrocytic development takes approx. 48 hours. Each replication cycle leads to a 5- to 8-fold increase in parasitemia. Parasites were cultured at low parasitemias and fed every second to third day for continuous culture. When cultured at high

parasitemias or during experiments, parasites were fed daily and the hematocrit was lowered by adding more medium to the cultures (if required). Cultures of NF54/iGP2-based parasites were cultured in the presence of 2.5 mM glucosamine (GlcN) to prevent overexpression of the gametocyte commitment factor GDV1 (Boltryk *et al.*, 2021).

2.2.16 Production of synchronous *P. falciparum* gametocytes

Gametocytes could be induced in NF54/iGP2-derived (Boltryk *et al.*, 2021) or 3D7CH-derived (Filarsky *et al.*, 2018) parasite lines following the established protocols.

i) NF54/iGP2 background

For the induction of gametocytes, synchronous ring stage cultures (2-3 % parasitemia) were washed in cRPMI to remove remaining GlcN and plated at 2.5-5% hematocrit (= day -1, generation 1). Gametocyte cultures were fed daily. After reinvasion (= day 1 of gametocytogenesis), asexual parasites were depleted using 50 mM GlcNAc in the culture medium. GlcNAc was added to the cell culture medium until day 6. From day 7 until day 14, gametocyte cultures were fed with culture medium containing 0.25 % Albumax + 5 % human serum (instead of 0.5 % Albumax). Gametocytes were cultured in the presence of GlcN from day 1 onwards. Gametocyte stages and gametocytemia were monitored using Giemsa-stained thin blood smears.

ii) 3D7CH background

For the induction of gametocytes, synchronous ring stage cultures were washed twice in cRPMI medium without choline (= day -1). Gametocyte cultures were fed daily. From day 1 of gametocytogenesis (generation 2) until day 6, asexual parasites were depleted using 50 mM GlcNAc in the culture medium (now again containing choline). From day 7 until day 14, gametocyte cultures were fed with culture medium containing 0.25 % Albumax + 5 % human serum (instead of 0.5 % Albumax) and choline. Gametocyte stages and gametocytemia were monitored using Giemsa-stained thin blood smears.

2.2.17 Giemsa staining of blood smears for routine culture and stage quantifications

To monitor parasite development and parasitemia, thin blood smears of parasite cultures were fixed with Methanol and stained with Giemsa solution for 10-15 min (Giemsa, 1904). After extensive rinsing with tap water, blood smears were examined at a Leica DM2000 LED microscope equipped with a Leica DMC2900 camera.

For stage quantification of asexual blood stages, Giemsa-stained blood smears of tightly synchronized parasite cultures were prepared at 24, 32, 40, 48, 60, and 72 hpi. Images of these smears were taken with a 63X objective. Per parasite line and day, at least 20 fields of view were recorded. Erythrocyte numbers were determined using the Parasitemia software

(<http://www.gburri.org/parasitemia/>). Infected RBCs were counted manually. For quantification of the number of daughter merozoites per schizont, the cysteine protease inhibitor E64 (10 μ M, Sigma) was added to tightly synchronized schizonts at 40 hpi. E64 prevents rupture of the RBCM but not the PVM. At 46–48 hpi, Giemsa smears were prepared and the number of daughter merozoites was counted. For the quantification of gametocyte maturation, Giemsa smears were taken daily. 20 fields of view were imaged per parasite line and day. Erythrocyte numbers were counted using the Parasitemia software. Gametocyte stages were counted manually. Gametocyte commitment rates were calculated as the ratio of parasitemia on day 6 / parasitemia on day 2. Gametocyte survival rates were calculated as the ratio of parasitemia on day 10 / parasitemia on day 6 (for 3D7CH-derived lines) or as the ratio of parasitemia on day 11 / parasitemia on day 5 (for NF54/iGP2-derived lines).

2.2.18 Freezing and Thawing of *Plasmodium* cryostabilates

For extended storage of (transgenic) parasite lines, 5–10 mL of ring stage culture were pelleted at 800 x g for 3 min. The supernatant was discarded and the pellet of infected and uninfected RBCs was resuspended in 1 mL Malaria Freezing Solution (MFS). The mix was transferred into a cryotube and immediately placed at -80 °C. For thawing of such cryostabilates, the stabilates were quickly thawed in a water bath (37 °C). The thawed culture was transferred into a 15-mL falcon tube and centrifuged at 800 x g for 3 min. The supernatant was discarded and the pellet was resuspended in 1 mL prewarmed Malaria Thawing Solution (MTS). After another centrifugation step, the pellet was washed once in cRPMI before transferring it into a cell culture dish for standard culture. For optimal growth conditions, fresh RBCs (final hematocrit 5 %) were added.

2.2.19 Isolation of parasites using saponin lysis

Treatment of infected RBCs with hemolytic saponin results in the disintegration of the RBCM and the PVM due to the higher cholesterol content compared to the parasite. Intact parasites can then be sedimented by centrifugation. For saponin lysis, infected RBCs were sedimented by centrifugation at 800 x g for 3 min. The supernatant was discarded. The pellet was resuspended in 0.03 % saponin in PBS (if not indicated otherwise; Sigma) and incubated on ice for 10 min. Saponin-freed parasites were sedimented by centrifugation at 2500 x g for 5 min at 4 °C. The samples were washed in ice-cold PBS until the supernatant was clear. Finally, the supernatant was taken off and the parasite pellet was stored at -20 °C until further processing. For Western Blot analysis, pellets of saponin-lysed parasites were resuspended in Western Blot lysis buffer and mixed with SDS Loading Dye before boiling and running on an SDS gel.

2.2.20 Isolation of schizonts using Percoll

To separate schizonts or gametocytes (stage III or later) from other stages and uninfected RBCs, 3-4 mL of 60 % Percoll solution were placed in a 15-mL falcon. Max. 10 mL of resuspended parasite culture were slowly layered on top before centrifugation at 800 x g for 5 min without acceleration or brake. Schizonts / Gametocytes could be found in a dark band at the interface of Percoll and medium while all other stages pellet with the uninfected RBCs at the bottom of the falcon tube. The schizont / gametocyte layer was taken off and transferred into a falcon with 5 mL fresh medium. After centrifugation at 800 x g for 3 min, the pellet was either used for reinvasion (schizonts) or for Western Blot analysis (schizonts / gametocytes). For Western Blot analysis, the pellets of gametocytes were resuspended in Western Blot lysis buffer and mixed with SDS Loading Dye before boiling and running on an SDS gel.

2.2.21 Synchronization of rings using sorbitol

P. falciparum cultures can be synchronized using sorbitol lysis (Lambros and Vandenberg, 1979) since Sorbitol treatment leads to lysis of trophozoite and schizont stages while leaving ring stages and RBCs intact. Of note, gametocytes are resistant to sorbitol treatment. For synchronization, the cultures were pelleted at 800 x g for 3 min before resuspending the pellet in prewarmed 5 % Sorbitol solution. After incubation for 10 min at room temperature, RBCs were pelleted at 800 x g for 3 min. The pellet was resuspended in fresh cRPMI and transferred into a fresh cell culture dish. Synchronized parasites were cultured again under standard conditions.

2.2.22 Tight synchronization of parasites via reinvasion

Sorbitol treatment allows for synchronization of ring stages. However, to tightly synchronize parasites to a narrow time window, reinvasion assays were performed. First, schizonts were isolated by Percoll density gradient centrifugation as described before. These schizonts were transferred into a sterile 1.5-mL Eppendorf reaction tube prepared with 250 µL fresh RBCs and 250 µL fresh cRPMI. The mix was incubated at 37 °C, 700 rpm, for 30 min before being transferred into a culture dish with fresh cRPMI. After another 2.5 hours of incubation at 37 °C, the cultures were synchronized by Sorbitol treatment. As only freshly re-invaded rings survive, this results in a synchronous culture within a three-hour window.

2.2.23 Transfection of *P. falciparum*

For the transfection of plasmid constructs, schizonts were enriched using Percoll and mixed with 50 µg of plasmid DNA dissolved in TE buffer. The mix was transferred into a cuvette and electroporated using program U-33 of the Lonza Nucleofector II device (Moon *et al.*, 2013). The electroporated parasites were immediately transferred into a sterile Eppendorf tube with

250 μ L prewarmed cRPMI and 250 μ L fresh RBCs, and incubated at 37 °C, 700 rpm, for 15-30 min. Afterward, the parasites were cultivated under standard conditions in cell culture dishes. 24 hours post transfection, drug selection pressure was applied using 3 nM WR99210. The medium was changed daily for five days. In our system, WR99210 allowed for the selection of episomal plasmids (Birnbaum *et al.*, 2017). For the selection of integrants, WR99210 was replaced by 400 μ g/mL Neomycin after the outgrowth of parasites. Again, the medium was changed daily for five days and cultures were monitored closely for the outgrowth of parasites (Birnbaum *et al.*, 2017). Successful integration of the pSLI constructs into the respective gene loci was confirmed by analytical PCR.

2.2.24 Immunofluorescence assays (IFA) of transgenic parasites

For immunostaining, thin blood smears were fixed in ice-cold methanol for 3 min and air-dried. Using a Dako pen, a barrier to liquid was drawn around the region of interest on the slide. The fixed blood smear was rehydrated using PBS before blocking unspecific binding sites with 3 % BSA in PBS for 30 min. Subsequently, the primary antibody (e.g., against the mScarlet tag) was added in 3 % BSA and incubated for 1 hour at room temperature. After extensive washing with PBS, a second primary antibody (targeting another protein of interest, e.g., an apical marker) was added and incubated for 1 hour at room temperature. After extensive washing with PBS, secondary antibodies linked to fluorophores were added and incubated for 1 hour at room temperature in the dark to avoid bleaching. Again, slides were washed extensively using PBS before adding 1 mg/mL DAPI in PBS for 10 min. After washing, one drop of Mowiol Mounting Medium was placed in the middle of the region of interest and covered with a cover slip. The edges were sealed using nail polish. The mounting medium was allowed to polymerize at 4 °C overnight before imaging.

2.2.25 Mitochondrial staining using MitoTracker or Rhodamine

For staining the mitochondrion/mitochondria of live parasites, two live-cell dyes were used:

i) MitoTracker

Tightly synchronized cultures were stained with 20 nM MitoTracker Red CMXRos (Invitrogen) in cRPMI for 15 min at 37 °C. For staining of the nuclei, 0.45 μ g/mL Hoechst were added to the mix. After incubation, cells were washed once in cRPMI and imaged to analyze the mitochondrial morphology. Staining was performed at several time points between 24 hpi and 40 hpi. Late-stage schizonts (40 hpi) were arrested using Compound 2 for 4 hours. For analysis, the age of the parasites was corrected using the number of nuclei (1, 2, 3+) to allow comparison of the staining patterns in WT and PNPLA2-KO parasites. Image acquisition was performed using the same settings for all samples and all replicates.

ii) Rhodamine123

Tightly synchronized cultures were stained with 0.1 µg/mL Rhodamine123 (for asexual stages) or 0.5 µg/mL Rhodamine123 (for gametocytes) in cRPMI for 30 min at 37 °C. 0.45 µg/mL Hoechst were added to the mix to visualize the nuclei. After incubation, cells were washed once in cRPMI before imaging. For asexual stages, Proguanil was included in the assay by treating tightly synchronized ring stage cultures with 200 nM Proguanil, 1 µM Proguanil, or DMSO (as solvent control) from 3 hpi until imaging. At 40 hpi, Compound 2 was added to the cultures to prevent egress. Rhodamine123 staining was performed at 48 hpi. For gametocytes, samples treated with 50 µM FCCP were included as a control since FCCP disrupts the mitochondrial membrane potential, thereby leading to a cytoplasmic Rhodamine123 signal. Gametocyte staining was performed on day 6 of gametocytogenesis. Image acquisition was performed using the same settings for all samples and for replicates.

2.2.26 Fluorescence microscopy

Parasites (live or fixed and stained in an IFA) were imaged on a Leica DM6 fluorescence microscope equipped with a Leica DFC9000GT camera and a Leica Plan Apochromat 100x/1.4 oil objective. Image processing was performed using ImageJ. The filter settings used were:

DAPI (325-375/435-485)

GFP (460-500/512-542)

TXR (542-582/604-644)

2.2.27 Electron microscopy

In general, the protocol for parasite fixation and embedding followed published procedures (Bisio *et al.*, 2020; Lentini *et al.*, 2021). *P. falciparum* parasites were synchronized to a three-hour time window by performing a reinvasion assay. At 38-40 hpi, schizonts were purified on 60% Percoll, washed in medium once, and arrested for four hours in the presence of 50 nM ML10 (Ressurreição *et al.*, 2020). Parasites were pelleted at 800 x g for 3 min, and washed in PBS once. All further centrifugation steps were performed at 800 x g for 2 min at room temperature. If the parasite pellet was stuck to one side, the tube was turned by 180° and the spin was repeated. Parasites were fixed with 2.5 % glutaraldehyde / 2 % paraformaldehyde in 0.1 M sodium cacodylate buffer at pH 7.4 for 1-2 hours at room temperature followed by three washes in 0.1 M sodium cacodylate buffer for 10 min each. Post-fixation was performed using 1 % osmium tetroxide and 1.5 % potassium ferrocyanide ("reduced osmium") in 0.1 M sodium cacodylate buffer, pH 7.4, 1 hour. Additional post-fixation was performed using 1 % osmium tetroxide in 0.1 M sodium cacodylate buffer, pH 7.4, for 1 hour. Parasites were then washed twice in double-distilled water for 10 min before embedding in 1% agarose. Embedded samples were stained with aqueous 1% uranyl acetate at 4°C overnight. The next day, samples were washed twice in double-distilled water for 5 min per wash. For dehydration, samples were incubated in graded ethanol series (2x 50%, 70%, 90%, 95%, 2x 100% EtOH) for 10 min

per wash. After dehydration, samples were infiltrated with graded series of Durcupan resin diluted with EtOH at 1:2, 1:1, 2:1 for 30 min each. Infiltration was completed with two 30-min infiltration steps in fresh Durcupan followed by 2-4 hours in fresh Durcupan. Samples were then embedded in Durcupan resin and polymerized at 60 °C for 24-48 hours. The sample in the resin block was cut out and glued onto a flat blank resin block with super glue. Silver conductive paste was applied on each side of the resin block to make it conductive and the mounted sample was coated with a 20 nm thick layer of gold.

The samples were imaged using a FEI Helios 660 NanoLab G3 UC DualBeam microscope (FEI). The ion beam was used in conjunction with a gas injection system to deposit a thick (~1.5 µm) layer of platinum on the top surface of the sample above the region of interest in order to reduce the FIB milling artefacts. The imaging surface was exposed by creating the front trench using 21 nA of focused ion beam current at 30 kV. Using the same parameters two side trenches were created. AutoSlice and View 4.2 software (FEI) were used to acquire the serial SEM images. A focused ion beam at a current of 2.5 pA and 30kV of acceleration voltage was applied to mill a 10 nm layer from the imaging face. The freshly exposed surface was imaged with a backscattered electron beam current of 400 pA at an acceleration voltage of 2 kV, a dwell time of 9 µs/pixel, and at the resolution of 5 nm/pixel.

Serial images through the selected region of interest were combined into single image stacks and aligned using the FIJI/ImageJ. Aligned images were scaled down by factor 2 in order to have a volume with isotropic voxels properties of the 10 nm/pixel in all x-, y- and z-dimension. For 3D reconstruction, the size of the final cell volume in x-, y- and z-dimension was 679 × 914 × 841 pixels corresponding to 6.79 × 9.14 × 8.41 µm for the 3D7 WT sample and 661 × 775 × 626 pixels corresponding to 6.61 × 7.75 × 6.26 µm for PNPLA2-KO sample respectively. For segmentation and 3D reconstruction, a semi-automated approach using the Ilastik software was used. Final 3D models were visualized using Blender.

2.2.28 Proliferation assay with *P. falciparum*

Flow cytometry is a fast and simple method to quantify parasitemia. Thus, it was used to follow parasite proliferation. Parasite nuclei were stained with dihydroethidium (DHE) and SYBR Green I to differentiate them from uninfected RBCs (that do not have a nucleus) (Malleret *et al.*, 2011). For staining, 20 µL resuspended parasite culture were incubated with 80 µL cRPMI, 5 µg/mL DHE and 0.25X SYBR Green for 30 min in the dark. At least 100,000 singlet events were recorded by the flow cytometer NovoCyte 1000 (ACEA). The gating strategy followed published protocols (Malleret *et al.*, 2011).

For a standard parasite proliferation assay, WT parasites (parental parasite line) and the transgenic parasite line of interest were tightly synchronized by reinvasion. At the trophozoite stage, the parasitemia was adjusted to 0.1 %. Parasite growth was monitored over two cycles with daily changes of the medium. In general, parasites were cultured in cRPMI.

For experiments in mFA medium, parasites were tightly synchronized in cRPMI. At the trophozoite stage, the parasitemia was adjusted to 0.1 % in mFA medium and cultures were maintained in mFA medium from then onwards. mFA medium was changed daily.

For the DCUQ supplementation assay, the proliferation assay was performed in the presence of DMSO (as solvent control) or different concentrations of DCUQ (Cayman, stock prepared in DMSO). As a positive control, WT parasites were treated with 1.15 nM Atovaquone (IC_{50} value according to Agarwal *et al.*, 2017) in addition to DMSO/DCUQ. Medium containing DMSO/DCUQ/Atovaquone was changed daily.

For the Trolox assay, parasite proliferation was monitored in the presence of DMSO, 10 μ M Trolox, or 100 μ M Trolox (stock prepared at 8 mM in RPMI) with daily medium changes.

2.2.29 Drug susceptibility assays

To study the susceptibility of WT and PNPLA2-KO parasites to antimalarial drugs, parasite cultures were tightly synchronized as described earlier. At 24 hpi, the parasitemia was determined by flow cytometry and adjusted to 0.1% starting parasitemia at 2% hematocrit (Wichers *et al.*, 2021). The assay was set up in black 96-well microtiter plates.

Drugs were prepared in PBS (Primaquine, freshly prepared for every assay) or DMSO (all other drugs). For each drug, serial drug dilutions were performed in duplicates in cRPMI. Parasite-infected RBCs were plated in a final volume of 200 μ L/well. The final concentration of DMSO did not exceed 0.5%. As positive control, infected RBCs were treated with the respective solvent; as negative control, uninfected RBCs were plated and used for background subtraction.

After 96 hours of incubation, parasite proliferation was determined: 100 μ L/well supernatant were discarded without disturbing the RBC layer before adding 100 μ L/well of lysis buffer (20 mM Tris, 5 mM EDTA, 0.008% saponin, 0.08% Triton X-100, 1xSYBR Gold). Plates were incubated at room temperature for 2 hours in the dark before measuring fluorescence using the EnVision Multimode plate reader (PerkinElmer) with excitation and emission wavelengths of FITC 485 / FITC 535. In order to calculate the 50 % inhibitory concentration (IC_{50}) values, the measured values were normalized to uninfected RBC and plotted in GraphPad Prism version 9 (GraphPad Software, USA) as a percentage of the value for the DMSO control. Dose-response curves were generated using nonlinear regression (curve fit > dose-response inhibition > (log) inhibitor versus normalized response—variable slope).

2.2.30 Measurement of oxygen consumption rates (Seahorse Assay)

Measurement of the oxygen consumption rate (OCR) was performed using a XFe96 Seahorse analyzer (Agilent). Coating of the CellTak plate to seed parasites and soaking of the sensors

were performed according to the manufacturer's instructions (Agilent). The protocol for measuring the OCR of *Plasmodium* followed published procedures (Sakata-Kato and Wirth, 2016; Hayward, Makota, *et al.*, 2022; Hayward, Rajendran, *et al.*, 2022).

For the measurement, *Plasmodium* parasites had to be freed from the surrounding RBCs and permeabilized. On the day of the assay, tightly synchronized schizonts were harvested at 38 hpi. 30 mL of culture at 5 % (v/v) hematocrit and >3% parasitemia were pelleted in 2x50 mL falcons. Pellets were lysed in 50 mL prewarmed 0.15 % (w/v) saponin (BDH Bioscience) each for 5 min at 37 °C. The obtained parasite pellets were washed with PBS twice and resuspended in MAS supplemented with BSA and malate (but without digitonin) for counting. Parasites were counted using a hemocytometer and prepared at 5×10^7 cells/mL in complete MAS (MAS supplemented with BSA, malate, digitonin and 0.1 % DMSO, final concentration). 100 μ L parasite suspension were plated into CellTak-coated wells of a XFe96 cell culture plate and centrifuged at 800 x g, 5 min, RT with the brake set to 1 to adhere parasites to the bottom. The plate was then turned by 180° and the spin was repeated to allow even settling. 75 μ L/well complete MAS were carefully added to all wells to avoid disturbance of the cell layer. Cells were plated in at least 8 wells per drug regimen. Drugs were prepared in MAS with a final DMSO concentration of 0.1 %. Drugs were loaded into the ports A-D of the XFe96 sensor cartridge in a volume of 25 μ L.

Port A: FCCP. Prepared at 8X concentration for final 2 μ M.

Port B: Atovaquone. Prepared at 9X concentration for final 1 μ M.

Port C: TMPD/Ascorbate. Prepared at 10X concentration for final 0.2 nM TMPD / 3.3 mM Ascorbate.

Port D: Sodium azide. Prepared at 11X concentration for final 10 mM.

The OCR was measured for five cycles of 20 s mixing, 1 min waiting, 2.5 min measuring at baseline and after each injection.

The first step of analysis included the subtraction of the background (corner wells without cells). Then, the average of the values obtained after injection of Atovaquone was calculated to determine the non-mitochondrial OCR which in turn was subtracted from the average of the values after injection of FCCP (maximal OCR; here same as basal OCR, OCR_{Basal}) or TMPD (for OCR_{TMPD}), respectively. The ratio OCR_{TMPD}/OCR_{Basal} illustrates the extent to which TMPD can rescue the defect of the mtETC. Large outliers that most likely result from improper injection of the drugs were removed during the analysis as suggested previously (Hayward, Rajendran, *et al.*, 2022).

2.2.31 Lipidomic analysis

For lipidomic analysis, parasites were tightly synchronized to a three-hour time window. Each individual reinvasion represents one biological replicate. Samples were treated independently of each other throughout the experiment(s).

At 40 hpi, parasites were treated with Compound 2 for 4 hours. The resuspended parasite culture was stained for flow cytometry according to the staining procedure used for proliferation assays. From the volume required for the acquisition of 100,000 events by flow cytometry, the absolute number of parasites in the respective culture was calculated. At 44 hpi, aliquots of 100-200 Mio. parasites were prepared for lipidomic analysis by transferring the respective amount of culture into 15-mL falcon tubes and centrifuging it at 800 x g for 5 min. The supernatant was discarded and the pellets were resuspended in 15 mL ice-cold 0.03 % saponin (Sigma) in DPBS to free the parasites from the RBCs. After a 10-min incubation step on ice, samples were spun at 3000 rpm for 5 min at 4 °C. After two washing steps in 15 mL ice-cold DPBS, pellets were resuspended in 1 mL ice-cold DPBS and transferred into 1.5 mL-screw cap PP vials (Sarstedt). The final spin was performed at 800 x g, 5 min, 4 °C. The supernatant was taken off and pellets were snap-frozen in liquid nitrogen. The samples were overlaid with nitrogen and stored at -80°C until shipment on dry ice to Dr. Markus Keller and Yvonne Wohlfarter, University of Innsbruck, Innsbruck, Austria, for lipid extraction and mass spectrometric analysis.

Cardiolipins (CL) and selected phospholipids were analyzed utilizing lipid extraction and sample analysis procedures as described previously (Oemer *et al.*, 2018, 2020; Wohlfarter *et al.*, 2022 (accepted for publication in CLMS)). Briefly, *P. falciparum* parasites were homogenized and lipids were extracted following the Folch method (Folch, Lees and Stanley, 1957) using 1 ml of 2/1 CHCl₃/MeOH extraction solvent containing 0.5 µM internal standards (CL(14:0)₄, PE(14:0)₂, PC(14:0)₂, PG(14:0)₂, PI(14:0)₂, PA(14:0)₂; Avanti Polar Lipids). Samples were dried under nitrogen gas flow and dissolved in salt-free starting solvent for subsequent HPLC-MS/MS analysis. Experiments were performed using a UHPLC-Elute system coupled with a trapped ion mobility spectrometry time-of-flight mass spectrometer (timsTOF, Bruker Daltonics, Bremen, Germany). Separation was carried out on a reverse phase Agilent Poroshell 120 EC-C8 2.7mm 2.1x100 mm column (Agilent Technologies, Santa Clara, USA) at 40°C. For CL and phospholipid separation, mobile phase A consisted of 60/40 ACN/H₂O, 10 mM ammonium formate, 0.2% formic acid, and mobile phase B of 90/10 IPA/ACN, 10 mM ammonium formate, 0.2% formic acid. HPLC gradients of respective methods are listed in Table 10. Spectrometric data were acquired in the 1000-1750 m/z range for CL and 150-1350 m/z for phospholipids in ESI-negative mode, monitored with a spectra rate of 5Hz. MS parameters for the respective methods are listed in Table 11.

For CL analysis, data were converted to .mzML format using MZmine3 (Version 3.0.0.0) and further analyzed in MZmine (Version 2.53) with the targeted feature extraction method (Pluskal *et al.*, 2010). Phospholipids were analyzed using TASQ (Bruker Daltonics, Bremen,

Germany) with targeted feature extraction. Extracted peak areas were processed with R (Version 4.1.1) and visualized in GraphPad Prism 9. Data were normalized to parasite number as counted by flow cytometry, or to 1 to obtain CL/phospholipid profiles. The unsaturation index was determined via the weighted average of the double bond number in CLs (Levental *et al.*, 2020; Symons *et al.*, 2021), whereas the double bond and carbon chain length were calculated as the sum of all species containing the respective amounts of carbons or double bonds in each sample.

CL ANALYSIS			PHOSPHOLIPID ANALYSIS		
Time [min]	Mobile Phase B [%]	Flow [ml/min]	Time [min]	Mobile Phase B [%]	Flow [ml/min]
0	50	0.4	0	40	0.4
2	50	0.4	3	40	0.4
14	73	0.4	20	65	0.4
15	99	0.4	22	99	0.5
18	99	0.4	25	99	0.5
19	50	0.4	26	40	0.4
20	50	0.4	28	40	0.4

Table 10. HPLC gradients for lipidomic analysis.

ESI SOURCE	CL METHOD	PHOSPHOLIPID METHOD
Polarity	Negative	Negative
End Plate Offset	500V	500V
Capillary	4500	4200
Nebulizer	2.5 Bar	3 Bar
Dry gas	10.0 L/min	10.0 L/min
Dry temperature	250°C	220°C
Tuning Parameters		
Deflection 1 Delta	-90 V	-80 V
Funnel 1 RF	317 Vpp	250 Vpp
Funnel 2 RF	503 Vpp	250 Vpp
isCID Energy	100 eV	0 eV
Multipole RF	1200.0 Vpp	200 Vpp
Ion Energy	10.0 eV	5.0 eV
Low Mass	1395.24 m/z	150 m/z
Collision Energy	20.0 eV	10.0 eV
Collision RF	4000.0 Vpp	1100.0 Vpp
Transfer Time	70 μ s	65 μ s
Pre-Pulse Storage	25.0 μ s	5.0 μ s

Table 11. Mass spectrometer parameters for lipidomic analysis.

2.2.32 Exflagellation assays of mature *P. falciparum* gametocytes

From day 11 until day 14 of gametocytogenesis, exflagellation was determined daily in technical duplicates. 250 μ L of resuspended gametocyte culture were spun down in an Eppendorf tube at 800 x g, 1 min. The supernatant was discarded and the pellet was resuspended in 250 μ L prewarmed (26 °C) ookinete medium supplemented with 20 % human serum. Preliminary experiments at 19 °C showed lower exflagellation rates (data not shown). Gametocytes were incubated for 12 min at 26 °C. Then, 6 μ L were placed on a slide and covered with a coverslip. For 5 min, all gametocytes as well as exflagellation events were counted using a 40x oil objective (aperture closed as much as possible to contrast the hemozoin). If indicated, the observation time was extended for another 10 min to detect a potential delay in exflagellation in non-exflagellating mutants.

2.2.33 Imaging-based egress assay of mature *P. falciparum* gametocytes

On day 14 of gametocytogenesis, the egress of mature male and female gametocytes was tested based on published protocols with minor modifications (Suarez-Cortés, Silvestrini and Alano, 2014; Neveu *et al.*, 2020). In brief, parasite-infected RBC were stained with iFluor555-WGA (stock 2 mg/mL, final concentration 5 μ g/mL) and 0.45 μ g/mL Hoechst at 37°C. After 30 min, the samples were washed in prewarmed Ringer solution. 5 μ L were placed on a slide and immediately covered with a cover slip. Imaging of this non-activated control was performed for 20 min. To study egress, gametocytes were activated by incubation in ookinete medium for 20 min at 26 °C before imaging for 20 min. As a control, gametocytes were activated in the presence of the PKG inhibitor Compound 2 and imaged for 20 min (data not shown). Fluorescence images were manually evaluated and gametocytes were assigned into one of four categories: falciform shape/WGA-positive (neither activated nor egressed), falciform shape/WGA-negative (not activated but lacking the RBCM, most like due to harsh conditions during handling), round shape/WGA-positive (activated but not egressed, parasites fail to dissolve the RBCM), and round shape/WGA-negative (successful activation and egress).

2.2.34 Protein sequence alignment

Amino acid sequences of the PNPLA2 protein and its orthologues in other species (as listed on PlasmoDB) were aligned using the multiple sequence alignment tool Clustal Omega (<https://www.ebi.ac.uk/Tools/msa/clustalo/>). Alignment was performed using default settings.

2.2.35 Modeling of protein structures

Protein structures were modeled using AlphaFold v2.2.0 (Jumper *et al.*, 2021; Varadi *et al.*, 2022). For modeling of the PNPLA domain of PNPLA2 the annotated amino acid residues

aa1130-1404 were used. The model of the full-length PNPLA2 was downloaded from the AlphaFold Protein Structure Database (<https://alphafold.ebi.ac.uk>). The crystal structure of the native *Solanum cardiophyllum* patatin (PDB: 4PK9, (Wijeyesakere, Richardson and Stuckey, 2014)) was downloaded from the RCSB Protein Data Bank (<https://www.rcsb.org>). Models were visualized and annotated using the ChimeraX software v1.4.0 (<https://www.cgl.ucsf.edu/chimerax/>) under the UCSF ChimeraX Non-Commercial License Agreement.

2.2.36 Statistical analysis

For statistical analysis of differences between two groups, ratio-paired or unpaired two-tailed students t-tests were used. For statistical analysis of more than two groups, a one-way analysis of variance (ANOVA), followed by a Holm-Sidak multiple-comparison test was performed. All statistical tests were done in GraphPad Prism. P values of <0.05 were considered significant. Statistical details (n numbers, tests used, definition of the error bars) are described in the figure legends.

3. Results

3.1 Characterization of the mitochondrial phospholipase PNPLA2

3.1.1 PF3D7_1358000 is a patatin-like phospholipase

PF3D7_1358000 encodes a protein of 2,012 amino acids (aa) with a calculated molecular weight (MW) of 238 kDa. Residues aa1130-1404 harbor a patatin-like phospholipase (PNPLA) domain including the catalytic serine hydrolase motif GX SXG (₁₁₆₅GTSGT₁₁₇₀) (Figure 6A). Based on this domain, the protein is subsequently referred to as patatin-like phospholipase 2 (PNPLA2) taking into account that PNPLA1 (PF3D7_0209100, (Singh et al., 2019; Flammersfeld et al., 2020)) has already been investigated. To get structural insight into PNPLA2 with no experimental protein structure available, the bioinformatic tool AlphaFold was applied that demonstrates accuracy competitive with experimental structures in a majority of cases (Jumper et al., 2021; Varadi et al., 2022). Its algorithm predicts the 3D protein structure based on the amino acid sequence. In the case of the PNPLA2 sequence, only the core region could be modeled with confidence scores >70 (Figure 6B, light and dark blue regions) implying that the folded domain might confer the protein function. The other regions have low confidence scores (Figure 6B, yellow and orange regions) indicating that the protein might be intrinsically disordered in these regions (Varadi *et al.*, 2022). The core region corresponds to the PNPLA domain (Figure 6C, gold). Independent modeling of only the PNPLA domain of PNPLA2 showed its typical compact fold of α -helices and β -sheets harboring the GTSTG motif in its core (Figure 6D, motif in red). Alignment with the crystal structure of the *Solanum cardiophyllum* patatin (PDB accession number 4PK9) revealed a strong overlap of the two structures (Figure 6E) supporting the annotation of PF3D7_1358000 as patatin-like phospholipase.

Despite the high conservation of the PNPLA domain, *P. falciparum* PNPLA2 shows less than 60 % sequence identity with its homologs in other human malaria species (ClustalW, (Sievers *et al.*, 2011), Table 12) that are similarly divergent to each other. The orthologue in the rodent malaria parasite *P. berghei*, PBANKA_1134300, shows about 50 % sequence identity to the PNPLA2 homologues in all human malaria species (Table 12).

Taken together, experimental approaches such as X-ray crystallography are needed to elucidate the overall structure of PNPLA2.

Results

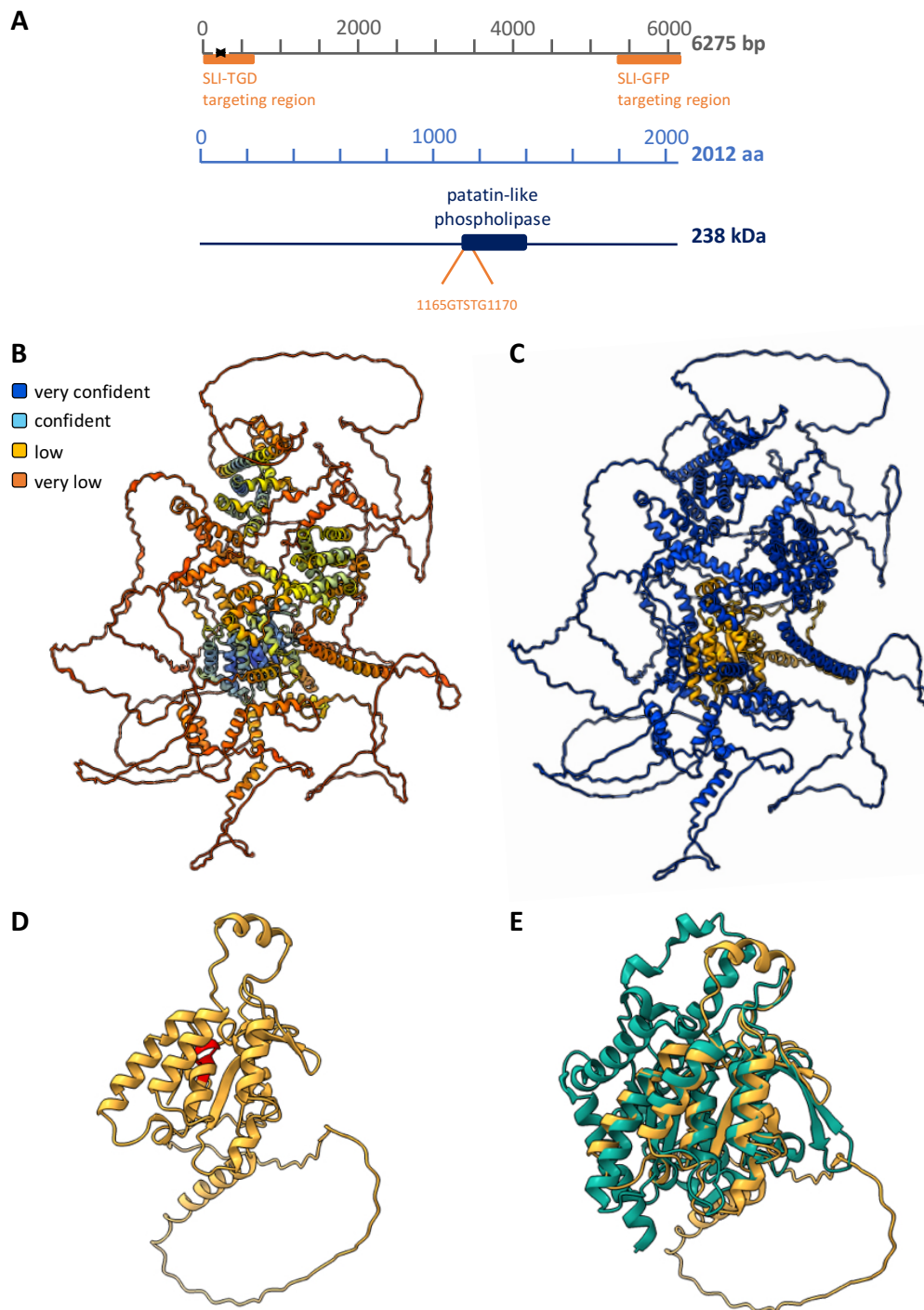


Figure 6. Predicted 3D structure of PF3D7_1358000 (PNPLA2). (A) Schematic representation of the *pnpla2* gene locus (grey) with the SLI targeting regions for homologous crossover (orange) and an intron-containing region (black ribbon). The PNPLA2 mRNA is depicted in light blue and the PNPLA2 protein in dark blue. The box indicates the predicted PNPLA domain containing the conserved GX SXG motif. (B) AlphaFold prediction of the PNPLA2 structure. Very high confidence: pLDDT > 90. High confidence: pLDDT 70-90. Low confidence: pLDDT 50-70. Very low confidence: pLDDT < 50. (C) AlphaFold prediction of the full-length PNPLA2 (blue) with the predicted PNPLA domain highlighted in gold. (D) AlphaFold prediction of the PNPLA domain of PNPLA2. The GTSTG motif is highlighted in red. (E) Alignment of the predicted PNPLA domain of PNPLA2 (gold) with the crystal structure of the native *Solanum cardiophyllum* patatin (PDB: 4PK9; green).

	<i>Pf</i>	<i>Pv</i>	<i>Po</i>	<i>Pm</i>	<i>Pk</i>	<i>Pb</i>
<i>P. falciparum</i> PF3D7_1358000	100.00	51.68	54.87	55.30	53.14	51.83
<i>P. vivax</i> PVP01_1113900	51.68	100.00	54.68	53.92	76.26	49.63
<i>P. ovale</i> POCGH01_11022500	54.87	54.68	100.00	60.92	55.75	57.33
<i>P. malariae</i> PMUG01_11028000	55.30	53.92	60.92	100.00	55.66	53.48
<i>P. knowlesi</i> PKNH_1113500	53.14	76.26	55.75	55.66	100.00	52.28
<i>P. berghei</i> PBANKA_1134300	51.83	49.63	57.33	53.48	52.28	100.00

Table 12. Sequence identities of PNPLA2 orthologs.

3.1.2 PNPLA2 localizes to the mitochondrion

To study protein localization, PNPLA2 was endogenously tagged on its C-terminus with GFP using the selection-linked integration (SLI) system (Figure 7A) (Birnbaum *et al.*, 2017; Burda *et al.*, 2021) and correct integration was confirmed by PCR (Figure 7B). Live cell fluorescence microscopy of PNPLA2-GFP schizonts and segmenters revealed that PNPLA2 colocalized with the live-cell dye MitoTracker CMXRos (Figure 7C) thereby confirming a mitochondrial localization, which is in line with a high MitoProt score of 0.9152 (Claros and Vincens, 1996). To exclude a localization to the apicoplast, which has a similar branched appearance in schizonts and is in close proximity to the mitochondrion, PNPLA2-GFP parasites were co-transfected with an acyl carrier protein (ACP)-mCherry construct that localizes to the apicoplast (Birnbaum *et al.*, 2020). There was little or no colocalization of PNPLA2-GFP and ACP-mCherry (Figure 7D) thus excluding localization to this organelle.

3.1.3 KO of PNPLA2 leads to a growth defect

To study PNPLA2 function during blood stage development, PNPLA2 was targeted for gene deletion (TGD) using the SLI system (Figure 8A) (Birnbaum *et al.*, 2017). PNPLA2-knockout (KO) parasites displaying correct integration as verified by PCR (Figure 8B) were viable which indicates that PNPLA2 is not essential for *in vitro* growth. However, PNPLA2-KO parasites showed ~50 % reduction in growth compared to 3D7 wildtype (WT) parasites over two cycles (Figure 8C).

Results

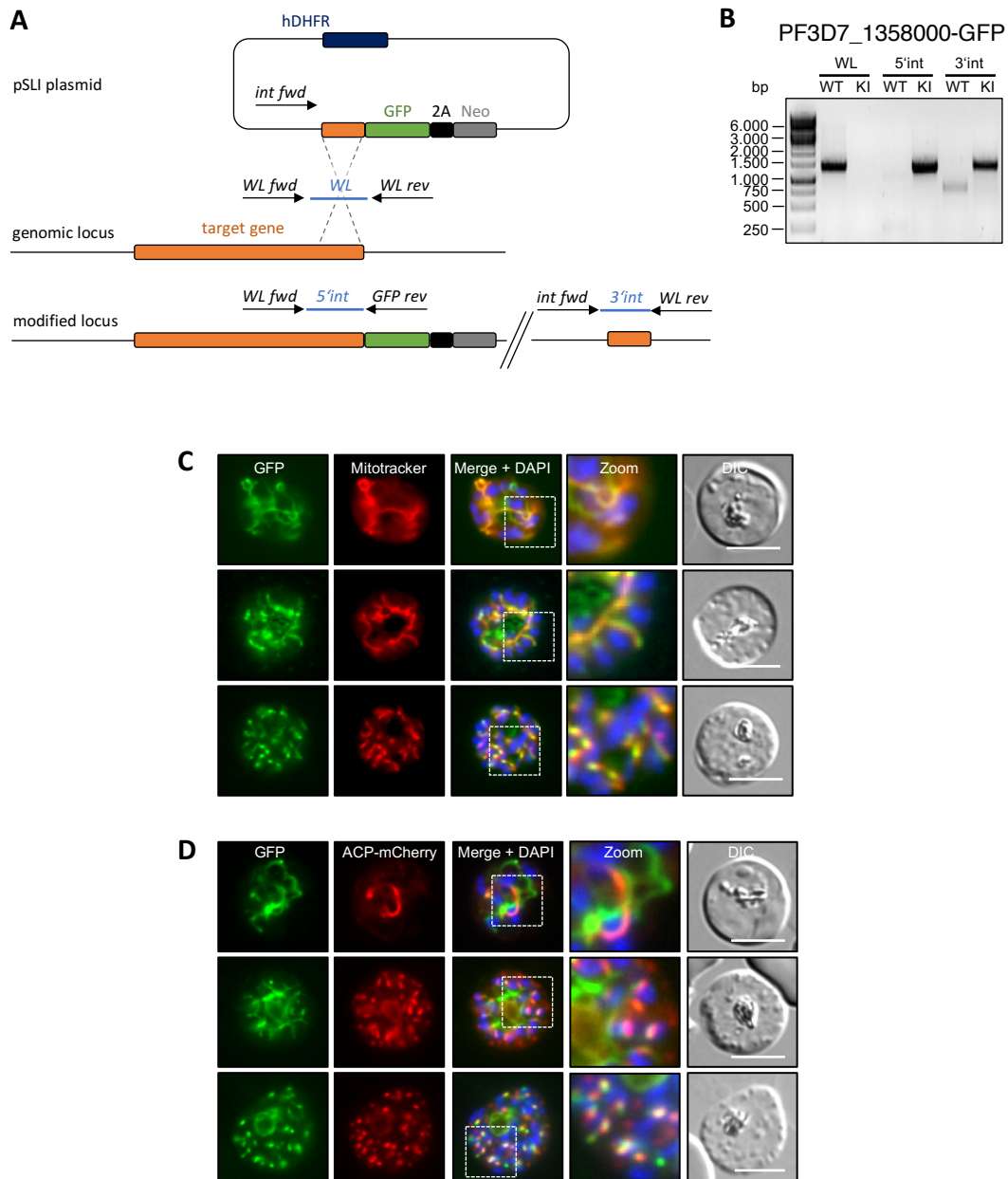


Figure 7. PNPLA2 localizes to the mitochondrion. (A) Schematic of the SLI targeting strategy for endogenous C-terminal tagging (Birnbaum *et al.*, 2017). Primers are indicated in italic and listed in Table 8. Indicated in blue and italic are the respective PCR products. *, stop codon; 2A, skip peptide; Neo, Neomycin resistance cassette; hDHFR, human dihydrofolate reductase. (B) Analytical PCR of PNPLA2-GFP parasites. WT, wildtype; KI, knock-in; WL, wildtype locus; 5'int, 5' integration; 3'int, 3' integration. (C) Live-cell microscopy of parasites expressing endogenously GFP-tagged PNPLA2 (PNPLA2-GFP). Parasites were stained with Mitotracker Red CMXRos and Hoechst. (D) Live-cell images of PNPLA2-GFP parasites co-expressing the apicoplast marker ACP-mCherry episomally. Nuclei were stained with Hoechst. All scale bars = 5 μ m. *Experiments were performed by Dr. Louisa Wilcke, Dr. Paul-Christian Burda and Sabrina Bielfeld.*

Results

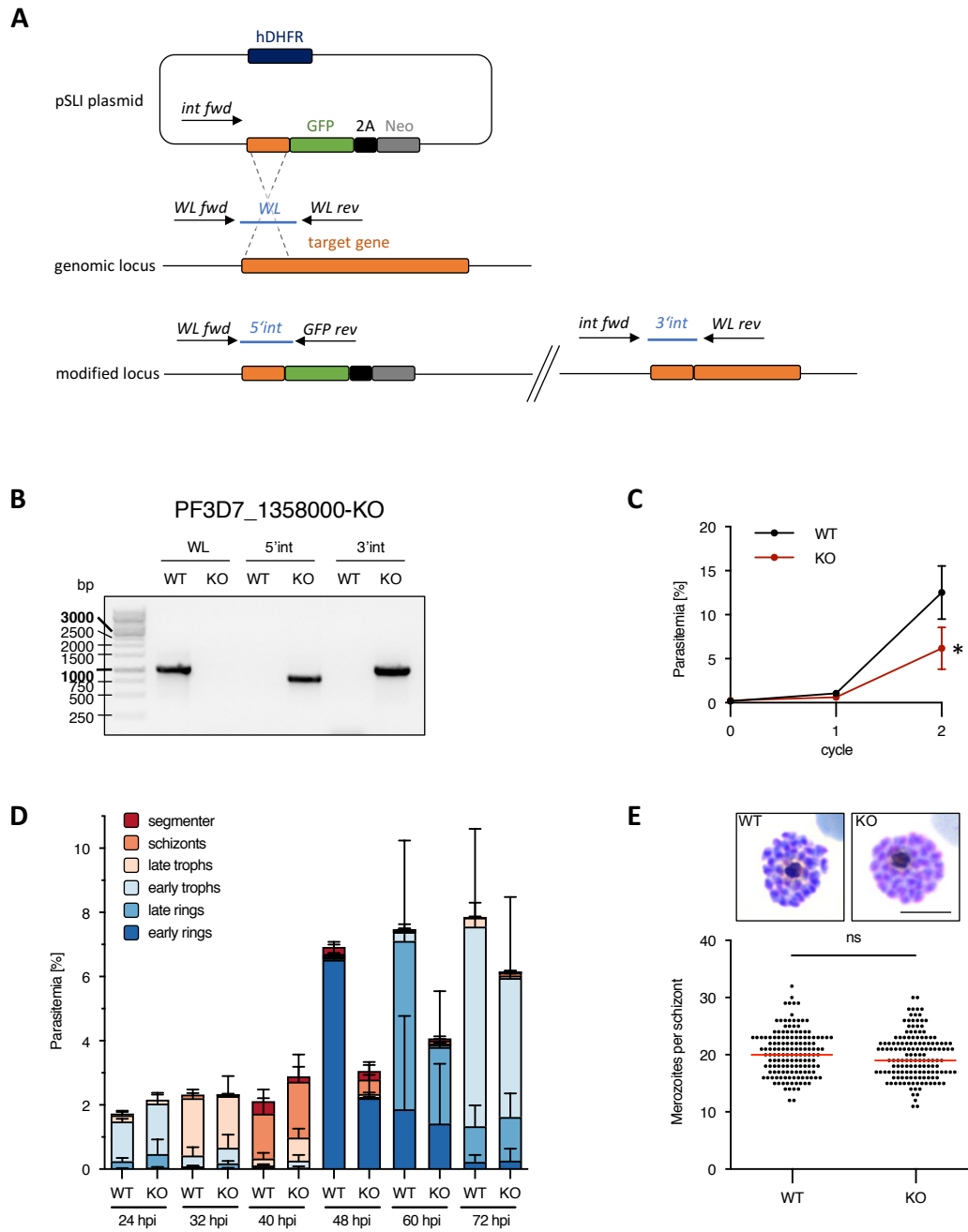


Figure 8. Deletion of PNPLA2 leads to slower asexual growth. (A) Schematic of the SLI targeting strategy for targeted gene deletion (TGD) (Birnbaum *et al.*, 2017). Primers are indicated in italic and listed in Table 8. Indicated in blue and italic are the respective PCR products. *, stop codon; 2A, skip peptide; Neo, Neomycin resistance cassette; hDHFR, human dihydrofolate reductase. (B) Analytical PCR of PNPLA2-KO parasites. (C) Proliferation of WT and PNPLA2-KO parasites over two cycles. Parasitemia was determined by flow cytometry. Mean \pm SD. $n=3$. Unpaired two-tailed students t-test (* $p<0.05$). (D) Stage quantification of WT and PNPLA2-KO parasites at the indicated time points. Stages were counted on Giemsa smears. Mean \pm SD. $n=3$. (E) Number of merozoites per schizont determined by counting nuclei of E64-treated parasites in Giemsa smears. Red line = median. Superplot of three independent experiments. Unpaired two-tailed students t-test (not significant (ns)). In each experiment, 50 schizonts were quantified. Experiments were performed by Dr. Paul-Christian Burda and Sabrina Bielfeld.

To characterize the growth defect of PNPLA2-KO parasites in more detail, the development of tightly synchronized parasites was analyzed in detail. Microscopic quantification of Giemsa-stained thin blood smears revealed that PNPLA2-KO parasites show delayed development in trophozoite and schizont stages (Figure 8D): while the vast majority of wildtype (WT) parasites at 40 hpi were schizonts and segmenters, a large proportion of PNPLA2-KO parasites were still at the trophozoite stage. As a consequence, at 48 hpi most WT parasites already reinvaded the next RBC and developed into ring stages while the majority of PNPLA2-KO parasites was still in the previous replication cycle as schizonts.

However, Giemsa-stained thin blood smears of schizonts treated with the PKG inhibitor Compound 2 (C2) that prevents merozoite egress revealed that mature PNPLA2-KO parasites showed similar numbers of daughter merozoites compared to WT schizonts (median: 20 merozoites in WT, 19 merozoites in PNPLA2-KO) (Figure 8E). In conclusion, the loss of PNPLA2 delays but does not compromise parasite maturation.

3.1.4 Loss of PNPLA2 leads to abnormal mitochondrial staining and an ultrastructural abnormality

Given the mitochondrial localization of PNPLA2, mitochondrial development and morphology of PNPLA2-KO parasites were studied next. For mitochondrial staining, the live-cell dye MitoTracker CMXRos was used. It stains the mitochondria in dependence on the mitochondrial membrane potential $\Delta\Psi_m$. Microscopic examination did not reveal any differences between WT and PNPLA2-KO in early trophozoites with only one nucleus (Figure 9A): most mitochondria displayed a typical “comma-like” structure while some already started to elongate. However, following the first round of nuclear duplication and division (2 nuclei) and thereafter (3+ nuclei) mitochondrial abnormalities became evident (Figure 9A). While in WT parasites the majority of mitochondria showed the expected elongated and branched morphology described previously (van Dooren *et al.*, 2005), about half of PNPLA2-KO parasites showed bright accumulations of mitochondrial staining. In PNPLA2-KO schizonts arrested with the egress inhibitor C2, more than 80 % of parasites showed abnormalities while these were evident in only 10 % of WT parasites (Figure 9B) hinting towards a potential defect in mitochondrial morphogenesis in PNPLA2-KO parasites.

For ultrastructural investigation, parasites were treated with the egress inhibitor ML10 and analyzed by FIB-SEM. Osmium-stained membranes in the individual sections did not reveal obvious mitochondrial abnormalities in the PNPLA2-KO parasites when compared to WT parasites (Figure 10-11). However, in the majority of PNPLA2-KO parasites but none of the WT parasites, a large structure with dark osmium-stained membranes was found close to the DV (Figure 11, yellow arrows). While its appearance and staining resembled the apicoplast, this structure contained mitochondria-like organelles in its lumen (Figure 11, yellow asterix). In most cases, the structure was connected to daughter merozoites in the depicted slice or above or below that as if it was about to be distributed to them (Figure 11). Notably, the

respective merozoites already contained a mitochondrion but no other apicoplast or apicoplast-like structure supporting the fact that this enlarged structure might be an abnormal apicoplast. To look at mitochondrial and apicoplast morphology in three dimensions, we performed computational three-dimensional modeling of mitochondria, apicoplast and other parasite organelles. The models were derived from one WT and one PNPLA2-KO schizont by segmentation and rendering of tomograms. Mitochondria of both, the WT and the PNPLA2-KO schizonts, showed the expected elongated ultrastructure with no obvious morphological differences between the two (Figure 12). They were already partially divided into the daughter merozoites indicating that indeed late-stage schizonts were sampled (Figure 12B). Additionally, every daughter merozoite contained two pear-shaped roptries indicating that there is likely no general defect in parasite maturation (Figure 12B). However, segmentation of the apicoplast in PNPLA2-KO schizonts showed the large apicoplast-like structure previously observed in the single sections (Figure 12B, yellow arrow). The 3D model confirmed that the respective merozoite connected to this structure already contained a mitochondrion but no other apicoplast (Figure 12B).

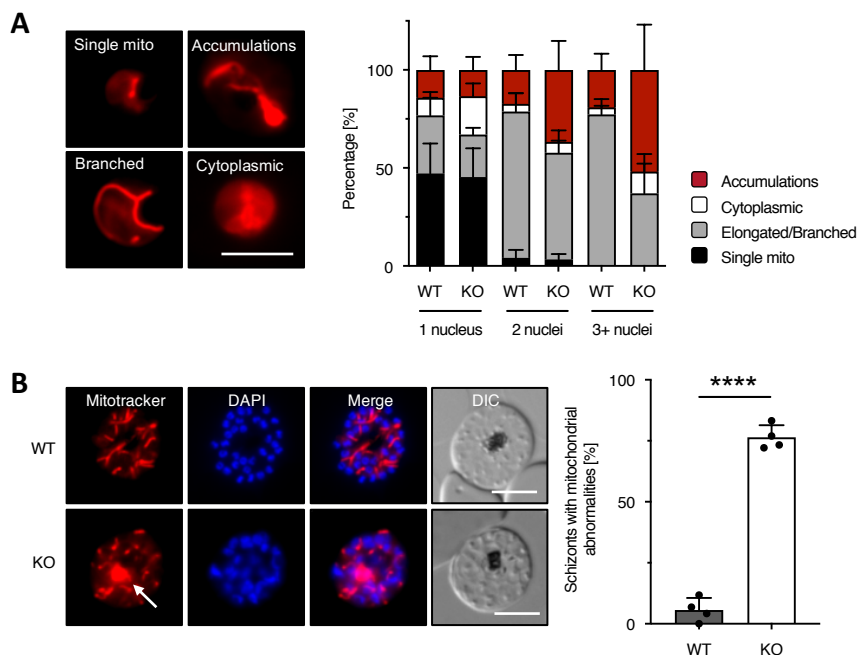


Figure 9. PNPLA2-KO parasites display an abnormal mitochondrial staining. (A) Mitotracker CMXRos staining pattern of tightly synchronized WT and PNPLA2-KO parasites at 24-40 hpi. Left: Representative images of the staining patterns. Right: Quantification based on the number of nuclei as indicated by Hoechst staining (not shown). Mean + SD, n=3. (B) Mitotracker CMXRos staining of C2-arrested WT and PNPLA2-KO schizonts at 48 hpi. Schizonts with at least one mitochondrial abnormality/accumulation were quantified. Data are normalized to the total number of schizonts. Bars show the mean + SD of n=4. Dots represent the mean of one individual experiment. WT: 381 parasites. KO: 376 parasites. Unpaired students t-test (****p<0.0001). Representative images are shown on the left. White arrow indicates a typical mitochondrial abnormality in PNPLA2-KO parasites. *Experiments of panel B were performed by Dr. Paul-Christian Burda and Sabrina Bielfeld.*

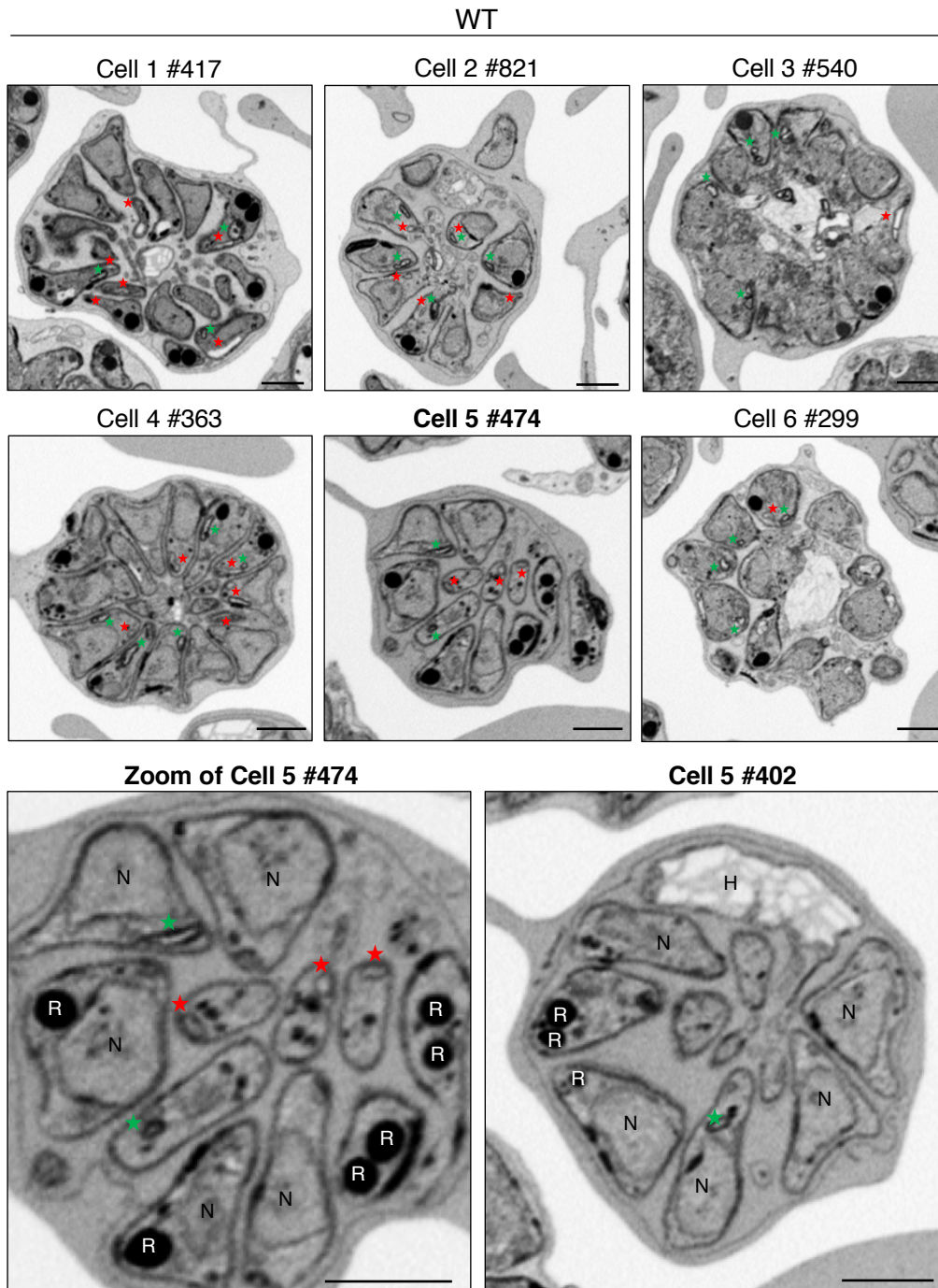
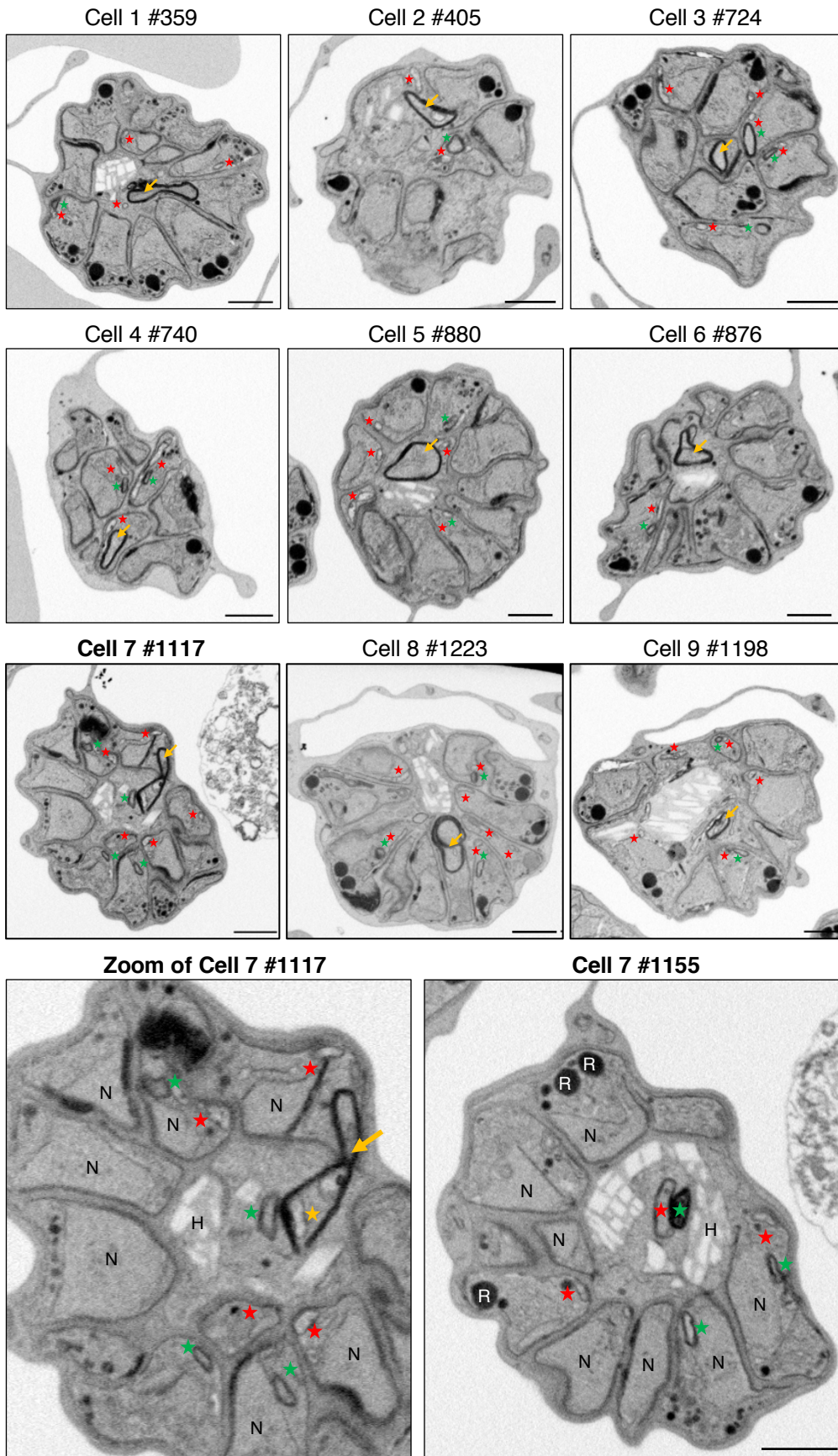


Figure 10. Ultrastructural analysis of WT parasites by FIB-SEM. Displayed are single slices from stacks of segmented schizonts of which the full volume was acquired. Indicated next to the cell number is the number of the slice. Red asterixes, mitochondrion; Green asterixes, apicoplast; R, rhoptry; N, nucleus; H, hemozoin. Cell 5 was selected for segmentation and rendering of a 3D model (Figure 12). Brightness and contrast of the images were adjusted. Scale bar = 1 μ m. Images were acquired by Dr. Bohumil Maco.

Results

PNPLA2-KO



Results

Figure 11. Ultrastructural analysis of PNPLA2-KO parasites by FIB-SEM. Displayed are single slices from stacks of segmented schizonts of which the full volume was acquired. Indicated next to the cell number is the number of the slice. Red asterixes, mitochondrion; Green asterixes, apicoplast; Yellow arrows/asterix: unidentified structures; R, rhoptry; N, nucleus; H, hemozoin. Cell 7 was selected for segmentation and rendering of a 3D model (Figure 12). Brightness and contrast of the images were adjusted. Scale bar = 1 μm . Images were acquired by Dr. Bohumil Maco.

Taken together, ultrastructural data indicate that the loss of PNPLA2 leads to an ultrastructural abnormality in form of an enlarged, strongly osmium-stained structure which might be derived from an apicoplast. Curiously, in its lumen mitochondria-like organelles can be seen. Moreover, loss of PNPLA2 leads to aberrant Mitotracker Red CMXRos staining. As Mitotracker Red CMXRos staining depends on $\Delta\Psi_m$ which in turn requires a fully functional mtETC, we next examined mitochondrial functions.

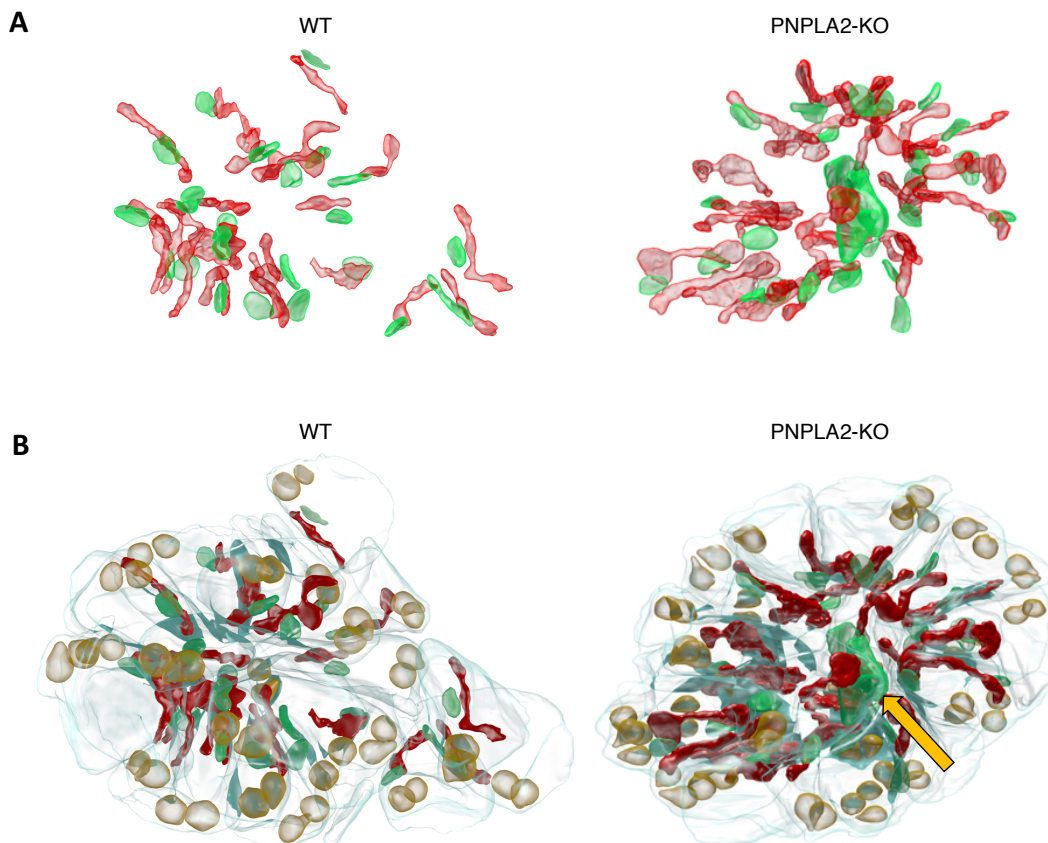


Figure 12. 3D reconstructions of segmented schizonts. (A) Segmentation of the mitochondria (red) and the apicoplasts (green) of one WT (Cell 5, Figure 10) and one PNPLA2-KO (Cell 7, Figure 11) schizont. (B) Segmentation of the mitochondria (red), the apicoplasts (green), the rhoptries (gold) and the parasite plasma membranes (blue) of the same schizonts as in A. Yellow arrow, unidentified structures observed exclusively in PNPLA2-KO parasites. Due to its dark staining it was annotated and segmented as apicoplast. Segmentation and 3D modeling were performed by Dr. Bohumil Maco.

3.1.5 PNPLA2-KO parasites are hypersensitive to drugs targeting the mtETC

The mitochondrion is an exploitable target for antimalarial drugs. Due to PNPLA2's mitochondrial localization and the aberrant Mitotracker staining in PNPLA2-KO parasites, we hypothesized that the loss of PNPLA2 might impair mitochondrial functions possibly resulting in hypersensitivity to drugs targeting the mitochondrion. Drug susceptibility of WT and PNPLA2-KO parasites was tested in 96-hour SYBR Gold assays (Wichers *et al.*, 2021) (Figure 13A-H). Interestingly, PNPLA2-KO parasites showed higher susceptibility to the Complex III inhibitors Atovaquone (5-fold, Figure 13A), Antimycin A (7-fold, Figure 13B) and Myxothiazol (6-fold, Figure 13C) as well as to Proguanil (13-fold, Figure 13D) as indicated by the lower IC₅₀ values. In contrast, no difference between WT and PNPLA2-KO parasites was observed for the DHODH inhibitor DSM1 (Figure 13E) or the antimalarials Primaquine (Figure 13F), BSD (Figure 13G) or Dihydroartemisinin (DHA, Figure 13H) thereby excluding a general effect of the loss of PNPLA2 on drug susceptibility.

The high susceptibility of PNPLA2-KO to Complex III inhibitors suggests that Complex III might be impaired. Complex III is crucial for the mtETC as it recycles ubiquinone (coenzyme Q) which is necessary for ubiquinone-dependent enzymes such as DHODH. To test whether the ubiquinone pool was affected by disruption of PNPLA2, parasites were treated with the ubiquinone analog decylubiquinone (DCUQ). In line with the literature (Ke *et al.*, 2011), DCUQ treatment rescued an Atovaquone-induced damage of WT parasites in a dose-dependent manner (Figure 13I). However, no rescue of PNPLA2-KO parasite growth was observed independently of the concentration of supplemented DCUQ. In conclusion, the loss of PNPLA2 does not impair ubiquinone recycling which is supported by the finding that PNPLA2-KO parasites showed similar sensitivity to DSM1 (Figure 13E). Taking into account the hypersensitivity to the Complex III inhibitors Atovaquone, Antimycin A and Myxothiazol, the PNPLA2-KO parasites likely have a defect in the mtETC downstream of Complex III which is independent of ubiquinone recycling.

The mtETC, especially Complex III, is a major site of the production of reactive oxygen species (ROS) and an imbalance between mitochondrial ROS production and antioxidant defense can result in oxidative stress with the potential to damage several cellular components (Gunjan *et al.*, 2016). Given the high susceptibility of PNPLA2-KO parasites to Complex III inhibitors, we tested whether the PNPLA2 deletion phenotype is linked to ROS activity. WT and PNPLA2-KO parasites were treated with 10 μ M or 100 μ M of the ROS scavenger Trolox for two parasite cycles. Parasite growth was monitored using flow cytometry. Trolox treatment, however, was not able to rescue the growth defect of PNPLA2-KO parasites, indicating that ROS activity does not play a major role in the observed phenotype (Figure 13J).

In conclusion, the loss of PNPLA2 leads to a defect in the mtETC downstream of Complex III but does not affect ubiquinone recycling. In addition, the growth defect cannot be explained by higher levels of ROS.

Results

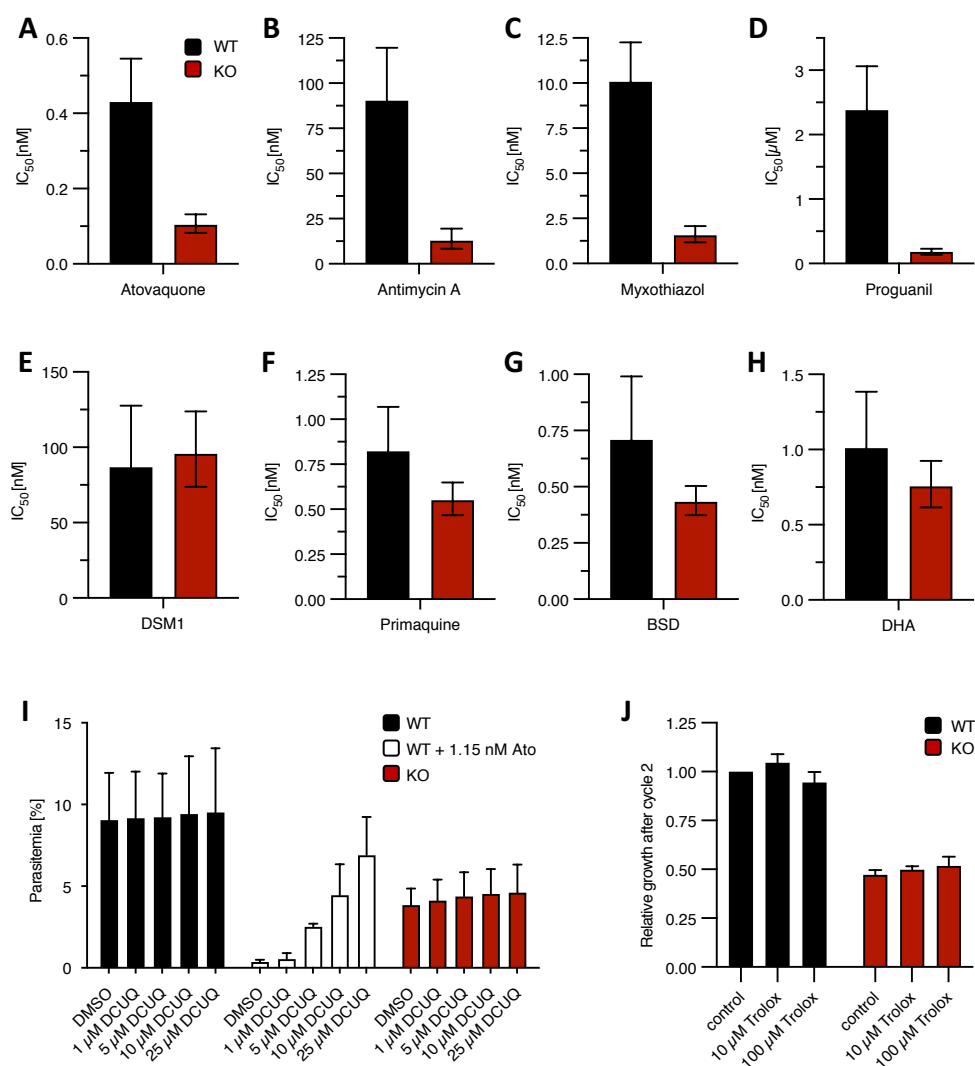


Figure 13. Susceptibility of PNPLA2-KO parasites to antimalarial drugs. Parasites were treated in 96-hour SYBR Gold assays using (A) Atovaquone, (B) Antimycin A, (C) Myxothiazol, (D) Proguanil, (E) DSM1, (F) Primaquine, (G) BSD, and (H) DHA. Growth of DMSO-treated control parasites was set to 100%. Based on this, IC_{50} values were calculated. Shown are means \pm 95% confidence interval. $n=3$. (I) Parasitemia of WT parasites treated with DMSO or 1.15 nM Atovaquone (IC_{50} according to Agarwal *et al.*, 2017) and PNPLA2-KO parasites after two cycles in the presence of the ubiquinone analog DCUQ. Parasitemia was determined by flow cytometry. Mean + SD. $n=3$. (J) Relative growth of WT and PNPLA2-KO parasites in the presence of Trolox. Parasitemia was determined by flow cytometry. Data were normalized to WT control parasites after 2 cycles. Mean + SD. $n=3$.

3.1.6 Loss of PNPLA2 leads to lower mitochondrial respiration

Our results so far indicated that PNPLA2-KO parasites might have a defect in mitochondrial function. To further characterize a potential defect in the mtETC, we next measured the oxygen consumption rate (OCR) of PNPLA2-KO parasites in an assay based on the Mito Stress Test (Agilent) using a Seahorse XFe96 analyzer as it has been done previously for *T. gondii* and *P. falciparum* (Figure 14A) (Sakata-Kato and Wirth, 2016; Jenni A Hayward *et al.*, 2022;

Jenni A. Hayward *et al.*, 2022a). Parasite schizonts were freed from the RBC using saponin and permeabilized using digitonin in the presence of malate which feeds electrons into the mtETC via MQO. Injection of the protonophore FCCP yields oxygen consumption at maximum capacity (Figure 14A-B). Remarkably, the resulting basal OCR was consistently reduced by 35-50% in PNPLA2-KO compared to WT parasites despite the high variations between the individual assays (Figure 14A, C). Subsequent injection of the Complex III inhibitor Atovaquone reduced the OCR to the detection limit with no difference between WT and PNPLA2-KO parasites (Figure 14B) indicating that the observed basal OCR (OCR_{Basal}) indeed represents mitochondrial respiration and is not masked by other cellular processes using oxygen. Next, reduced N,N,N,N'-tetramethyl-p-phenylenediamine (TMPD) was injected that donates electrons directly to CytC thereby bypassing the inhibited Complex III (Figure 14A-B) before finally injecting the Complex IV inhibitor sodium azide (NaN_3) to validate that the measured TMPD-elicited OCR (OCR_{TMPD}) is indeed mediated by the mtETC upstream of Complex IV (Figure 14A-B). If in a given KO parasite Complex III was impaired, the OCR would be rescued by the addition of TMPD while a defect of Complex IV would prevent this rescue. Interestingly, the injection of TMPD led to an increase of the OCR in WT and PNPLA2-KO parasites (Figure 14B) indicating that Complex IV is principally active and functional. However, the TMPD-elicited OCR (OCR_{TMPD}) of PNPLA2-KO was significantly reduced by 27-48% compared to WT parasites (Figure 14C) while the fold stimulation of OCR_{TMPD} relative to the basal OCR was comparable between WT and PNPLA2-KO parasites (Figure 14D). As TMPD fails to rescue the OCR of PNPLA2-KO parasites back to WT levels, the mtETC defect likely occurs downstream of CytC in the electron transport from CytC to Complex IV or in Complex IV activity resulting in the observed reduction of both, the basal OCR and the OCR_{TMPD} . These results support our previous findings that the loss of PNPLA2 impairs key mitochondrial functions.

3.1.7 PNPLA2-KO parasites show a lower mitochondrial membrane potential

Apart from ubiquinone recycling at Complex III, which is necessary to provide orotate for pyrimidine synthesis, parasites rely on a functional mtETC to generate the mitochondrial membrane potential $\Delta\Psi_m$ because critical processes such as protein and metabolite import mediated by mitochondrial carriers rely on $\Delta\Psi_m$. To test whether the loss of PNPLA2 impairs the parasite's ability to generate $\Delta\Psi_m$, C2-arrested schizonts were stained using the $\Delta\Psi_m$ -dependent mitochondrial live-cell dye Rhodamine123 as described previously (Matz *et al.*, 2018).

Microscopic examination allowed the differentiation of parasites into three categories: i) strong mitochondrial signal, ii) weak mitochondrial signal (some with high cytoplasmic background), and iii) no signal or only cytoplasmic/peripheral signal. Interestingly, more PNPLA2-KO schizonts showed only weak or no mitochondrial staining compared to WT parasites (Figure 14E) indicating that disruption of PNPLA2 impairs a mitochondrial function required for sustaining a normal $\Delta\Psi_m$.

Results

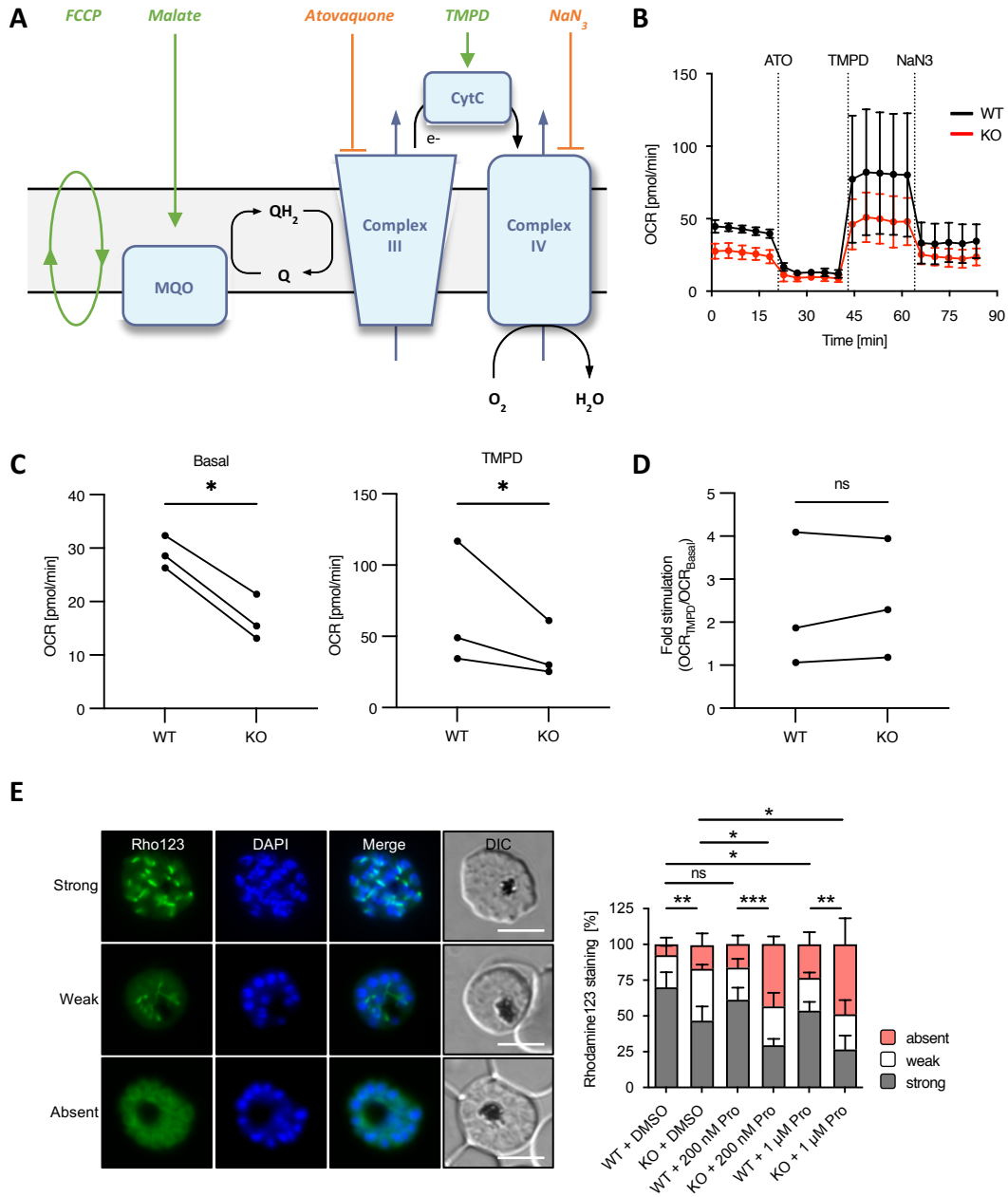


Figure 14. PNPLA2-KO parasites show lower oxygen consumption rates (OCRs) and a lower $\Delta\psi_m$. (A) Schematic of the Seahorse assay used to determine the OCRs. FCCP and malate are injected to saponin-freed parasites ($\text{OCR}_{\text{Basal}}$) before adding Atovaquone. Injection of TMPD feeds electrons directly to CytC (OCR_{TMPD}) before Complex IV is inhibited by NaN_3 . (B) OCR of WT and PNPLA2-KO parasites. Mean \pm SD. $n=3$. (C) $\text{OCR}_{\text{Basal}}$ and OCR_{TMPD} of 3 independent experiments. Dots represent means of independent experiments. (D) Fold stimulation as indicated by the ratio of $\text{OCR}_{\text{TMPD}}/\text{OCR}_{\text{Basal}}$. Ratio-paired students t-test (* $p<0.05$). (E) Analysis of the mitochondrial membrane potential $\Delta\psi_m$. Parasites were treated with DMSO (solvent control), 200 nM or 1 μM of proguanil. Schizonts were arrested with C2 and stained with Rhodamine123 (Rho123, green) at 48 hpi. Parasites with a strong, weak or absent mitochondrial Rho123 signal were quantified by fluorescence microscopy. Shown are means + SD of 4 independent experiments, in which a total of 352 to 414 schizonts were analyzed per cell line and condition. One-way analysis of variance (ANOVA) followed by a Holm-Sidak multiple comparison test was performed (* $p<0.05$; ** $p<0.01$; *** $p<0.001$; ns, not significant). Representative images are shown on the left. DAPI-stained nuclei are shown in blue. DIC, differential interference contrast. Scale bars = 5 μm .

Given that PNPLA2-KO parasites showed a remarkable hypersensitivity to Proguanil, whose activity had previously been linked to $\Delta\Psi_m$ (Srivastava and Vaidya, 1999; Painter *et al.*, 2007), parasites were treated with Proguanil to test how this drug treatment affects $\Delta\Psi_m$. Treatment with 200 nM Proguanil (the approximate IC_{50} in KO parasites) led to a significant increase in PNPLA2-KO parasites displaying weak or cytoplasmic Rhodamine123 staining compared to the DMSO-treated control (Figure 14E). This significant increase could not be observed in WT parasites (Figure 14E). However, treatment with 1 μ M Proguanil resulted in significantly more parasites displaying abnormal staining patterns in both, WT and PNPLA2-KO parasites, indicating that Proguanil treatment alone affects $\Delta\Psi_m$ (Figure 14E).

In conclusion, these data imply that PNPLA2-KO parasites may have a lower $\Delta\Psi_m$ under physiological conditions and fail to maintain $\Delta\Psi_m$ when treated with Proguanil.

3.1.8 Deletion of PNPLA2 is associated with changes in the mitochondrial phospholipid cardiolipin

Given that PNPLA2 is annotated as a phospholipase based on a conserved PNPLA domain harboring the characteristic GX SXG lipase motif, we next performed targeted lipidomic analysis of C2-arrested schizonts to further characterize the PNPLA2-deletion phenotype. We hereby focused on the mitochondrion-specific phospholipid cardiolipin, due to its established key role in mitochondrial functions and the mtETC (Mancuso *et al.*, 2007; Baker *et al.*, 2016; Hoffmann and Becker, 2022). In addition, we analyzed the levels of several other highly abundant phospholipids, including several PE species, given that PE has been demonstrated to influence mtETC activity (Baker *et al.*, 2016).

Lipidomic analysis revealed that CL species in *P. falciparum* are surprisingly long-chained compared to prokaryotes and fungi (Oemer *et al.*, 2018) and that cardiolipin species with even-numbered carbon chains showed a higher abundance than those with uneven-numbered carbon chains (Figure 15A). In addition, we found that malaria CLs showed a remarkable variability in the number of their double bonds (Figure 15B), and observed that PNPLA2-KO parasites displayed a trend towards shorter and more saturated CL species compared to WT parasites, the latter being reflected in the reduced overall unsaturation index (Figure 15C). However, the total abundance of CLs per parasite remained unchanged (Figure 15D). Of note, our analysis did not reveal any changes in the profile of non-cardiolipin lipid species (Figure 15E) thereby excluding a general effect of PNPLA2 deletion on the lipid metabolism and highlighting the mitochondrion-specific function of PNPLA2.

Recent studies have shown that the FA- and lipid composition of cell culture media has a strong impact on the CL profile (Oemer *et al.*, 2022). In turn, the supplementation of culture medium with certain FAs can cause strong changes in certain lipid classes, such as CLs (Oemer *et al.*, 2021). Thus, we tested whether supplementation of selected fatty acids might rescue the growth phenotype.

Results

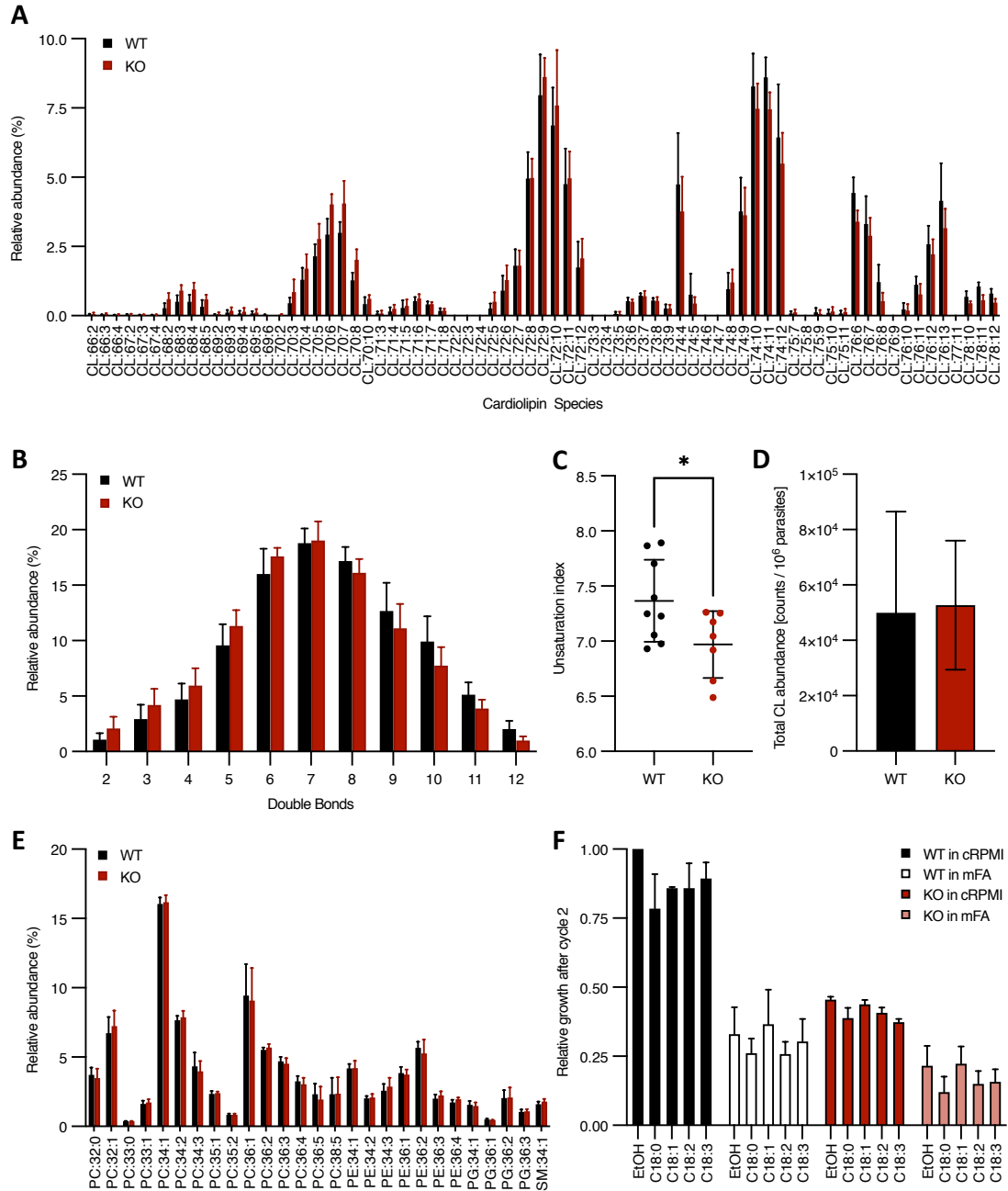


Figure 15. Lipidomic analysis of PNPLA2-KO parasites. (A) Relative CL abundance of WT and PNPLA2-KO parasites at 44 hpi (treated with C2). Mean \pm SD. Nine (WT) and seven (KO) independent biological replicates. (B) Abundance of double bonds in CL species. Mean \pm SD. (C) Unsaturation index. Mean \pm SD. Dots represent the values of each independent replicate. Unpaired students t-test (* $p < 0.05$). (D) Total CL abundance. Mean \pm SD. Unpaired students t-test (not significant). (E) Relative abundance of highly expressed phospholipids in WT and PNPLA2-KO parasites 44 hpi (treated with C2). Mean \pm SD. (F) Relative growth of WT (black) and PNPLA2-KO (red) parasites in complete RPMI (dark bars) or minimal fatty acid medium (light bars) supplemented with 30 μ M of the respective fatty acid after two cycles. C18:0, stearic acid; C18:1, vaccenic acid; C18:2, linoleic acid; C18:3, α -linolenic acid. Data were normalized to WT control (EtOH) in cRPMI. Mean \pm SD. $n = 3$. *The lipidomic analysis was performed by Yvonne Wohlfarter and Dr. Markus A. Keller.*

Growth assays were performed over two cycles in complete cell culture medium containing albumax (cRPMI) or minimal fatty acid medium (mFA) which only contained palmitic acid (C_{16:0}) and oleic acid (C_{18:1,n-9}) as lipid sources. These media were complemented with ethanol as solvent control or one of the following: stearic acid (C_{18:0}), vaccenic acid (C_{18:1,n-7}), linoleic acid (C_{18:2,n-6}), or α -linolenic acid (C_{18:3,n-3}). The fatty acids included in the experiments were chosen based on Mi-Ichi *et al.* (2006) who tested combinations of three FAs that would support long-term *in vitro* culture of *P. falciparum*. They found that palmitic acid and oleic acid (= mFA) combined with mono-, di- or triunsaturated C18 fatty acids supported continuous parasite culture. Stearic acid (C_{18:0}) was included as the C18 saturated control (Mi-Ichi, Kita and Mitamura, 2006). Notably, levels of linoleic acid (C_{18:2}) and its isomers have been shown to strongly affect CLs (Oemer *et al.*, 2020).

We observed that the growth of WT parasites in mFA medium was strongly reduced compared to cRPMI indicating that parasite fitness requires rich lipid sources (Figure 15F). Interestingly, even the addition of single FAs to mFA medium did not restore growth of WT parasites back to WT growth rates in cRPMI (Figure 15F). The supplementation of FAs to PNPLA2-KO parasites in cRPMI did not improve parasite growth indicating that a shortage of the tested fatty acids cannot explain the observed growth phenotype (Figure 15F). When comparing the growth of WT and PNPLA2-KO parasites, we observed a similar growth defect of about 50 % for PNPLA2-KO parasites in both growth media, cRPMI and mFA, compared to the respective WT parasites independent of the supplemented C18 FAs (Figure 15F).

Taken together, the loss of PNPLA2 resulted in shorter and more saturated CL species which supports a mitochondrial function of PNPLA2. Supplementation of selected FAs that might influence the CL profile did not rescue the observed growth defect.

3.1.9 PNPLA2-KO parasites fail to form mature gametocytes

It has been reported that mitochondrial functions including the mtETC and the TCA cycle become increasingly important for parasite physiology during gametocytogenesis (MacRae *et al.*, 2013; Ke *et al.*, 2015; Evers *et al.*, 2021). To study the effect of PNPLA2 loss on gametocyte development, we performed targeted gene deletion of PNPLA2 in a 3D7 line that can be induced to commit to sexual development by the depletion of choline from the cell culture medium, and that subsequently fully supports gametocyte development (3D7CH, (Filarsky *et al.*, 2018)). Correct integration of the pSLI-TGD construct into the *pnpla2* locus was verified by PCR (Figure 16A) and the KO-associated growth defect in asexual blood stage development was confirmed (Figure 16B). Gametocyte commitment was induced by choline depletion in 3D7CH (WT) and the newly generated PNPLA2-KO parasites as described previously (Brancucci *et al.*, 2017; Filarsky *et al.*, 2018), and gametocyte maturation was followed for 10 days (Figure 16C-D).

Results

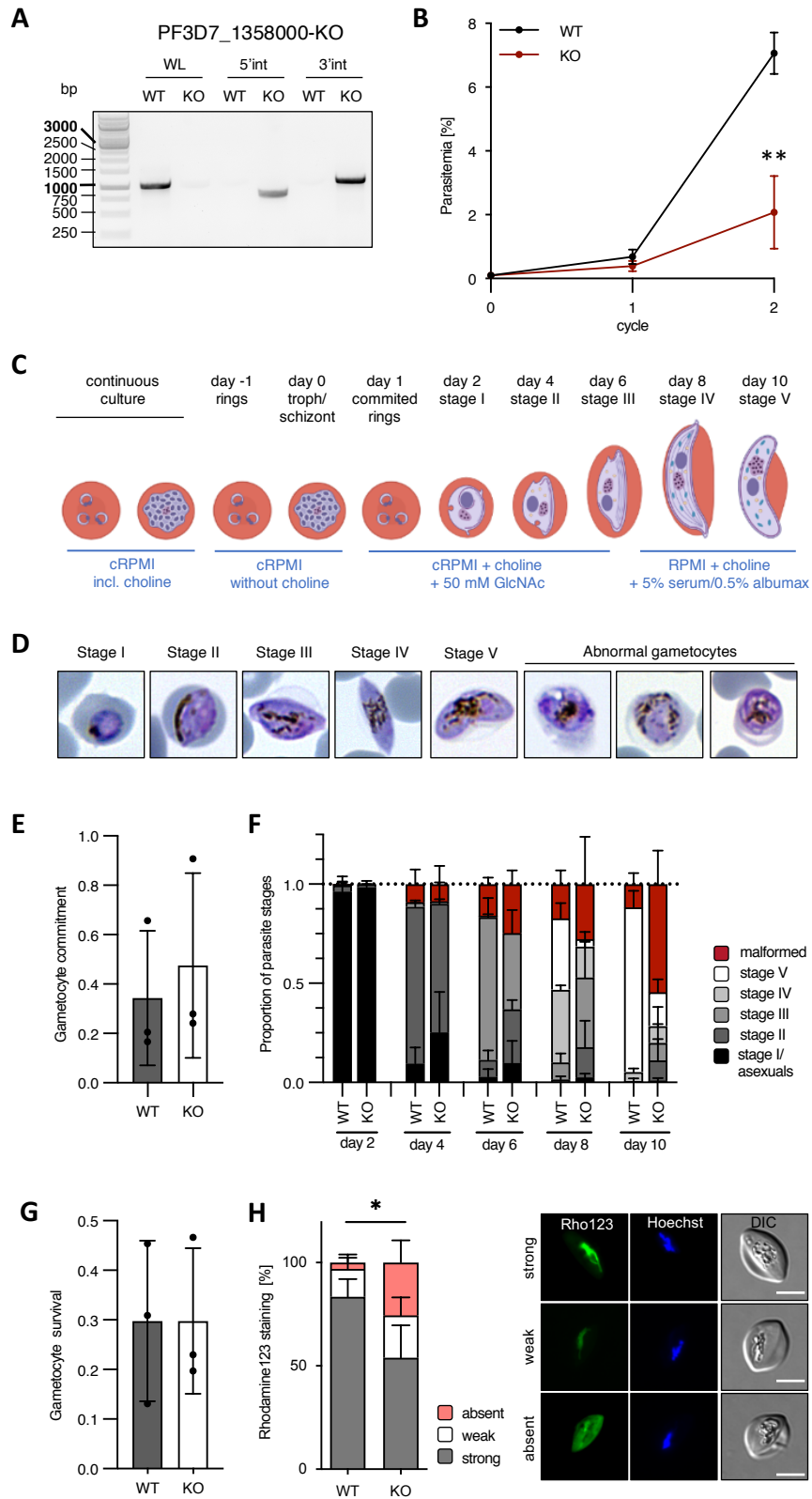


Figure 16. PNPLA2-KO parasites show defects in gametocyte development. (A) Analytical PCR of PNPLA2-KO parasites in the 3D7CH background that fully supports gametocyte development. (B) Proliferation assay of WT and PNPLA2-KO parasites (3D7CH background). Mean \pm SD. n=3. Unpaired students t-test (**p<0.05). (C) Schematic of the experimental strategy to study gametocyte development of PNPLA2-KO parasites. Created with Biorender.com. (D) Representative images of Giemsa-stained gametocyte stages. (E) Gametocyte commitment rates calculated from the parasitemia on day 6 divided by the parasitemia on day 2. Dots represent the 3 independent experiments. Mean \pm SD. Unpaired students t-test (not significant). (F) Gametocyte maturation of WT and PNPLA2-KO parasites by counting parasites on Giemsa-stained blood smears on the respective days. Means + SD. n=3. (G) Gametocyte survival rates calculated as the ratio of the parasitemia on day 10 / the parasitemia on day 6. Dots represent the values of individual experiments. Bars represent the means \pm SD. n=3. Unpaired students t-test (not significant). (H) Analysis of $\Delta\Psi_m$ in WT and PNPLA2-KO gametocytes at day 6 of gametocyte development. Gametocytes were stained with Rhodamine123 (Rho123, green) and gametocytes with a strong, weak or absent mitochondrial Rhodamine123 signal were quantified by fluorescence microscopy. Shown are means + SD of four independent experiments, in which a total of 146 WT and 106 KO gametocytes were analyzed. Unpaired students t-test (*p<0.05). Representative images are shown on the right. Hoechst-stained nuclei are shown in blue. DIC, differential interference contrast. Scale bars = 5 μ m.

After induction of gametocytogenesis, no difference in gametocyte commitment between WT and PNPLA2-KO parasites could be observed although the variation between assays was high (Figure 16E). However, quantification of gametocyte stages revealed that from day 6 onwards, PNPLA2-KO parasites showed a higher proportion of malformed gametocytes (Figure 16F). Only very few gametocytes reached late stages by day 10, while more than half of the gametocytes showed an abnormal (rounded) morphology (Figure 16F). Nevertheless, gametocyte survival rates were comparable between WT and PNPLA2-KO parasites (as calculated by dividing the parasitemia on day 10 - the final day of the assay - by the parasitemia on day 6 - when all asexual stages should have been depleted from the culture) (Figure 16G). To probe into the mitochondrial membrane potential $\Delta\Psi_m$, we finally stained WT and PNPLA2-KO gametocytes with Rhodamine123 on day 6 of gametocyte development (stage III) when PNPLA2-KO parasites still displayed a normal morphology. Similar to asexual blood stages, a significantly higher proportion of PNPLA2-KO gametocytes showed a weak or absent Rhodamine123 staining in comparison to WT parasites, arguing that PNPLA2 is important for normal mtETC function in gametocyte development (Figure 16H).

Taken together, our study of PNPLA2 in gametocytes suggests that PNPLA2 fulfills a crucial function in the parasite's mtETC throughout blood stage development.

3.2 Characterization of phospholipases in gametocytes

Plasmodium possesses a large family of about 27 (putative) phospholipases (Burda *et al.*, 2021), whose importance for asexual blood stage development was previously analyzed in great detail by our lab (Burda *et al.*, 2021). In contrast to the data in asexual blood stages, our knowledge regarding phospholipase function in gametocytes is relatively scarce.

In total, 15 out of the 27 *Plasmodium* (phospho)lipases are expressed in stage V gametocytes based on mass spectrometric evidence (Table 13). Out of these, three have a predicted signal peptide or N-terminal transmembrane domain (PF3D7_0731800 (LPL4), PF3D7_1411900 (PL39), PF3D7_1412000 (PL38), Table 1, Table 13) which suggest they might be targeted into the secretory pathway and could be involved in the egress process. They were selected for functional characterization in gametocytes. Additionally, PF3D7_0924000 (PNPLA3) was selected since two other patatin-like phospholipases, PNPLA1 and PNPLA2, have already been shown to fulfill important functions during intraerythrocytic parasite development thereby highlighting the special role patatin-like phospholipases play in key cellular processes (Table 1, Table 13) (Flammersfeld *et al.*, 2018, 2020; Singh *et al.*, 2019; Burda *et al.*, 2021). The functional characterization of phospholipases in gametocytes also included PF3D7_1476700 (LPL1, Table 1, Table 13) given that its role in gametocytes remained previously unexplored (Asad *et al.*, 2021; Burda *et al.*, 2021). Mass spectrometric evidence suggests that LPL1 is expressed in male gametocytes suggesting it might fulfill a sex-specific function (Lasonder, Sanna R Rijpma, *et al.*, 2016). Lastly, we included PF3D7_0709700 (PARE, Table 1, Table 13) in our analysis since transcriptomic data suggest it might be a female-specific phospholipase (Lasonder, Sanna R Rijpma, *et al.*, 2016). Moreover, PARE has been shown to have esterase activity (Istvan *et al.*, 2017). However, its phospholipase activity has not been investigated. Interestingly, PlasmoDB suggests four orthologs and paralogs for PARE which match with the four predicted orthologs and paralogs for LPL1 (Table 1).









GENE ID	ANNOTATION	ESSENTIAL?	SP?
PF3D7_0209100	Patatin-like phospholipase PNPLA1		<input type="checkbox"/>
PF3D7_0709700	Prodrug activation and resistance esterase	<input type="checkbox"/>	<input type="checkbox"/>
PF3D7_0731800	Alpha/beta hydrolase (LPL4)	<input type="checkbox"/>	
PF3D7_0908000	Plasma membrane protein 1	<input type="checkbox"/>	<input type="checkbox"/>
PF3D7_0924000	Patatin-like phospholipase PNPLA3	<input type="checkbox"/>	<input type="checkbox"/>
PF3D7_0937200	Lysophospholipase		<input type="checkbox"/>
PF3D7_1038900	Esterase	<input type="checkbox"/>	<input type="checkbox"/>
PF3D7_1126600	Steryl ester hydrolase		<input type="checkbox"/>
PF3D7_1238600	Sphingomyelin phosphodiesterase	<input type="checkbox"/>	<input type="checkbox"/>
PF3D7_1358000	Patatin-like phospholipase PNPLA2	<input type="checkbox"/>	<input type="checkbox"/>
PF3D7_1416300	NAPE-hydrolyzing phospholipase D		<input type="checkbox"/>
PF3D7_1411900	P1/s1 nuclease (PL39)	<input type="checkbox"/>	
PF3D7_1412000	P1/s1 nuclease (PL38)	<input type="checkbox"/>	
PF3D7_1476700	Lysophospholipase (LPL1)		<input type="checkbox"/>
PF3D7_1476800	Lysophospholipase	<input type="checkbox"/>	<input type="checkbox"/>

Table 13. Putative lipases with mass spectrometric evidence for expression in gametocytes. Bold: Phospholipases selected for characterization. Essentiality according to Burda *et al.* (2021). Red boxes, essential; white boxes, dispensable; grey boxes, n.d. Signal peptide (SP) according to SignalP or by the presence of an N-terminal transmembrane domain (TM) according to data deposited on PlasmoDB. White boxes, no SP/ TM; black boxes, SP or N-terminal TM present.

Based on the criteria outlined above, six members of the phospholipase gene family were selected to study their localization and characterize their importance for gametocyte development and gamete egress.

3.2.1 The six selected phospholipases show various localization patterns in blood stages

To study protein localization, the respective gene loci were targeted for endogenous C-terminal tagging with a fluorescent tag using a modified SLI-GFP construct (Figure 7A) (Birnbaum *et al.*, 2017), in which the GFP had been replaced by mScarlet. As the parental line, we made use of the inducible NF54/iGP2 line that allows for the production of high numbers of synchronous gametocytes and is transmission-competent, meaning it has maintained its ability to form gametes (Boltryk *et al.*, 2021). In this line, gametocyte commitment is driven by conditional overexpression of the sexual commitment factor GDV1 (Boltryk *et al.*, 2021).

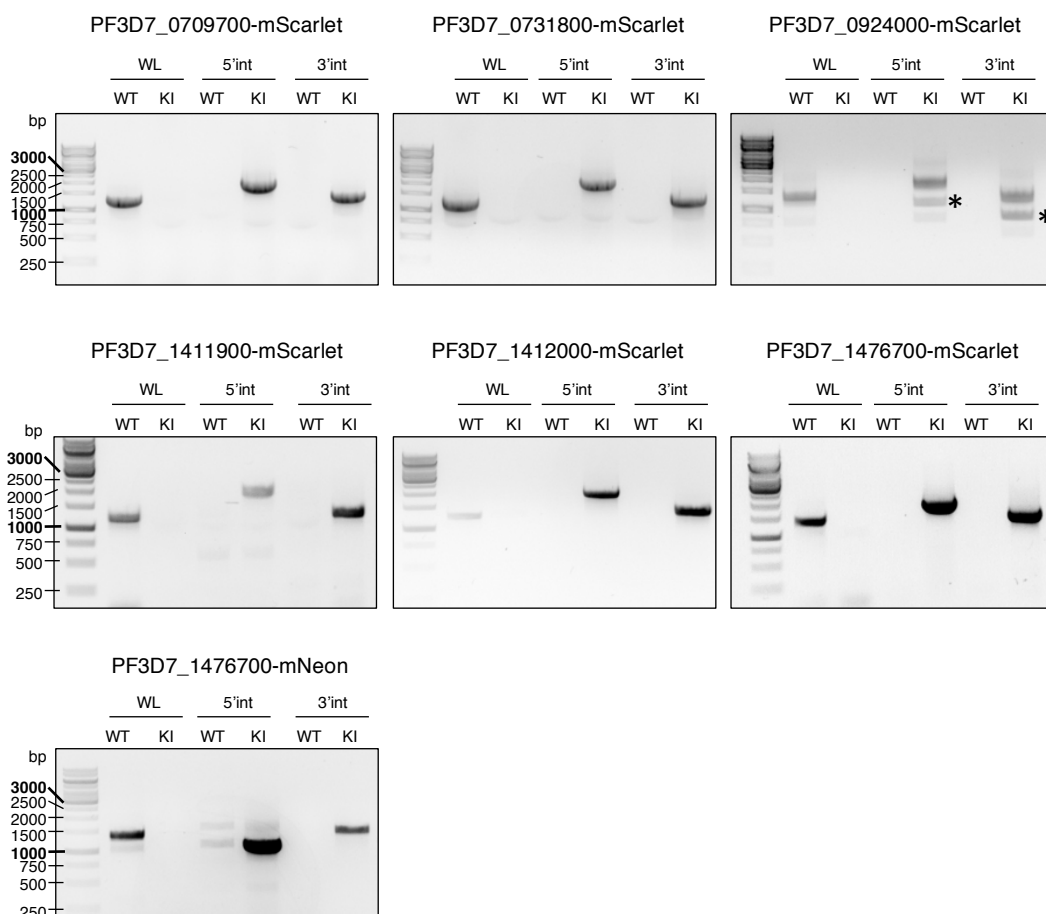


Figure 17. Analytical PCRs of mScarlet/mNeon-tagged parasite lines in the NF54/iGP2 and 3D7CH background. The SLI targeting strategy and the primer localizations are depicted in Figure 7A. GFP was replaced by mScarlet or mNeonGreen-glmS (mNeon), respectively. Instead of the *GFP rev* primer the primer *Neo rev* was used. Primers are listed in Table 8. WL, wildtype locus; 5'int, 5' integration; 3'int, 3' integration; KI, knock-in; *, unspecific double-band.

Results

All of the selected phospholipase candidates were tagged with mScarlet to avoid potential artifacts of (or overlaps with) the GDV1-GFP protein of the parental NF54/iGP2 line. Additionally, PF3D7_1476700 was tagged with mNeonGreen-glmS in the 3D7CH background which fully supports gametocyte development (Filarsky *et al.*, 2018). Correct integration of the respective constructs was confirmed by PCR (Figure 17).

PF3D7_0709700 is annotated as the prodrug activation and resistance esterase (PARE, Table 1) and has a predicted phospholipase activity. It is a protein with a molecular weight of 42 kDa. Its amino acid residues (aa) 30-362 are annotated as an α/β -hydrolase domain (Figure 18A). Transcriptomic data indicate PARE peak expression in trophozoites and schizonts (Wichers *et al.*, 2019) as well as in gametocytes (López-Barragán *et al.*, 2011).

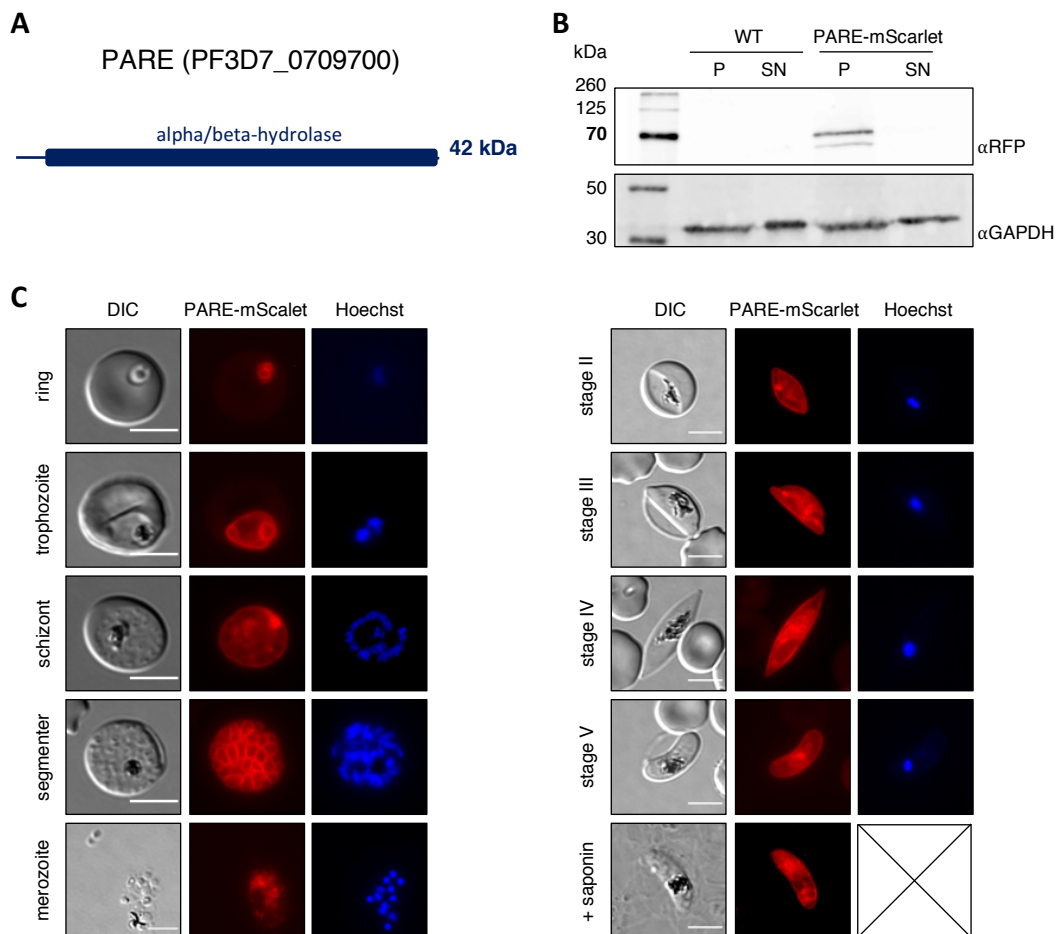


Figure 18. PARE localizes to the PPM. (A) Schematic of the PARE protein. (B) Western Blot of saponin-lysed C2-arrested schizonts. SN, supernatant; P, pellet. Expected sizes: 70 kDa (PARE-mScarlet), 38 kDa (GAPDH). (C) Live-cell microscopy of asexual blood stages (left) and gametocytes (right). Nuclei were stained with Hoechst. + saponin indicates that parasites were treated with 0.03% saponin for 5 min at room temperature before washing and imaging. Scale bars = 5 μ m.

To confirm the expression of the full-length PARE-mScarlet fusion protein, we performed a Western Blot analysis of C2-arrested, saponin-lysed schizonts. Saponin treatment of infected RBCs results in the disintegration of the RBCM and the PVM due to their high cholesterol content (Benting, Mattei and Lingelbach, 1994; Ansorge *et al.*, 1996). Intact parasites can be sedimented by centrifugation. Western Blot analysis revealed expression of the full-length PARE-mScarlet fusion protein in the pellet fraction indicating that the protein is not a soluble protein of the PV or the host cell cytoplasm (Figure 18B). Interestingly, some of the parasite cytoplasmic marker GAPDH leaked into the supernatant fraction after saponin lysis suggesting that the saponin treatment might have partially permeabilized the parasite plasma membrane (PPM) providing more indications that PARE is not localizing in the host cell cytoplasm. Live cell fluorescence microscopy revealed a peripheral localization of PARE-mScarlet in all asexual and sexual blood stages (Figure 18C), while the signal in merozoites appeared diffuse. Furthermore, treatment of stage V gametocytes with saponin did not abolish the peripheral localization (Figure 18C). Taken together, we conclude that PARE localizes to the PPM and is expressed throughout the intraerythrocytic life cycle.

PF3D7_0731800 has been annotated as lysophospholipase 4 (LPL4, Table 1). The protein has a molecular weight of 79 kDa and harbors a predicted phospholipase/monoglyceride lipase domain (aa113-672) with an α/β -hydrolase fold (aa288-503) (Figure 19A). Interestingly, it has a predicted N-terminal transmembrane domain (aa1-24) which might indicate that LPL4 is directed into the secretory pathway (Figure 19A). Western Blot analysis of stage V gametocytes revealed expression of full-length LPL4-mScarlet (Figure 19B). According to transcriptomic data, LPL4 shows the highest expression in late schizonts, free merozoites and young rings (Wichers *et al.*, 2019) as well as in stage II and stage V gametocytes (López-Barragán *et al.*, 2011). In line with the transcriptomic data, there was no fluorescence signal detectable in ring and trophozoite stages while schizont stages showed a weak punctuate pattern of LPL4-mScarlet in the cytoplasm and some signal in the food vacuole (Figure 19C). Throughout gametocyte development, LPL4-mScarlet localized to the DV (Figure 19D). The bright signal is in line with the higher expression in gametocytes compared to asexual stages. To exclude that the signal arose from autofluorescence of the hemozoin within the DV, NF54/iGP2 parasites from the parental line were imaged under the same conditions. Here, only in stage IV and V gametocytes some weak autofluorescence could be detected supporting our observation that LPL4-mScarlet localizes to the DV in gametocyte stages (Figure 19E). Notably, some parasites showed some additional LPL4-mScarlet signal in the parasite periphery (Figure 19D, stage II).

Pf3d7_0924000 encodes a putative patatin-like phospholipase, here termed patatin-like phospholipase 3 (PNPLA3, Table 1) since PNPLA1 and PNPLA2 have already been described (Singh *et al.*, 2019; Flammersfeld *et al.*, 2020; Burda *et al.*, 2021). PNPLA3 has a molecular weight of 151 kDa and contains a triacylglycerol lipase domain (aa126-241) as well as a patatin-like phospholipase domain (aa604-749) (Figure 20A). In addition, it harbors two predicted transmembrane domains (aa36-59 and aa269-289).

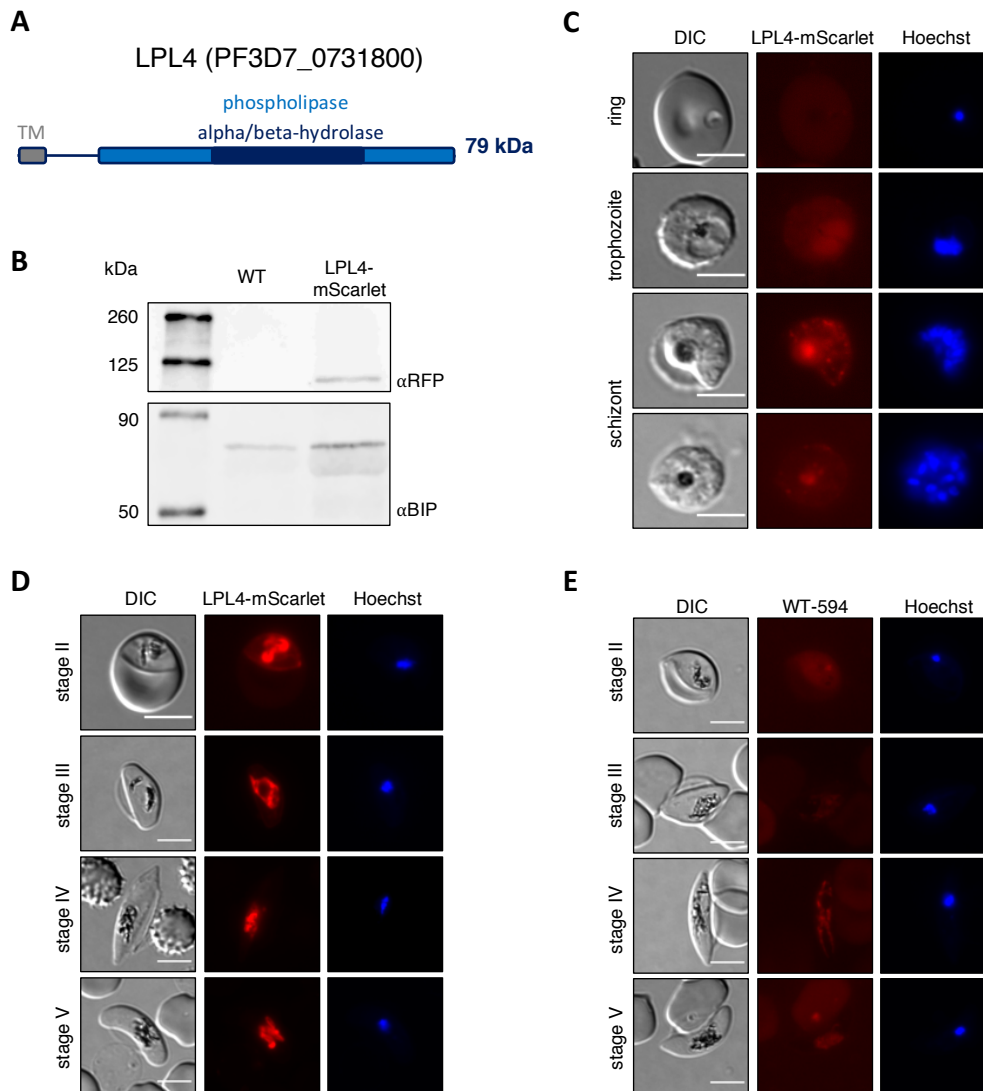


Figure 19. LPL4 localizes mainly to the DV. (A) Schematic of the LPL4 protein. TM, transmembrane domain. (B) Western Blot of Percoll-purified stage V gametocytes. Expected sizes: 107 kDa (LPL4-mScarlet), 70 kDa (BIP). (C-E) Live-cell microscopy of (C) asexual blood stages of LPL4-mScarlet, (D) gametocytes of LPL4-mScarlet, and (E) NF54/iGP2 wildtype gametocytes stained with Hoechst. Wildtype parasites were imaged under the same conditions as (C,D). Scale bars = 5 μ m.

Western Blot analysis of stage V gametocytes revealed expression of the full-length PNPLA3-mScarlet fusion protein as well as some free mScarlet (Figure 20B, loading control is missing). According to transcriptomic data, PNPLA3 has its peak expression in late schizonts (Wichers *et al.*, 2019) and in ookinetes (López-Barragán *et al.*, 2011). Interestingly, using live cell microscopy no PNPLA3-mScarlet signal could be detected in asexual stages except for the potential autofluorescence of the DV (Figure 20C). In gametocytes, the PNPLA3-mScarlet localization was irregular and diffuse, likely pointing towards a cytoplasmic localization that might be partially masked by the bright autofluorescence signal of the DV (Figure 20D-E). Additionally, the diffuse localization pattern might be caused by some fluorescence signal of

cleaved mScarlet that masks the true localization of the full-length PNPLA3-mScarlet fusion protein. Taken together, PNPLA3 localization remains elusive.

The gene *pf3d7_1411900* encodes a putative phospholipase, here termed phospholipase 39 (PL39, Table 1) due to its molecular weight of 39 kDa. It has a predicted signal peptide and contains a phospholipase C/P1 nuclease domain (aa23-315) (Figure 21A). Enzymes harboring these domains are typically involved in phosphate ester hydrolysis of lipids or nucleic acids (Coleman, 1992; Desai and Shankar, 2003). While some transcriptomic data indicate PL39 peak expression in young rings (Otto *et al.*, 2010; Wichers *et al.*, 2019), another study detects its transcript in late trophozoites and stage II gametocytes (López-Barragán *et al.*, 2011).

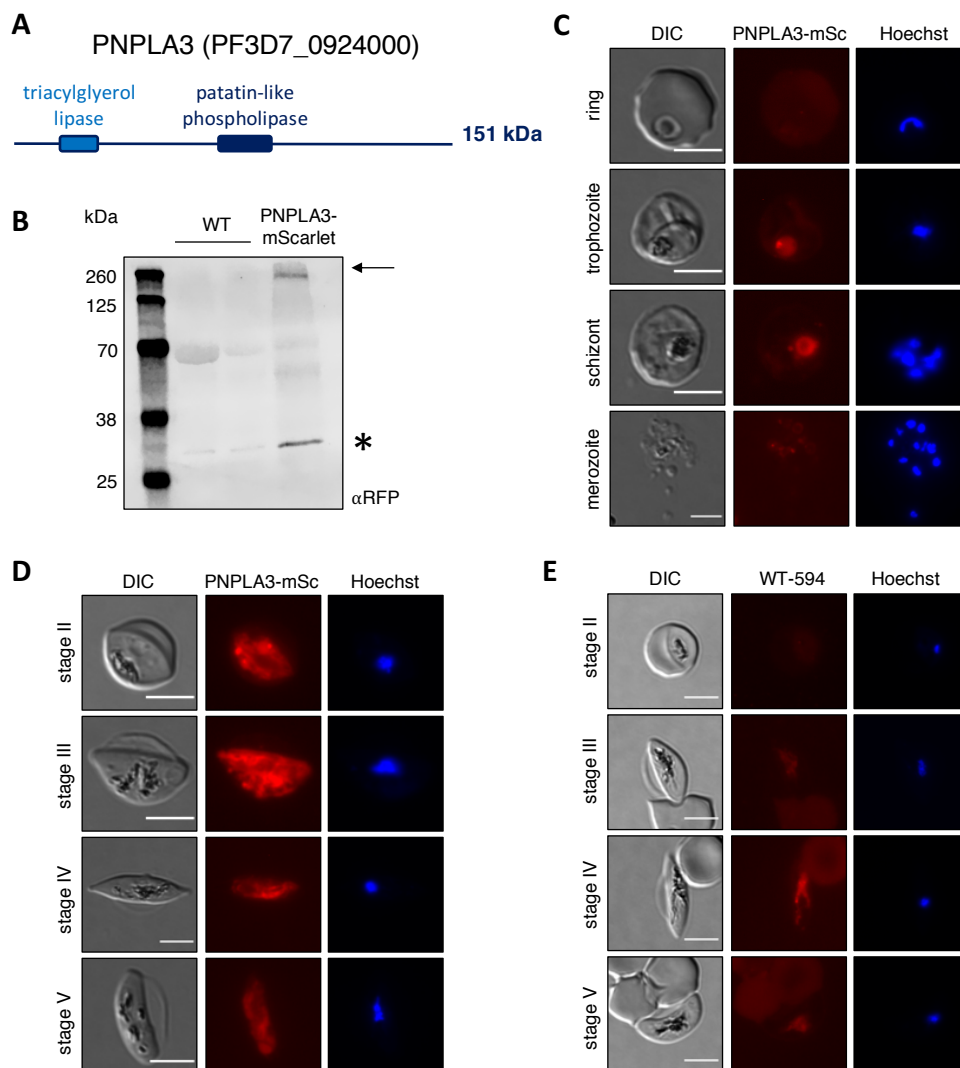


Figure 20. PNPLA3 shows an unspecific localization pattern. (A) Schematic of the PNPLA3 protein. (B) Western Blot of Percoll-purified stage V gametocytes. Expected size: 179 kDa. The asterisk indicates free mScarlet (28 kDa). (C-E) Live-cell microscopy of (C) asexual blood stages of PNPLA3-mScarlet, (D) gametocytes of PNPLA3-mScarlet, and (E) NF54/iGP2 wildtype gametocytes stained with Hoechst. Wildtype parasites were imaged under the same conditions as (C,D). Scale bars = 5 μ m.

Results

Western Blot analysis of C2-arrested schizonts revealed an inconclusive pattern (Figure 21B). Although the expected size for the PL39-mScarlet fusion protein is 67 kDa, a double band ran slightly lower than that and was also (partially) detected in the WT control lane, which points towards some cross-reactivity of the antibody. In addition, a band at higher molecular weight (around 120 kDa) corresponding to an unknown protein, and some free mScarlet were detected (Figure 21B). In stage V gametocytes, no bands for PL39-mScarlet were detected which is in line with the transcriptomic data that indicate an earlier expression peak (Figure 21B).

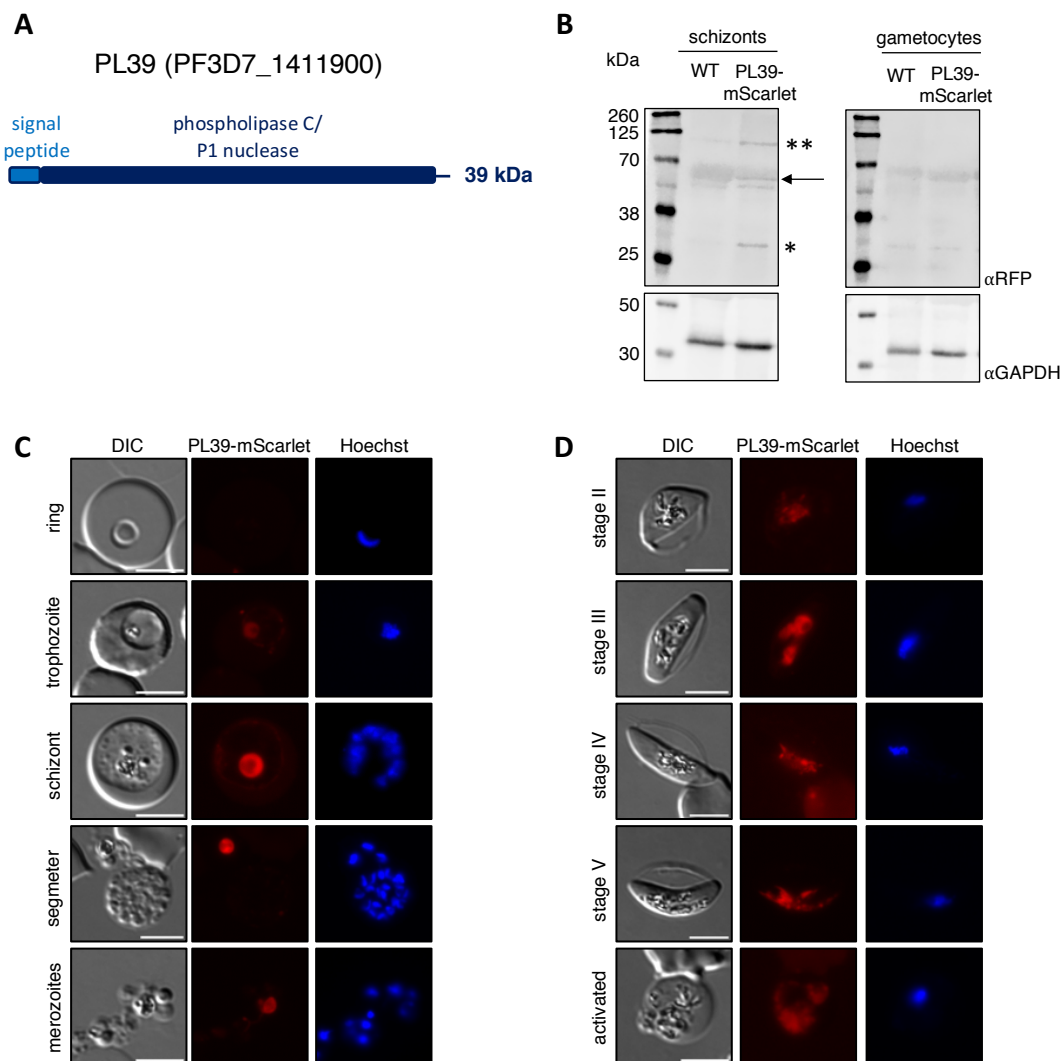


Figure 21. PL39 cannot be localized with high confidence. (A) Schematic of the PL39 protein. (B) Western Blot of Percoll-purified C2-arrested schizonts (left) and stage V gametocytes (right). Expected size: 67 kDa. The asterix indicates free mScarlet (28 kDa). Two asterixes indicate a likely unspecific band. (C-D) Live-cell microscopy of (C) asexual blood stages of PL39-mScarlet and (D) gametocytes of PL39-mScarlet. Nuclei were stained with Hoechst. Scale bars = 5 μ m.

Live cell fluorescence microscopy revealed localization of PL39-mScarlet to the DV in all asexual and sexual blood stages (Figure 21C-D) with a brighter signal than in the NF54/iGP2 parental line (Figure 19E, 20E) indicating that PL39 might localize to the hemozoin-containing DV. The presence of a (putative) signal peptide would argue for the export of PL39 into the PV. However, some exported proteins are diverted to or endocytosed into the DV where they might be further degraded (Adisa *et al.*, 2003). In conclusion, PL39-mScarlet localization needs to be further investigated.

The neighboring gene locus *pf3d7_1412000* encodes another putative phospholipase, here termed phospholipase 38 (PL38, Table 1) due to its molecular weight of 38 kDa. The genomic proximity of *pl39* and *pl38* and the presence of only one single orthologue in the rodent malaria parasite *P. berghei* at this genomic location (according to PlasmoDB) suggests that these loci are the result of gene duplication. However, since PL39 and PL38 show only 46 % sequence identity (according to ClustalW), they may have evolved to fulfill different functions. Similar to PL39, PL38 has a predicted signal peptide and contains a phospholipase C/P1 nuclease domain (aa19-312) (Figure 22A). However, in contrast to PL39, PL38 shows the highest expression in late-stage schizonts (Otto *et al.*, 2010; López-Barragán *et al.*, 2011; Wichers *et al.*, 2019) with some indication that it is also highly expressed in ookinetes (López-Barragán *et al.*, 2011). Surprisingly, we failed to detect PL38-mScarlet in C2-arrested schizonts by Western Blot analysis (Figure 22B). In stage V gametocytes, bands running at the correct size for PL38-mScarlet (66 kDa) and free mScarlet (28 kDa) were detected (Figure 22B). In live-cell microscopy, PL38-mScarlet shows a punctuate localization pattern in schizonts and free merozoites (Figure 22C) while in all other intraerythrocytic asexual stages and gametocytes no signal or only autofluorescence of the hemozoin could be observed (Figure 22C-D). The detection of PL38 in schizonts and merozoites is in line with the transcriptomic data but contrary to our Western Blot analysis highlighting the need to further verify this analysis. As the punctuate pattern of PL38-mScarlet was similar to an expected localization of apical markers, an immunofluorescence staining assay was performed which allowed co-staining with the marker Rap1 (for rhoptries) or SUB1 (for exonemes) (Figure 22E-F). PL38-mScarlet showed strong co-localization with Rap1 indicating that PL38 is a rhoptry protein (Figure 22E). The SUB1 staining was diffuse and did not show a strong overlap with the diffuse PL38-mScarlet signal suggesting that PL38 does not localize to the exonemes although additional staining assays and potentially super-resolution microscopy will be needed to verify this result (Figure 22E).

PF3D7_1476700 has been described as lysophospholipase 1 (LPL1, Table 1). The 41-kDa protein contains a phospholipase domain with an alpha/beta hydrolase fold (aa17-350) (Figure 23A) and recombinant LPL1 showed concentration-dependent lysophospholipase activity (Asad *et al.*, 2021). According to transcriptomic data it is expressed throughout asexual intraerythrocytic development (Otto *et al.*, 2010; Wichers *et al.*, 2019) but peaks in stage V gametocytes (López-Barragán *et al.*, 2011) with higher expression in female than in male gametocytes (Lasonder, Sanna R Rijpma, *et al.*, 2016).

Results

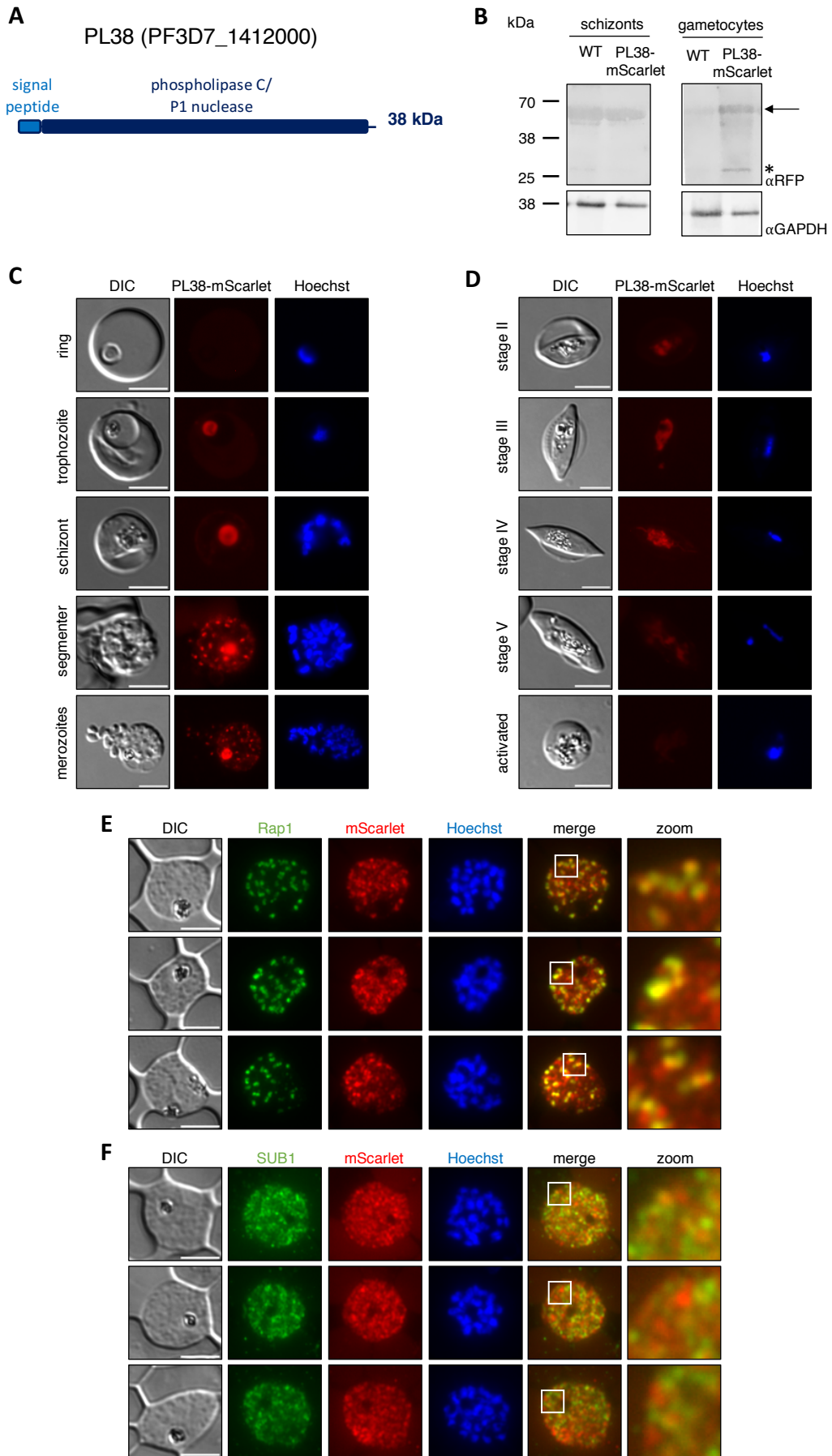


Figure 22. PL38 localizes to rhoptries. (A) Schematic of the PL38 protein. (B) Western Blot of Percoll-purified C2-arrested schizonts (left) and stage V gametocytes (right). Expected size of PL38-mScarlet: 66 kDa. The asterix indicates free mScarlet (28 kDa). Note that the Western Blot image of gametocytes has been mirrored from the original due to a likely swap of the samples. (C-D) Live-cell microscopy of (C) asexual blood stages of PL38-mScarlet and (D) gametocytes of PL38-mScarlet. Nuclei were stained with Hoechst. (E-F) Fluorescence microscopy of C2-arrested schizonts stained with anti-RFP (red), Hoechst (blue) and an apical marker (green): (E) Rap1 for rhoptries and (F) SUB1 for exonemes. Scale bars = 5 μ m.

Surprisingly, there was no fluorescence signal detected for LPL1-mScarlet in asexual stages except for some signal within the DV that might be explained by autofluorescence of the hemozoin (Figure 23B). However, in gametocyte stages, apart from the signal in the DV, some LPL1-mScarlet could be detected in the parasite periphery, even in activated gametocytes that egressed from the PV and RBC suggesting a localization at the PPM (Figure 23C). This localization is in partial conflict with published data localizing LPL1 to a multi-vesicular neutral lipid-rich body next to the DV in asexual blood stages (Asad *et al.*, 2021). To exclude an aberrant localization due to the mScarlet tag, LPL1 was also tagged with mNeonGreen-glmS (LPL1-mNeon). Tagging was performed in the non-fluorescent 3D7CH background. In ring and trophozoite stages, the LPL1-mNeon signal was very weak and localized mostly to the cytoplasm and in the periphery. A stronger LPL1-mNeon signal was detected in the periphery of schizont stages (with some fluorescence signal in the DV) and merozoites (with some cytoplasmic signal) (Figure 23D). In gametocyte stages, LPL1-mNeon was much more highly expressed and displayed a clear peripheral localization (Figure 23E). As LPL1-mNeon could be detected in the periphery of merozoites and LPL1-mScarlet was shown to localize in the periphery of activated gametocytes, we conclude that LPL1 likely localizes to the PPM.

Taken together, the six selected phospholipases show different gene expression patterns and localizations throughout intraerythrocytic development.

3.2.2 LPL1 is not essential for asexual intraerythrocytic development

To probe into the function of the six phospholipases for gametocyte development and egress, the respective gene loci were targeted for gene deletion in the NF54/iGP2 background (Boltryk *et al.*, 2021) using the SLI-TGD system (Figure 8A) (Birnbaum *et al.*, 2017). Correct integration of the respective constructs into the gene loci was verified by PCR (Figure 24A). Subsequently, the parasite lines will be referred to as knockout (KO) lines.

Previously, five of the six phospholipases (PARE, LPL4, PNPLA3, PL39, and PL38) were shown to be dispensable for asexual blood stage development using the same constructs used in this thesis but in the 3D7 background (Burda *et al.*, 2021). To complete the characterization of the six phospholipases in asexual blood stages, proliferation of LPL1-KO parasites was followed for three cycles. The growth assay revealed that LPL1 is dispensable for asexual growth (Figure 24B).

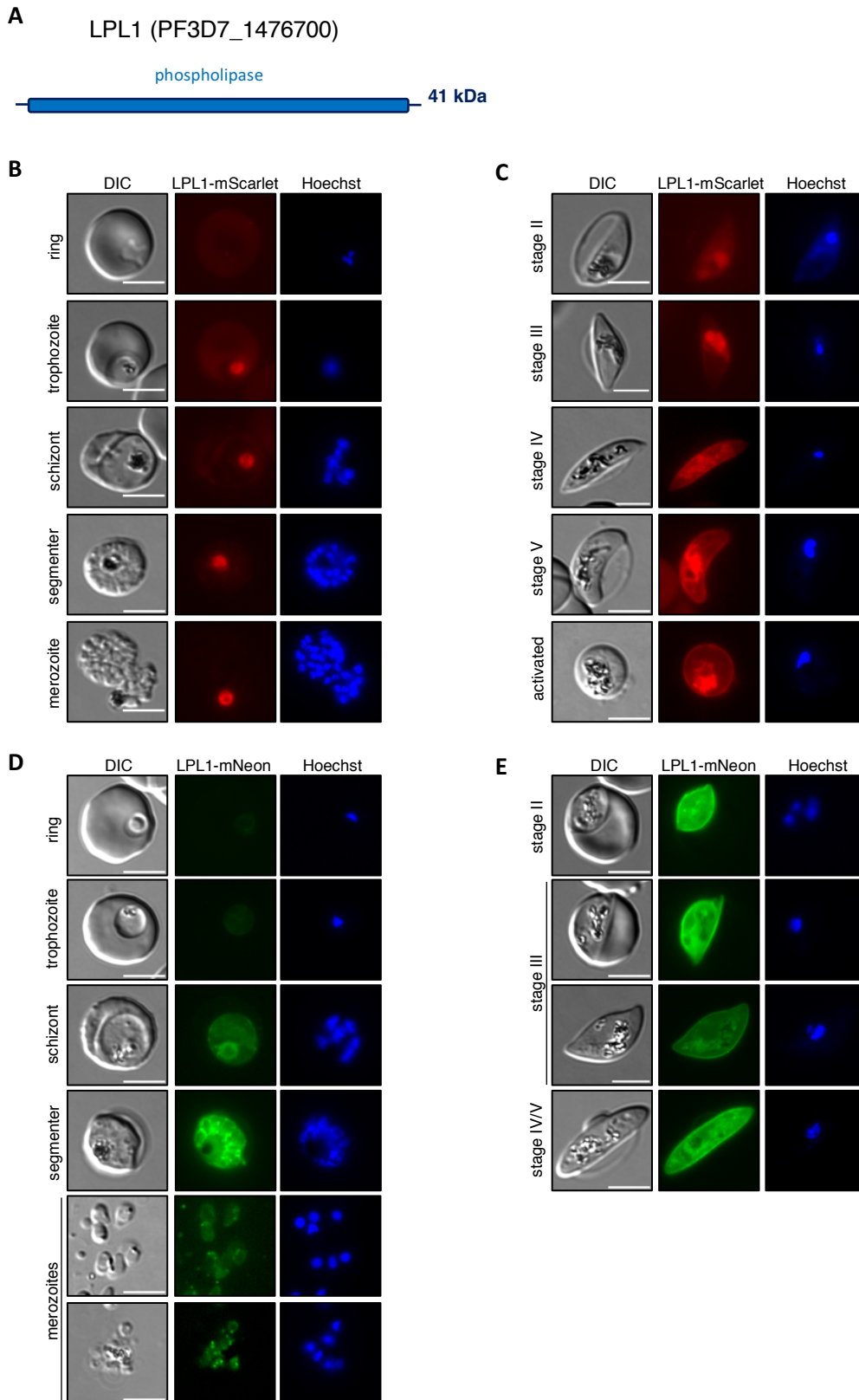


Figure 23. LPL1 localizes to the PPM. (A) Schematic of the LPL1 protein. (B-E) Live-cell microscopy of (B) LPL1-mScarlet asexual blood stages, (C) LPL1-mScarlet gametocytes, (D) LPL1-mNeon asexual blood stages, and (E) LPL1-mNeon gametocytes. Nuclei were stained with Hoechst. Scale bars = 5 μ m.

Results

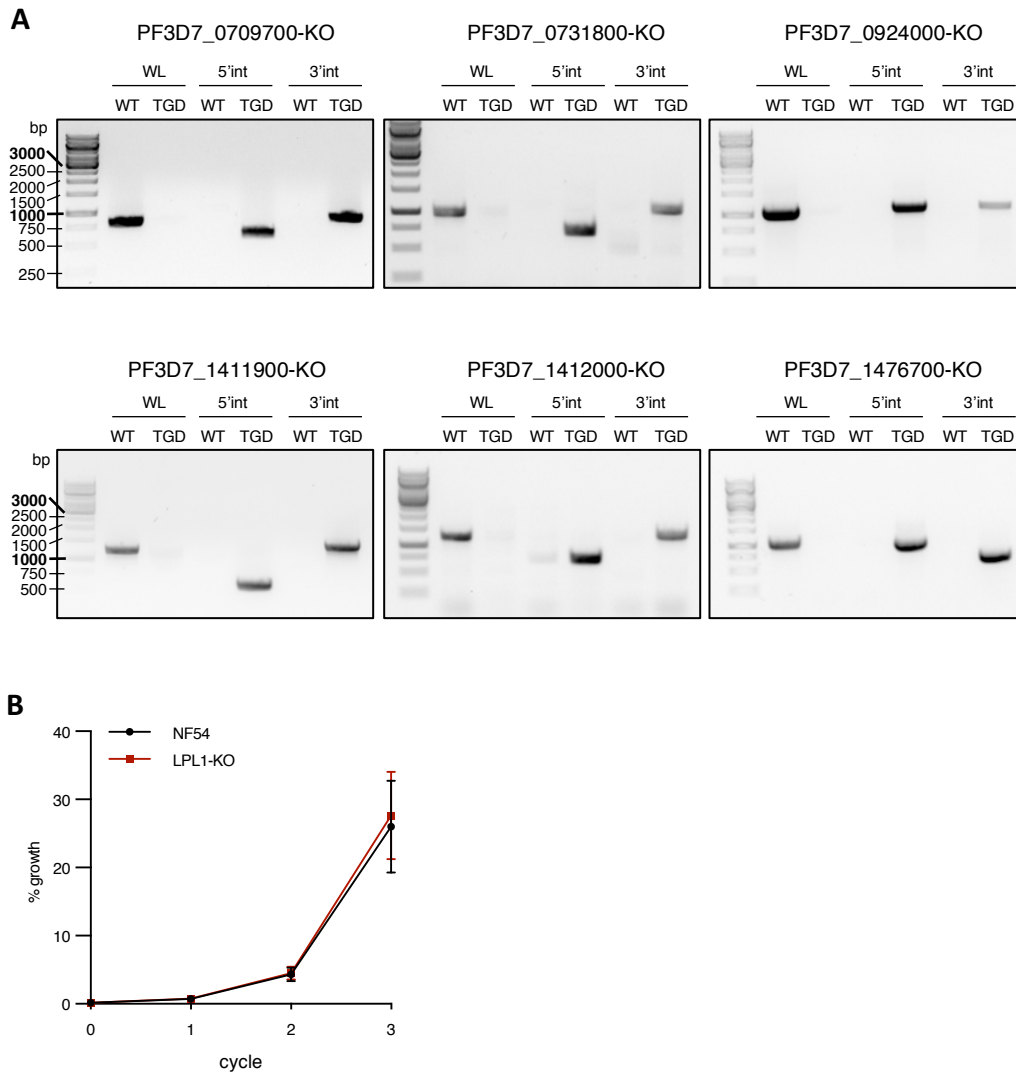


Figure 24. Analytical PCRs of KO parasite lines in the NF54/iGP2 background. (A) PCR images of the respective analytical PCRs. The SLI targeting strategy and the primer localizations are depicted in Figure 8A. Primers are listed in Table 8. WL, wildtype locus; 5'int, 5' integration; 3'int, 3' integration, TGD, targeted gene deletion. (B) Growth assay of LPL1-KO parasites over three cycles. Parasites were diluted 1:10 after the second cycle to prevent overgrowth. Mean \pm SD. $n=3$. Unpaired students t-test (not significant).

3.2.3 Loss of individual phospholipases does not impair gametocyte development

To study the function of the selected phospholipases in gametocyte development, gametocyte commitment was induced as described previously and gametocyte development was followed over two weeks (Figure 25A) (Boltryk *et al.*, 2021). Gametocyte survival rates describe the gametocytemia of stage V gametocytes in relation to the gametocytemia of stage III gametocytes. Quantification of gametocyte survival rates revealed that PARE-KO gametocytes had slightly lower gametocyte survival than WT gametocytes although this trend was not significant (Figure 25B). The other five phospholipase-KO lines showed similar gametocyte survival rates compared to the WT although the variations between the individual assays were high (Figure 25C-G).

Results

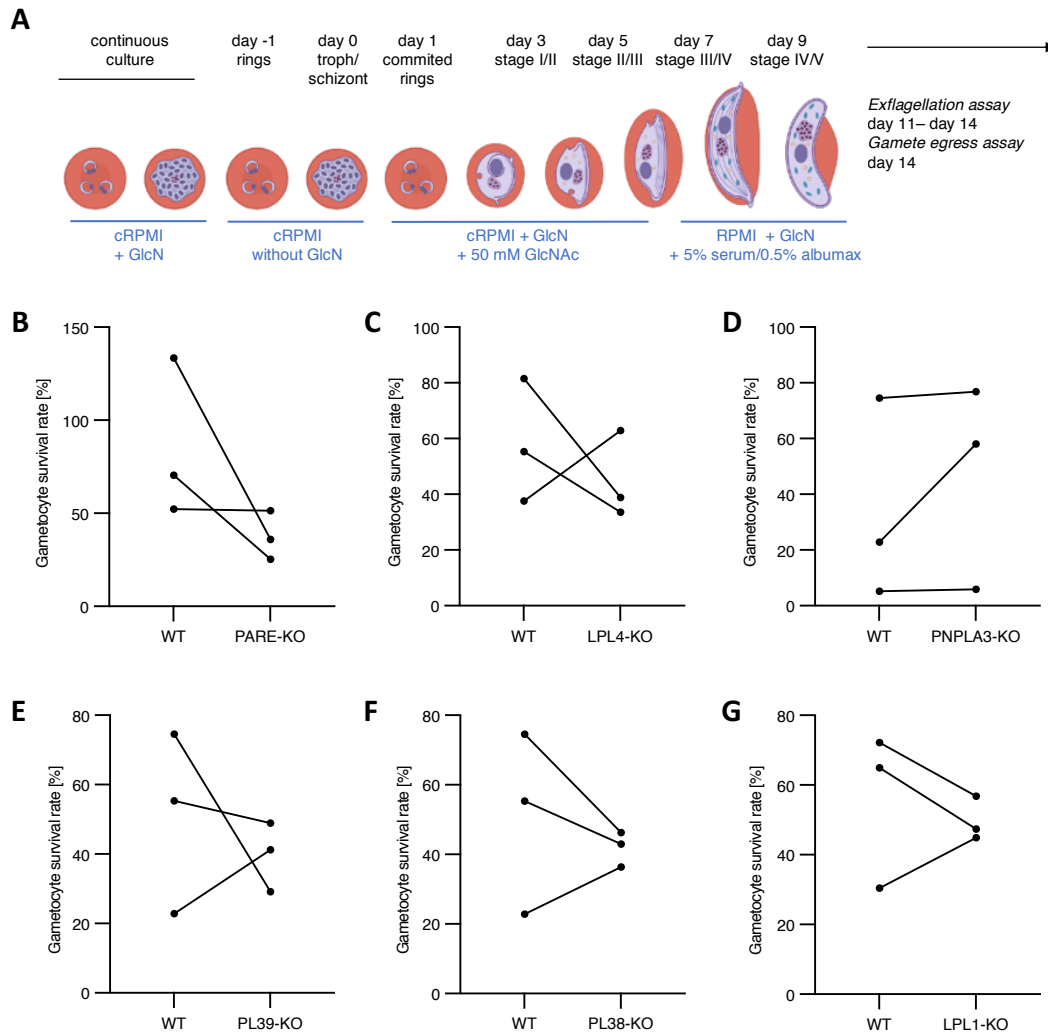


Figure 25. Individual KO of the six phospholipases does not impair gametocyte survival. (A) Schematic of the experimental strategy to study gametocyte development and gamete egress of phospholipase-KO lines in the NF54/iGP2 background. (B-G) Gametocyte survival rates as calculated by the ratio of gametocytemia of day 11/gametocytemia on day 5. Dots represent independent experiments. Lines connect the KO with the respective WT control. Please note that in some assays NF54/iGP2 WT gametocytes served as a control for several KO lines in parallel. (B) PARE-KO, (C) LPL4-KO, (D) PNPLA3-KO, (E) PL39-KO, (F) PL38-KO and (G) LPL1-KO. Unpaired students t-test for all lines (not significant).

Quantification of the gametocyte stages over the 11-day course of gametocytogenesis revealed that none of the phospholipase-KO lines showed a general defect in gametocyte maturation (Figure 26A-F). Notably, PNPLA3-KO parasites displayed a trend for more abnormal gametocyte stages on day 11 compared to the WT control but standard deviations were high (Figure 26C).

3.2.4 None of the tested phospholipases is required for gametogenesis

Next, we tested the exflagellation and general gamete egress of mature stage V gametocytes in the KO parasite lines. Exflagellation assays of the six phospholipase-KO lines were

Results

performed on four subsequent days (day 11 until day 14) in technical duplicates (Figure 27). While PARE-KO and LPL1-KO gametocytes showed similar exflagellation rates to WT parasites (Figure 27A, F), the three parasite lines LPL4-KO, PL39-KO and PL38-KO showed significantly higher exflagellation rates than WT parasites (Figure 27B, D-E). We can thus conclude that none of the five phospholipases plays an essential role in gametocyte exflagellation.

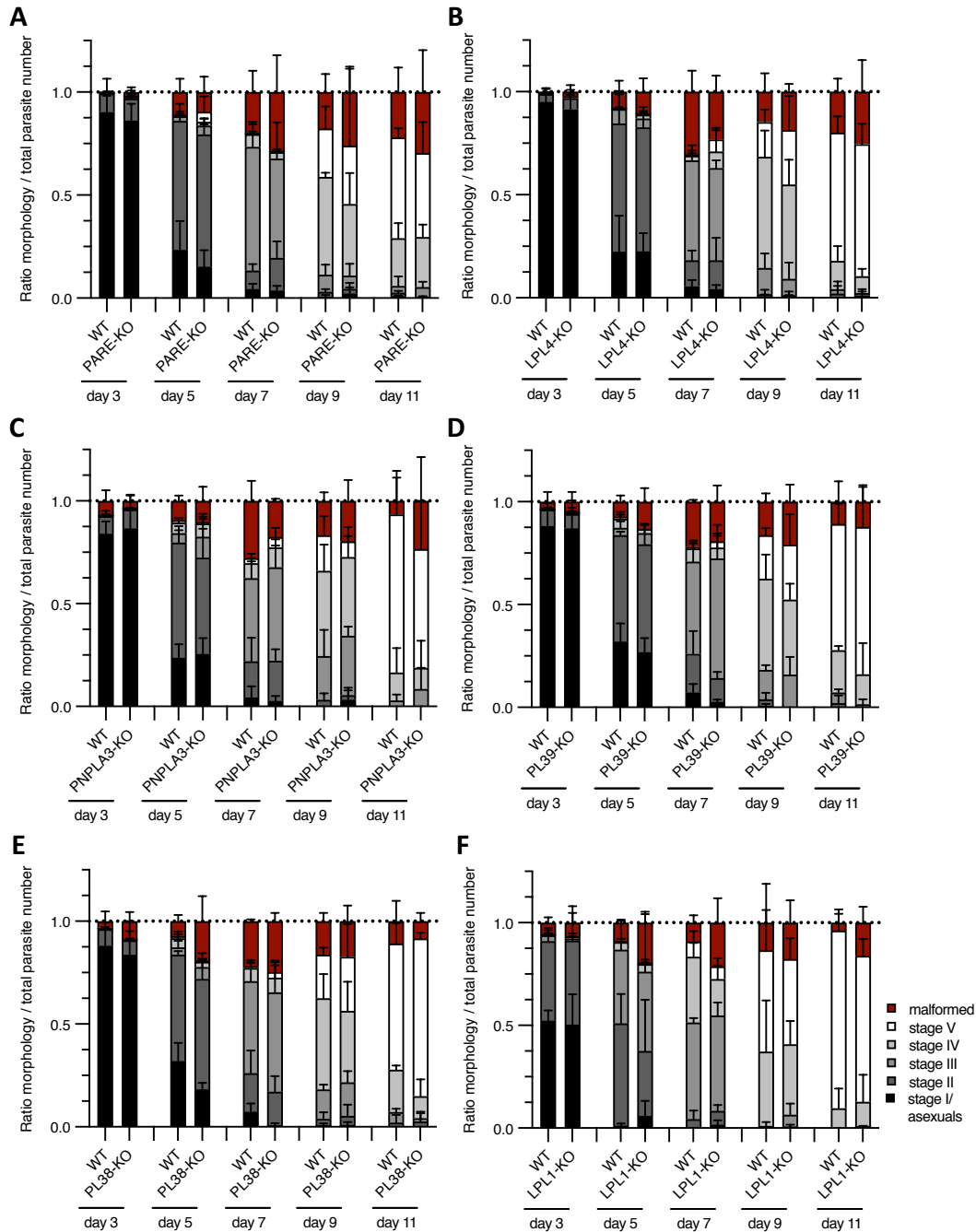


Figure 26. Individual KO of the six phospholipases does not impair gametocyte maturation. (A-F) Quantification of gametocyte stages on the days indicated below the graphs by counting Giemsa-stained thin blood smears. Mean + SD. $n=3$. Please note that in some assays NF54/iGP2 WT gametocytes served as a control for several KO lines in parallel. (A) PARE-KO, (B) LPL4-KO, (C) PNPLA3-KO, (D) PL39-KO, (E) PL38-KO and (F) LPL1-KO.

Results

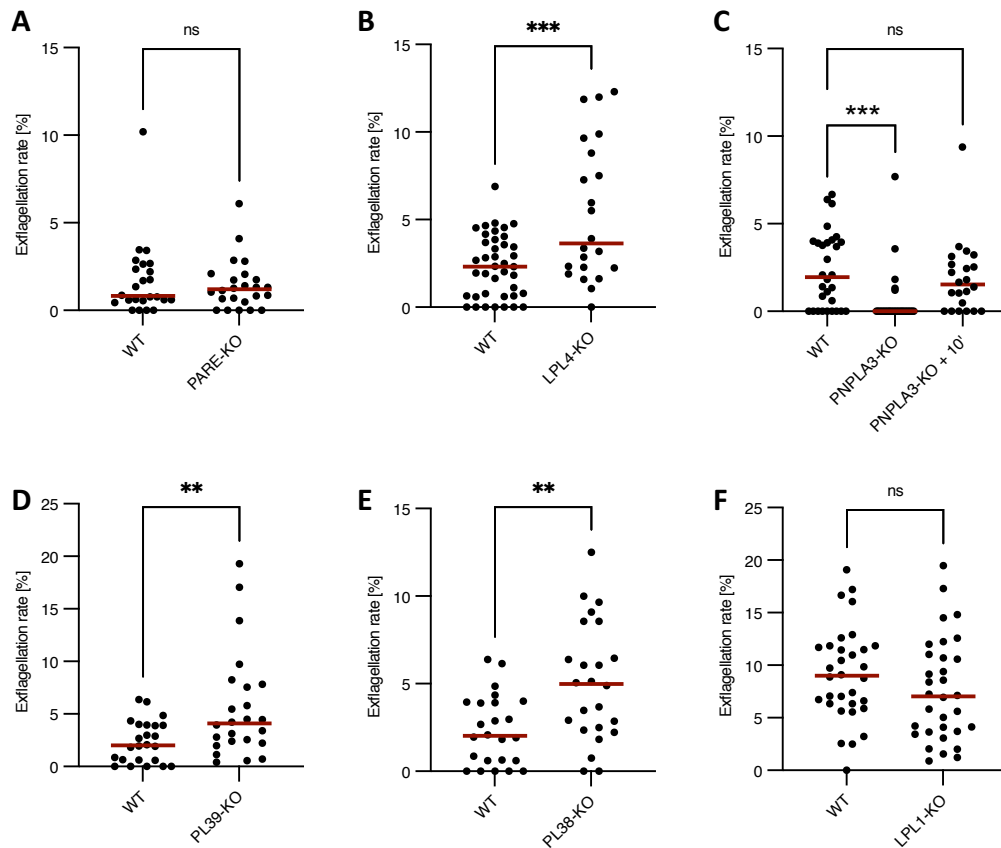


Figure 27. PNPLA3-KO shows a delay in exflagellation. (A-F) Exflagellation assays of (A) PARE-KO, (B) LPL4-KO, (C) PNPLA3-KO with 10 additional minutes of exflagellation time, (D) PL39-KO, (E) PL38-KO, and (F) LPL1-KO gametocytes. Graphs display superplots of three independent experiments. For each experiment, exflagellation was checked in technical duplicates on four subsequent days (day 11 – day 14). Red lines indicate the median of all exflagellation rates observed across all days and experiments for the respective parasite line. Unpaired students t-test (** $p < 0.01$, *** $p < 0.0005$). Please note that some assays were run in parallel with NF54/iGP2 gametocytes serving as control for several KO lines.

PNPLA3-KO gametocytes showed a significant reduction in exflagellation within the five minutes of observation time. Interestingly, exflagellation rates similar to WT parasites were achieved when the observation time was extended by 10 min (Figure 27C) indicating that loss of PNPLA3 might delay efficient exflagellation but is not deleterious.

While male gametocytes undergo a dramatic transformation leading to the formation of eight haploid motile microgametes, female gametes retain their spherical shape after egress from the RBC (Kuehn and Pradel, 2010). To study the egress capacity of female gametocytes, we made use of an established egress assay that uses live-cell fluorescence microscopy (Figure 28A) (Suarez-Cortés, Silvestrini and Alano, 2014; Neveu *et al.*, 2020). Before activation, the RBCM of RBCs infected with mature stage V gametocytes was stained using the live-cell dye iFluor555-wheat germ agglutinin (WGA). Subsequently, gametocytes were activated for 20 minutes and parasite morphology (falciform shape versus spherical shape) as well as the

Results

staining pattern (WGA-positive versus WGA-negative) were analyzed (Figure 28B) (Suárez-Cortés, Silvestrini and Alano, 2014; Neveu *et al.*, 2020).

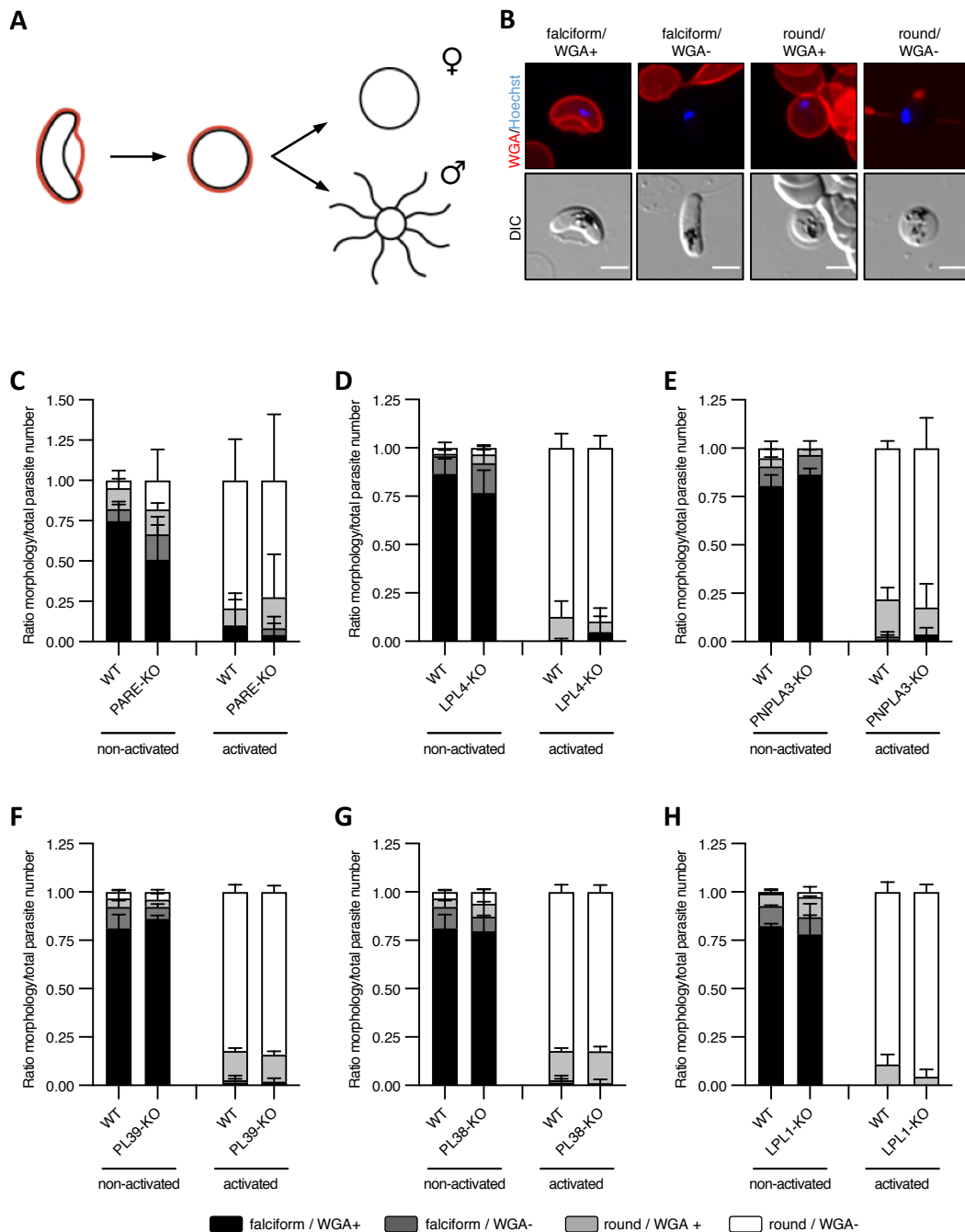


Figure 28. None of the phospholipase-KO lines shows a defect in gamete egress. (A) Schematic of the gamete egress assay. On day 14 of gametocytogenesis, the RBCM was stained with iFluor555-WGA (red). Upon activation, gametocytes first round up before egressing from the RBC thereby losing the iFluor555-WGA signal. Female gametocytes remain round while male gametocytes form eight motile flagella. (B) Representative images of the four categories used to categorize gametocytes/gametes in the gamete egress assay. Staining with iFluor555-WGA (red) and Hoechst (blue). DIC, differential interference contrast. Scale bar = 5 μ m. (C-H) Imaging-based gamete egress assays with (C) PARE-KO, (D) LPL4-KO, (E) PNPLA3-KO, (F) PL39-KO, (G) PL38-KO, and (H) LPL1-KO gametocytes. Activated samples: Gametocytes were activated for 20 min before imaging. At least 20 parasites were imaged per condition. Mean + SD. n=3.

The vast majority of non-activated gametocytes showed the expected falciform shape with strong iFluor555-WGA staining of the membrane (Figure 28C-H). We found that all of the six phospholipase-KO lines showed normal egress after activation indicated by rounding up and loss of the WGA signal (Figure 28C-H). Hence, we conclude that all of the six tested phospholipases are dispensable for general gamete egress.

Taken together, we found that all six phospholipase candidates are dispensable for gametocyte maturation and gamete egress. However, PNPLA3 might play a role in efficient exflagellation of male gametocytes.

4. Discussion

4.1 PNPLA2 is an important mitochondrial phospholipase for intraerythrocytic parasite development

Maintaining mitochondrial functions is crucial for parasite survival and several antimalarial drugs targeting these functions are effective. Here, I showed that *P. falciparum* parasites critically depend on the mitochondrial phospholipase PNPLA2 for asexual intraerythrocytic development and gametocytogenesis.

4.1.1 Loss of the mitochondrial phospholipase PNPLA2 leads to ultrastructural aberrations

Using GFP-tagging of the endogenous gene product, we localized PNPLA2 to the mitochondrion (Figure 7) which is supported by the presence of a predicted mitochondrial targeting sequence (MitoProt, (Claros and Vincens, 1996)) as well as by the identification of PNPLA2 in a recent proteomic analysis of the parasite mitochondrion using proximity-dependent biotinylation (Lamb *et al.*, 2022). Interestingly though, its predicted ortholog in the related apicomplexan parasite *Toxoplasma gondii* (TgPL2, TGME49_231370) localizes to the apicoplast (Lévêque *et al.*, 2017). Previous transcriptomic analyses indicated that peak expression of PNPLA2 in asexual blood stage parasites occurs during schizont development, roughly 36-48 hpi (Otto *et al.*, 2010; Toenhake *et al.*, 2018; Wichers *et al.*, 2019), which is in line with the observed expression of PNPLA2-GFP by microscopy.

Ultrastructural investigation of PNPLA2-KO parasites revealed no mitochondrial aberrations for the majority of mitochondria (Figure 10-12). However, KO parasites displayed a large, abnormal structure with dark osmium-stained membranes resembling the apicoplast in close proximity to the DV that could not be found in the WT (Figure 10-11). These structures contained other organelles in their lumen that were reminiscent of mitochondria (Figure 11). Of note, TgPL2 deletion results in an uncontrolled accumulation of membrane material in the apicoplast severely perturbing its homeostasis and function and ultimately resulting in parasite death (Lévêque *et al.*, 2017). However, a study in murine embryonic fibroblasts has shown that mitochondria can undergo active conversion between their normal morphology and a large spherical morphology in which they enwrap cytoplasm, membranes, vesicles and even another mitochondrion in response to the mitochondrial uncoupler carbonyl cyanide *m*-chlorophenylhydrazine (CCCP) (Ding *et al.*, 2012). This shows a remarkable resemblance to the PNPLA2-KO parasites that show a lower mitochondrial membrane potential (Figure 14E) and these large spherical structures (Figure 11). Moreover, an ultrastructural study in *T. gondii* tachyzoites similarly describes such large structures of mitochondrial origin and warns that these so-called ovoid mitochondrial cytoplasmic (OMC) complexes might be mistaken for the apicoplast (Köhler, 2006). While the *Toxoplasma* mitochondrial ultrastructure

typically displays a dual-membraned wall with cristae, the described *Toxoplasma* wildtype parasites also harbored oval-shaped organelles consisting of one or two evaginations of the single mitochondrion with six, eight or more membranous layers giving them the dark appearance in osmium staining (Köhler, 2006). The OMC was often found in proximity to the apicoplast or the Golgi and was detected at the end of the tachyzoite's lytic life cycle (Köhler, 2006). The large structure we observed in PNPLA2-KO parasites is also roughly spherical and resembles the multi-membranous apicoplast. In line with the *Toxoplasma* data, we found this structure in late-stage schizonts that are almost fully segmented as indicated by the divided and distributed mitochondria (Figure 11-12). Typically, the apicoplast divides and is distributed to the daughter parasites before the mitochondrion undergoes fission (van Dooren *et al.*, 2005; Rudlaff *et al.*, 2020) supporting the hypothesis that the aberrant structure in PNPLA2-KO parasites might be indeed derived from mitochondria. In disagreement with this hypothesis, nascent daughter merozoites, which harbor parts of the large structure, already contained a mitochondrion but no other apicoplast strongly arguing for an origin from the apicoplast rather than the mitochondrion. However, since mitochondria in *Plasmodium* asexual blood stages are acristae (Krungkrai, Prapunwattana and Krungkrai, 2000), further studies, potentially involving immunolabelling or using correlative light and electron microscopy methods, will be needed to investigate the origin of these curious large structures in detail.

Given the different localization of TgPL2 and PNPLA2, it is striking to observe that the loss of the respective proteins results in ultrastructural aberrations that might be linked to the apicoplast in both cases. However, the loss of the respective proteins differs greatly in its phenotypic severity: while KO of PNPLA2 leads to a growth defect of about 50 %, loss of TgPL2 is lethal. This difference in phenotypic severity might again be linked to the apicoplast. *Plasmodium* and *Toxoplasma* show different levels of dependence on the apicoplast-resident type II fatty acid biosynthesis pathway which is dispensable for intraerythrocytic development of *P. falciparum* but essential for *T. gondii* development (Mazumdar *et al.*, 2006; Yu *et al.*, 2008; Tarun, Vaughan and Kappe, 2009; Vaughan *et al.*, 2009; van Schaijk *et al.*, 2014) which may explain why the ultrastructural aberrations are not correlated with the severity of the loss-of-function phenotypes. Notably, the different localization of the orthologues raises the question whether TgPL2 and PNPLA2 are indeed true orthologues. Searching for other *Toxoplasma* candidates, we made use of proteomic hyperLOPIT data and identified two other (putative) mitochondrial phospholipases: TGME49_309940 and TGME49_246530. However, both are members of the phospholipase D family and thus can be excluded as true orthologues of PNPLA2 which belongs to the class of patatin-like phospholipases that exhibit phospholipase A2 activity (Barylyuk *et al.*, 2020).

In addition to the observed ultrastructural aberrations in the PNPLA2-KO parasites, we found that loss of PNPLA2 leads to abnormal, very bright patches (accumulations) of mitochondrial staining when using the live-cell dye MitoTracker CMXRos (Figure 9) suggesting a putative function of PNPLA2 in or during mitochondrial morphogenesis. Assuming that the large

organellar structure found by FIB-SEM is indeed of mitochondrial origin, we could speculate that loss of PNPLA2 impairs mitochondrial dynamics. In blood stages, the mitochondrion is a highly dynamic organelle that potentially undergoes self-fusion events (Van Dooren, Stimmler and McFadden, 2006) although no components of a fusion machinery have been identified. In mammalian cells, mitochondrial hyperfusion has been described as a compensatory mechanism during starvation signals (Rambold *et al.*, 2011). A similar mechanism was suggested for the formation of the spherical mitochondrion in murine embryonic fibroblasts when treated with CCCP (Ding *et al.*, 2012). Hence, the abnormal MitoTracker CMXRos staining in PNPLA2-KO parasites and the presence of the large spherical structure could suggest that the mitochondria might undergo a similar process of hyperfusion in response to the lower mitochondrial membrane potential or the starvation signals induced by a potential shortage of required phospholipid precursors generated by the putative phospholipase A2 function of PNPLA2. Interestingly, in *C. elegans* and mammalian cells, mitochondrial hyperfusion could also be induced by lowering Complex IV activity (Rolland *et al.*, 2013). The authors propose that mitochondrial hyperfusion is critical to maintaining cellular functions that require Complex IV activity. This is particularly intriguing considering that our Seahorse data suggest a decrease in Complex IV activity in PNPLA2-KO parasites.

4.1.2 PNPLA2 might be required for full activity of Complex IV

One of the main functions of the parasite's mtETC and especially Complex III is the recycling of ubiquinone. This reaction is of vital importance for the asexual blood stage parasite as ubiquinone is required for the DHODH and thus for the pyrimidine biosynthesis pathway. Although it might be tempting to speculate that loss of PNPLA2 impairs ubiquinone recycling thereby reducing pyrimidine synthesis and resulting in a slow-growing phenotype, our results do not support this hypothesis. We show that the ubiquinone pool is not affected as supplementation with DCUQ does not restore WT growth in PNPLA2-KO parasites (Figure 13I). Additionally, PNPLA2-KO parasites are similarly sensitive to the DHODH inhibitor DSM1 (Figure 13E). Taken together, this argues against an impaired pyrimidine biosynthesis pathway in PNPLA2-KO parasites.

A closer investigation of the mtETC revealed that PNPLA2-KO parasites show lower mitochondrial oxygen consumption rates (Figure 14B-C). Interestingly, even after TMPD treatment during the assay, PNPLA2-KO respiratory rates were lower than WT levels indicating that either Complex IV activity is impaired (but not completely abolished) or that the electron transfer from CytC to Complex IV is inefficient. In line with these results, PNPLA2-KO parasites are hypersensitive to drugs targeting the mtETC at or downstream of Complex III (Figure 13A-D).

Research has shown that the composition of Complex IV in *P. falciparum* is highly divergent to classic model systems but similar to the composition of Complex IV in the related

Apicomplexan parasite *T. gondii* (Evers *et al.*, 2021) where it was shown to associate with Complex III dimers. Notably, in mammalian cells, certain phospholipids of the inner mitochondrial membrane, in particular CL and PE, are required for full activity of the mtETC by affecting supercomplex formation of Complex III and IV and by regulating Complex IV activity (Pfeiffer *et al.*, 2003; Böttinger *et al.*, 2012). This way, CL and PE are also involved in the efficient generation of $\Delta\Psi_m$. Whether CL and PE are similarly required for the stabilization of supercomplexes in Apicomplexan parasites remains to be elucidated. However, a role of phospholipids in central mitochondrial functions in Apicomplexa seems likely as the KO of the likely phospholipid-hydrolyzing enzyme PNPLA2 results in a mitochondrial defect. Along these lines, the mitochondrial phospholipase iPLA₂ γ has been demonstrated to be required for full Complex IV activity in mice (Mancuso *et al.*, 2007): the loss of iPLA₂ γ resulted in impaired Complex IV activity associated with decreased (18:2)₄CL (Mancuso *et al.*, 2007). The authors conclude that the phospholipase iPLA₂ γ is essential for maintaining efficient bioenergetic mitochondrial function through tailoring mitochondrial membrane lipid metabolism and composition. One plausible explanation for the observed defects in PNPLA2-KO parasites would thus be a deregulated mitochondrial phospholipid metabolism which negatively affects the activity of the mtETC.

4.1.3 Loss of PNPLA2 might affect cardiolipin composition

To study whether PNPLA2 is involved in mitochondrial lipid metabolism, we performed targeted lipidomic analysis of WT and PNPLA2-KO parasites. We hereby focused on the mitochondria-specific CLs and - to our knowledge - study their composition in *P. falciparum* for the first time. We can mostly exclude that the measured CLs are derived from the host RBCs because mature RBCs expel their mitochondria and thus lose the vast majority of their CLs (Alberts *et al.*, 2002). Moreover, parasites were freed from the host RBCs by saponin lysis. Our lipidomic analysis of *P. falciparum* parasites revealed that *P. falciparum* showed a high abundance of CLs with long, even-numbered carbon chains and a remarkable variety in the number of double bonds with a peak at 8 (Figure 15). Interestingly, the profile resembled in carbon chain length and broadness the CL species in the murine cerebellum which show highly unsaturated and long carbon chains over a certain range around CL76:10 (Oemer *et al.*, 2020). In *T. gondii*, CL species show similar length and broadness as in our *Plasmodium* study with the same bias towards an even carbon chain length but *Toxoplasma* CLs seemed to have a higher degree of saturation (Fu *et al.*, 2018). Prokaryotic organisms generally display shorter CLs, also with odd chain length, that are typically highly saturated (Oemer *et al.*, 2018) suggesting that despite having the “bacterial” cardiolipin synthase CLS_pld (Tian, Feng and Wen, 2012), malaria parasites undergo CL remodeling which is only performed in eukaryotic organisms.

Upon loss of PNPLA2, parasites displayed a lower unsaturation index for CLs and their CL profile was slightly shifted towards shorter-chained CLs (Figure 15). However, the total abundance of CLs remained unchanged (Figure 15). Taken together, this suggests that loss of

PNPLA2 might not impair CL biosynthesis but rather CL remodeling. In the first step of CL remodeling, nascent CL is deacylated by a phospholipase to form monolysocardiolipin (MLCL). While the CLD1 has been described to fulfill this function in yeast, *Drosophila*, and mammalian cells, enzymes of the class of iPLA2 β or γ have been reported to catalyze this reaction (Beranek *et al.*, 2009; Malhotra *et al.*, 2009; Zachman *et al.*, 2010). Interestingly, PNPLA2 has been identified as the predicted iPLA2 γ homolog in *P. falciparum* (Tian, Feng and Wen, 2012) supporting a role for PNPLA2 in CL remodeling. However, the phylogenetic clade of Alveolata (incl. *Plasmodium* spp.) apparently lacks the second maturation enzyme required for CL remodeling, a homolog for TAZ or ALCAT (Tian, Feng and Wen, 2012). Thus, it remains unknown how MLCL would be reacylated to form a mature CL. One study identified the *T. gondii* ankyrin repeat-containing protein TgACBP2 (TGGT1_234510) as a key factor in cardiolipin metabolism (Fu *et al.*, 2018). However, its molecular function remains to be elucidated. Interestingly, loss of TgACBP2 had no effects on mitochondrial morphology but resulted in a reduced $\Delta\Psi_m$ and elevated ROS levels (Fu *et al.*, 2018) thereby linking CL remodeling to mitochondrial function rather than morphology. In line with this, we found that $\Delta\Psi_m$ was reduced in PNPLA2-KO parasites (Figure 14E) thereby supporting a link between PNPLA2, CL remodeling and mitochondrial function in *Plasmodium*.

If the PNPLA2 enzyme is indeed the *P. falciparum* homolog of the iPLA2 γ involved in CL remodeling, this gives rise to several hypotheses that could explain the observed phenotypes although until further investigation they remain speculative. As mentioned before, the loss of iPLA2 γ in mice leads to an accumulation of shorter-chained CL species; in particular, a decrease in (18:2)₄CL species was observed (Mancuso *et al.*, 2007, 2009). These alterations in the CL content were accompanied by a decrease in Complex IV activity and by enlarged, aberrant mitochondria (Mancuso *et al.*, 2007, 2009). Similarly, in our KO of PNPLA2 we observed an accumulation of shorter-chained CL species (Figure 15) as well as a decrease in OCRs that could be explained by a decrease in Complex IV activity (Figure 14). The resemblance is remarkable, especially when considering that (18:2)₄CL is CL72:8, given that CL species with a carbon chain length of 72 are highly abundant in *P. falciparum* (Figure 15A). In HEK cells, elevated levels of polyunsaturated FA18:2 and FA18:3 (α -linolenic acid) shifted the CL profile towards longer and more unsaturated acyl chains (Oemer *et al.*, 2022) and elevated levels of FA18:2 were linked to higher efficiency of mitochondrial respiration (Oemer *et al.*, 2018). Given that loss of PNPLA2 results in shorter, more saturated CL species and lower respiration, we could speculate that PNPLA2 is important for CL remodeling using C18 FA species.

Given the link between phospholipases, CL species and mitochondrial functions, we further investigated whether the growth phenotype of PNPLA2-KO parasites could be rescued by supplementation of the media with selected FAs. FA18:2 (linoleic acid with isomers) and FA18:1 (oleic acid and isomers) were shown to be the most influential acyl chains within the FA pools of CLs (Oemer *et al.*, 2020). As oleic acid is essential for parasite propagation (Mitamura *et al.*, 2000; Mi-Ichi, Kita and Mitamura, 2006; Mi-Ichi, Kano and Mitamura, 2007),

it was always supplemented in minimal FA medium next to palmitic acid (C16:0). Supplementation of mFA or cRPMI with stearic acid, vaccenic acid, linoleic acid or α -linolenic acid could not rescue the growth phenotype of PNPLA2-deficient parasites (Figure 15F). In conclusion, the loss of PNPLA2 shifts the CL profile towards shorter, more saturated carbon chains. However, this shift most likely cannot simply be explained by the shortage of the FAs that have previously been identified to be the most influential for CLs. This suggests that PNPLA2 might be directly involved in CL remodeling rather than in providing the required free FAs.

Notably, our analysis did not reveal any changes in the profile of non-cardiolipin lipid species (Figure 15E) thereby excluding a general effect of PNPLA2 deletion on lipid metabolism. In contrast, the loss of PNPLA1 was shown to result in increased levels of phospholipids and particularly higher absolute PC levels (Flammersfeld *et al.*, 2020) highlighting the different cellular functions of patatin-like phospholipases in the malaria parasite.

It is interesting to note, that fission and fusion of mitochondria have been shown to be functionally dependent on CL (Dudek, 2017). In the eukaryotic unicellular parasite *Trypanosoma brucei*, KO of the cardiolipin synthase resulted in reduced cellular CL levels and aberrant mitochondrial morphology (Serricchio and Bütikofer, 2012). Given that PNPLA2 seems to be important for the CL profile, we could speculate that the imbalance of CLs, albeit not changes in the total abundance of CLs, in the PNPLA2-KO might impair the fission of mitochondria late in intraerythrocytic development resulting in the large aberrant structures observed by FIB-SEM (Figure 11). Further experiments might shed light on this potential functional link.

In addition, the balance of phospholipid species, and especially of CLs, in the mitochondria is crucial for several mitochondrial tasks such as proton gradient buffering (Haines and Dencher, 2002), cristae formation (Ikon and Ryan, 2017), and mitochondrial respiration because the formation of mtETC supercomplexes depends on CLs (Pinheiro and Watts, 1994; Pfeiffer *et al.*, 2003; Mileykovskaya and Dowhan, 2009; Bazán *et al.*, 2013). Additionally, CLs have been shown to directly interact with CytC (Hanske *et al.*, 2012). We could speculate that the shift in the CL profile observed in PNPLA2-KO parasites (Figure 15) affects supercomplex formation in the mtETC and/or impairs the efficient electron transport from CytC to Complex IV. As a consequence, the electron flow through the mtETC might be lower which is in line with the measurements in the Seahorse assay (Figure 14). Moreover, sequestration of CLs in protein supercomplexes has been shown to be critical to protect CLs from degradation via the intermediate MLCL. The protein association was promoted by unsaturated CL species (Xu *et al.*, 2016). Although PNPLA2-KO did not result in lower CL abundance, we could speculate that the higher degree of saturation might impair supercomplex formation providing another strong argument for a link between PNPLA2 and efficient mitochondrial respiration. Future studies will need to test this hypothesis.

Malaria parasites rely on a functional and efficient mtETC for ubiquinone recycling and for generation of $\Delta\Psi_m$. To quantify $\Delta\Psi_m$ in the PNPLA2-KO, parasites were stained with the fluorescent mitochondrial dye Rhodamine123 which is readily sequestered by functioning mitochondria but easily washed out once the cells experience a loss in $\Delta\Psi_m$. Our analysis revealed that a higher proportion of PNPLA2-KO parasites show only weak or no mitochondrial staining in both, schizonts and gametocytes, while the majority of WT parasites displays the typical strong mitochondrial staining pattern (Figure 14E, 16H). This indicates that $\Delta\Psi_m$ might be lower in the PNPLA2-KO. Interestingly, the difference was enhanced by treatment of schizonts with Proguanil: While only few WT parasite lose their $\Delta\Psi_m$ when treated with 200 nM Proguanil, the majority of PNPLA2-KO parasites experiences $\Delta\Psi_m$ loss (Figure 14E). Notably, 200 nM is the approximate IC_{50} of Proguanil in PNPLA2-KO parasites (Figure 13D). At a concentration of 1 μ M Proguanil – which is even lower than the expected IC_{50} in WT parasites (Figure 13D) –, both WT and PNPLA2-KO parasites show an impaired ability to sustain the $\Delta\Psi_m$ (Figure 14E). Treatment of parasites with Atovaquone but not Proguanil alone has previously been described to disrupt $\Delta\Psi_m$ (Srivastava and Vaidya, 1999; Painter *et al.*, 2007). However, the Atovaquone concentration required to collapse $\Delta\Psi_m$ is reduced in the presence of Proguanil indicating that Proguanil inhibits a function to generate the $\Delta\Psi_m$ that only becomes essential when the electron flow over the mtETC is inhibited (Painter *et al.*, 2007). As PNPLA2-KO parasites have an impaired mtETC (Figure 14), we might argue that they rely more heavily on the Proguanil-sensitive pathway to generate $\Delta\Psi_m$ under physiological conditions. As a consequence, KO parasites might be hypersensitive to Proguanil, and Proguanil treatment might lead to a fast collapse of $\Delta\Psi_m$ as the parasites fail to sustain $\Delta\Psi_m$ via their impaired mtETC (Figure 13D).

Notably, the presence of a Proguanil-sensitive pathway to generate $\Delta\Psi_m$ was recently questioned by a study in yeast (Mounkoro, Michel and Meunier, 2021). The authors propose that Proguanil does not have a specific target but rather accumulates in the mitochondria to concentrations that impair multiple mitochondrial functions finally leading to cell death. They further suggest that Proguanil-resistant mutants show a decrease in ubiquinone levels which possibly alters the properties of the mitochondrial membranes and thus lowers the intramitochondrial level of Proguanil (Mounkoro, Michel and Meunier, 2021). Our data indicate that the ubiquinone pool of PNPLA2-KO parasites is unaffected (Figure 13I) although we cannot exclude it might be higher than in WT parasites. If it was higher, it might render parasites hypersensitive to Proguanil as this would be the opposite of the proposed mechanism for Proguanil resistance (Mounkoro, Michel and Meunier, 2021). Proguanil would then accumulate at high concentrations and could act as a factor that promotes the collapse of the $\Delta\Psi_m$. However, this hypothesis requires detailed investigation and extensive testing as the mtETC in *Plasmodium* is highly divergent from mtETC in yeast and other eukaryotic organisms.

Taken together, our data suggest that PNPLA2 is important for sustaining $\Delta\Psi_m$ via the mtETC indicating that PNPLA2 is important for full mitochondrial function. Loss of PNPLA2 leads to

a shift in the CL profile towards shorter-chained and more saturated CL species which could provide an explanation for the observed lower mitochondrial respiration and the lower $\Delta\Psi_m$.

4.1.4 Is the phospholipase activity of PNPLA2 required for regular mitochondrial function?

Many of the metabolites used in mitochondrial energy metabolism possess dual roles in modulating signaling cascades (e.g., acyl-CoA, acylcarnitines, fatty acids, and lysophosphatidic acid), thereby integrating lipid energy metabolism and cellular signaling functions (Mancuso *et al.*, 2007). Mitochondrial phospholipases are known to be important players in the regulation of mitochondrial function and signaling by exerting their enzymatic activity. However, biochemical activity of PNPLA2 as a hydrolyzing phospholipase has yet to be established.

Patatin-like phospholipases are highly conserved enzymes of prokaryotic and eukaryotic organisms with major roles in lipid homeostasis. Via their phospholipase A2 (PLA2) activity, PNPLAs are able to generate lysophospholipids and FAs, including polyunsaturated fatty acids, which are either further processed within the lipid metabolism pathway or may act as signaling molecules (Kienesberger *et al.*, 2009; Ramanadham *et al.*, 2015; Lévêque *et al.*, 2017; Wilson and Knoll, 2018). An important feature of patatin-like phospholipases is the catalytic Serine-Aspartate dyad of which the Serine is embedded within the conserved GX SXG motif (Arpigny and Jaeger, 1999; Banerji and Flieger, 2004; Ramanadham *et al.*, 2015). PNPLA2 harbors all these features of a functional enzyme but phospholipase activity remains to be tested. One possibility would be the recombinant expression of PNPLA2 and subsequent *in vitro* enzymatic profiling. In addition, recombinant expression would allow experimental determination of the 3D protein structure, e.g., by X-ray crystallography, NMR spectroscopy, or single-particle electron microscopy (Parker, 2003; Doerr, 2016; Hu *et al.*, 2021). Compared to the AlphaFold prediction (Figure 6), an experimental protein structure could provide reliable information about the folding of the full-length protein including the large, seemingly unstructured protein regions which might have an unknown fold or might represent true intrinsically disordered regions. Intrinsically disordered regions have been described to mediate peptide interactions and to be involved in regulating protein function, e.g., by undergoing posttranslational modifications (Babu, 2016). An experimental structure could thus give deeper insight into PNPLA2 function. Another possibility to test for phospholipase activity would be the complementation of PNPLA2-KO parasites with active site mutants. However, due to the size of PNPLA2 (240 kDa), cloning of the respective constructs with active site mutations poses a challenge. In addition, it would be favorable if the expression of the complementation constructs would be under the endogenous promoter to avoid effects resulting from different expression levels. Alternatively, CRISPR-Cas9 could be used to introduce active site or silent mutations into the endogenous locus of the enzyme, an approach that was performed for TgPL2 in *T. gondii* (Lévêque *et al.*, 2017). Although this approach as well as the complementation approach would not provide direct proof of

phospholipase activity, the failure to outgrow viable parasites with mutant PNPLA2 would strongly suggest that the enzymatic activity is important for PNPLA2 function.

Importantly, we provide two lines of genetic evidence that the observed mitochondrial phenotype in PNPLA2-KO mutants is indeed due to a loss of PNPLA2. Targeted gene deletion and DiCre-based conditional gene excision both lead to a similar growth phenotype with aberrant mitochondrial MitoTracker CMXRos staining (Burda *et al.*, 2021). However, additional studies are necessary to investigate potential (partial) compensatory mechanisms that are exploited by KO parasites which might explain why the mitochondrial function of PNPLA2 is important but not essential. The enzyme PfXL1 (PF3D7_1001400, annotated as exported lipase) could be an interesting candidate for detailed analysis for two reasons: i) it has a predicted lipase activity and ii) the MitoProt tool predicts the probability of this protein's export to the mitochondria with 0.94 (Claros and Vincens, 1996) indicating that PNPLA2 and XL1 might be redundant. However, overexpression of a GFP-tagged XL1 did not reveal a mitochondrial localization (Spillman, Dalmia and Goldberg, 2016). Thus, it remains to be determined whether PNPLA2 acts in concert with other phospholipases or whether it plays a unique role in blood stage parasites.

4.1.5 PNPLA2 is required for gametocyte maturation

Apart from analyzing the role of PNPLA2 in asexual blood stage development, its function was also characterized during gametocytogenesis. Interestingly, PNPLA2-KO parasites showed a strong maturation defect with about 50 % of gametocytes failing to form elongated late stages and instead displaying an abnormal rounded morphology (Figure 16). Additionally, PNPLA2-KO parasites showed an impaired ability to sustain the mitochondrial membrane potential in stage III gametocytes (Figure 16). Our results support the hypothesis that PNPLA2 is required for mitochondrial function(s) throughout asexual and sexual intraerythrocytic development. Moreover, our results would argue that gametocytes rely more heavily on mitochondrial functions which is in line with previous studies that investigated the importance of the mtETC and the TCA cycle during gametocytogenesis (MacRae *et al.*, 2013; Ke *et al.*, 2015; Evers *et al.*, 2021). Future studies should probe into the role of PNPLA2 in mosquito stages that rely on functional mitochondria even more including central carbon pathways such as the TCA cycle (Ke *et al.*, 2015; Srivastava *et al.*, 2016).

In conclusion, our study reveals the importance of PNPLA2 for mitochondrial function in both asexual blood stages and gametocytes. Thereby, it highlights the mitochondrial lipid metabolism as a potential target for future antimalarial drugs with activity against the disease-causing asexual blood stages and the transmission-competent gametocytes.

4.2 Phospholipases show high redundancy in gameto(cyto)genesis

Phospholipases were shown to be important players in asexual intraerythrocytic development and egress from liver stages (Burda *et al.*, 2015, 2021; Srivastava and Mishra, 2022). The second part of this thesis aimed to expand the functional characterization of phospholipases and explore their role in gametocytogenesis and gamete development.

Six individual phospholipases were characterized. Five of them had previously been shown to be dispensable for asexual growth by our group (Burda *et al.*, 2021). In contrast to published data (Asad *et al.*, 2021), here I showed that LPL1 is dispensable for asexual growth (Figure 24B). The discrepancy between the two findings might be explained by the different genetic systems used to generate the data: Asad *et al.* (2021) used a conditional knockdown system in which the gene of interest is tagged with the *E. coli* degradation domain that allows for fast downregulation of protein translation by degrading the mRNA transcript (Asad *et al.*, 2021). In contrast, in this thesis, I used the SLI system that leads to gene truncation and thus a functional KO but requires parasite selection over several cycles using drug selection markers (Figure 8A) (Birnbaum *et al.*, 2017). This extended culture in absence of the protein might upregulate compensatory mechanisms thereby masking the true function of protein candidates. Lysophospholipases such as LPL1 likely play a key role in lysoPC degradation by producing glycerophosphocholine that is then further cleaved to choline by a glycerophosphodiesterase (PfGDPD) and used for PC biosynthesis (Ramaprasad *et al.*, 2022). Loss of PfGDPD could be rescued by supplementation with exogenous choline that could be directly metabolized by the parasite thereby bypassing the KO of PfGDPD (Ramaprasad *et al.*, 2022). As the continuous culture of our LPL1-KO line was performed in a cell culture medium with a high concentration of choline to prevent gametocyte commitment (Filarsky *et al.*, 2018; Boltryk *et al.*, 2021), we could speculate that the high levels of exogenous choline may complement the LPL1 deletion phenotype in a similar manner to the rescue of a PfGDPD-KO. This provides another explanation for the observed differences in the LPL1 deletion phenotype. However, this thesis and the study by Asad *et al.* (2021) also observe different LPL1 localizations: I localized LPL1 to the PPM using two different fluorescent tags (Figure 21) which is different from its published localization in foci in the ER and close to the DV (Asad *et al.*, 2021). Asad *et al.* (2021) present clear evidence that the foci that LPL1 localizes to correspond to lipid storage vesicles and that they are distinct from membrane labeling despite their vicinity to the PPM. For their analysis, they tagged LPL1 endogenously using GFP and HA and performed live-cell imaging. However, their immunoblots suggest that some of the respective HA and GFP tag was cleaved (Asad *et al.*, 2021) which might prevent proper assessment of protein localization. Nevertheless, localization in lipid storage vesicles would be in line with the suggested role of LPL1 in neutral lipid generation and heme detoxification (Asad *et al.*, 2021). In contrast, LPL1 localization at the PPM as presented in this thesis would suggest a different role for this enzyme during intraerythrocytic development. Further detailed functional characterization will be needed to explain the different findings between the studies and to clarify and elucidate the role of LPL1 during blood stage development.

Phospholipases fulfill several cellular functions during blood stage development which is highlighted by the different localization patterns of the six phospholipase candidates selected for characterization. We showed that PARE and LPL1 both localize to the PPM. However, PARE was shown to be expressed in asexual stages and gametocytes (Figure 16) while LPL1 seemed to be higher expressed in gametocytes (Figure 21). Interestingly, both candidates harbor a predicted $\alpha\beta$ -hydrolase domain. The $\alpha\beta$ -hydrolase fold is common to a number of hydrolytic enzymes of widely differing phylogenetic origin and catalytic function. The core of each enzyme is an $\alpha\beta$ -sheet containing eight strands that are connected by helices (according to InterPro). Individual KO of the LPL1 and PARE did not result in a defect in gametocytogenesis or gamete egress (Figure 23-24). Although it is tempting to speculate about the redundancy of these two enzymes due to their similar localization and structure, future studies will need to provide proof for this hypothesis.

In contrast to LPL1 and PARE, PL38 could not be detected in gametocytes using live-cell microscopy. Instead, PL38 localizes to the rhoptries which is in line with transcriptomic data suggesting a late expression peak in asexual intraerythrocytic development (López-Barragán *et al.*, 2011). However, in disagreement with these data, the respective Western Blot analysis detects PL38-mScarlet in gametocytes but not schizonts (Figure 20). Loss of PL38 did not impair gametocytogenesis or gamete egress (Figure 23-24) which would be in line with a function in late asexual blood stages. Further analysis will be required to clarify PL38 expression. Notably, PL38 is the first phospholipase that has been shown to localize to an apical organelle. Phospholipases have been suggested to play a role in invasion for a long time since they might be involved in creating the pore between rhoptry contents and the host cell cytoplasm (Saffer and Schwartzman, 1991). In line with this hypothesis, the *T. gondii* patatin-like phospholipase TgPL3 (TGME49_305140) has been localized to the apical pole and its phospholipase activity was shown to be necessary for rhoptry secretion (Wilson *et al.*, 2020). We could speculate that the phospholipase activity of PL38 might be involved in the invasion process by pore formation or by influencing membrane composition or curvature. However, gene deletion did not result in an impairment of invasion processes (Burda *et al.*, 2021). Future studies might explore the interplay of PL38 with rhoptry-resident invasion factors and with the membranes of the parasite and its host cell.

Similar to the three candidates described above, LPL4 and PL39 were dispensable for gametocyte maturation and egress including exflagellation (Figure 23-24). LPL4 seemed to be expressed throughout intraerythrocytic development which is in line with transcriptomic data (Otto *et al.*, 2010; López-Barragán *et al.*, 2011; Wichers *et al.*, 2019). It was mainly localized to the DV (Figure 17). In contrast, the localization and expression of PL39 remain to be elucidated (Figure 19).

The last remaining phospholipase candidate, PNPLA3, is expressed in stage V gametocytes as confirmed by Western Blot analysis (Figure 18). However, its exact localization remains elusive as the signal in gametocytes was irregular and diffuse (Figure 18). Interestingly,

PNPLA3-KO gametocytes showed a notable delay in - but not complete abolishment of - exflagellation (Figure 24). Of note, PNPLA3 expression peaks in ookinetes (López-Barragán *et al.*, 2011) which is in line with an important role during gametogenesis and transition into the subsequent zygote and ookinete stage.

Our screen of six selected phospholipase candidates in gametocytes revealed that none of those is essential for gametocyte and gamete development suggesting functional redundancy of these enzymes during this complex cellular process. In line with this, the high degree of redundancy of phospholipases in *P. falciparum* was already described in our global screen of asexual blood stages (Burda *et al.*, 2021). However, our screen does not exclude important functions in other life stages such as ookinetes. Future experiments might aim to explore the dependency of phospholipases on each other and to elucidate potential compensatory mechanisms, e.g., by generating double/triple/multiple lipase KO parasites.

An unexplored but nevertheless interesting aspect of this study is the gametocyte sex ratio. It is known that the sex ratio is affected by environmental factors which may optimize parasite transmission as well as by epigenetic components (Josling and Llinás, 2015). In *P. falciparum*, ordinarily one male gametocyte is observed for three or four females. As male gametocytes form eight flagella, this establishes an approximate 1:1 ratio in the mosquito midgut. However, large fluctuations in the gametocyte sex ratio are observed (Talman *et al.*, 2004). The high variability of the sex ratio might explain why some KO parasite lines – namely LPL4-KO, PL39-KO and PL38-KO - seemingly exflagellated better than the WT parasites (Figure 27), especially when considering that PL38 might not be expressed in gametocytes at all (Figure 22). Alternatively, in the respective KO parasite lines, the sex ratio might be increased towards males thereby increasing the number of exflagellation events that can be observed. In support of this hypothesis, PL39 is higher expressed in female than male gametocytes according to transcriptomic data (Lasonder, Sanna R Rijpma, *et al.*, 2016). Thus, the KO of PL39 might drive parasites to differentiate into male gametocytes. However, LPL4 shows higher expression levels in males (Lasonder, Sanna R Rijpma, *et al.*, 2016), thereby contradicting our hypothesis.

In conclusion, we characterized six (putative) phospholipases during gametocytogenesis revealing a high level of redundancy. Exploring their interplay might allow a deeper understanding of the parasite's lipid metabolism during asexual and sexual blood stage development.

4.3 Future perspectives

P. falciparum parasites are heavily reliant on a functional and correctly regulated lipid metabolism. In this thesis, I provided a functional analysis of the mitochondrial patatin-like phospholipase (PNPLA2, PF3D7_1358000) in asexual stages and gametocyte development,

and characterized six phospholipase-KO lines for potential defects in gametocyte development.

I showed that PNPLA2 is required for regular mitochondrial function of asexual blood stages and gametocytes and is involved in cardiolipin metabolism. Future studies might explore the link between CLs and mitochondrial functions in *Plasmodium* further as their connection has been established for several other (eukaryotic) organisms such as yeast and mammalian cells (Serricchio and Bütikofer, 2012; Baker *et al.*, 2016). As deletion of PNPLA2 is not lethal for the parasite, its exploitation as a potential drug target is questionable. However, the PNPLA2-KO could be a valuable tool to investigate the lipid metabolism of *P. falciparum* and could guide future studies of asexual blood stages and gametocytes. Modulation of lipid supplementation and inactivation of other phospholipases or acyltransferases with a putative function in cardiolipin metabolism might help us move forward and push the boundaries of our current knowledge of the parasite's lipid metabolism.

In addition, I showed that *P. falciparum* gametocytes express several phospholipases during gametocyte development that do not play essential roles in *in vitro* gametocyte maturation or gametogenesis when individually targeted for gene deletion. Taken together with our study in asexual blood stages (Burda *et al.*, 2021), this reveals a high level of redundancy in the class of *Plasmodium* phospholipases, highlighting the need for further investigation of their interplay. Although the six selected phospholipases do not represent attractive drug targets *per se* due to their dispensability, broadly acting phospholipase inhibitors might be suitable antimalarials when they inhibit several members of this class that are involved in various critical cellular processes. Drug specificity might be given by the divergence of *Plasmodium* and their mammalian hosts. In line with this, the antimalarial drug Salinipostin A has been identified as a broadly acting α/β serine hydrolase inhibitor that favors plasmodial hydrolases over mammalian ones (Yoo *et al.*, 2020). Interestingly, PNPLA2 and PARE (among others) were identified as targets of Salinipostin A and of the pan-lipase inhibitor isopropyl dodecylfluorophosphonate (Elahi *et al.*, 2019; Yoo *et al.*, 2020) highlighting the potential of this enzyme class as a target for antimalarial drug development. In order to guide future development, we require a profound understanding of the parasite's lipid metabolism. This thesis provides a first step in that direction.

References

- Absalon, S., Robbins, J.A. and Dvorin, J.D. (2016) 'An essential malaria protein defines the architecture of blood-stage and transmission-stage parasites', *Nature Communications*, 7(1). doi:10.1038/ncomms11449.
- Adisa, A. *et al.* (2003) 'The signal sequence of exported protein-1 directs the green fluorescent protein to the parasitophorous vacuole of transfected malaria parasites', *Journal of Biological Chemistry*, 278(8), pp. 6532–6542. doi:10.1074/jbc.M207039200.
- Agarwal, P. *et al.* (2017) 'In vitro susceptibility of Indian Plasmodium falciparum isolates to different antimalarial drugs & antibiotics', *The Indian Journal of Medical Research*, 146(5), pp. 622–628. doi:10.4103/ijmr.IJMR_1688_15.
- Agnandji, S.T. *et al.* (2014) 'Efficacy and Safety of the RTS,S/AS01 Malaria Vaccine during 18 Months after Vaccination: A Phase 3 Randomized, Controlled Trial in Children and Young Infants at 11 African Sites', *PLoS Medicine*, 11(7), p. e1001685. doi:10.1371/journal.pmed.1001685.
- Aktas, M. *et al.* (2014) 'Membrane lipids in Agrobacterium tumefaciens: biosynthetic pathways and importance for pathogenesis', *Frontiers in Plant Science*, 5, p. 109. doi:10.3389/fpls.2014.00109.
- Alberts, B. *et al.* (2002) *Molecular Biology of the Cell*. 4th editio. Garland Science.
- Aldritt, S.M., Joseph, J.T. and Wirth, D.F. (1989) 'Sequence identification of cytochrome b in Plasmodium gallinaceum', *Molecular and Cellular Biology*, 9(9), pp. 3614–3620. doi:10.1128/mcb.9.9.3614-3620.1989.
- Amino, R. *et al.* (2006) 'Quantitative imaging of Plasmodium transmission from mosquito to mammal', *Nature Medicine*, 12(2), pp. 220–224. doi:10.1038/nm1350.
- Amos, B. *et al.* (2022) 'VEuPathDB: The eukaryotic pathogen, vector and host bioinformatics resource center', *Nucleic Acids Research*, 50(D1), pp. D898–D911. doi:10.1093/nar/gkab929.
- Andreadaki, M. *et al.* (2018) 'Sequential Membrane Rupture and Vesiculation during Plasmodium berghei Gametocyte Egress from the Red Blood Cell', *Scientific Reports*, 8(1), pp. 1–13. doi:10.1038/s41598-018-21801-3.
- Angulo, I. and Fresno, M. (2002) 'Cytokines in the pathogenesis of and protection against malaria', *Clinical and Diagnostic Laboratory Immunology*, 9(6), pp. 1145–52. doi:10.1128/cdli.9.6.1145-1152.2002.
- Ansorge, I. *et al.* (1996) 'Protein sorting in Plasmodium falciparum-infected red blood cells permeabilized with the pore-forming protein streptolysin O', *Biochemical Journal*, 315(1), pp. 307–314. doi:10.1042/bj3150307.
- Arbon, D. *et al.* (2022) 'Repurposing of mitochondria-targeted tamoxifen: Novel anti-cancer drug exhibits potent activity against major protozoan and fungal pathogens', *bioRxiv* [Preprint]. doi:10.1101/2022.03.24.485593.
- Arpigny, J.L. and Jaeger, K.E. (1999) 'Bacterial lipolytic enzymes: classification and properties', *The Biochemical Journal*, 343(1), pp. 177–83. Available at: <http://www.ncbi.nlm.nih.gov/pubmed/10493927>.
- Asad, M. *et al.* (2021) 'An essential vesicular-trafficking phospholipase mediates neutral lipid synthesis and contributes to hemozoin formation in Plasmodium falciparum', *BMC Biology*, 19(1). doi:10.1186/s12915-021-01042-z.
- Aurrecochea, C. *et al.* (2009) 'PlasmoDB: a functional genomic database for malaria parasites', *Nucleic Acids Research*, 37(Database), pp. D539–D543. doi:10.1093/nar/gkn814.
- Babu, M.M. (2016) 'The contribution of intrinsically disordered regions to protein function, cellular

- complexity, and human disease', *Biochemical Society Transactions*, 44(5), pp. 1185–1200. doi:10.1042/BST20160172.
- Baker, C.D. *et al.* (2016) 'Specific requirements of nonbilayer phospholipids in mitochondrial respiratory chain function and formation', *Molecular Biology of the Cell*, 27(14), pp. 2161–2171. doi:10.1091/mbc.E15-12-0865.
- Baker, D.A. *et al.* (2017) 'A potent series targeting the malarial cGMP-dependent protein kinase clears infection and blocks transmission', *Nature Communications*, 8(1), pp. 1–9. doi:10.1038/s41467-017-00572-x.
- Banerji, S. and Flieger, A. (2004) 'Patatin-like proteins: a new family of lipolytic enzymes present in bacteria?', *Microbiology*, 150(Pt 3), pp. 522–525. doi:10.1099/mic.0.26957-0.
- Bannister, L.H. *et al.* (2000) 'A brief illustrated guide to the ultrastructure of *Plasmodium falciparum* asexual blood stages', *Parasitology Today*, 16(10), pp. 427–33. doi:10.1016/S0169-4758(00)01755-5.
- Barylyuk, K. *et al.* (2020) 'A Comprehensive Subcellular Atlas of the *Toxoplasma* Proteome via hyperLOPIT Provides Spatial Context for Protein Functions', *Cell Host & Microbe*, 28(5), pp. 752–766.e9. doi:10.1016/j.chom.2020.09.011.
- Baum, J. *et al.* (2006) 'Regulation of apicomplexan actin-based motility', *Nature Reviews Microbiology*, 4(8), pp. 621–628. doi:10.1038/nrmicro1465.
- Bazán, S. *et al.* (2013) 'Cardiolipin-dependent reconstitution of respiratory supercomplexes from purified *Saccharomyces cerevisiae* complexes III and IV', *Journal of Biological Chemistry*, 288(1), pp. 401–411. doi:10.1074/jbc.M112.425876.
- Beaumelle, B.D. and Vial, H.J. (1986) 'Modification of the fatty acid composition of individual phospholipids and neutral lipids after infection of the simian erythrocyte by *Plasmodium knowlesi*.', *Biochimica et biophysica acta*, 877(2), pp. 262–70. doi:10.1016/0005-2760(86)90303-6.
- Belikova, N.A. *et al.* (2006) 'Peroxidase Activity and Structural Transitions of Cytochrome c Bound to Cardiolipin-Containing Membranes', *Biochemistry*, 45(15), pp. 4998–5009. doi:10.1021/bi0525573.
- Bennink, S., Kiesow, M.J. and Pradel, G. (2016) 'The development of malaria parasites in the mosquito midgut', *Cellular Microbiology*, 18(7), pp. 905–918. doi:10.1111/cmi.12604.
- Bennink, S. and Pradel, G. (2021) 'Vesicle dynamics during the egress of malaria gametocytes from the red blood cell', *Molecular and Biochemical Parasitology*, 243(111372). doi:10.1016/j.molbiopara.2021.111372.
- Benting, J., Mattei, D. and Lingelbach, K. (1994) 'Brefeldin A inhibits transport of the glycoporphin-binding protein from *Plasmodium falciparum* into the host erythrocyte', *Biochemical Journal*, 300(3), pp. 821–826. doi:10.1042/bj3000821.
- Beranek, A. *et al.* (2009) 'Identification of a cardiolipin-specific phospholipase encoded by the gene CLD1 (YGR110W) in yeast', *Journal of Biological Chemistry*, 284(17), pp. 11572–11578. doi:10.1074/jbc.M805511200.
- Billker, O. *et al.* (1998) 'Identification of xanthurenic acid as the putative inducer of malaria development in the mosquito', *Nature*, 392(6673), pp. 289–292. doi:10.1038/32667.
- Birnbaum, J. *et al.* (2017) 'A genetic system to study *Plasmodium falciparum* protein function', *Nature Methods*, 14(4), pp. 450–456. doi:10.1038/nmeth.4223.
- Birnbaum, J. *et al.* (2020) 'A Kelch13-defined endocytosis pathway mediates artemisinin resistance in malaria parasites', *Science*, 367(6473), pp. 51–59. doi:10.1126/science.aax4735.
- Bisio, H. *et al.* (2020) 'The ZIP Code of Vesicle Trafficking in Apicomplexa: SEC1/Munc18 and SNARE Proteins', *mBio*. Edited by L.M. Weiss, 11(5). doi:10.1128/mBio.02092-20.
- Boltryk, S.D. *et al.* (2021) 'CRISPR/Cas9-engineered inducible gametocyte producer lines as a valuable

- tool for Plasmodium falciparum malaria transmission research', *Nature Communications*, 12(1), p. 4806. doi:10.1038/s41467-021-24954-4.
- Böttinger, L. *et al.* (2012) 'Phosphatidylethanolamine and cardiolipin differentially affect the stability of mitochondrial respiratory chain supercomplexes', *Journal of Molecular Biology*, 423(5), pp. 677–686. doi:10.1016/j.jmb.2012.09.001.
- Boysen, K.E. and Matuschewski, K. (2011) 'Arrested oocyst maturation in Plasmodium parasites lacking type II NADH:Ubiquinone dehydrogenase', *Journal of Biological Chemistry*, 286(37), pp. 32661–32671. doi:10.1074/jbc.M111.269399.
- Bozdech, Z. *et al.* (2003) 'The transcriptome of the intraerythrocytic developmental cycle of Plasmodium falciparum', *PLoS Biology*, 1(1), p. E5. doi:10.1371/journal.pbio.0000005.
- Bozdech, Z. and Ginsburg, H. (2004) 'Antioxidant defense in Plasmodium falciparum - data mining of the transcriptome', *Malaria Journal*, 3, p. 23. doi:10.1186/1475-2875-3-23.
- Brancucci, N.M.B. *et al.* (2017) 'Lysophosphatidylcholine Regulates Sexual Stage Differentiation in the Human Malaria Parasite Plasmodium falciparum', *Cell*, 171(7), pp. 1532-1544.e15. doi:10.1016/j.cell.2017.10.020.
- Bullen, H.E. *et al.* (2016) 'Phosphatidic Acid-Mediated Signaling Regulates Microneme Secretion in Toxoplasma', *Cell Host & Microbe*, 19(3), pp. 349–360. doi:10.1016/j.chom.2016.02.006.
- Burda, P.-C. *et al.* (2015) 'A Plasmodium Phospholipase Is Involved in Disruption of the Liver Stage Parasitophorous Vacuole Membrane', *PLoS Pathogens*, 11(3), p. e1004760. doi:10.1371/journal.ppat.1004760.
- Burda, P.-C. *et al.* (2021) 'Global analysis of putative phospholipases in the malaria parasite Plasmodium falciparum reveals critical factors for parasite proliferation', *bioRxiv*, p. 2021.06.28.450158. doi:10.1101/2021.06.28.450158.
- Canfield, C.J., Pudney, M. and Gutteridge, W.E. (1995) 'Interactions of atovaquone with other antimalarial drugs against Plasmodium falciparum in vitro', *Experimental Parasitology*, 80(3), pp. 373–381. doi:10.1006/expr.1995.1049.
- Cao, J. *et al.* (2004) 'A Novel Cardiolipin-remodeling Pathway Revealed by a Gene Encoding an Endoplasmic Reticulum-associated Acyl-CoA:Lysocardiolipin Acyltransferase (ALCAT1) in Mouse', *Journal of Biological Chemistry*, 279(30), pp. 31727–31734. doi:10.1074/jbc.M402930200.
- Claros, M.G. and Vincens, P. (1996) 'Computational method to predict mitochondrially imported proteins and their targeting sequences', *European Journal of Biochemistry*, 241(3), pp. 779–786. doi:10.1111/j.1432-1033.1996.00779.x.
- Cobbold, S.A. *et al.* (2013) 'Kinetic flux profiling elucidates two independent acetyl-coa biosynthetic pathways in plasmodium falciparum', *Journal of Biological Chemistry*, 288(51), pp. 36338–36350. doi:10.1074/jbc.M113.503557.
- Coleman, J.E. (1992) 'Structure and Mechanism of Alkaline Phosphatase', *Annual Review of Biophysics and Biomolecular Structure*, 21(1), pp. 441–483. doi:10.1146/annurev.bb.21.060192.002301.
- Collins, C.R. *et al.* (2013) 'Malaria Parasite cGMP-dependent Protein Kinase Regulates Blood Stage Merozoite Secretory Organelle Discharge and Egress', *PLoS Pathogens*, 9(5), p. e1003344. doi:10.1371/journal.ppat.1003344.
- Cowman, A.F. *et al.* (2016) 'Malaria: Biology and Disease', *Cell*, 167(3), pp. 610–624. doi:10.1016/j.cell.2016.07.055.
- Cowman, A.F. and Crabb, B.S. (2006) 'Invasion of red blood cells by malaria parasites', *Cell*, 124(4), pp. 755–766. doi:10.1016/j.cell.2006.02.006.
- Crabb, B. *et al.* (1997) 'Stable transgene expression in Plasmodium falciparum', *Molecular and Biochemical Parasitology*, 90(1), pp. 131–144. doi:10.1016/S0166-6851(97)00143-6.

- Creasey, A. *et al.* (1994) 'Maternal inheritance of extrachromosomal DNA in malaria parasites', *Molecular and Biochemical Parasitology*, 65(1), pp. 95–98. doi:10.1016/0166-6851(94)90118-X.
- Daubenberger, C.A. *et al.* (2000) 'Identification and recombinant expression of glyceraldehyde-3-phosphate dehydrogenase of *Plasmodium falciparum*', *Gene*, 246(1–2), pp. 255–264. doi:10.1016/S0378-1119(00)00069-X.
- Day, K.P. *et al.* (1998) 'CD36-dependent adhesion and knob expression of the transmission stages of *Plasmodium falciparum* is stage-specific', *Molecular and Biochemical Parasitology*, 93(2), pp. 167–177. doi:10.1016/S0166-6851(98)00040-1.
- Dearnley, M.K. *et al.* (2012) 'Origin, composition, organization and function of the inner membrane complex of *Plasmodium falciparum* gametocytes', *Journal of Cell Science*, 125(Pt 8), pp. 2053–63. doi:10.1242/jcs.099002.
- Déchamps, S. *et al.* (2010) 'Glycerophospholipid acquisition in *Plasmodium* - a puzzling assembly of biosynthetic pathways', *International Journal for Parasitology*, 40(12), pp. 1347–65. doi:10.1016/j.ijpara.2010.05.008.
- Desai, N.A. and Shankar, V. (2003) 'Single-strand-specific nucleases', *FEMS Microbiology Reviews*, 26(5), pp. 457–491. doi:10.1111/j.1574-6976.2003.tb00626.x.
- Ding, W.X. *et al.* (2012) 'Electron microscopic analysis of a spherical mitochondrial structure', *Journal of Biological Chemistry*, 287(50), pp. 42373–42378. doi:10.1074/jbc.M112.413674.
- Dixon, M.W.A. and Tilley, L. (2021) '*Plasmodium falciparum* goes bananas for sex', *Molecular and Biochemical Parasitology*, 244. doi:10.1016/j.molbiopara.2021.111385.
- Dodge, J.T. and Phillips, G.B. (1967) 'Composition of phospholipids and of phospholipid fatty acids and aldehydes in human red cells.', *Journal of Lipid Research*, 8(6), pp. 667–75. Available at: <http://www.ncbi.nlm.nih.gov/pubmed/6057495>.
- Doerr, A. (2016) 'Single-particle cryo-electron microscopy', *Nature Methods*, 13(1), pp. 23–23. doi:10.1038/nmeth.3700.
- van Dooren, G.G. *et al.* (2005) 'Development of the endoplasmic reticulum, mitochondrion and apicoplast during the asexual life cycle of *Plasmodium falciparum*', *Molecular Microbiology*, 57(2), pp. 405–19. doi:10.1111/j.1365-2958.2005.04699.x.
- Van Dooren, G.G., Stimmler, L.M. and McFadden, G.I. (2006) 'Metabolic maps and functions of the *Plasmodium* mitochondrion', *FEMS Microbiology Reviews*, 30(4), pp. 596–630. doi:10.1111/j.1574-6976.2006.00027.x.
- Van Dooren, G.G. and Striepen, B. (2013) 'The algal past and parasite present of the apicoplast', *Annual Review of Microbiology*, 67, pp. 271–289. doi:10.1146/annurev-micro-092412-155741.
- Dorn, A. *et al.* (1995) 'Malarial haemozoin/ β -haematin supports haem polymerization in the absence of protein', *Nature*, 374(6519), pp. 269–271. doi:10.1038/374269a0.
- Dudek, J. (2017) 'Role of Cardiolipin in Mitochondrial Signaling Pathways', *Frontiers in Cell and Developmental Biology*, 5, p. 90. doi:10.3389/fcell.2017.00090.
- Dunst, J., Kamena, F. and Matuschewski, K. (2017) 'Cytokines and Chemokines in Cerebral Malaria Pathogenesis', *Frontiers in Cellular and Infection Microbiology*, 7. doi:10.3389/fcimb.2017.00324.
- Elahi, R. *et al.* (2019) 'Functional annotation of serine hydrolases in the asexual erythrocytic stage of *Plasmodium falciparum*', *Scientific Reports*, 9(1), pp. 1–11. doi:10.1038/s41598-019-54009-0.
- Evers, F. *et al.* (2021) 'Composition and stage dynamics of mitochondrial complexes in *Plasmodium falciparum*', *Nature Communications*, 12(1), pp. 1–17. doi:10.1038/s41467-021-23919-x.
- Feagin, J.E. (1992) 'The 6-kb element of *Plasmodium falciparum* encodes mitochondrial cytochrome genes', *Molecular and Biochemical Parasitology*, 52(1), pp. 145–148. doi:10.1016/0166-6851(92)90046-

M.

Ferreira, J.L. *et al.* (2022) 'Form follows function: Variable microtubule architecture in the malaria parasite', *bioRxiv*, p. 2022.04.13.488170.

Filarsky, M. *et al.* (2018) 'GDV1 induces sexual commitment of malaria parasites by antagonizing HP1-dependent gene silencing', *Science*, 359(6381), pp. 1259–1263. doi:10.1126/science.aan6042.

Fisher, N. *et al.* (2014) 'Mitochondrial Electron Transport Chain of *Plasmodium falciparum*', in *Encyclopedia of Malaria*. Springer New York, pp. 1–14. doi:10.1007/978-1-4614-8757-9_12-1.

Flammersfeld, A. *et al.* (2018) 'Phospholipases during membrane dynamics in malaria parasites', *International Journal of Medical Microbiology*, 308(1), pp. 129–141. doi:10.1016/j.ijmm.2017.09.015.

Flammersfeld, A. *et al.* (2020) 'A patatin-like phospholipase functions during gametocyte induction in the malaria parasite *Plasmodium falciparum*', *Cellular Microbiology*, 22(3). doi:10.1111/cmi.13146.

Flannery, E.L., Markus, M.B. and Vaughan, A.M. (2019) '*Plasmodium vivax*', *Trends in Parasitology*, 35(7), pp. 583–584. doi:10.1016/j.pt.2019.04.005.

Folch, J., Lees, M. and Stanley, G.H.S. (1957) 'A simple method for the isolation and purification of total lipides from animal tissues', *Journal of Biological Chemistry*, 226(1), pp. 497–509. doi:10.1016/S0021-9258(18)64849-5.

Frischknecht, F. and Matuschewski, K. (2017) '*Plasmodium* sporozoite biology', *Cold Spring Harbor Perspectives in Medicine*, 7(5). doi:10.1101/cshperspect.a025478.

Fu, Y. *et al.* (2018) 'Comprehensive characterization of toxoplasma acyl coenzyme a-binding protein tgacbp2 and its critical role in parasite cardiolipin metabolism', *mBio*, 9(5), pp. 1–20. doi:10.1128/mbio.01597-18.

Garcia, G.E. *et al.* (1998) 'Xanthurenic acid induces gametogenesis in *Plasmodium*, the malaria parasite', *Journal of Biological Chemistry*, 273(20), pp. 12003–12005. doi:10.1074/jbc.273.20.12003.

Gardner, M.J. *et al.* (2002) 'Genome sequence of the human malaria parasite *Plasmodium falciparum*', *Nature*, 419(6906), pp. 498–511. doi:10.1038/nature01097.

Gautret, P. and Motard, A. (1999) 'Periodic infectivity of *Plasmodium* gametocytes to the vector. A review', *Parasite*, 6(2), pp. 103–111. doi:10.1051/parasite/1999062103.

Geoghegan, N.D. *et al.* (2021) '4D analysis of malaria parasite invasion offers insights into erythrocyte membrane remodeling and parasitophorous vacuole formation', *Nature Communications*, 12(1). doi:10.1038/s41467-021-23626-7.

Gerald, N., Mahajan, B. and Kumar, S. (2011) 'Mitosis in the human malaria parasite *Plasmodium falciparum*', *Eukaryotic Cell*, 10(4), pp. 474–482. doi:10.1128/EC.00314-10.

Giemsa, G. (1904) 'Eine Vereinfachung und Vervollkommnung meiner Methylenblau-Eosin-Färbemethode zur Erzielung der Romanowsky-Nocht'schen Chromatinfärbung', *Centralblatt für Bakteriologie I*, 32, pp. 307–313.

Goñi, F.M., Montes, L.-R. and Alonso, A. (2012) 'Phospholipases C and sphingomyelinases: Lipids as substrates and modulators of enzyme activity', *Progress in Lipid Research*, 51(3), pp. 238–66. doi:10.1016/j.plipres.2012.03.002.

Goodman, C.D., Buchanan, H.D. and McFadden, G.I. (2017) 'Is the Mitochondrion a Good Malaria Drug Target?', *Trends in Parasitology*, 33(3), pp. 185–193. doi:10.1016/j.pt.2016.10.002.

Gu, Z. *et al.* (2003) 'Aberrant cardiolipin metabolism in the yeast *taz1* mutant: a model for Barth syndrome', *Molecular Microbiology*, 51(1), pp. 149–158. doi:10.1046/j.1365-2958.2003.03802.x.

Guca, E. *et al.* (2016) 'Phosphatidylcholine and Phosphatidylethanolamine Biosynthesis Pathways in *Plasmodium*', in *Comprehensive Analysis of Parasite Biology: From Metabolism to Drug Discovery*. Weinheim, Germany: Wiley-VCH Verlag GmbH & Co. KGaA, pp. 171–191.

doi:10.1002/9783527694082.ch7.

Gulati, S. *et al.* (2015) 'Profiling the Essential Nature of Lipid Metabolism in Asexual Blood and Gametocyte Stages of *Plasmodium falciparum*', *Cell Host and Microbe*, 18(3), pp. 371–381. doi:10.1016/j.chom.2015.08.003.

Guler, J.L. *et al.* (2013) 'Asexual Populations of the Human Malaria Parasite, *Plasmodium falciparum*, Use a Two-Step Genomic Strategy to Acquire Accurate, Beneficial DNA Amplifications', *PLoS Pathogens*. Edited by X. Su, 9(5), p. e1003375. doi:10.1371/journal.ppat.1003375.

Gunjan, S. *et al.* (2016) 'Mefloquine induces ROS mediated programmed cell death in malaria parasite: *Plasmodium*', *Apoptosis*, 21(9), pp. 955–964. doi:10.1007/s10495-016-1265-y.

Haines, T.H. and Dencher, N.A. (2002) 'Cardiolipin: A proton trap for oxidative phosphorylation', *FEBS Letters*, 528(1–3), pp. 35–39. doi:10.1016/S0014-5793(02)03292-1.

Hall, R. *et al.* (1983) 'Antigens of the erythrocytic stages of the human malaria parasite *Plasmodium falciparum* detected by monoclonal antibodies', *Molecular and Biochemical Parasitology*, 7(3), pp. 247–265. doi:10.1016/0166-6851(83)90025-7.

Hanske, J. *et al.* (2012) 'Conformational properties of cardiolipin-bound cytochrome c', *Proceedings of the National Academy of Sciences*, 109(1), pp. 125–130. doi:10.1073/pnas.1112312108.

Hartmann, A. *et al.* (2014) 'Phosphatidylethanolamine Synthesis in the Parasite Mitochondrion Is Required for Efficient Growth but Dispensable for Survival of *Toxoplasma gondii*', *Journal of Biological Chemistry*, 289(10), pp. 6809–6824. doi:10.1074/jbc.M113.509406.

Hayward, J.A., Makota, F.V., *et al.* (2022) 'A screen of drug-like molecules identifies chemically diverse electron transport chain inhibitors in apicomplexan parasites', *bioRxiv*, p. 2022.02.13.480284. doi:10.1101/2022.02.13.480284.

Hayward, J.A., Rajendran, E., *et al.* (2022) 'Real-Time Analysis of Mitochondrial Electron Transport Chain Function in *Toxoplasma gondii* Parasites Using a Seahorse XFe96 Extracellular Flux Analyzer', *Bio-protocol*, 12(1), pp. 1–38. doi:10.21769/BioProtoc.4288.

Hoffmann, J.J. and Becker, T. (2022) 'Crosstalk between Mitochondrial Protein Import and Lipids', *International Journal of Molecular Sciences*. MDPI. doi:10.3390/ijms23095274.

Holz, G.G. (1977) 'Lipids and the malarial parasite', *Bulletin of the World Health Organization*, 55(2–3), pp. 237–248.

Hu, Y. *et al.* (2021) 'NMR-Based Methods for Protein Analysis', *Analytical Chemistry*, 93(4), pp. 1866–1879. doi:10.1021/acs.analchem.0c03830.

Hudson, A.T. (1993) 'Atovaquone - a novel broad-spectrum anti-infective drug', *Parasitology Today*, 9(2), pp. 66–68. doi:10.1016/0169-4758(93)90040-M.

Ikon, N. and Ryan, R.O. (2017) 'Cardiolipin and mitochondrial cristae organization', *Biochimica et Biophysica Acta - Biomembranes*, 1859(6), pp. 1156–1163. doi:10.1016/j.bbamem.2017.03.013.

Inoue, H., Nojima, H. and Okayama, H. (1990) 'High efficiency transformation of *Escherichia coli* with plasmids', *Gene*, 96(1), pp. 23–28. doi:10.1016/0378-1119(90)90336-P.

Istvan, E.S. *et al.* (2017) 'Esterase mutation is a mechanism of resistance to antimalarial compounds', *Nature Communications*, 8, pp. 1–8. doi:10.1038/ncomms14240.

Jaber, S.M., Yadava, N. and Polster, B.M. (2020) 'Mapping mitochondrial respiratory chain deficiencies by respirometry: Beyond the Mito Stress Test', *Experimental Neurology*, 328, p. 113282. doi:10.1016/j.expneurol.2020.113282.

Janouškovec, J. *et al.* (2010) 'A common red algal origin of the apicomplexan, dinoflagellate, and heterokont plastids', *Proceedings of the National Academy of Sciences of the United States of America*, 107(24), pp. 10949–10954. doi:10.1073/pnas.1003335107.

- Janse, C.J. *et al.* (1988) 'DNA synthesis in gametocytes of *Plasmodium falciparum*', *Parasitology*, 96, pp. 1–7. doi:10.1017/s0031182000081609.
- Jensen, M.D., Conley, M. and Helstowski, L.D. (1983) 'Culture of *Plasmodium falciparum*: the role of pH, glucose, and lactate', *The Journal of Parasitology*, 69(6), pp. 1060–7. Available at: <http://www.ncbi.nlm.nih.gov/pubmed/6371212>.
- Josling, G.A. and Llinás, M. (2015) 'Sexual development in *Plasmodium* parasites: knowing when it's time to commit', *Nature Reviews Microbiology*, 13(9), pp. 573–587. doi:10.1038/nrmicro3519.
- Jumper, J. *et al.* (2021) 'Highly accurate protein structure prediction with AlphaFold', *Nature*, 596(7873), pp. 583–589. doi:10.1038/s41586-021-03819-2.
- Kats, L.M. *et al.* (2007) 'Protein Trafficking to Apical Organelles of Malaria Parasites - Building an Invasion Machine', *Traffic*, 9(2), pp. 176–186. doi:10.1111/j.1600-0854.2007.00681.x.
- Ke, H. *et al.* (2011) 'Variation among *Plasmodium falciparum* strains in their reliance on mitochondrial electron transport chain function', *Eukaryotic Cell*, 10(8), pp. 1053–61. doi:10.1128/EC.05049-11.
- Ke, H. *et al.* (2015) 'Genetic investigation of tricarboxylic acid metabolism during the *Plasmodium falciparum* life cycle', *Cell Reports*, 11(1), pp. 164–174. doi:10.1016/j.celrep.2015.03.011.
- Keller, M.A. (2021) 'Interpreting phospholipid and cardiolipin profiles in rare mitochondrial diseases', *Current Opinion in Systems Biology*, 28(Icimd), p. 100383. doi:10.1016/j.coisb.2021.100383.
- Khan, S.M. *et al.* (2005) 'Proteome analysis of separated male and female gametocytes reveals novel sex-specific *Plasmodium* biology', *Cell*, 121(5), pp. 675–687. doi:10.1016/j.cell.2005.03.027.
- Kienesberger, P.C. *et al.* (2009) 'Mammalian patatin domain containing proteins: a family with diverse lipolytic activities involved in multiple biological functions', *Journal of Lipid Research*, 50, pp. S63–8. doi:10.1194/jlr.R800082-JLR200.
- Kilian, N. *et al.* (2018) 'Role of phospholipid synthesis in the development and differentiation of malaria parasites in the blood', *Journal of Biological Chemistry*, 293(45), pp. 17308–17316. doi:10.1074/jbc.R118.003213.
- Köhler, S. (2006) 'Multi-membrane-bound structures of Apicomplexa: II. The ovoid mitochondrial cytoplasmic (OMC) complex of *Toxoplasma gondii* tachyzoites', *Parasitology Research*, 98(4), pp. 355–369. doi:10.1007/s00436-005-0066-y.
- Kono, M. *et al.* (2012) 'Evolution and architecture of the inner membrane complex in asexual and sexual stages of the malaria parasite', *Molecular Biology and Evolution*, 29(9), pp. 2113–32. doi:10.1093/molbev/mss081.
- Kono, M. *et al.* (2013) 'The apicomplexan inner membrane complex', *Frontiers in Bioscience*, 18(3), pp. 982–992. doi:10.2741/4157.
- Krotoski, W.A. *et al.* (1982) 'Demonstration of hypnozoites in sporozoite-transmitted *Plasmodium vivax* infection', *American Journal of Tropical Medicine and Hygiene*, 31(6), pp. 1291–1293. doi:10.4269/ajtmh.1982.31.1291.
- Krungkrai, J. *et al.* (1999) 'Mitochondrial oxygen consumption in asexual and sexual blood stages of the human malarial parasite, *Plasmodium falciparum*', *The Southeast Asian Journal of Tropical Medicine and Public Health*, 30(4), pp. 636–42. Available at: <http://www.ncbi.nlm.nih.gov/pubmed/10928353>.
- Krungkrai, J., Prapunwattana, P. and Krungkrai, S.R. (2000) 'Ultrastructure and function of mitochondria in gametocytic stage of *Plasmodium falciparum*', *Parasite*, 7(1), pp. 19–26. doi:10.1051/parasite/2000071019.
- Kuehn, A. and Pradel, G. (2010) 'The coming-out of malaria gametocytes', *Journal of Biomedicine & Biotechnology*, 2010, p. 976827. doi:10.1155/2010/976827.
- Lalève, A. *et al.* (2016) 'The antimalarial drug primaquine targets Fe-S cluster proteins and yeast

- respiratory growth', *Redox Biology*, 7, pp. 21–29. doi:10.1016/j.redox.2015.10.008.
- Lamb, I.M. *et al.* (2022) 'Mitochondrially targeted proximity biotinylation and proteomic analysis in *Plasmodium falciparum*', *PLoS ONE*. Edited by G. Langsley, 17(8 August), p. e0273357. doi:10.1371/journal.pone.0273357.
- Lambros, C. and Vandenberg, J.P. (1979) 'Synchronization of *Plasmodium falciparum* Erythrocytic Stages in Culture', *Journal Parasitology*, 65(3), pp. 418–420.
- Lasonder, E., Rijpma, Sanna R., *et al.* (2016) 'Integrated transcriptomic and proteomic analyses of *P. falciparum* gametocytes: molecular insight into sex-specific processes and translational repression', *Nucleic Acids Research*, 44(13), pp. 6087–6101. doi:10.1093/nar/gkw536.
- Lasonder, E., Rijpma, Sanna R., *et al.* (2016) 'Integrated transcriptomic and proteomic analyses of *P. falciparum* gametocytes: molecular insight into sex-specific processes and translational repression', *Nucleic Acids Research*, 44(13), pp. 6087–101. doi:10.1093/nar/gkw536.
- Lentini, G. *et al.* (2021) 'Structural insights into an atypical secretory pathway kinase crucial for *Toxoplasma gondii* invasion', *Nature Communications*, 12(1), p. 3788. doi:10.1038/s41467-021-24083-y.
- Levental, K.R. *et al.* (2020) 'Lipidomic and biophysical homeostasis of mammalian membranes counteracts dietary lipid perturbations to maintain cellular fitness', *Nature Communications*, 11(1), p. 1339. doi:10.1038/s41467-020-15203-1.
- Lévêque, M.F. *et al.* (2017) 'TgPL2, a patatin-like phospholipase domain-containing protein, is involved in the maintenance of apicoplast lipids homeostasis in *Toxoplasma*', *Molecular Microbiology*, 105(1), pp. 158–174. doi:10.1111/mmi.13694.
- Lim, L. and McFadden, G.I. (2010) 'The evolution, metabolism and functions of the apicoplast', *Philosophical Transactions of the Royal Society B: Biological Sciences*, 365(1541), pp. 749–763. doi:10.1098/rstb.2009.0273.
- López-Barragán, M.J. *et al.* (2011) 'Directional gene expression and antisense transcripts in sexual and asexual stages of *Plasmodium falciparum*', *BMC Genomics*, 12(1), p. 587. doi:10.1186/1471-2164-12-587.
- Luévano-Martínez, L.A. *et al.* (2015) 'Cardiolipin is a key determinant for mtDNA stability and segregation during mitochondrial stress', *Biochimica et Biophysica Acta - Bioenergetics*, 1847(6–7), pp. 587–598. doi:10.1016/j.bbabi.2015.03.007.
- MacRae, J.I. *et al.* (2013) 'Mitochondrial metabolism of sexual and asexual blood stages of the malaria parasite *Plasmodium falciparum*', *BMC Biology*, 11. doi:10.1186/1741-7007-11-67.
- Maguire, P.A. and Sherman, I.W. (1990) 'Phospholipid composition, cholesterol content and cholesterol exchange in *Plasmodium falciparum*-infected red cells.', *Molecular and Biochemical Parasitology*, 38(1), pp. 105–12. doi:10.1016/0166-6851(90)90210-d.
- Mair, G.R. *et al.* (2006) 'Regulation of sexual development of *Plasmodium* by translational repression', *Science*, 313(5787), pp. 667–9. doi:10.1126/science.1125129.
- Malhotra, A. *et al.* (2009) 'Role of calcium-independent phospholipase A 2 in the pathogenesis of Barth syndrome', *Proceedings of the National Academy of Sciences*, 106(7), pp. 2337–2341. doi:10.1073/pnas.0811224106.
- Malleret, B. *et al.* (2011) 'A rapid and robust tri-color flow cytometry assay for monitoring malaria parasite development', *Scientific Reports*, 1(1), p. 118. doi:10.1038/srep00118.
- Mamoun, C. Ben *et al.* (1999) 'A set of independent selectable markers for transfection of the human malaria parasite *Plasmodium falciparum*', *Proceedings of the National Academy of Sciences*, 96(15), pp. 8716–8720. doi:10.1073/pnas.96.15.8716.
- Mancuso, D.J. *et al.* (2007) 'Genetic ablation of calcium-independent phospholipase A2 γ leads to

- alterations in mitochondrial lipid metabolism and function resulting in a deficient mitochondrial bioenergetic phenotype', *Journal of Biological Chemistry*, 282(48), pp. 34611–34622. doi:10.1074/jbc.M707795200.
- Mancuso, D.J. *et al.* (2009) 'Genetic ablation of calcium-independent phospholipase A2 γ leads to alterations in hippocampal cardiolipin content and molecular species distribution, mitochondrial degeneration, autophagy, and cognitive dysfunction', *Journal of Biological Chemistry*, 284(51), pp. 35632–35644. doi:10.1074/jbc.M109.055194.
- Marsh, K. *et al.* (1995) 'Indicators of life-threatening malaria in African children', *The New England Journal of Medicine*, 332(21), pp. 1399–404. doi:10.1056/NEJM199505253322102.
- Matz, J.M. *et al.* (2018) 'An Unusual Prohibitin Regulates Malaria Parasite Mitochondrial Membrane Potential', *Cell Reports*, 23(3), pp. 756–767. doi:10.1016/j.celrep.2018.03.088.
- Mazumdar, J. *et al.* (2006) 'Apicoplast fatty acid synthesis is essential for organelle biogenesis and parasite survival in *Toxoplasma gondii*', *Proceedings of the National Academy of Sciences*, 103(35), pp. 13192–13197. doi:10.1073/pnas.0603391103.
- McLean, A.R.D. *et al.* (2015) 'Malaria and immunity during pregnancy and postpartum: a tale of two species', *Parasitology*, 142(8), pp. 999–1015. doi:10.1017/S0031182015000074.
- McRobert, L. *et al.* (2008) 'Gametogenesis in malaria parasites is mediated by the cGMP-dependent protein kinase', *PLoS Biology*, 6(6), pp. 1243–1252. doi:10.1371/journal.pbio.0060139.
- Meis, J.F.G.M. *et al.* (1983) 'Malaria parasites - Discovery of the early liver form', *Nature*, 302(5907), pp. 424–426. doi:10.1038/302424a0.
- Mesén-Ramírez, P. *et al.* (2019) 'EXP1 is critical for nutrient uptake across the parasitophorous vacuole membrane of malaria parasites', *PLOS Biology*. Edited by T.F. de Koning-Ward, 17(9), p. e3000473. doi:10.1371/journal.pbio.3000473.
- Mi-Ichi, F., Kano, S. and Mitamura, T. (2007) 'Oleic acid is indispensable for intraerythrocytic proliferation of *Plasmodium falciparum*', *Parasitology*, 134(12), pp. 1671–1677. doi:10.1017/S0031182007003137.
- Mi-Ichi, F., Kita, K. and Mitamura, T. (2006) 'Intraerythrocytic *Plasmodium falciparum* utilize a broad range of serum-derived fatty acids with limited modification for their growth', *Parasitology*, 133(4), pp. 399–410. doi:10.1017/S0031182006000540.
- Mileykovskaya, E. and Dowhan, W. (2009) 'Cardiolipin membrane domains in prokaryotes and eukaryotes', *Biochimica et Biophysica Acta (BBA) - Biomembranes*, 1788(10), pp. 2084–2091. doi:10.1016/j.bbamem.2009.04.003.
- Mitamura, T. *et al.* (2000) 'Serum factors governing intraerythrocytic development and cell cycle progression of *Plasmodium falciparum*', *Parasitology International*, 49(3), pp. 219–229. doi:10.1016/S1383-5769(00)00048-9.
- Mohammad, A.H. *et al.* (2022) 'Narrative Review of the Control and Prevention of Knowlesi Malaria', *Tropical Medicine and Infectious Disease*, 7(8), p. 178. doi:10.3390/tropicalmed7080178.
- Moon, R.W. *et al.* (2013) 'Adaptation of the genetically tractable malaria pathogen *Plasmodium knowlesi* to continuous culture in human erythrocytes', *Proceedings of the National Academy of Sciences of the United States of America*, 110(2), pp. 531–536. doi:10.1073/pnas.1216457110.
- Morrisette, N.S. and Sibley, L.D. (2002) 'Cytoskeleton of Apicomplexan Parasites', *Microbiology and Molecular Biology Reviews*, 66(1), pp. 21–38. doi:10.1128/MMBR.66.1.21.
- Moser, K.A. *et al.* (2020) 'Strains used in whole organism *Plasmodium falciparum* vaccine trials differ in genome structure, sequence, and immunogenic potential', *Genome Medicine*, 12(1), p. 6. doi:10.1186/s13073-019-0708-9.
- Mounkoro, P., Michel, T. and Meunier, B. (2021) 'Revisiting the mode of action of the antimalarial

- proguanil using the yeast model', *Biochemical and Biophysical Research Communications*, 534, pp. 94–98. doi:10.1016/j.bbrc.2020.12.004.
- Mukherjee, S. *et al.* (2022) 'Maturation and substrate processing topography of the *Plasmodium falciparum* invasion/egress protease plasmepsin X', *Nature Communications*, 13(1), p. 4537. doi:10.1038/s41467-022-32271-7.
- Nair, S.C. *et al.* (2022) 'The mitochondrion of *Plasmodium falciparum* generates essential acetyl-CoA for protein acetylation', *bioRxiv* [Preprint]. doi:10.1101/2022.03.02.482627.
- Nawabi, P. *et al.* (2003) 'Neutral-lipid analysis reveals elevation of acylglycerols and lack of cholesterol esters in *Plasmodium falciparum*-infected erythrocytes', *Eukaryotic Cell*, 2(5), pp. 1128–1131. doi:10.1128/EC.2.5.1128-1131.2003.
- Neveu, G. *et al.* (2020) '*Plasmodium falciparum* sexual parasites develop in human erythroblasts and affect erythropoiesis', *Blood*, 136(12), pp. 1381–1393. doi:10.1182/blood.2019004746.
- Ngotho, P. *et al.* (2019) 'Revisiting gametocyte biology in malaria parasites', *FEMS Microbiology Reviews*, 43(4), pp. 401–414. doi:10.1093/femsre/fuz010.
- Nina, P.B. *et al.* (2011) 'ATP synthase complex of *Plasmodium falciparum*: Dimeric assembly in mitochondrial membranes and resistance to genetic disruption', *Journal of Biological Chemistry*, 286(48), pp. 41312–41322. doi:10.1074/jbc.M111.290973.
- Nozawa, A. *et al.* (2020) 'Characterization of mitochondrial carrier proteins of malaria parasite *Plasmodium falciparum* based on in vitro translation and reconstitution', *Parasitology International*, 79, p. 102160. doi:10.1016/j.parint.2020.102160.
- Oakley, M.S. *et al.* (2011) 'Clinical and molecular aspects of malaria fever', *Trends in Parasitology*, 27(10), pp. 442–449. doi:10.1016/j.pt.2011.06.004.
- Oemer, G. *et al.* (2018) 'Molecular structural diversity of mitochondrial cardiolipins', *Proceedings of the National Academy of Sciences of the United States of America*, 115(16), pp. 4158–4163. doi:10.1073/pnas.1719407115.
- Oemer, G. *et al.* (2020) 'Phospholipid Acyl Chain Diversity Controls the Tissue-Specific Assembly of Mitochondrial Cardiolipins', *Cell Reports*, 30(12), pp. 4281–4291.e4. doi:10.1016/j.celrep.2020.02.115.
- Oemer, G. *et al.* (2021) 'Fatty acyl availability modulates cardiolipin composition and alters mitochondrial function in HeLa cells', *Journal of Lipid Research*, 62, p. 100111. doi:10.1016/j.jlr.2021.100111.
- Oemer, G. *et al.* (2022) 'The lipid environment modulates cardiolipin and phospholipid constitution in wild type and tafazzin-deficient cells', *Journal of Inherited Metabolic Disease*, 45(1), pp. 38–50. doi:10.1002/jimd.12433.
- Okamoto, N. *et al.* (2009) 'Apicoplast and mitochondrion in gametocytogenesis of *Plasmodium falciparum*', *Eukaryotic Cell*, 8(1), pp. 128–132. doi:10.1128/EC.00267-08.
- Olszewski, K.L. and Llinás, M. (2011) 'Central carbon metabolism of *Plasmodium* parasites', *Molecular and Biochemical Parasitology*, 175(2), pp. 95–103. doi:10.1016/j.molbiopara.2010.09.001.
- Otto, T.D. *et al.* (2010) 'New insights into the blood-stage transcriptome of *Plasmodium falciparum* using RNA-Seq', *Molecular Microbiology*, 76(1), pp. 12–24. doi:10.1111/j.1365-2958.2009.07026.x.
- Otto, T.D. *et al.* (2014) 'A comprehensive evaluation of rodent malaria parasite genomes and gene expression', *BMC Biology*, 12, p. 86. doi:10.1186/s12915-014-0086-0.
- Painter, H.J. *et al.* (2007) 'Specific role of mitochondrial electron transport in blood-stage *Plasmodium falciparum*', *Nature*, 446(7131), pp. 88–91. doi:10.1038/nature05572.
- Palmieri, F. and Pierri, C.L. (2010) 'Mitochondrial metabolite transport', *Essays in Biochemistry*, 47, pp. 37–52. doi:10.1042/BSE0470037.

References

- Parker, M.W. (2003) 'Protein Structure from X-Ray Diffraction', *Journal of Biological Physics*, 29(4), pp. 341–62. doi:10.1023/A:1027310719146.
- Patra, K.P. and Vinetz, J.M. (2012) 'New ultrastructural analysis of the invasive apparatus of the plasmodium ookinete', *American Journal of Tropical Medicine and Hygiene*, 87(3), pp. 412–417. doi:10.4269/ajtmh.2012.11-0609.
- Pegoraro, M. and Weedall, G.D. (2021) 'Malaria in the "Omics Era"', *Genes*, 12(6), p. 843. doi:10.3390/genes12060843.
- Pfeiffer, K. *et al.* (2003) 'Cardiolipin Stabilizes Respiratory Chain Supercomplexes', *Journal of Biological Chemistry*, 278(52), pp. 52873–52880. doi:10.1074/jbc.M308366200.
- Phillips, M.A. *et al.* (2008) 'Triazolopyrimidine-Based Dihydroorotate Dehydrogenase Inhibitors with Potent and Selective Activity against the Malaria Parasite *Plasmodium falciparum*', *Journal of Medicinal Chemistry*, 51(12), pp. 3649–3653. doi:10.1021/jm8001026.
- Pinheiro, T.J.T. and Watts, A. (1994) 'Resolution of Individual Lipids in Mixed Phospholipid Membranes and Specific Lipid-Cytochrome c Interactions by Magic-Angle Spinning Solid-State Phosphorus-31 NMR', *Biochemistry*, 33(9), pp. 2459–2467. doi:10.1021/bi00175a014.
- Pluskal, T. *et al.* (2010) 'MZmine 2: Modular framework for processing, visualizing, and analyzing mass spectrometry-based molecular profile data', *BMC Bioinformatics*, 11(1), p. 395. doi:10.1186/1471-2105-11-395.
- Pöyry, S. *et al.* (2013) 'Atomistic simulations indicate cardiolipin to have an integral role in the structure of the cytochrome bc1 complex', *Biochimica et Biophysica Acta*, 1827(6), pp. 769–78. doi:10.1016/j.bbabi.2013.03.005.
- Radloff, P.D. *et al.* (1996) 'Atovaquone and proguanil for *Plasmodium falciparum* malaria', *Lancet*, 347(9014), pp. 1511–4. doi:10.1016/s0140-6736(96)90671-6.
- Rajaram, K. *et al.* (2022) 'Metabolic changes accompanying the loss of fumarate hydratase and malate–quinone oxidoreductase in the asexual blood stage of *Plasmodium falciparum*', *Journal of Biological Chemistry*, 298(5), p. 101897. doi:10.1016/j.jbc.2022.101897.
- Ralph, S.A. *et al.* (2004) 'Metabolic maps and functions of the *Plasmodium falciparum* apicoplast', *Nature Reviews Microbiology*, 2(3), pp. 203–216. doi:10.1038/nrmicro843.
- Ramanadham, S. *et al.* (2015) 'Calcium-independent phospholipases A2 and their roles in biological processes and diseases', *Journal of Lipid Research*, 56(9), pp. 1643–68. doi:10.1194/jlr.R058701.
- Ramaprasad, A. *et al.* (2022) 'A choline-releasing glycerophosphodiesterase essential for phosphatidylcholine biosynthesis and blood stage development in the malaria parasite', *bioRxiv* [Preprint]. doi:10.1101/2022.06.14.496138.
- Rambold, A.S. *et al.* (2011) 'Tubular network formation protects mitochondria from autophagosomal degradation during nutrient starvation', *Proceedings of the National Academy of Sciences*, 108(25), pp. 10190–10195. doi:10.1073/pnas.1107402108.
- Razak, M.R.M.A. *et al.* (2014) 'Effect of choline kinase inhibitor hexadecyltrimethylammonium bromide on *Plasmodium falciparum* gene expression.', *The Southeast Asian Journal of Tropical Medicine and Public Health*, 45(2), pp. 259–66. Available at: <http://www.ncbi.nlm.nih.gov/pubmed/24968665>.
- Ren, M., Phoon, C.K.L. and Schlame, M. (2014) 'Metabolism and function of mitochondrial cardiolipin', *Progress in Lipid Research*, 55(1), pp. 1–16. doi:10.1016/j.plipres.2014.04.001.
- Rénia, L. *et al.* (2012) 'Cerebral malaria', *Virulence*, 3(2), pp. 193–201. doi:10.4161/viru.19013.
- Ressurreição, M. *et al.* (2020) 'Use of a highly specific kinase inhibitor for rapid, simple and precise synchronization of *Plasmodium falciparum* and *Plasmodium knowlesi* asexual blood-stage parasites', *PloS One*, 15(7), p. e0235798. doi:10.1371/journal.pone.0235798.

- Ridgway, M.C. *et al.* (2022) 'Analysis of sex-specific lipid metabolism of *Plasmodium falciparum* points to the importance of sphingomyelin for gametocytogenesis', *Journal of Cell Science*, 135(5). doi:10.1242/jcs.259592.
- Rogers, N.J. *et al.* (1996) 'CD36 and intercellular adhesion molecule 1 mediate adhesion of developing *Plasmodium falciparum* gametocytes', *Infection and Immunity*, 64(4), pp. 1480–1483. doi:10.1128/iai.64.4.1480-1483.1996.
- Rolland, S.G. *et al.* (2013) 'Impaired complex IV activity in response to loss of LRPPRC function can be compensated by mitochondrial hyperfusion', *Proceedings of the National Academy of Sciences of the United States of America*, 110(32). doi:10.1073/pnas.1303872110.
- Rosenthal, P.J. and Meshnick, S.R. (1996) 'Hemoglobin catabolism and iron utilization by malaria parasites', *Molecular and Biochemical Parasitology*, 83(2), pp. 131–139. doi:10.1016/S0166-6851(96)02763-6.
- Rudlaff, R.M. *et al.* (2020) 'Three-dimensional ultrastructure of *Plasmodium falciparum* throughout cytokinesis', *PLoS Pathogens*, 16(6). doi:10.1371/journal.ppat.1008587.
- Saffer, L.D. and Schwartzman, J.D. (1991) 'A Soluble Phospholipase of *Toxoplasma gondii* Associated with Host Cell Penetration', *The Journal of Protozoology*, 38(5), pp. 454–460. doi:10.1111/j.1550-7408.1991.tb04816.x.
- Sakata-Kato, T. and Wirth, D.F. (2016) 'A Novel Methodology for Bioenergetic Analysis of *Plasmodium falciparum* Reveals a Glucose-Regulated Metabolic Shift and Enables Mode of Action Analyses of Mitochondrial Inhibitors', *ACS Infectious Diseases*, 2(12), pp. 903–916. doi:10.1021/acscinfecdis.6b00101.
- Sato, S. (2021) 'Plasmodium—a brief introduction to the parasites causing human malaria and their basic biology.', *Journal of Physiological Anthropology*, 40(1), p. 1. doi:10.1186/s40101-020-00251-9.
- van Schaijk, B.C.L. *et al.* (2014) 'Type II fatty acid biosynthesis is essential for *Plasmodium falciparum* sporozoite development in the midgut of anopheles mosquitoes', *Eukaryotic Cell*, 13(5), pp. 550–559. doi:10.1128/EC.00264-13.
- Schlame, M. and Greenberg, M.L. (2017) 'Biosynthesis, remodeling and turnover of mitochondrial cardiolipin', *Biochimica et Biophysica Acta (BBA) - Molecular and Cell Biology of Lipids*, 1862(1), pp. 3–7. doi:10.1016/j.bbalip.2016.08.010.
- Schwall, C.T., Greenwood, V.L. and Alder, N.N. (2012) 'The stability and activity of respiratory Complex II is cardiolipin-dependent.', *Biochimica et Biophysica Acta*, 1817(9), pp. 1588–96. doi:10.1016/j.bbabi.2012.04.015.
- Serricchio, M. and Bütikofer, P. (2012) 'An essential bacterial-type cardiolipin synthase mediates cardiolipin formation in a eukaryote', *Proceedings of the National Academy of Sciences of the United States of America*, 109(16). doi:10.1073/pnas.1121528109.
- Shen, B. and Sibley, L.D. (2012) 'The moving junction, a key portal to host cell invasion by apicomplexan parasites', *Current Opinion in Microbiology*, 15(4), pp. 449–55. doi:10.1016/j.mib.2012.02.007.
- Sheokand, P.K. *et al.* (2021) 'A *Plasmodium falciparum* lysophospholipase regulates fatty acid acquisition for membrane biogenesis to enable schizogonic asexual division', *bioRxiv* [Preprint].
- Siciliano, G. *et al.* (2020) 'Critical Steps of *Plasmodium falciparum* Ookinete Maturation', *Frontiers in Microbiology*, 11(March), pp. 1–9. doi:10.3389/fmicb.2020.00269.
- Sievers, F. *et al.* (2011) 'Fast, scalable generation of high-quality protein multiple sequence alignments using Clustal Omega', *Molecular Systems Biology*, 7(1), p. 539. doi:10.1038/msb.2011.75.
- Silvestrini, F. *et al.* (2010) 'Protein export marks the early phase of gametocytogenesis of the human malaria parasite *Plasmodium falciparum*', *Molecular & Cellular Proteomics*, 9(7), pp. 1437–48.

doi:10.1074/mcp.M900479-MCP200.

Singh, P. *et al.* (2019) 'Role of a patatin-like phospholipase in *Plasmodium falciparum* gametogenesis and malaria transmission', *PNAS*, 116(35), pp. 17498–17508. doi:10.1073/pnas.1900266116.

Skinner-Adams, T.S. *et al.* (2019) 'Cyclization-blocked proguanil as a strategy to improve the antimalarial activity of atovaquone', *Communications Biology*, 2(1). doi:10.1038/s42003-019-0397-3.

Spillman, N.J., Dalmia, V.K. and Goldberg, D.E. (2016) 'Exported Epoxide Hydrolases Modulate Erythrocyte Vasoactive Lipids during *Plasmodium falciparum* Infection', *mBio*. Edited by L.H. Miller, 7(5). doi:10.1128/mBio.01538-16.

Srivastava, A. *et al.* (2016) 'Stage-Specific Changes in *Plasmodium* Metabolism Required for Differentiation and Adaptation to Different Host and Vector Environments', *PLoS Pathogens*, 12(12). doi:10.1371/journal.ppat.1006094.

Srivastava, I.K. and Vaidya, A.B. (1999) 'A Mechanism for the Synergistic Antimalarial Action of Atovaquone and Proguanil', *Antimicrobial Agents and Chemotherapy*, 43(6), pp. 1334–1339. doi:10.1128/AAC.43.6.1334.

Srivastava, P.N. and Mishra, S. (2022) 'Disrupting a *Plasmodium berghei* putative phospholipase impairs efficient egress of merozoites', *International Journal for Parasitology*, 52(8), pp. 547–558. doi:10.1016/j.ijpara.2022.03.002.

Storm, J. *et al.* (2014) 'Phosphoenolpyruvate Carboxylase Identified as a Key Enzyme in Erythrocytic *Plasmodium falciparum* Carbon Metabolism', *PLoS Pathogens*, 10(1). doi:10.1371/journal.ppat.1003876.

Struck, N.S. *et al.* (2005) 'Re-defining the Golgi complex in *Plasmodium falciparum* using the novel Golgi marker PfGRASP', *Journal of Cell Science*, 118(23), pp. 5603–5613. doi:10.1242/jcs.02673.

Struck, N.S. *et al.* (2008) 'Spatial dissection of the cis- and trans-Golgi compartments in the malaria parasite *Plasmodium falciparum*', *Molecular Microbiology*, 67(6), pp. 1320–30. doi:10.1111/j.1365-2958.2008.06125.x.

Sturm, A. *et al.* (2006) 'Manipulation of host hepatocytes by the malaria parasite for delivery into liver sinusoids', *Science*, 313(5791), pp. 1287–90. doi:10.1126/science.1129720.

Suarez-Cortés, P., Silvestrini, F. and Alano, P. (2014) 'A fast, non-invasive, quantitative staining protocol provides insights in *Plasmodium falciparum* gamete egress and in the role of osmiophilic bodies', *Malaria Journal*, 13(1). doi:10.1186/1475-2875-13-389.

Symons, J.L. *et al.* (2021) 'Lipidomic atlas of mammalian cell membranes reveals hierarchical variation induced by culture conditions, subcellular membranes, and cell lineages', *Soft Matter*, 17(2), pp. 288–297. doi:10.1039/d0sm00404a.

Talman, A.M. *et al.* (2004) 'Gametocytogenesis: The puberty of *Plasmodium falciparum*', *Malaria Journal*, 3(24). doi:10.1186/1475-2875-3-24.

Tan, M.S.Y. and Blackman, M.J. (2021) 'Malaria parasite egress at a glance', *Journal of Cell Science*, 134(5). doi:10.1242/jcs.257345.

Tarun, A.S., Vaughan, A.M. and Kappe, S.H.I. (2009) 'Redefining the role of de novo fatty acid synthesis in *Plasmodium* parasites', *Trends in Parasitology*, 25(12), pp. 545–550. doi:10.1016/j.pt.2009.09.002.

Tian, H.F., Feng, J.M. and Wen, J.F. (2012) 'The evolution of cardiolipin biosynthesis and maturation pathways and its implications for the evolution of eukaryotes', *BMC Evolutionary Biology*, 12(1), p. 32. doi:10.1186/1471-2148-12-32.

Toenhake, C.G. *et al.* (2018) 'Chromatin Accessibility-Based Characterization of the Gene Regulatory Network Underlying *Plasmodium falciparum* Blood-Stage Development', *Cell Host & Microbe*, 23(4), pp. 557–569.e9. doi:10.1016/j.chom.2018.03.007.

- Torrentino-Madamet, M. *et al.* (2010) 'Microaerophilic Respiratory Metabolism of Plasmodium falciparum Mitochondrion as a Drug Target', *Current Molecular Medicine*, 10(1), pp. 29–46. doi:10.2174/156652410791065390.
- Trager, W. and Jensen, J.B. (1976) 'Human Malaria Parasites in Continuous Culture', *Science*, 193(4254), pp. 673–675. doi:10.1126/science.781840.
- Tran, P.N. *et al.* (2016) 'Changes in lipid composition during sexual development of the malaria parasite Plasmodium falciparum', *Malaria Journal*, 15(1), pp. 1–13. doi:10.1186/s12936-016-1130-z.
- Uyemura, S.A. *et al.* (2004) 'Oxidative Phosphorylation and Rotenone-insensitive Malate- and NADH-Quinone Oxidoreductases in Plasmodium yoelii yoelii Mitochondria in Situ', *Journal of Biological Chemistry*, 279(1), pp. 385–393. doi:10.1074/jbc.M307264200.
- Vaidya, A.B., Akella, R. and Suplick, K. (1989) 'Sequences similar to genes for two mitochondrial proteins and portions of ribosomal RNA in tandemly arrayed 6-kilobase-pair DNA of a malarial parasite', *Molecular and Biochemical Parasitology*, 35(2), pp. 97–107. doi:10.1016/0166-6851(89)90112-6.
- VanWye, J.D. and Haldar, K. (1997) 'Expression of green fluorescent protein in Plasmodium falciparum', *Molecular and Biochemical Parasitology*, 87(2), pp. 225–229. doi:10.1016/S0166-6851(97)00059-5.
- Varadi, M. *et al.* (2022) 'AlphaFold Protein Structure Database: Massively expanding the structural coverage of protein-sequence space with high-accuracy models', *Nucleic Acids Research*, 50(D1), pp. D439–D444. doi:10.1093/nar/gkab1061.
- Vaughan, A.M. *et al.* (2009) 'Type II fatty acid synthesis is essential only for malaria parasite late liver stage development', *Cellular Microbiology*, 11(3), pp. 506–520. doi:10.1111/j.1462-5822.2008.01270.x.
- Vaughan, A.M. *et al.* (2012) 'Complete Plasmodium falciparum liver stage development in liver-chimeric mice', *Journal of Clinical Investigation*, 122(10), pp. 3618–3628. doi:10.1172/JCI62684.
- Vaughan, J.A. (2007) 'Population dynamics of Plasmodium sporogony', *Trends in Parasitology*, pp. 63–70. doi:10.1016/j.pt.2006.12.009.
- Vergeade, A. *et al.* (2016) 'Cardiolipin fatty acid remodeling regulates mitochondrial function by modifying the electron entry point in the respiratory chain', *Mitochondrion*, 28, pp. 88–95. doi:10.1016/j.mito.2016.04.002.
- Verhoef, J.M.J., Meissner, M. and Kooij, T.W.A. (2021) 'Organelle dynamics in apicomplexan parasites', *mBio*. American Society for Microbiology. doi:10.1128/mBio.01409-21.
- Vial, H.J. *et al.* (1989) 'Phospholipid metabolism in Plasmodium -infected erythrocytes: guidelines for further studies using radioactive precursor incorporation', *Parasitology*, 98(3), pp. 351–357. doi:10.1017/S0031182000061424.
- Vielemeyer, O. *et al.* (2004) 'Neutral lipid synthesis and storage in the intraerythrocytic stages of Plasmodium falciparum', *Molecular and Biochemical Parasitology*, 135(2), pp. 197–209. doi:10.1016/j.molbiopara.2003.08.017.
- Ward, K.E., Fidock, D.A. and Bridgford, J.L. (2022) 'Plasmodium falciparum resistance to artemisinin-based combination therapies', *Current Opinion in Microbiology*, p. 102193. doi:10.1016/j.mib.2022.102193.
- Wein, S. *et al.* (2018) 'Contribution of the precursors and interplay of the pathways in the phospholipid metabolism of the malaria parasite', *Journal of Lipid Research*, 59(8), pp. 1461–1471. doi:10.1194/jlr.M085589.
- Wendel, W.B. (1946) 'The influence of naphthoquinones upon the respiratory and carbohydrate metabolism of malarial parasites', *Federation proceedings*, 5, p. 406.
- WHO (2021) *World Malaria Report 2021*, *World Malaria Report*. Geneva.

- Wichers, J.S. *et al.* (2019) 'Dissecting the Gene Expression, Localization, Membrane Topology, and Function of the Plasmodium falciparum STEVOR Protein Family', *mBio*. Edited by J.C. Boothroyd, 10(4). doi:10.1128/mBio.01500-19.
- Wichers, J.S. *et al.* (2021) 'Characterization of Apicomplexan Amino Acid Transporters (ApiATs) in the Malaria Parasite Plasmodium falciparum', *mSphere* [Preprint]. Edited by M. Phillips. doi:10.1128/mSphere.00743-21.
- Wijeyesakere, S.J., Richardson, R.J. and Stuckey, J.A. (2014) 'Crystal Structure of Patatin-17 in Complex with Aged and Non-Aged Organophosphorus Compounds', *PLoS ONE*. Edited by I. Silman, 9(9), p. e108245. doi:10.1371/journal.pone.0108245.
- Wilson, S.K. *et al.* (2020) 'A toxoplasma gondii patatin-like phospholipase contributes to host cell invasion', *PLoS Pathogens*, 16(7). doi:10.1371/journal.ppat.1008650.
- Wilson, S.K. and Knoll, L.J. (2018) 'Patatin-like phospholipases in microbial infections with emerging roles in fatty acid metabolism and immune regulation by Apicomplexa', *Molecular Microbiology*, 107(1), pp. 34–46. doi:10.1111/mmi.13871.
- Wu, Y. *et al.* (1995) 'Transfection of Plasmodium falciparum within human red blood cells', *Proceedings of the National Academy of Sciences*, 92(4), pp. 973–977. doi:10.1073/pnas.92.4.973.
- Wu, Y., Kirkman, L.A. and Wellems, T.E. (1996) 'Transformation of Plasmodium falciparum malaria parasites by homologous integration of plasmids that confer resistance to pyrimethamine', *Proceedings of the National Academy of Sciences*, 93(3), pp. 1130–1134. doi:10.1073/pnas.93.3.1130.
- Xu, Y. *et al.* (2016) 'Loss of protein association causes cardiolipin degradation in Barth syndrome', *Nature Chemical Biology*, 12(8), pp. 641–647. doi:10.1038/nchembio.2113.
- Xu, Y. *et al.* (2019) 'Assembly of the complexes of oxidative phosphorylation triggers the remodeling of cardiolipin', *Proceedings of the National Academy of Sciences of the United States of America*, 166(23), pp. 11235–11240. doi:10.1073/pnas.1900890116.
- Yang, M. *et al.* (2022) 'Genetic disruption of isocitrate dehydrogenase arrests the full development of sexual stage parasites in Plasmodium falciparum', *bioRxiv* [Preprint]. doi:10.1101/2022.08.05.502965.
- Ye, C., Shen, Z. and Greenberg, M.L. (2016) 'Cardiolipin remodeling: a regulatory hub for modulating cardiolipin metabolism and function', *Journal of Bioenergetics and Biomembranes*, 48(2), pp. 113–123. doi:10.1007/s10863-014-9591-7.
- Yeoh, S. *et al.* (2007) 'Subcellular discharge of a serine protease mediates release of invasive malaria parasites from host erythrocytes', *Cell*, 131(6), pp. 1072–83. doi:10.1016/j.cell.2007.10.049.
- Yeoman, J.A. *et al.* (2011) 'Tracking glideosome-associated protein 50 reveals the development and organization of the inner membrane complex of Plasmodium falciparum', *Eukaryotic Cell*, 10(4), pp. 556–564. doi:10.1128/EC.00244-10.
- Yoo, E. *et al.* (2020) 'The Antimalarial Natural Product Salinipostin A Identifies Essential α/β Serine Hydrolases Involved in Lipid Metabolism in P. falciparum Parasites', *Cell Chemical Biology*, 27(2), pp. 143-157.e5. doi:10.1016/j.chembiol.2020.01.001.
- Young, J.A. *et al.* (2005) 'The Plasmodium falciparum sexual development transcriptome: A microarray analysis using ontology-based pattern identification', *Molecular and Biochemical Parasitology*, 143(1), pp. 67–79. doi:10.1016/j.molbiopara.2005.05.007.
- Yu, M. *et al.* (2008) 'The Fatty Acid Biosynthesis Enzyme FabI Plays a Key Role in the Development of Liver-Stage Malarial Parasites', *Cell Host and Microbe*, 4(6), pp. 567–578. doi:10.1016/j.chom.2008.11.001.
- Zachman, D.K. *et al.* (2010) 'The role of calcium-independent phospholipase A2 in cardiolipin remodeling in the spontaneously hypertensive heart failure rat heart', *Journal of Lipid Research*, 51(3), pp. 525–534. doi:10.1194/jlr.M000646.

Publications

Results of this PhD thesis are published as a preprint.

Burda PC, Ramaprasad A, **Pietsch E**, Bielfeld S, Söhnchen C, Wilcke L, Strauss J, Schwudke D, Sait A, Collinson LM, Blackman MJ, Gilberger TW (2021) **Global analysis of putative phospholipases in the malaria parasite *Plasmodium falciparum* reveals critical factors for parasite proliferation.** biorxiv <https://doi.org/10.1101/2021.06.28.450158>.

In addition, Emma Luise Pietsch is listed as a co-author on the following publications and preprints.

Publications in peer-reviewed journals

Alder A, Wilcke L, **Pietsch E**, von Thien H, Pazicky S, Löw C, Mesén-Ramirez P, Bachmann A, Burda PC, Kunick C, Sondermann H, Wilson D, Gilberger TW (2022) **Functional inactivation of *Plasmodium falciparum* glycogen synthase GSK3 modulates erythrocyte invasion and blocks gametocyte maturation.** JBC 298(9) 102360.

Wichers JS, Gelder Cv, Fuchs G, Ruge JM, **Pietsch E**, Ferreira JL, Safavi S, Thien Hv, Burda PC, Mesén-Ramirez P, Spielmann T, Strauss J, Gilberger TW, Bachmann A (2021) **Characterization of apicomplexan amino acid transporters (ApiATs) in the malaria parasite *Plasmodium falciparum*.** mSphere 6(6)e00743-21.

Burda PC, Crosskey T, Lauck K, Zurborg S, Söhnchen C, Liffner B, Wilcke L, **Pietsch E**, Strauss J, Jeffries CM, Svergun DI, Wilson DW, Wilmanns M, Gilberger TW (2020) **Structure-based identification and functional characterization of a lipocalin in the malaria parasite *Plasmodium falciparum*.** Cell Rep 31:107817.

Hübner K, Karwelat D, **Pietsch E**, Beinborn I, Winterberg S, Bedenbender K, Benedikter BJ, Schmeck B, Vollmeister E (2020) **NF- κ B-mediated inhibition of microRNA-149-5p regulates Chitinase-3-like 1 expression in human airway epithelial cells.** Cellular Signalling 67:109498.

Preprints

Ferreira JL, Prazak V, Vasishtan D, Siggel M, Hentzschel F, **Pietsch E**, Kosinski J, Frischknecht F, Gilberger TW, Grünewald K (2022) **Form follows function: Variable microtubule architecture in the malaria parasite.** biorxiv <https://www.biorxiv.org/content/10.1101/2022.04.13.488170v1>

Kehrer J, Ricken D, Strauss L, **Pietsch E**, Heinze JM, Frischknecht F (2020) **APEX-based proximity labeling in *Plasmodium* identifies a membrane protein with dual functions during mosquito infection.** biorxiv <https://www.biorxiv.org/content/10.1101/2020.09.29.318857v1.full>

Presentations

This work was presented at two conferences.

BioMalPar XVIII: biology and pathology of the malaria parasite.

23 – 25 May 2022

Heidelberg, Germany

Poster: The patatin-like phospholipase PfPNPLA2 and its link to the parasite's electron transport chain.

Molecular Parasitology Meeting (MPM) XXXIII

18 – 22 September 2022

Woods Hole, MA, USA

Poster: The patatin-like phospholipase PfPNPLA2 is important for mitochondrial function in malaria parasites.